Accuracy Problems in Weighing Vehicles during Motion

Author: PLAMEN ATANASSOV POPOV

Thesis submitted for the Degree of
Doctor of Philosophy in
Measurement and Instrumentation.

Supervised by: Dr Faruq Abdullah

THE CITY UNIVERSITY - LONDON
SCHOOL OF ENGINEERING
DEPARTMENT OF ELECTRICAL ELECTRONIC AND INFORMATION ENGINEERING

October 1992

DECLARATION

I grant powers of discretion to the University Librarian to allow this thesis to be copied in whole or in part without further reference to me. This permission covers only single copies made for study purposes, subject to normal conditions of acknowledgement.

ACKNOWLEDGEMENTS

Many people provided assistance and support in the course of this work. At this final moment my deepest gratitude goes to:

First and foremost to my supervisor Dr Abdullah for his guidance and especially his patience in helping to produce this thesis.

Prof. Finkelstein and Prof. Grattan who welcomed me to the City University, for their constant support and supervision.

My parents who helped me choose science as the direction of my life, the rest of my family, and above all my wife Nicky for their love, encouragement and persistence.

All those members of the City University staff whom I have consulted along these years for their time and helpfulness.

The Bulgarian Committee for Science and Technology for financial support.

The Transport and Road Research Laboratory, and particularly Robin Moore for their technical assistance and advice.

Finally all the friends I met at the City University for the useful discussions on related and unrelated topics. Peter Burton in particular who made this foreign land to me feel more like home.

ABSTRACT

The objective of this study is to help solving some of the measurement accuracy and reliability problems of present WIM systems. The theoretical part of the study is focused on vehicle dynamic effects since they have long been identified as one of the major causes of error in high speed dynamic vehicle weighing.

A detailed system analysis describes the functionality of the basic elements of the WIM process - vehicle suspension dynamics, sensor system, and signal processing. In the metrological analysis the standard measurement categories accuracy, repeatability, reproducibility etc., are defined for the technique, and the main sources of measurement errors are identified. Mathematical models are presented of the vehicle suspension/tyres, and a rigid sensor platform with its ground foundation, which are later used in a series of vehicle - roadsurface dynamic interaction computer simulations. A locally developed interactive modelling package is used to run the simulations. Two major sets of simulations are performed - 1) vehicle interaction with road profiles of deterministic shapes, 2) vehicle interaction with road surfaces of stochastic description. The effects of different factors influencing the outcome of the measurement, e.g. vehicle speed, platform protrusion level, vehicle physical parameters, etc., are investigated.

As part of the experimental work a concept for a capacitive sensor is proposed in line with the trend of developing low-cost, easy to install WIM systems. Finite element modelling is used to derive the optimal sensor strip profile. Finally a frequency modulated capacitance measurement circuit incorporating frequency drift compensation is developed and tested with good results.

Most of the study results are presented in both tabular and graphical form. The corresponding conclusions are drawn on the basis of the obtained data, regarding the design, installation and usage of WIM equipment.

Keywords: dynamic weighing, vehicle modelling, road surface simulation, weighing sensors, capacitance measuring circuits.

TABLE OF CONTENTS

LIST OF ABBREVIATIONS

AC - Alternating Current
A/D - Analogue to Digital
AVCS - Automatic Vehicle Classifcation System
DAC - Digital to Analogue Converter
DC - Direct Current
DLC - Dynamic Load Coefficient
DOF - Degree of Freedom
DPU - Data processing Unit
FCE - Frequency Control Element
FE - Finite Elements
FM - Frequency Modulation
HGV - Heavy Goods Vehicle
IC - Integrated Circuit
IF - Impact Factor
MEDIEM - Multi Energy Domain Interactive Elements Modelling
MIRA - Motor Industry Research Association
PDF - Probability Density Function
PSD - Power Spectral Density
PVDF - Polyvinylidene fluoride
RF - Radio Frequency
RRL - Road Research Laboratory
SAE - Society of Autotmotive Engineers
TRRL - Transport and Road Research Laboratory
WIM - Weigh in Motion

LIST OF FIGURES

LIST OF TABLES

INTRODUCTION

Although Weighing Vehicles in Motion, (WIM) has been practised for more than three decades now, no systematic investigation into its problems in metrological terms has been undertaken yet. Various authors have tackled different aspects of the process and a variety of systems have been described mainly in terms of the different force/weight sensors used. Despite the great number of different types and makes of WIM systems in use at present, no functional classification, standard set of technical specifications, metrological requirements, methods of calibration etc., have been developed yet.

The relatively poor accuracy of existing WIM systems (rarely better than 10% of static weight), show that the measurement process is impaired by specific error contributing factors inherent to the technique. These are apparently due to the dynamic character of the measurand and the short measurement period insufficient to provide an adequate signal sample for efficient processing. Identification of factors influencing the outcome of the WIM measurement, as well as quantifying their effect is therefore necessary if improvement in accuracy is sought. The dynamic effects of vehicle/wheel interaction with the road surface and WIM equipment are of primary importance in that respect. The nature and magnitudes of the dynamic wheelforces have been the subject of a number of theoretical and experimental studies, but not yet in the context of dynamic weighing accuracy.

With the growing demand in the last decade for vehicle/axle weight data, a considerable effort has been dedicated to the development of lightweight, easy to install, low-cost WIM installations. This effort has largely been directed towards the introduction in the area of new types of force/displacement transducers, refining the signal processing methods, and automating data gathering and presentation.

A feasibility study was undertaken at The City University in 1985 of dynamic weighbridge systems, as part of a contract with the Transport and Road Research Laboratory, (TRRL) to evaluate the performance of existing WIM

installations and identify prospective candidate sensor systems for the technology. Soon after the completion of the contract a decision was taken to continue the research in the area of computer simulation of the dynamic weighing process. Also to be continued was the theoretical and experimental study on the feasibility of capacitive strip deflection sensors for use in WIM systems, as well as the development of a measurement circuit for that type of sensor. Part of the work was done at the request of the TRRL, and relevant documentation and experimental results at the Laboratory were made available for the purposes of the study. The research work that followed is described in this thesis.

The objectives set before the study were:

- Conduct an extensive survey of existing WIM systems to build a comprehensive classification with respect of system installation method, rules of operation, primary transducers used, operational accuracy, cost etc.
- Build a generalised model of the weighing process, and present a structure of a typical WIM system incorporating information flow and influencing factors.
- Analyse the process in metrological terms and identify the major causes of measurement errors. Review methods to improve accuracy, e.g. WIM site preparation, signal processing techniques etc.
- Build representative mathematical models of vehicle suspension and tyre, typical road profiles, as well as sensor platforms in order to perform simulations of vehicle – road/sensor interactions.
- Simulate dynamic interactions between vehicle wheels/axles and road or sensor profiles of deterministic and stochastic description, representing typical cases of the measurement process.
- Develop a capacitive sensor and a measuring circuit with possible application in low cost, fast installation WIM systems.

The theoretical part of the study makes extensive use of the computer aided mathematical modelling tools developed earlier at the Measurements and Instrumentation Centre of The City University. The thesis is structured in six chapters followed by a study summary and directions for further research in the area.

Chapter 1 begins with an introduction to WIM principles and the historical background of the technology. Examples of systems currently in use are given and the method of their operation is explained. The various fields of application of dynamic vehicle weight data are listed. System classification is performed on the basis of purpose of measurement, sensor dimensions, methods of installation etc.

In Chapter 2 a detailed analysis is carried out of a typical WIM system. All the components of the measurement setup are handled in detail. Special attention is paid to the dynamic behaviour of vehicle suspensions and sensor platforms. Typical sensor signals and available signal conditioning and processing techniques are discussed.

Chapter 3 is an analysis of the dynamic weighing process in metrological terms. The standard measurement categories, e.g. accuracy, repeatability, reproducibility etc., are defined for dynamic weighing, and respective classifications are derived. All possible major sources of error are then explained and analysed in detail. Methods for improving WIM accuracy are also discussed.

Chapter 4 describes the development of mathematical models of WIM components. The two main approaches in modelling methodologies are introduced, and existing vehicle model examples are surveyed. The selection of the working suspension/tyre models is explained. Different graphical interface modelling techniques are described and the main modelling package used in the study is introduced.

In Chapter 5 the results of the simulation trials of dynamic vehicle/road surface interaction are presented. The main simulation tasks are described and the planning of the modelled situations is explained. The effects of different factors influencing the dynamic behaviour of the vehicle are investigated and the respective conclusions are drawn.

Chapter 6 describes a novel concept for a capacitive line sensor for in-motion weighing, as well as the practical design and testing of an associated electronic circuit. The properties and relationships of capacitive force/deflection transducers are presented. The profile and dimensions of a prospective strip sensor are derived using finite element modelling methods. A frequency modulated capacitance measuring circuit incorporating drift correction technique is described, and the experimental results of the device's performance are

presented.

Finally in Chapter 7 the study findings are summarised and directions for possible further research are suggested.

Most of the results of the study are presented in graphical or tabular form. Though a large part of the study was performed employing theoretical methods, WIM equipment developers and manufacturers might find the results and the suggested devices of practical value for their work.

Chapter I: Definitions and Classifications.

1. 1 BACKGROUND.

Weighing vehicles in motion, **(WIM)** is the procedure of measuring the wheel forces applied by moving vehicles to roads and tracks. Sometimes called ***Dynamic Vehicle Weighing***, it is now a well established technology and there is a wide variety of systems in use worldwide.

Vehicle weight data have been collected for almost 60 years now for numerous reasons. Initially weight measurements were taken statically, with the vehicle, (or axle), at rest on top the scales designed for static operation. Static weighing, however, proved to be inefficient and unsafe for heavy traffic volumes. Furthermore it is impossible through static weighing to obtain data about dynamic pavement loading caused by moving vehicles which is of increasing interest to road and pavement structure designers. For many years traffic operators and weighing equipment specialists have been working to perfect techniques of weighing vehicles while they are in motion.

1. 2 WIM QUALITIES.

Compared to static weighing, the weighing of vehicles during motion offers the following advantageous features:

a) High vehicle processing rate and minimal traffic disruption: With static weighscales the vehicle normally has to leave the road in order to be placed on the weighing platform. Weighing in motion avoids this procedure since most dynamic weighscales are placed/embedded directly on the road and vehicle diversion is not required. This has also the added effect of minimal scale avoidance by drivers hence providing less biased information.

b) Improved safety both for drivers and equipment operators: No special manoeuvring or other activities are normally required in the dynamic weighing process which might endanger the driver or the vehicle. In the cases when WIM

installations are manned the crew is usually accommodated in a nearby building or a van avoiding any contact with the traffic. In addition, WIM systems sometimes are installed in advance of bridge structures to detect and divert overweight vehicles that might cause accidents.

c) High degree of system automation: The process of measurement and data presentation in most contemporary WIM systems is fully automated. Their electronics involve microprocessor based digital signal processing and data handling techniques. Combining weight information with other vehicle data such as speed, time of passage, destination etc, allows for creating automatic real time vehicle classification systems. It also becomes possible to reduce staff and management requirements.

d) Reduced unit cost per vehicle weighed: Fully automated unmanned and low maintenance WIM systems result in considerable long term savings for the user.

e) Availability of dynamic wheel load information preferred by pavement and bridge design researchers: Modern techniques for roadway construction and pavement design depend on data regarding the dynamics of vehicle-road interactions. The only practical way to gather that information is by measuring the loads applied by moving vehicles on roads using WIM equipment.

However, some of the disadvantages of the technique have to be mentioned too. These are:

a) Relative inaccuracy in comparison with static weighers: Due to the dynamic character of the inputs, WIM data are inherently approximate when static weights have to be deduced from the measurement. Normal accuracy for current systems is within $\pm 10\%$ of static weights, compared with $\pm (1-2)\%$ for a static scale. For that reason WIM scales are still not certified for legislative and enforcement weighing utilisation.

b) Unavailability of information which sometimes can only be provided by the driver: Sometimes specific information, (i.e. nature of load, origin and destination, type of fuel etc.), can be obtained only from the driver when the vehicle is stopped.

c) Complexity of installation, activating and deactivating of a WIM site and the resulting traffic disruptions: These activities might necessitate temporary

closure of the road section with all the involved inconveniences and expenses.

d) High initial costs: Due to the high costs of the above activities, the advanced technology level of the equipment, and the increased staff technical requirements, WIM systems are still expensive to install and activate.

1. 3 HISTORY OF WIM DEVELOPMENT.

Most of the early examples of WIM devices were similar in construction to existing static weighers and consisted of heavy platforms supported by loadcells situated in specially prepared road pits.

One of the earliest attempts to develop dynamic weighing equipment was reported in 1952 by the U.S. Bureau of Public Roads, [102]. The weighing platform measuring (3.7×0.9m) was situated in a specially prepared 0.3m deep concrete reinforced pit dug into the traffic lane. The platform was supported at each corner by 4 columns to which resistance strain gages were bonded and electrically connected into a Wheatstone bridge circuit. The system's output was obtained as photographs of oscilloscope traces from the load cells and data about axle weights, axle spacings and vehicle speeds were computed by manually analysing the oscilloscope readings.

The first British system was similar in construction and was built by the Road Research Laboratory, (RRL), in 1957, [143]. An improved version was developed in 1963 and is still in use at about 30 locations throughout the U.K., [91], [142]. The installation normally consists of 3 separate platforms, (0.6 × 0.6m each), assembled side by side in order to span the near-side traffic lane, [115]. Each module is supported by 4 loadcells located at its corners and connected in a bridge circuit. The amplified and filtered outputs are sent for processing in a load classifying unit which is usually a part of an Automatic Vehicle Classification System, (AVCS) installed at some of the TRRL weighbridge sites, [139].

By the mid 1960s research in the area was concentrating on designing lighter and cheaper systems involving different constructions of weighing platforms with alternative strain gage positioning and improved signal detection,

[76]. The extensive construction efforts and costs of the heavy platforms as well as their lack of portability meant that they could be used only at expensively built locations. Their maintenance also proved costly with significant levelling and lateral translation problems as well as load cells performance deteriorating due to moisture effects.

One result of this research was the Radian Corporation WIM System, developed at the University of Texas and used extensively throughout the U.S.A., [77]. The weigh platform measuring (1.4×0.5m) had a depth of only 0.05m and was supported by 8 load cells connected in a Wheatstone bridge circuit together with 8 passive strain resistors for temperature compensation. Accuracies of $\pm 5\%$ for gross vehicle weights and $\pm 10\%$ for individual axles were claimed at low speeds, [35].

A different principle was used in the dynamic weigher developed by the German Bundesanstalt fur Strassenwessen, (BAST), [14], [19], [35]. The strain gages were bonded to specially milled grooves on the underside of the weighing platform, ($1.2 \times 0.5 \times 0.016$m). The whole assembly required only 0.05m road excavation for the base frame. Another German development used a hydraulically operated sensor, [62]. It consisted of an elastic steel hollow plate filled with a blend of silicone oil. It was connected to a rigid hydraulic vessel partially divided by a flexible membrane. Application of load on the upper plate forced the fluid out causing the membrane to deflect proportionally. The deflection was monitored by an inductive distance transducer and interpreted as axle weight. However, the system was difficult to install because it required nearly 1m deep road excavation.

The search for lower cost portable WIM systems and the recent advances in sensor technology have brought about the introduction of alternative methods of force transduction into the area. Two of the major efforts in this direction that have resulted in the development of commercially viable systems are the capacitive and the piezo-electric based sensors.

The capacitive sensors in the form of a weighmat or a strip normally consist of two or more conductive plates separated by elastic dielectric material and encapsulated in weatherproof rubber. As a wheel passes over the sensor the deflection of the plates brings about proportional change in the capacitance which is detected either by the output voltage of a reactive bridge, or by the

frequency shift in an oscillator circuit. A flexible capacitive weighpad design was first patented in 1968 by Trott and Grainger, [141], [142]. It consisted of 3 perforated plates separated by layers of natural rubber and sealed in a rubber enclosure. Subsequent developments, [12], [87], were devices of slightly different construction, but operating on the same design principles. One of the first commercially available capacitive mat sensors was developed in 1967 by South Africa's National Inst. for Road Research, [13], [14], [104], and marketed as the "Viatec Axle Weight Analyser" by *'Plessey'* S. Africa. Similar capacitive sensors have been developed later in Sweden, (The Telub Traffic Data Analyser), in England by the TRRL, the Golden River system, [75] etc. Several recent capacitive sensor developments, [29], [37], [126] prove the practicality of the technique, especially when used with modern microprocessor based electronics.

Piezo-electric sensors use the properties of some crystalline materials to develop electrical charges of opposite polarities on certain parallel faces when a force is applied on them. The piezo-effect is dynamic so that a charge is generated only when the forces are changing. The earliest piezo-electric WIM system was developed in 1967 in France by the Laboratoire Central des Ponts et Chausees. Three crystal assemblies are used to support a weighing platform and produce an electrical signal proportional to the applied load, [131]. Over 50 of these systems were installed in France.

Another piezo-electric based system also developed in France uses a coaxial cable filled with pressure-sensitive piezoelectric ceramic powder, [125]. The cable, (commonly known as Vibracoax), is placed in a shallow groove across the traffic lane and covered with a sand-epoxy mixture. The wheel load is transmitted through the sealing material causing the cable to deform thus generating electric charge on the copper shield and the core of the cable. Initially the Vibracoax sensor exhibited poor accuracy and repeatability due to longitudinal sensitivity variation, output dependence on the length of cable over which the pressure was exerted, bending effects etc, [93]. However improved methods of sensor packaging and mounting have brought the accuracy to acceptable levels. The simple installation, robustness and reliability of the sensor have provided the possibility of an affordable WIM system of reasonable accuracy. Many examples of piezo-electric cable systems have been installed in France, Germany, England, Denmark, U.S.A. etc., [10], [52], [93], [125]. The recently developed polymeric piezoelectric films, (PVDF) might also find

application as WIM transducers, [26], [133]. They are pliant, flexible, tough and lightweight. Thinness and large voltage response make them very attractive although they also present some accuracy problems associated with their considerable sensitivity to temperature, electromagnetic interference, out-of-plane stresses etc. PVDF material is manufactured by several companies including "Metal Box Ltd" and "Yarsley Research Labs Ltd" in the U.K., as well as the "Pennwalt Corp." in the U.S.A.

At present both the older type deep excavation platform as well as the modern light sensor installations can be seen in use around the world. The recently installed systems tend to be of the latter type underlining the tendency of adopting the low cost easy to install and maintain system for the majority of measurements. A more detailed description of the operational principles of some of the common WIM systems is given in Section 1.6, and for a survey of existing equipment refer to App. A.

1. 4 ALTERNATIVE WIM METHODS.

Two of the more commonly used alternative techniques of dynamic vehicle weight measurements are the instrumented road bridges and on-board vehicle systems.

1. 4. 1 Bridge WIM Systems.

These make use of the response of strain gages attached to the main supporting beams of road bridges under traffic, [27], [94], [95], [108]. Thus the bridge acts as a massive scale reducing dynamic load fluctuations by its inertia. System installation is usually easy and unobstructive to traffic. Weighing is completely undetectable by drivers. However, the technique can only be applied to bridge structures with sufficient deformability. Accuracy is relatively poor and it is difficult to isolate measurements when there is more than one vehicle on the bridge. In general the method is well suited for determination the load spectrum of bridge structures under traffic for which the knowledge of individual axle weights is not indispensable.

1. 4. 2 Vehicle mounted Systems.

On-board vehicle weighing systems are generally used for obtaining continuous records of the dynamic loads on vehicle suspensions during travel. Strain gages are attached to axle/suspension parts that experience strain during motion, [11], [100]. In some cases, [135], [150], measuring the changes in tyre pressure under load provides a simple and convenient real-time indication of the dynamic forces experienced by the vehicle during motion. The wider use of such systems is hampered by their high cost, generally low accuracy and poor reliability. However, various applications of on-board systems where dynamic loads may serve as a useful parameter are being developed at present. These include load-sensitive braking and suspension systems, on-board freight monitoring etc. It seems likely that with the advent of microelectronics and new sensor developments the uses of on-board systems will increase and will probably be even made compulsory for lorries in some countries, [11].

Research into the area of dynamic weighing is centred on improving the performance of existing systems by perfecting the sensor's physical construction and the signal processing algorithms, as well as studying the properties of other potential force transducers and their feasibility for dynamic weighing.

1. 5 APPLICATIONS OF WIM SYSTEMS.

The opportunity of measuring axle loads in an economical way offers wide activity scope in numerous fields of traffic and road engineering. The uses of vehicle weight data can be categorised into the following areas:

- Pavement design and performance studies.
- Road structures engineering and monitoring.
- Vehicle weight and size enforcement.
- Traffic trends evaluation and planning.
- Vehicle suspension research.

1. 5. 1 Pavement design and performance studies.

When designing the road superstructure, as with every engineering construction, an assumption has to be made regarding the applied work loading. Whilst a building or a bridge is designed primarily for a given maximum load, pavement design has to be based on the cumulative traffic loading expected to pass over the road during its design life. A knowledge of the magnitude and frequency of application of wheel loads to road surfaces is therefore of major importance in the structural design of the pavement cross section, and in anticipating future road maintenance problems. The mechanism of pavement deterioration under traffic has been investigated by many authors, [22], [23], [24], [73], [74], [88], [113], [135], [144], [150], and through dynamic weighing of vehicle axles information is provided of the stress inputs the pavement is receiving under traffic.

The AASHO Road Test, [137], was one of the first attempts to quantify the contribution of different axle loads to pavement lifetime. The following relationship between the damaging power of an axle, D and its weight W was derived empirically:

$$D = \left(\frac{W}{W_S}\right)^n \qquad (1.1)$$

where W_S is a standard axle load against which the damaging power of all other axle loads are compared, and n is the value of the exponent which can range from 2 to 6 depending on the thickness of the pavement and the strength of the subgrade. For average conditions a value of 4 is commonly accepted, hence expression (1.1) has become known as the "***Fourth Power Law***". Adopting a standard load $W_S = 100$kN, which in most European countries corresponds to the maximum allowed single axle load [20], and $W_S = 168.5$kN for a twin axle, the following equivalent damage factors D can be obtained for various vehicles using Eq. 1.1 - Table 1.1:

Axle load	Axle Load	Damage Factor, D	
[kN]	*[t]*	*Single Axle*	*Tandem Axle*
10	*1.01*	*0.0001*	--
50	*5.0*	*0.063*	*0.0078*
100	*10.0*	*1.0*	*0.12*
110	*11.0*	*1.46*	*0.18*
150	*15.0*	*5.06*	*0.63*
200	*20.0*	*16.0*	*1.98*
250	*25.0*	*39.06*	*4.84*

Table 1.1. Pavement Damage Factors for Single and Twin axle loads calculated by the 4th power law, Eq.(1.1).

It follows from the results that:

- the influence of lightly loaded axles, (cars, light commercial vehicles etc.), is negligible;
- the number of medium and heavy axle loads decidedly influence pavement durability;
- maximum permissible axle loads should be properly maintained since a 10% excess load could reduce the durability of the pavement by 46%.

However, the general validity of the *"Fourth Power Law"* has since been questioned as it referred to global deterioration of road surface rather than local pavement failures. Furthermore, parts of the AASHO test, were performed in unrepresentative conditions, but above all it failed to consider the effect of fluctuating wheel loads which were later proved to have a major contribution in pavement deterioration. Sweatman, [135] used a hub mounted transducer to measure the dynamic loads generated by a single wheel on 9 different types of commercial vehicle suspensions at a range of speeds on road surfaces of different roughness. Assuming that the wheel forces followed a Gaussian distribution and implementing the Fourth Power Law, he derived a ***Road Stress Factor, Φ:***

$$\Phi = K.W_{st}^4.[1 + 6s^2 + 3s^4]$$

where:

s - Dynamic Load Coefficient: $s = \frac{\sigma}{W_{st}}$,

W_{st} - Static Wheel Load,
σ - Standard Deviation of Wheel Load,
K - Constant.

Sweatman then defined the ***Dynamic Road Stress Factor*** v:

$$v = \frac{\Phi}{KW_{st}^4} = [1 + 6s^2 + 3s^4], \qquad (1.2)$$

and suggested that this factor should account for the damaging effects of the dynamic component of wheel loads. For typical motorway conditions of roughness and speed this factor was found to vary between 1.11 and 1.46, depending on the suspension system.

Cebon, [22] developed a number of road damage criteria by calculating the stresses and strains of the road structure during the passage of a set of randomly oscillating moving loads. The criteria are implemented in the theoretical evaluation of the damaging power of three popular articulated vehicles using their mathematical representation and a simple roadway model. The study indicated that the dynamic component of wheel forces may reduce substantially the service life of typical UK motorways. The results were dependent on the roughness of the road, and the configuration, suspension system and speed of the vehicle.

Other authors, [73], [74], [88], [113], [144], [150], examine the effects on road failure mechanisms of pavement structure, vehicle design parameters, types

of vehicles and axle configurations etc. WIM equipment is used to verify the predicted results or to gather dynamic wheel load information to be related to pavement damage.

1. 5. 2 Road structures engineering and monitoring.

Traffic loading data are also essential to bridge and tunnel design, monitoring and research, [18], [94], [95], [96]. Since the early 1950's when the modern basis of bridge design was formulated a significant increase in both size and weights of HGV-s has occurred prompting engineers to investigate the relationships between applied load and bridge stress and reassess bridge designs in accordance with new traffic conditions. Since both maximum loading and the frequency distribution of heavy load applications are important for road structures, complete information about the weight characteristics of the traffic stream is needed. Information about axle spacings is essential to determine the application frequency of axle loads. Inter-vehicle spacing is also important since maximum loading is likely to occur when several HGV-s are present on the structure. Because bridges are normally long relative to axle spacing, gross vehicle weight accuracy is usually more important than individual axle loads.

1. 5. 3 Vehicle size and Weight enforcement.

Control of the sizes and weights of heavy vehicles on motorways is of crucial importance for the proper management of those facilities. As it was pointed out earlier in that section and in other reports, [25], [56], excessive weights can cause premature failure of pavements and bridges. Overweight vehicles may present safety roadway hazards both because of poor manoeuvrability and the increased likelihood of mechanical failure. Largely because of the increasing number of overweight HGV-s in the traffic stream enforcement legislations have been developed in the last decade across the world. Although WIM equipment has not yet been certified in this country as sufficiently accurate to be used for enforcement weighing, its use in conjunction with certified static scales is now commonplace. The WIM equipment is normally situated ahead of the static scales and used to pick out suspected overweight trucks that can be stopped for static enforcement weighing. A real-time enforcement WIM device has been installed in this country ahead of a

historic bridge to identify overweight trucks and trigger a warning preventing them from crossing, [93].

1. 5. 4 Traffic trends evaluation and planning.

Vehicle weight data are utilised in various ways for the assessment and development of traffic policies and regulations. Estimates of annual vehicle-miles of travel by a vehicle type and ton-miles of goods movement on the motorway system are important for regional economic activities and motorway network planning. Information obtained from vehicle weight studies provides the basis for developing trends in vehicle sizes and types, axle configuration and weight distribution which can be useful in traffic policy formulation and motorway planning.

1. 5. 5 Vehicle suspension research.

The aggressiveness of vehicle interaction with pavement is strongly dependent on the vehicle's suspension type and parameters. Many researchers, [48], [73], [74], [88], [110], [113], [114], [129], [130], [135], [150], have studied the interaction between heavy vehicles and road surfaces during travel and related the dynamic behaviour of the axles to the specific suspension type. Air cushion suspensions have generally emerged as the least aggressive type with regard to pavement damage. Different types of HGVs and axle configurations have also been studied, [74], [113], [144].

1. 6 CLASSIFICATION OF WIM SYSTEMS.

Weighing in motion is now an established technology and there is a wide variety of systems in use. The existing road-embedded WIM systems employ different principles of operation, types of sensors, signal detection modes, etc.

1. 6. 1 Purpose of measurement.

An initial distinction has to be made regarding the function of the WIM system. According to the measurement task they perform, two types of systems can be distinguished:

a) Systems producing an estimate of the ***True vehicle weight*** – as taken at static conditions. The information gathered with these systems is used for goods weight measurements, taxation, enforcement of vehicle weight limits, traffic trends, road capacity studies etc.

b) Systems measuring the actual ***Dynamic loads*** transmitted by moving vehicles on pavements and road structures. The data is mainly used in pavement performance evaluation, for the design and construction of road structures – bridges, flyovers and tunnels, vehicle suspension studies etc.

1. 6. 2 Measurement Period.

Since a reliably accurate static weight indication of a fast moving vehicle is difficult to obtain, tight speed restrictions are usually enforced upon vehicles before a measurement is taken. Such systems are known as slow speed or quasi-static dynamic weighing systems and gross vehicle weight, (sum of axle weights) is often required to be displayed. It is usual for these systems to be sited off the main highway in a lay-by or a slip road in order that they may operate without interference to the traffic flow, [69], [115]. The vehicle is driven slowly over the weighbridge (at a speed of no more than 2.5 mph), so that no substantial suspension oscillations are excited. If any vibrations do occur anyway, several cycles will normally elapse during the time for which the axle is being weighed. If

the sensor signal is averaged over the measuring period the mean value will be representative of the load imposed by the axle.

High speed axle weighers are in more common use as they are installed directly onto the highway and measurements are taken with vehicles travelling at their normal speeds. This type of system is the main subject of the study. Also since mostly truck weights and dynamic wheel forces are of interest the study is mainly concerned with Truck and Heavy-Goods-Vehicles in-motion weighing. Hence most of the subsequent classifications apply to high speed HGV WIM systems.

1. 6. 3 Sensor Dimensions.

In terms of sensor system dimensions and configuration two distinctive types of systems exist presently, profoundly differing in signal shape, interpretation and processing.

For the purpose of describing the two different systems and for future use, three characteristic sets of length l, and width b, dimensions are assigned (Fig. 1.1) to:

- vehicle: l_v , b_v
- tyre print: l_t , b_t
- sensing system: l_s , b_s

The distinction is made on the basis of comparing the length of the sensing system in forward direction, l_s, with the tyre print length, l_t.

1. 6. 3. 1 Line sensors: These are usually built as cables or narrow strips laid over the road or buried under the road surface. Tyreprint length must considerably exceed sensor length in the direction of travel, i.e., $l_t >> l_s$ and $b_s >> b_t$, (Fig 1.2a). In some cases (mainly buried lines) due to sensor sensitivity to pressures in its vicinity, l_s is defined as length of the zone where the sensor exhibits sensitivity above a certain threshold.

In reality, tyreprint shape is not strictly rectangular and the pressure under it is not uniform, [82]. This will lead to corresponding rounding and

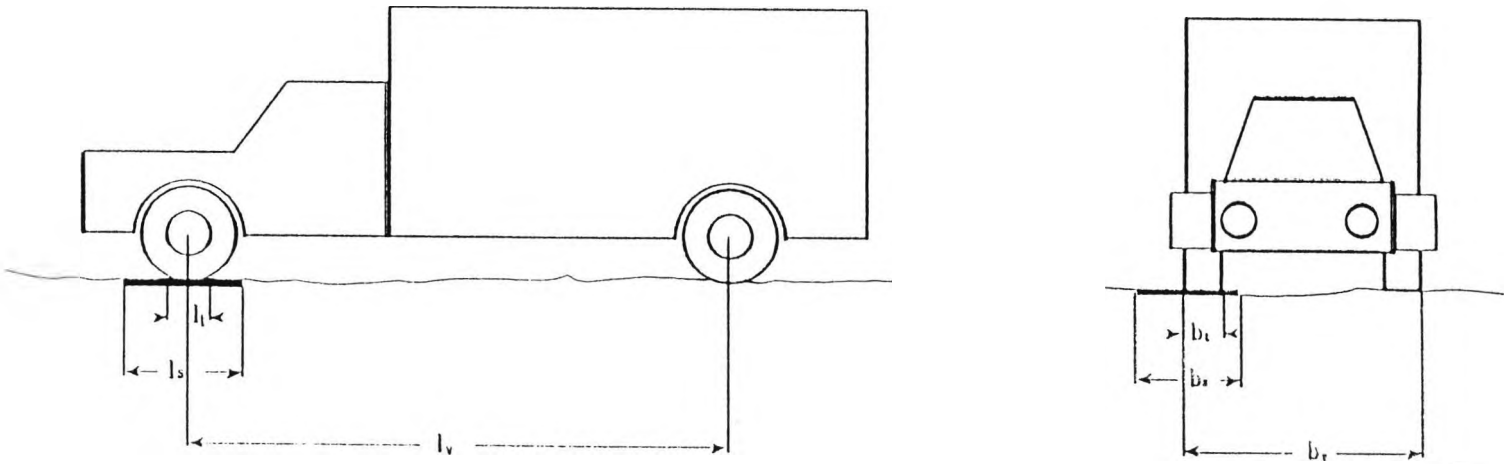

Fig. 1.1 Relative dimensions of Vehicle, Tyre, and Weighing Sensor.

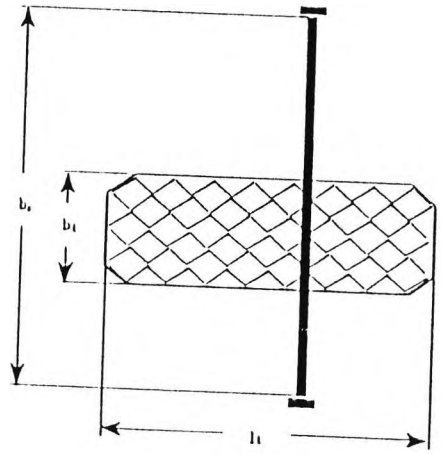

a) Sensor/Tyre Relative Dimensions

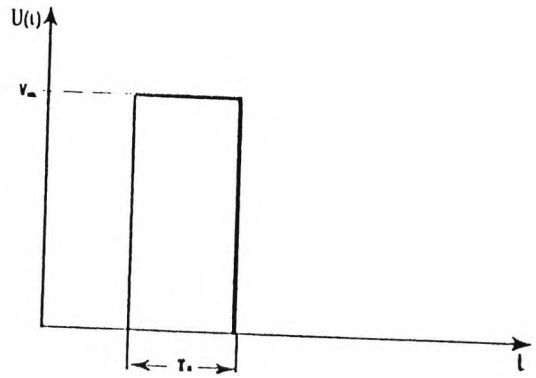

b) Ideal Sensor Output

Fig. 1.2 Line Sensor Operation.

distortion of the expected sensor signal. In the analysis however, an idealised rectangular tyreprint with uniformly distributed pressure, p_t, under it have been assumed leading to an ideally rectangular sensor response - Fig. 1.2(b):

$$p_t = \frac{\textit{halfaxle load}}{\textit{tyreprint area}} = \frac{W}{A_t} = \frac{W}{l_t \times b_t} \quad [N/m^2]$$

The signal's amplitude V_m will be proportional to the product of tyreprint compression pressure p_t and the length of line over which it acts, i.e. the tyreprint width b_t :

$$V_m = p_t \times b_t = \frac{W}{l_t} \quad [V] \qquad (1.3)$$

It is obvious that information about tyreprint length l_t is necessary to provide an accurate indication of the halfaxle weight W. The time it takes the tyre to traverse the sensor is the signal's duration T_S:

$$T_S = \frac{l_t}{U}$$

where U is the forward speed of the vehicle. Then:

$$V_m = \frac{W}{T_S \cdot U}$$

and for the halfaxle load W:

$$W = \frac{\overset{Signal\ Area}{\overbrace{\underset{Signal\ Ampl.}{p_t} \times b_t \times T_S}} \times \underset{Veh.\ Speed}{U}}{} \qquad (1.4)$$

i.e. indication about halfaxle weight is given by the product of area under the sensor signal and vehicle velocity. The additional measurement of vehicle horizontal speed is therefore necessary for the accurate in-motion estimation of axle weights. Sensor induced impact errors may appear when it is laid on the road surface without smoothing ramps. However those are greatly reduced by the enveloping effect of vehicle tyres.

Line sensors in most common use today are the Piezo-electric cable sensors, [10], [111], [131], [138], as well as some recently developed capacitive strip sensors, [29], [147]. Studying the experience with the over 200 "Vibracoax" WIM installations in France circa 1985, [131], reports the accuracy levels achieved by two types of installations differing in the complexity of sensor configuration and signal processing methods. The simplified equipment is built around the assumption that, as a first approximation the product $(p_t \times b_t)$, (contact pressure times tyreprint width), is directly proportional to axle load. For these types of systems 90% of heavy truck axle measurements were reported to be within 15% of their static weight. The more sophisticated group of equipment includes a second piezo cable accordingly spaced from the first one and making it possible to measure the vehicle's speed in the direction of travel, as well as to use the inputs from both cables in the signal processing algorithm. The claimed accuracy in this case is within 10% of static weight for 90% of the measured axles.

1. 6. 3. 2 Area Sensors: These have to be large enough to accommodate a complete tyre print so $l_s > l_t$ and $b_s > b_t$, (typical $l_t \times b_t$ being 300mm x 250mm). Fig. 1.3 shows a typical dimension relationship and an idealised sensor signal. The ramp-up/down portions of the signal correspond to the time when the tyre is not fully supported by the sensor platform, i.e. coming up or down the platform. When the whole tyre sits on the platform the sensor output's amplitude is proportional to the semiaxle's weight W.

Depending on their principle of operation area type sensors fall into two

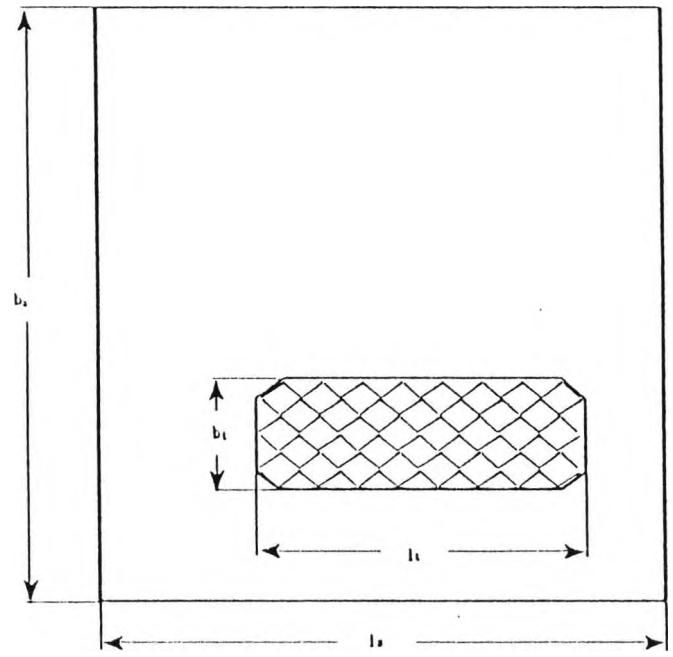

a) Sensor/Tyre Relative Dimensions

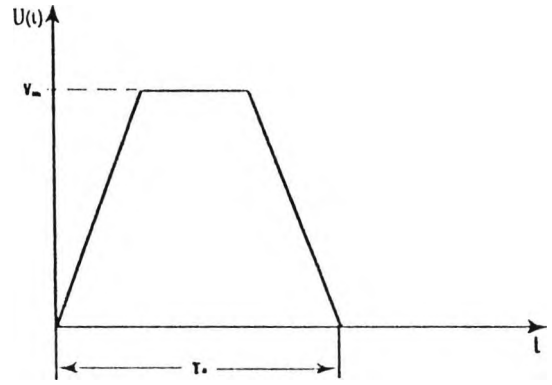

b) Ideal Sensor Output

Fig. 1.3 Line Sensor Operation.

categories: Point-sensor systems and Pressure integrating sensors.

a) ***Point-sensor*** systems employ a number of individual force transducers situated under the platform and their combined outputs are passed on to the signal conditioning unit. Most rigid platform weighscales such as the strain gage types as well as the piezocrystal loadcell system mentioned earlier, [131] are based on this principle.

b) ***Pressure integrating sensor*** systems - their whole sensor area is pressure sensitive and the electrical output is either generated by sensor compression under tyre load or derived as a change in the electro-magnetic properties due to sensor deformation. The sensor is normally a thin mat of pressure/deformation sensitive structure or material. Typical examples are the capacitive mat systems, as well as the prospective polymeric piezoelectric film, (PVDF) systems, [26], [133].

1. 6. 4 Sensor Installation.

In terms of operational lifetime and mode of installation WIM systems can be generally classified as: Temporary and Permanent systems.

a) Temporary systems require minimum road preparation, usually are of low cost design and normally employ surface laid sensors. Some of them are portable and operational lifetime spans from one day to a couple of months. The capacitive mat as well as some of the piezocable systems fall in this sensor category.

b) Permanent systems are normally road embedded hence require more time and effort to prepare the location and install. Their operational lifetime with regular maintenance could last up to 10 years. Most shallow and deep excavation weighscale systems can be put in this group including the buried piezocable installations.

WIM systems can further be categorised depending on their applications, vehicle operational speeds, Signal processing electronics, etc.

Chapter II: WIM System Analysis.

INTRODUCTION

In this Chapter a more detailed investigation is undertaken into the structure and operation of WIM systems. A typical system is decomposed into its constituitive blocks and the signal flow during measurement is explained. Some of the measurement influencing factors are outlined and special attention is paid to vehicle dynamic effects - the Impact Factor.

Each of the basic building parts of the system and their operation are then studied in separate sections. Vehicle suspension dynamics are explained from the point of view of their dynamic interaction with roadtracks and weighing platforms. Since mathematical modelling of that interaction is a major part of the study, an analysis of vehicle suspension as a physical system is performed. A generalised suspension model is presented and its elements and their properties explained. A frequency analysis of the suspension system is also carried out.

WIM sensors are discussed in a separate section. Basic sensor classification is introduced and some dimension, weighing period and frequency response relationships are derived based on that classification. A mathematical model is developed for a sensor platform and its foundation, and its frequency response investigated.

Finally weighing signal processing is discussed and the structure and operation of WIM systems electronics is explained. An example of a typical WIM electronics block is presented and its functionality explained. Different signal detection and conditioning techniques are discussed and their qualities are compared in terms of accuracy and measurement reliability.

2. 1 STRUCTURE AND OPERATION OF WIM SYSTEMS

Regardless of their type and technical specifications most road embedded WIM systems have similar structure and operational philosophy. It is assumed that the vehicle's axle weight is to be determined by some type of pressure/displacement transducer that measures the force imparted via tyre contact. A functional diagram of a typical system in its measurement environment is shown in Fig. 2.1.

The instantaneous pressure p exerted on the ***Sensing System*** in the moment of axle passage is the output of the ***Vehicle Dynamics*** section and represents the mechanical input to the ***Sensing System.*** The transducer's electrical output – voltage V, is fed into the ***Signal Processing Unit*** to produce the output of the system $O(W_s)$ as a reading or a record of the data required by the measurement. The output is a function of the static vehicle weight W_s and a number of influencing factors some of which are shown on the figure.

The physical parameters of the vehicle will be of primary importance for its dynamic behaviour on the road. The type of the vehicle, (number of axles, articulated etc.), tyre pressures, suspension stiffness and damping, vehicle mass distribution, as well as its speed at the moment of contact will define its interaction with the sensing system. Provided the primary factors likely to cause dynamic wheel forces differing from static wheel loads are identified accounted for in the design and site selections of the WIM system, satisfactory measurement results can be obtained.

Measurements may be distorted by environmental factors such as temperature and pressure variations, electrical interferences etc. Sensor installation and maintenance, as well as road structure and surface conditions ahead of the sensor system may seriously affect measurement accuracy. Undesirable dynamic forces could also arise from the tyres hitting the unlevelled edges of the weighscale platform. The influencing factors in dynamic weighing of vehicles will be discussed in more detail in the metrological analysis in Ch.3.

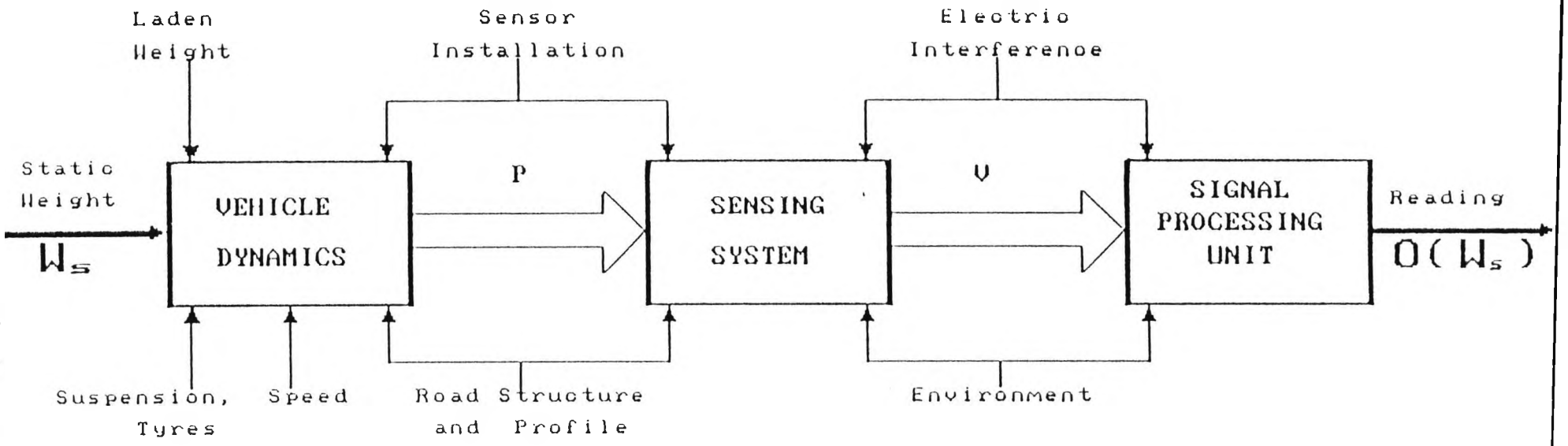

Fig.2.1 WIM System decomposition.

2. 2 STATIC AND DYNAMIC AXLE LOADS. IMPACT FACTOR

A vehicle with perfectly round and dynamicaly balanced wheels travelling at a constant speed along a horizontal, straight and perfectly smooth road would theoretically apply constant vertical force to the pavement through its tyres, equal to its static wheel load. These conditions, however, never exist in practice and the moving vehicle is excited by the interaction of its tyres with the road surface. The load applied to the pavement therefore is a vibratory signal comprising a dynamic component superimposed onto the static vehicle weight. It can be regarded as a random oscillation around a DC value corresponding to the static weight, and within a relatively narrow frequency band determined by the natural frequencies of the vehicle.

The dynamic component will inevitably appear as unwanted noise in the input to the WIM system. Being a function of the interaction between the vehicle and road surfaces, it will depend on a number of roadway, sensor installation and vehicular factors. This will make it particularly difficult to predict its pattern and magnitude for individual measurements.

Each vehicle is a mechanical system consisting of masses, springs and dampers and its dynamic behaviour on the road depends on these parameters. The physical parameters of the vehicle also affect the amplitudes of the wheel forces, but these are mainly influenced by the uniformity of the road profile and the vehicle's horizontal speed.

A measure of the magnitude of the dynamic wheel load at any moment of time is the ratio of its amplitude and the static vehicle weight known as the ***Impact Factor, (IF):***

$$IF = \frac{Static\ weight + Dynamic\ load}{Static\ weight} = 1 + \frac{Dynamic\ load}{Static\ weight}$$

On a motorway class road at normal vehicle speeds the range of IF is usually within *0.7* and *1.3*, [115]. This would mean that errors up to $\pm 30\%$ have to be expected if static vehicle weights are approximated from the sampled signal and no filtering devices are used.

In the studies of road pavement damage however, when the effects of large numbers of vehicle passages are considered, variations in speed and suspension characteristics introduce randomness into dynamic loads so that the mean impact factors are closer to *1.0*. The average impact factor recorded at a number of **TRRL** weighbridge sites lies between *0.9* and *1.1* centred slightly above *1.0*, [92].

Unwanted impact forces may also arise from the tyres hitting the weighscale when the platform is not flush with the road. Efforts must be therefore concentrated on the proper sensor installation, making it as level as possible with the road surface, thus eliminating the impact peak at its origin. On some slow speed weighers the impact peak is avoided by introducing a time delay after the tyres hit the platform before taking the measurement, [46].

Numerous studies have been dedicated to the identification of dynamic load factors, prediction and measurement of dynamic forces transmitted to the road, and methods to reduce them. Page, [106], [107], theoretically investigated the dynamic behaviour of a simple vehicle passing over common types of surface irregularities and examined the effect of varying the vehicle's parameters on the dynamic loads applied to the road.

Laker, [72], simulated vehicle runs over computer generated road profiles of different roughness. He compared them with experimental results measured on a vehicle with matching parameters over various road surfaces.

Whittemore et al, [150] tackled the measurement and prediction of dynamic tyre-road forces of heavy trucks. The development of equipment to provide a continuous accurate measurement of tyre forces was described. Three pavement load prediction techniques are discussed including a time-domain analogue simulation procedure.

Page, [108], measured the dynamic wheel loads exerted by a two-axle goods vehicle on a number of bridges to establish the impact factor and implement the results in the design of bridge structures.

Other dynamic wheel force measurements have been performed for different purposes using both road-embedded and vehicle-mounted systems - Dickerson and Mace [39], Cebon [22],[23],[24], Mitschke [89], Leonard and Grainger [74], etc.

A major part of this study is also dedicated to Impact factor investigation and dynamic forces prediction. The dynamic behaviour of truck axles over road irregularities of deterministic shape as well as random surfaces are studied and quantitative data are provided for use by pavement designers and traffic load estimators.

2. 3 VEHICLE SUSPENSION DYNAMICS

Vehicles are complex mechanical structures with many degrees of freedom, with linear and non-linear springs and various types of damping. A schematic of a simple 2-D model of a two-axle vehicle is presented in Fig. 2.2.

2. 3. 1 Suspension Components.

For the investigation of dynamic interaction between vehicles and tracks, the vehicle is assumed to be composed of three basic components: masses, springs and damping elements:

a) Masses: In vehicles masses are usually concentrated in several lumped units and all gravitational and inertial forces are assumed to be acting on their centres of gravity. This idealisation is justified if the lumped body's rigidity is much greater than that of adjoining parts. Along with the forces of gravity and inertia, the vehicle's masses are also subjected to restoring and damping forces as well as the reaction of the road.

b) Springs: The individual parts of vehicles are bound together by springs. The general equation describing spring movement is:

$$F = k_1 + k_2 y + k_2 y^2 + \ldots + k_n y^{n-1}$$

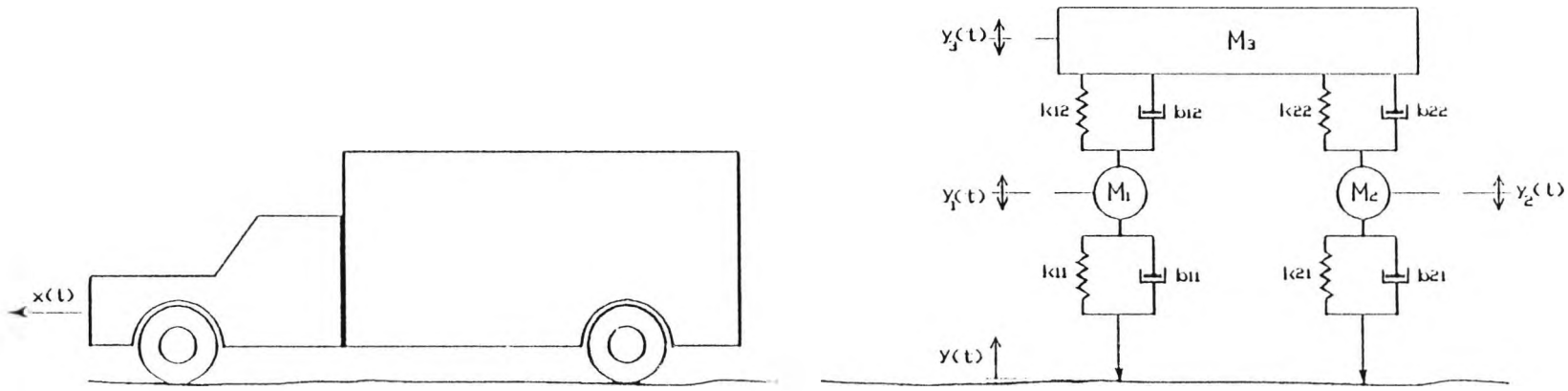

Fig.2.2 A Two-axle Vehicle representation.

where F is the applied force, y is the resulting deflection and k are spring constants.

The simplest spring is the linear one, whose load-deflection characteristic is represented by the stiffness constant k:

$$F = k \, . \, y$$

c) Damping Elements: The role of damping elements in vehicle suspensions is to restrict vibrations associated with motion. Two major types of damping elements are defined in vehicle suspension modelling:

• Viscous damping, corresponding to the movement of a mass in a liquid. The damping force, B_v, depends on the velocity of vibration $\dot{y}$:

$$B_v = b \, . \, \dot{y}$$

where b is the viscous damping coefficient. Exponential diminishing amplitude of the free vibrations is characteristic of this type of damping.

• Coulomb dry friction assumes that the damping force B_c is proportional to the normal force N:

$$B_c = \begin{cases} +\mu N & \text{for } y > 0 \\ -\mu N & \text{for } y < 0 \end{cases}$$

where μ is the coefficient of friction. The dry friction is characterised by linearly diminishing amplitudes of the free vibrations.

2. 3. 2 System Equations.

The equations of motion are derived on the basis of Newton's second law and D'Alembert principle:

$$[M].\{\ddot{y}\} + [b].\{\dot{y}\} + [k].\{y\} = \{F\} \qquad (2.1)$$

where:

$\{y\}$ - vector of generalised displacement of the system of lumped masses, (points denote derivation with respect to time),

$[M]$ - mass matrix,

$[b]$ - damping matrix,

$[k]$ - stiffness matrix,

$\{F\}$ - vector of model forces and force acting between vehicle and track.

The movement of the vehicle along the x axis is usually assumed to be uniform with velocity, U:

$$x = U.t,$$

so that the longitudinal motion is excluded from the Eq.(2.1). The external forces $\{F\}$ may be deterministic, however the stochastic approach has been adopted recently due to the assumption that the road surface irregularities possess random character.

2. 3. 3 Suspension Model.

A simplified suspension model representing a half axle/single wheel part of the vehicle was used for the theoretical investigations in this study. A survey of suspension models used by other authors as well as the reasoning behind choosing this particular vehicle approximation is given in Ch.4. The schematic of the quarter-vehicle suspension model is shown in Fig. 2.3. The body of the vehicle is represented by the ***Sprung mass*** m_1. The mass of the axle and wheel of the vehicle is generally referred to as the ***Unsprung mass*** m_2, although in

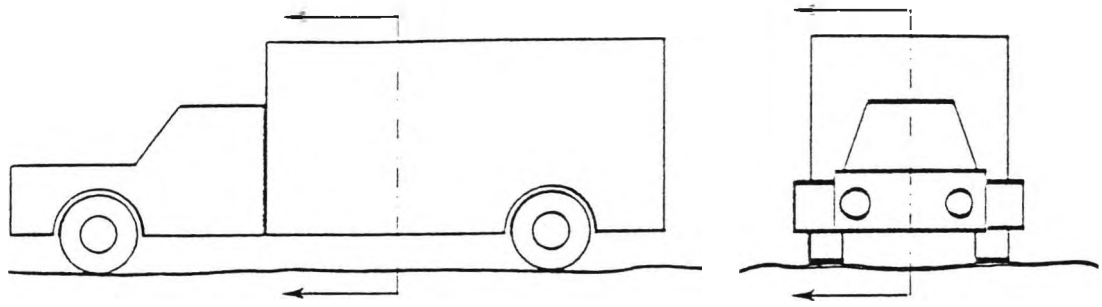

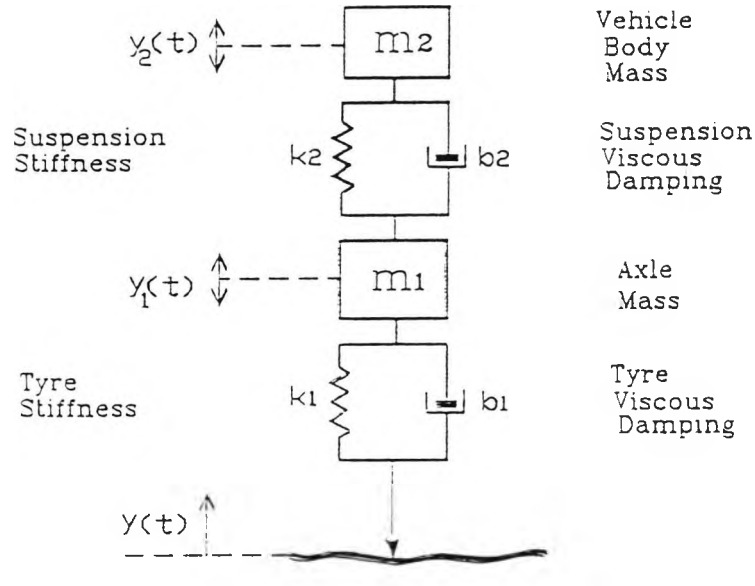

Fig.2.3 Quarter-vehicle, (Single wheel) Vehicle model.

fact it is sprung by the tyre. For a real vehicle where the spring has mass, that mass is proportionally divided between the sprung and unsprung masses in a way depending on the type of spring. For a leaf spring it is common for two-thirds of its mass to be included in the sprung mass and one third in the unsprung mass.

The correct mathematical representation of the suspension elements: springs, shock absorbers and bump stoppers is of primary importance for the accuracy of simulation.

2. 3. 3. 1 Model parameters. Some of the model parameter identification methods used by different authors are presented below.

Cebon, [22] performed an extensive experimental study into the mathematical behaviour of leaf springs to derive their parameters and guiding relationships. In the models he used, suspension pivot friction was simulated by friction torques. Hydraulic dampers were not fitted on the experimental vehicle so they were excluded from the model. Rubber stop bumpers were also considered.

Whittemore et al, [150] identified suspension parameters by driving a test vehicle over bumps of deterministic shape and measuring the resultant dynamic forces. The same obstacle shapes were then simulated as inputs to the basic computer model and the correct parameter values were determined by adjustment to obtain the best match between measured and computed pavement loads. As a first approximation, a linear spring in parallel with a viscous damper were selected, but were found unsatisfactory at low frequencies. Good agreement in signal frequency content was achieved when the combination of viscous and friction dampers were introduced. The three friction elements set at different breakaway levels represented the friction coupling between the leaves of the suspension assembly.

The equations in Page's model, [106] were written so that the spring could have either linear or non-linear load deflection characteristics. For the non-linear case it was assumed that the stiffness of the spring is at a minimum at its zero load position and increases progressively as the spring is displaced in either direction.

The linear spring model was found adequate for the purposes of the current simulation. The spring is represented by a single stiffness term k_2 and:

$$F_{s2} = k_2 \cdot (y_1 - y_2)$$

The suspension damping in Page's model includes both viscous, b_2, and Coulombs friction, c_2, terms. However, Page showed that the latter's effect on dynamic wheel forces was negligible provided the value of c_2 was within realistic limits. If very high values for c_2 were selected this would "lock" the suspension springs leaving only tyre damping to dissipate the energy of the system. Therefore the Coulomb's friction term, c_2 was left out of this model, and for the damping force we have:

$$F_{d1} = b_2 \cdot (\dot{y}_1 - \dot{y}_2)$$

With their elastic properties pneumatic vehicle tyres are a constituent part of vehicle's suspension. They are also the dynamic interface of the vehicle with the track it is traversing. Many authors [3], [21], [22], [34], [81], [83], [106], [119], [150], have tackled the problem of pneumatic tyre simulation and a considerable number of models have been produced. These will be reviewed in more detail later when a more sophisticated tyre model used in this study is analysed.

In the present model the elastic properties of the tyre are represented by a stiffness term, k_1, and its inherent damping by a viscous damping term b_1 so that:

$$F_{s1} = k_1 \cdot (y - y_1)$$

$$F_{d1} = b_1 \cdot (\dot{y} - \dot{y}_1)$$

The tyre stiffness is assumed to be linear within the entire load range of the vehicle. This assumption is backed by measurements carried out with commonly used vehicle tyres [150], [106]. Not so straightforward is the question of what value for k_1 should be adopted. Albert, [3] has shown that differences between static and rolling tyre stiffness rates may amount to 20% for low tyre inflation

pressures (10psi), but for highly inflated standard tyres, (30psi), the stiffnesses are virtually identical. The easily measured standing tyre stiffness has been used in the present model.

The model's parameter values represent the *front end* of a **TRRL** test vehicle (a two axled ***AEC "Mandator"***) for which some experimental data are available. The parameter values are listed in Table 2.1:

Parameter				Value
Sprung mass	=	m_2	=	*2400. 0 kgf*
Unsprung mass	=	m_1	=	*336. 0 kgf*
Suspension spring stiffness	=	k_2	=	*250. 0 kN/m*
Tyre stiffness	=	k_1	=	*1564. 0 kN/m*
Suspension viscous damping	=	b_2	=	*4. 0 kN/m/s*
Tyre viscous damping	=	b_1	=	*1. 0 kN/m/s*

Table 2.1: Parameter values for "front end" of TRRL *"Mandator"* test vehicle.

Values of unsprung mass and suspension spring stiffness have been obtained from manufacturer's data. Spring mass and tyre stiffness were measured in the laboratory and suspension damping was calculated through comparison of experimental and theoretical data and adjustment to obtain the best fit. As no measurement results of truck tyre damping were known the adopted value was adjusted from previous measurements of car tyre damping. Anyway, as it was proved later, variations of this value had little effect on the dynamic behaviour of the model.

2. 3. 3. 2 Model equations. The equations of motion are derived directly from Fig. 2.3 by considering the forces acting on the sprung and unsprung masses:

a) Equilibrium of vehicle body:

$$m_2 . \ddot{y}_2 = -\,[m_2 . g + F_{s2} + F_{d2}], \quad \text{or} \quad m_2 . (\ddot{y}_2 + g) = F_{s2} + F_{d2} \ ,$$

giving:

$$m_2 . \ddot{y}_2 = - [m_2 . g + k_2 . (y_1 - y_2) + b_2 . (\dot{y}_1 - \dot{y}_2)] \qquad (2.2)$$

b) Equilibrium of axle:

$$m_1 . \ddot{y}_1 = F_{s2} + F_{d2} - [\, m_1 . g + F_{s1} + F_{d1} \,], \text{ or}$$

$$m_1 . \ddot{y}_1 = k_2 . (y_1 - y_2) + b_2 . (\dot{y}_1 - \dot{y}_2) -$$

$$-[m_1 . g + k_1 . (y - y_1) + b_1 . (\dot{y} - \dot{y}_1)] \qquad (2.3)$$

The dynamic force imparted to the road by the wheels is calculated as the force required to compress the tyre spring k_1 and overcome tyre viscous damping c_1. The total force F_w is given by:

$$F_w = (F_{s1} + F_{d1}) = - [k_1 . (y - y_1) + b_1 . (\dot{y} + \dot{y}_1)]$$

After replacing from the previous expressions:

$$F_w = (m_1 + m_2) . g + m_1 . \ddot{y}_2 + m_2 . \ddot{y}_1 \qquad (2.4)$$

and at rest:

$$F_w = (m_1 + m_2) . g$$

The input to the model is the road profile elevation $y(t)$. This is normally

a computer generated profile of typical deterministic shape: impulse, step, ramp, haversine bump, or some form of stochastic description of the road surface.

2. 3. 4 Vehicle Oscillation Modes.

The dynamic response of the vehicle is a complex vibration usually within a narrow frequency range: $0.5Hz - 20Hz$. Normally there are two major natural frequencies of vibration determined by the physical parameters of the vehicle:

a) Wheel hop frequency:

$$f_w = \frac{1}{2\pi}\sqrt{\frac{k_1 + k_2}{m_1}} \qquad (2.5)$$

This is the vibration frequency of the axle suspended between the tyre and suspension springs. It is called wheel hop because it often seems as though the wheel is *hopping* as it is going over the road irregularity. It normally lies in the range between 8Hz and 18Hz and for the test vehicle: $f_w = 11.7\ Hz$.

b) Body bounce frequency:

$$f_b = \frac{1}{2\pi}\sqrt{\frac{k_2}{m_2}} \qquad (2.6)$$

This is the frequency of vibration of the body mass sprung by the suspension of the vehicle. Depending on the laden weight, the frequency is usually within 1Hz to 4Hz. For the values chosen for the test vehicle: $f_b = 1.62\ Hz$.

A third characteristic frequency of vibration can be introduced for the purpose of the analysis. It describes the state when the suspension is "locked" and the whole vehicle is suspended only by the tyre. It is the so called "locked spring body bounce":

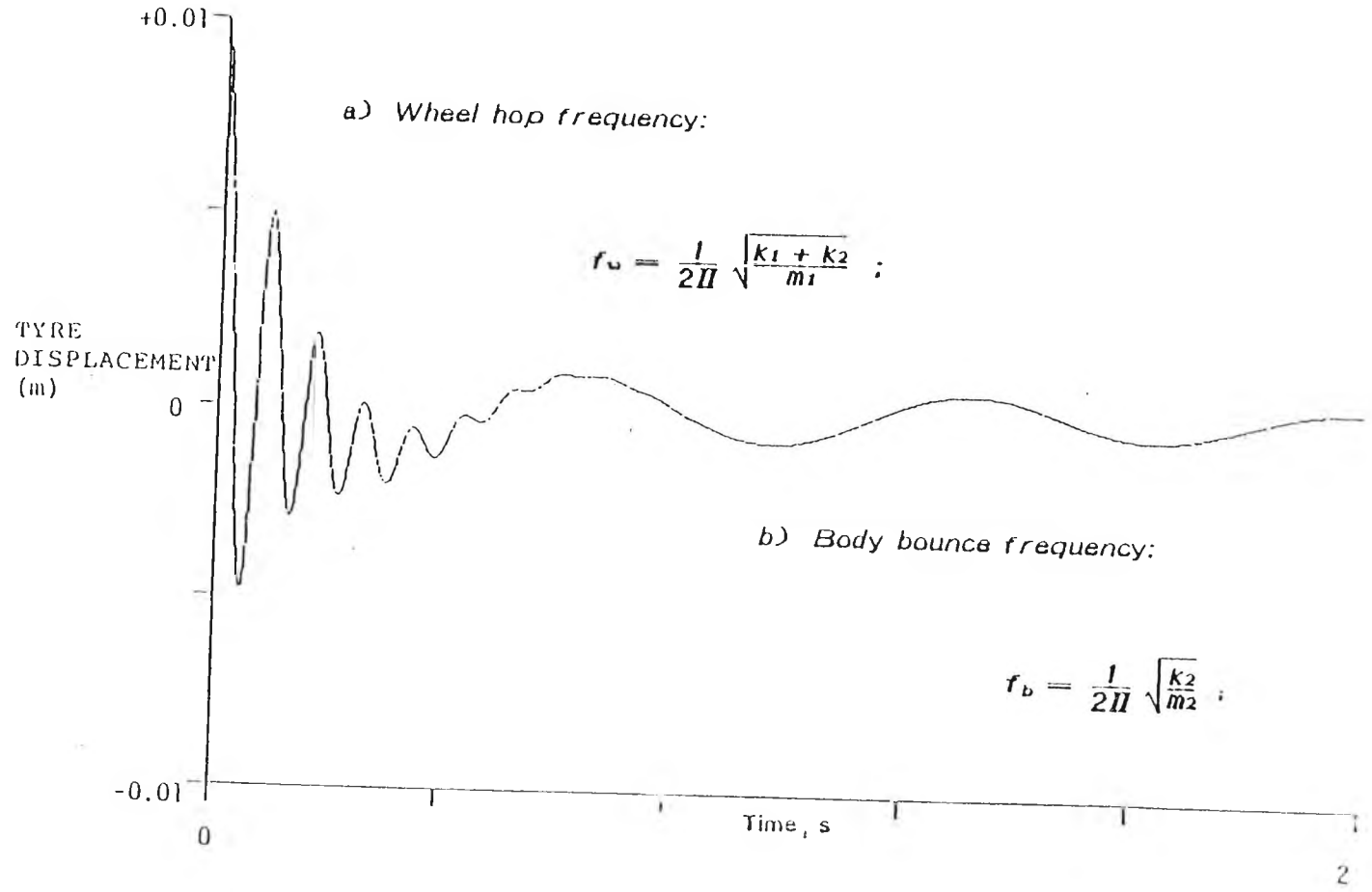

Fig.2.4 Suspension Dynamics for a Step Profile, $U = 140km/h$.

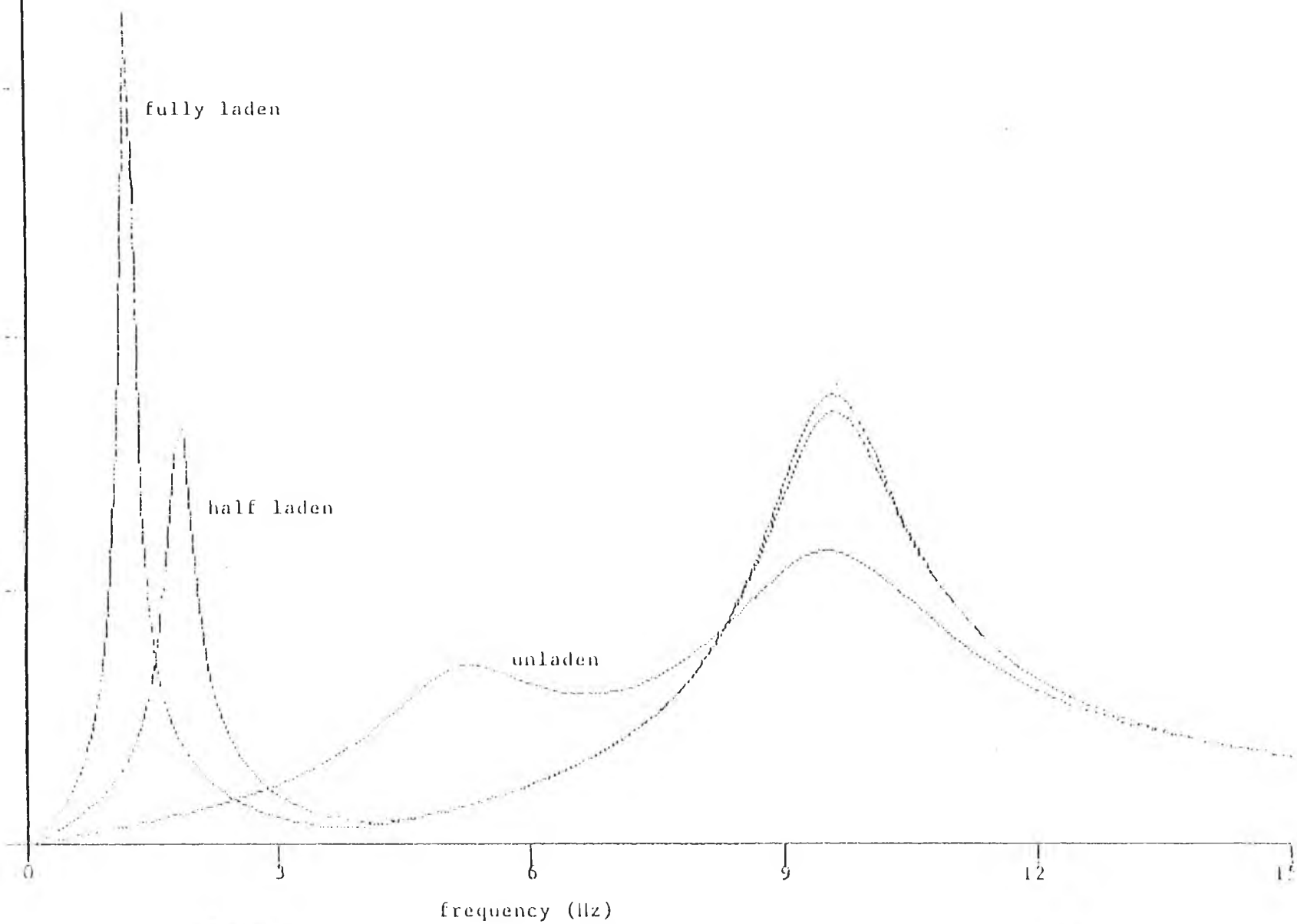

Fig.2.5 Frequency response of a Vehicle suspension with different laden weights.

$$f_l = \frac{1}{2\pi}\sqrt{\frac{k_1}{m_1 + m_2}};$$

and for the vehicle model: $f_l = 3.81\ Hz.$

The wheel hop and body bounce frequencies are illustrated well in a simulation of the wheel going over and abrupt step in the road – Fig. 2.4. The initial high frequency oscillations are wheel hop and they occur because the inertia of the sprung mass, m_2, delays its response. The tyre displacements are large and dynamic forces imparted to the road will be correspondingly large. As energy is transferred to the body of the vehicle, the lower body bounce frequency is excited. The tyre deflection is less as wheel hop dies away and the motion is now transmitted through the vehicle suspension to its body.

Frequency analyses of dynamic wheel force records [150], as well as theoretical simulations in the frequency domain [2], suggest that the lower frequency body bounce vibration component dominates the dynamic wheel forces, except for some poorly damped 'bogie' group suspensions.

The characteristic frequencies in the simulated response of a vehicle running over step/bump profiles were analysed for three laden weights of a test vehicle – Fig. 2.5, [2]. The domination of the low frequency is particularly pronounced for large body masses (laden weights), and it diminishes with reduction of the laden weight. It can also be seen that the high, (wheel hop) frequency changes very little with laden weight, whereas a significant shift is observed in the low, (body bounce) frequency.

2. 4 SENSOR SYSTEM

This section is aimed at giving an insight into the process of dynamic vehicle weighing from the point of view of sensor system design. Part of the analysis is performed by computer simulation of the measurement process and some conclusions concerning the practical design of the system are presented.

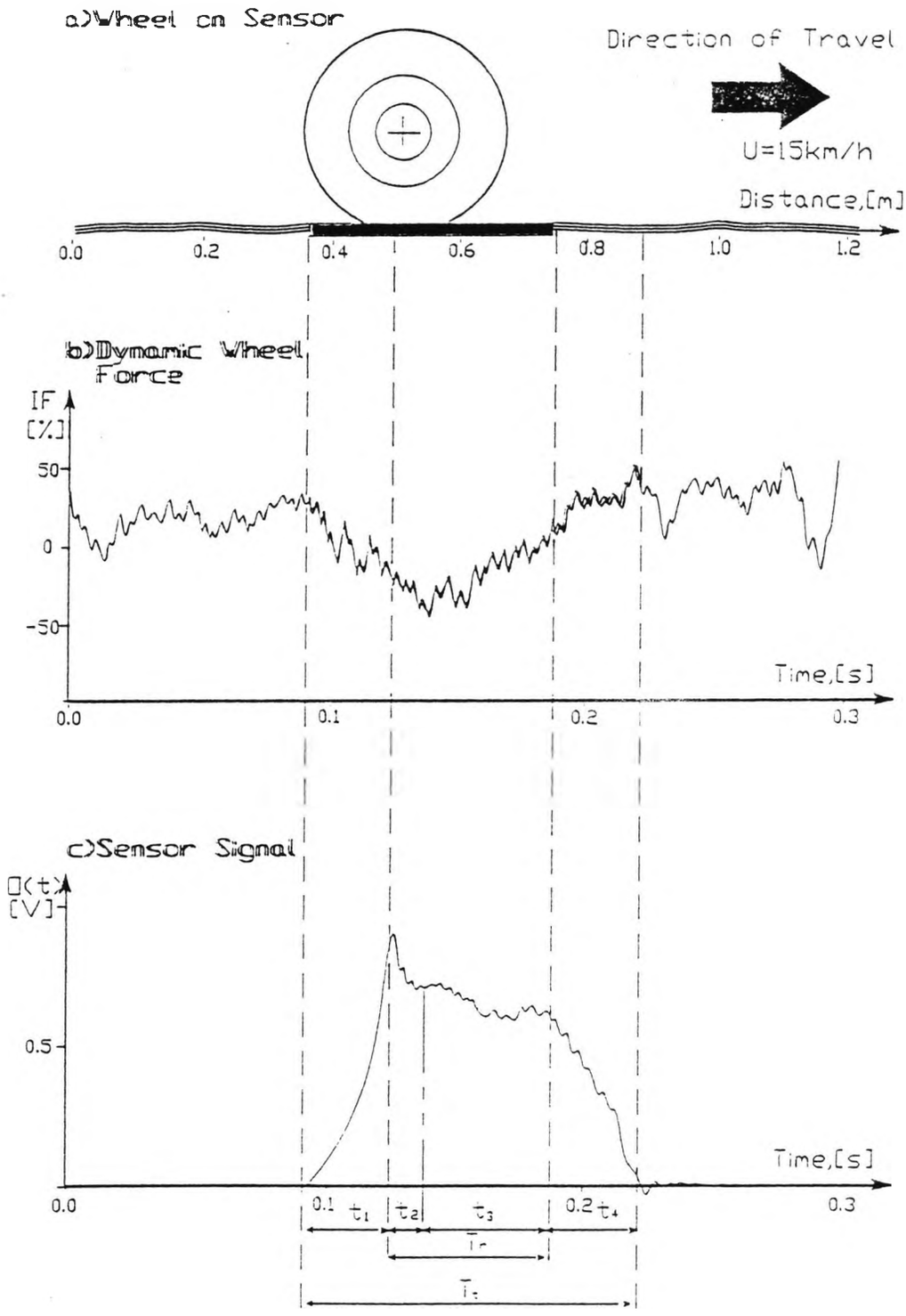

Fig.2.6 Typical Weigh-in motion sequence, (Area type Sensor).

2. 4. 1 Sensor Output Signals.

In Fig. 2.6(b) a typical record of dynamic wheel load is shown presented in terms of the corresponding ***Impact Factor***. Also shown is the way it is sampled by a typical *area* type weighing sensor – Fig. 2.6(a), and the resulting transducer signal – Fig. 2.6(c).

Experiments have shown that the wheel force patterns of a specific vehicle proceeding along the same track at the same speed tend to repeat within only a small scatter – [74], [76], [150]. However, this does not apply when the wheel forces of a variety of passing vehicles travelling at different speeds have to be considered. It is therefore accepted that the weighscale "sees" a randomly sampled portion of the dynamic signal marked on the graph with a thick line –Fig. 2.6(b). Several characteristic sections can be recognised in the resulting sensor signal – Fig. 2.6(c). The rise/fall parts t_1, t_4, correspond to the time when the tyre is not fully supported by the sensor. The extent of the ringing that occurs in part t_2 depends on the mechanical properties of the sensor and its frequency response. A time delay can be introduced by means of hardware to skip the transient parts during $(t_1 + t_2)$. The useful part of the signal, representative of the sampled random "window" in the dynamic force, corresponds therefore to part t_3, the ***axle residency*** time.

2. 4. 2 Weighing Period and Sensor Frequency Response.

What part of the signal's cycle will be sampled by the sensor depends on the latter's length in the direction of travel, the major frequencies of vehicle vibrations and the horizontal speed of the vehicle.

A twin-axle HGV is considered passing over a line or area sensing system of dimensions $l_s \times b_s$ at speed U. It is assumed that the two axle suspensions are completely decoupled. Ignoring axle dynamics the following *ideal* sensor signals will be expected as outputs of the line and area type sensors - Fig. 2.7. The tyre print dimensions l_t and b_t are recalled from Ch.1, Section 1.6.2, and values $l_t = 0.3m$ and $b_t = 0.25m$ are assigned typical for HGV's, [21], [82]. The shortest axle separation distance likely to be encountered in HGV vehicles, $l_a = 1m$ between axle centres is adopted.

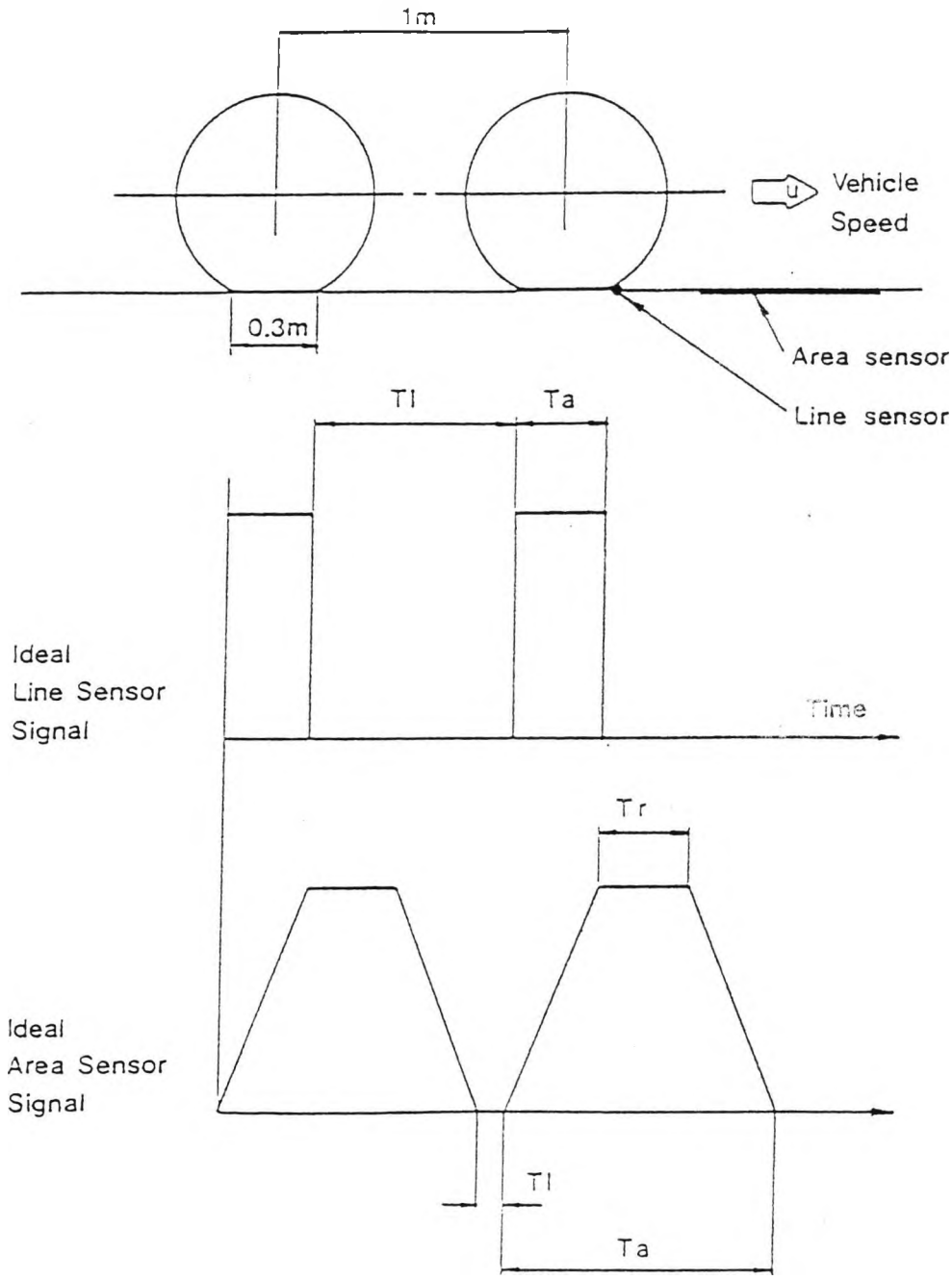

Fig.2.7 Ideal Line and Area Sensor Signals.

The total vehicle transit time, T can be decomposed into the following parts:

- T_a : Axle transit time: the time when the tyre is in contact with the sensor,
- T_l : Latency time: the duration between the two axle signals,
- T_r : Residency time: when an axle is completely supported by the sensor.

2. 4. 2. 1 Line Sensor System. For an ideal line sensor $l_s = 0$. The different sensor transit times can be derived from the expressions in Table 2.2. The corresponding plots are shown in Fig. 2.8. It can be seen from the plots that the shortest possible transit times for an axle (T_a) could be less than 10msec. These correspond to highest transit frequencies of more than 100Hz. If signal distortion is to be avoided the frequency response of the sensor should be about 10 times this, i.e. flat to well above 1000Hz.

2. 4. 2. 2 Area Sensor System. The various transit times for area sensors are presented in Table 2.3:

$l_t = 0.25m;$ $b_t = 0.2m;$ $l_a = 1.0m;$ $l_s = x$			
T_a	T_l	T_r	T
$\frac{l_s + l_t}{U}$	$\frac{l_a - l_t - l_s}{U}$	$\frac{l_s - l_t}{U}$	$\frac{l_s + l_a + l_t}{U}$

Table 2.3 Area Sensor Transit Times: U [m/s]

In area sensor systems the measurement relies upon the whole wheel weight being simultaneously supported by the sensor therefore its length must be at least that of the tyreprint length l_t. In practice l_t varies with tyre size, wheel weight and tyre inflation pressure. The adopted value of $l_t = 0.25m$ is an approximate figure for an HGV with correctly inflated tyres, and must be

$l_t = 0.25m;$	$b_t = 0.2m;$	$l_a = 1.0m;$	$l_s \sim 0$
T_a	T_l	T_r	T
$\frac{l_t}{U}$	$\frac{l_a}{U}$	-----	$\frac{l_a + l_t}{U}$

Table 2.2 Line Sensor Transit Times: U [m/s]

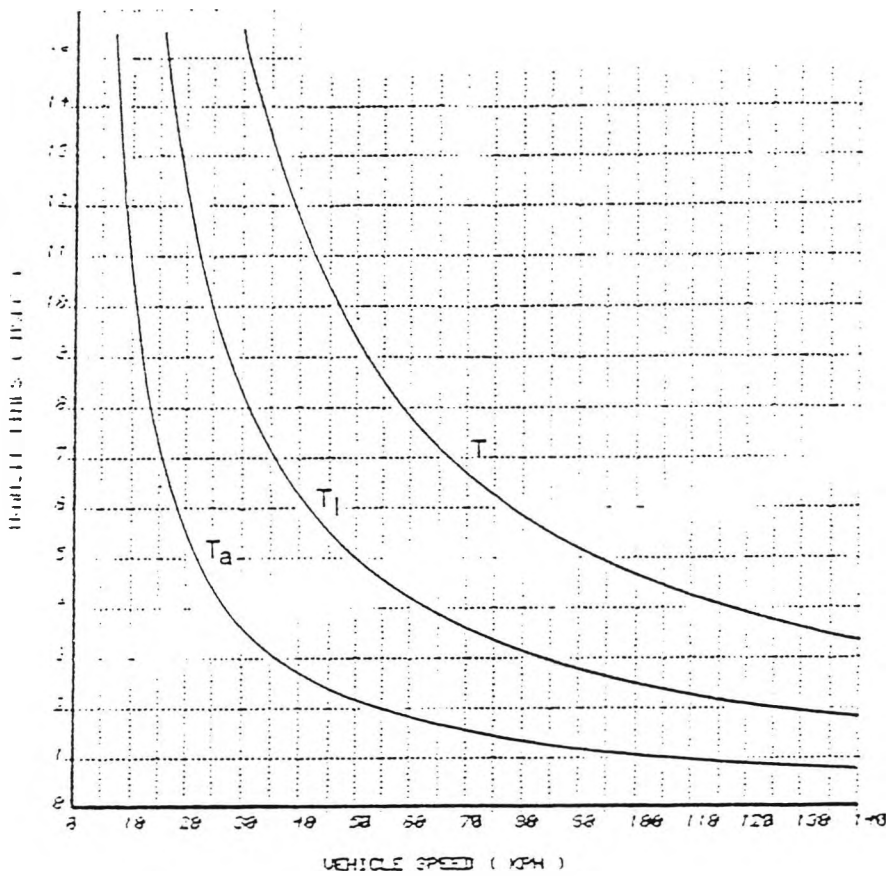

Fig.2.8 Line Sensor Transit times.

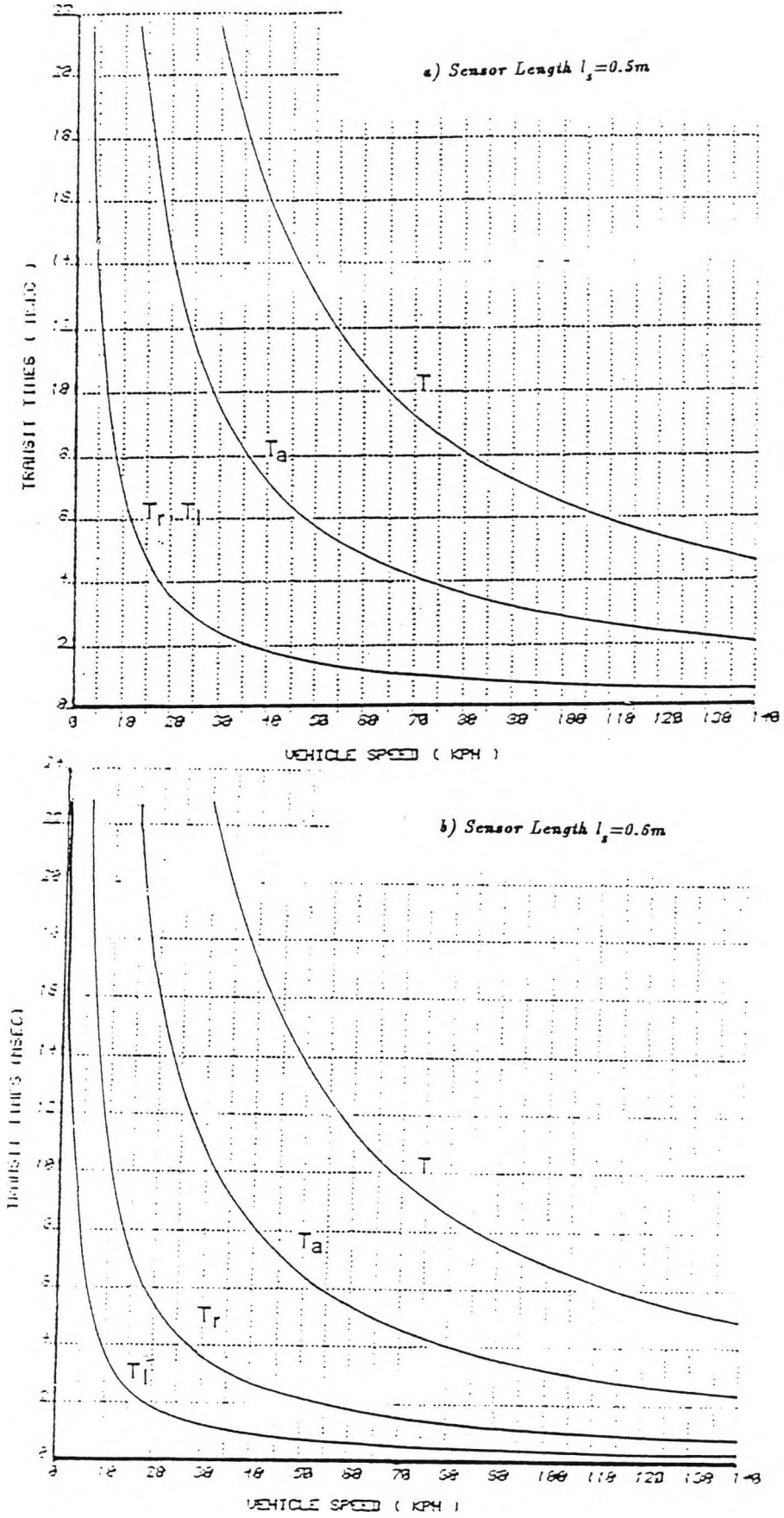

Fig.2.9 Area Sensor Transit times.

therefore regarded as an absolute minimum, (zero residency time) for sensor platform length. However, module length must not be such that the wheel on the next axle arrives before the departure of the first. With the adopted vehicle dimensions this would correspond to an upper limit of $l_s = 0.7m$, (zero latency time). Module length therefore should lie somewhere between $0.3 - 0.7$m. However, leaving a comfortable margin for tyre contact length variation, this range can be modified to 0.4m - 0.6m, and preferably the higher end of the range should be chosen to allow for greater residency times.

Plots of transit times as a function of vehicle speed U are provided in Fig. 2.9 (a) and (b), respectively for two module lengths. The shortest contact time T_a corresponds to the shorter module, $(l_s = 0.5m)$, and is about 20ms at a speed $U = 140kmh$. The highest transit frequencies will therefore be in the range of 50Hz. However, when area sensors are concerned the useful parts of the signal occur during the residency time T_r, when the tyre is fully supported by the sensor. For the same sensor module this will translate into shortest residence time $T_r \sim 5ms$, and transit frequencies of the order of 200Hz, requiring flat frequency sensor response up to 2kHz.

The residency time plateaus in the area sensor outputs plot in Fig. 2.7 are flat only in the case of ideal sensor signal. In practice the residency time part of the signal will represent randomly sampled "windows" of the dynamic loads imposed by moving vehicles on the road. On its part the weighing platform will respond with vibrations of its own depending on its mechanical properties and the properties of the weighbridge foundation.

For the application of effective vehicle vibration filtering, a sufficient signal sample has to be taken, containing at least one vibration period. What portions of the vehicle's natural oscillation cycles that will be captured by the sensor will depend on the length of the weighing platform, the tyre contact length, the forward speed of the vehicle, and finally on its natural frequencies of vibration. From the axle transit time expressions in Table 2.3 the relationship between vehicle speed and vibration period captured by the sensor was derived. The two natural frequencies, $(f_b = 1.62Hz,\ f_w = 11.7Hz)$, of the standard vehicle, $(l_t = 0.25m)$ were studied at vehicle passages over the TRRL weighing platform, $(l_s = 0.6m)$. The graphs in Fig. 2.10 show the portions of signal cycles sampled at different speeds. The results show that a complete cycle can be accommodated only at speeds lower than 20km/h, and that is only for the higher frequency of

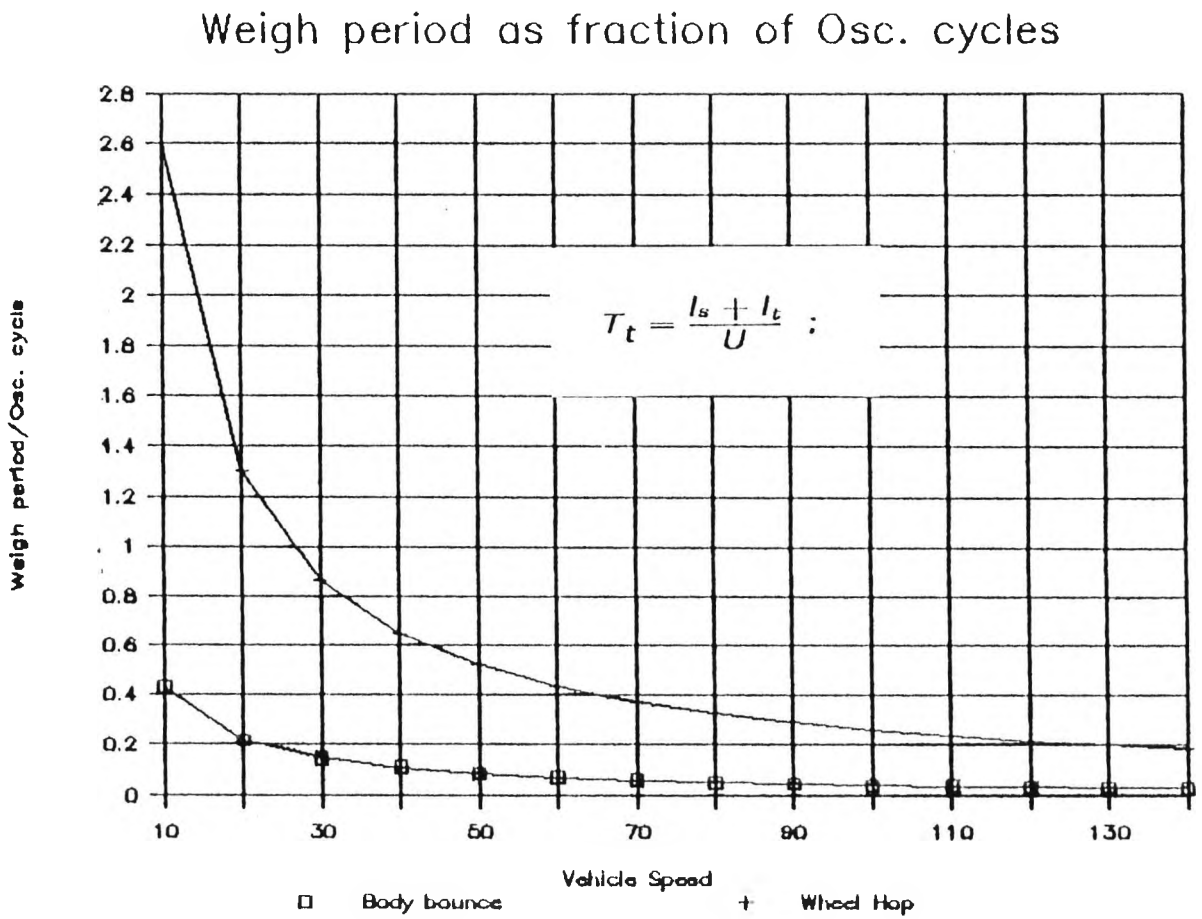

Fig.2.10 Weighing time as a fraction of Vehicle Oscillation cycles.

the wheel hop. For the body bounce oscillation even at this low speed only less than half of the cycle will be captured by the sensor.

An illustration of how the dynamic loads will vary with distance as the vehicle moves at two different speeds is presented in Fig. 2.11. The vehicle vibrations are approximated to a single sinusoid of frequency 2Hz corresponding to the body bounce. The distance relationship of the cycle to a 3ft long sensor platform is also shown.

The situation will be even worse if the transient parts have to be eliminated which will effectively "shorten" the sensor length, leaving only the residency part of the signal to be processed:

$$T_r = \frac{l_s - l_t}{U} \quad ;$$

Obviously signal samples of these relative sizes will be insufficient if the DC value (static weight) has to be extracted. Speed restrictions of no more than 20km/h inevitably have to be imposed if accuracies of less than 10% are required.

An obvious way to increase the measurement period is to use long weighing platforms or an array of multiple weighing sensors, the latter appearing to be a more feasible solution. The signal sample (or the number of discrete samples), will now be sufficient to ensure that the filtered DC value is much closer to the true static weight. This concept seems even more attractive now that cheap and easy to install transducers can be used – e.g. piezoelectric cables/films, capacitive mats/strips etc., and efficient real time digital techniques can be applied for signal processing.

2. 4. 3 WIM Sensor Dynamics Analysis.

A typical weighbridge installation consists of the sensor platform supported by specially prepared foundation or just by the road surface.

2. 4. 3. 1 Road surface deflections and strains. As the vehicle tyre moves along the road surface, a dish of approximately 2-3m diameter centred on

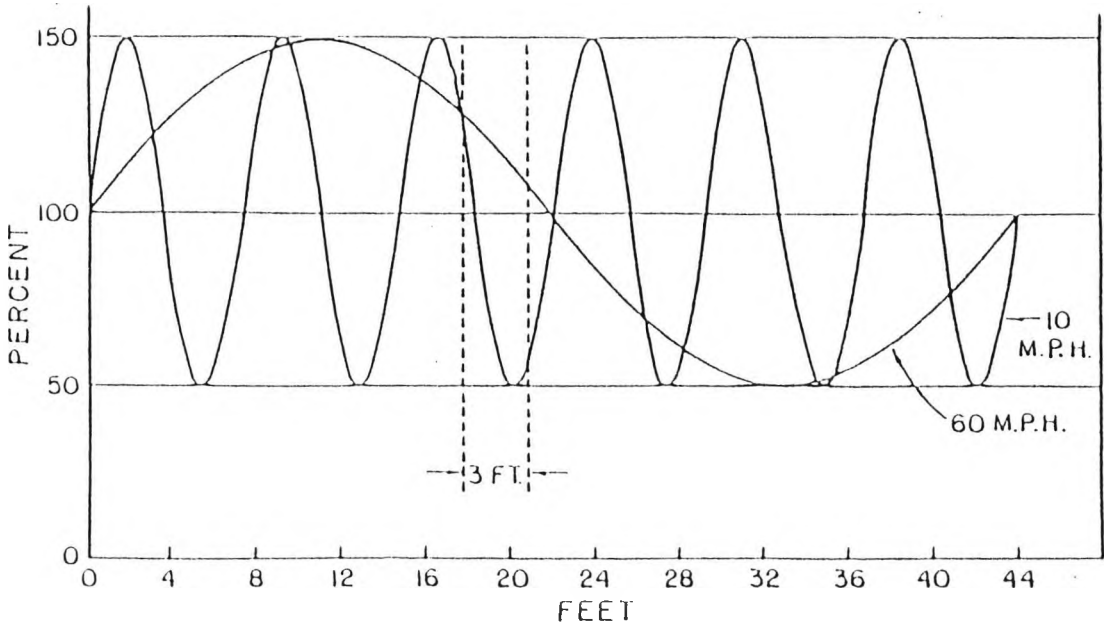

Fig.2.11 Body bounce Oscillations at different Vehicle Speeds.

the tyre print moves with the vehicle. The maximum deflection at the centre of the dish varies according to whether the pavement is flexible or rigid. For a flexible pavement typical maximum static deflections are in the range of 0.2 to 0.6mm, [63]. Typical maximum static strains on the surface of flexible pavement are 0.001, (1000μstrain). Motion of a vehicle tends to reduce these deflections and strains by a factor of about 3 between speeds of 0 to 30kmh. Above this speed they remain almost constant. These typical deflection and strain values are necessary when consideration is given to the coupling of sensor systems to the road.

2. 4. 3. 2 Weighbridge and Foundation mathematical modelling. A typical shallow excavation weighbridge is considered for this investigation consisting of a metal platform supported by loadcells which are coupled to a foundation base. The platform is assumed to be a rigid mass and the base is integral with pavement structure. The load-cells are characterised with their stiffness and damping, (natural or added), and part of their mass is attributed to the plate mass. The whole assembly can therefore be represented by a simple arrangement of a mass, spring and a damper.

The Finite Elements, (FE) study of the (0.6 x 0.6m) TRRL module, [142], [147] has shown a top centre deflection of 0.5mm for a 12tonnef load applied centrally on the weighbridge, corresponding to a stiffness of $k_w = 2.35.10^8\ N/m$. With the observed first natural resonance frequency of $f_p = 317Hz$, an effective mass of 60kgf can be calculated from the equation:

$$f_p = \frac{1}{2\pi}\sqrt{\frac{k_w}{m_e}}$$

The actual mass of the top plate is $m_w = 85kgf$, so this corresponds to an effective mass ratio of 0.7. The viscous damper coefficient, b_w is unknown but can be computed assuming various damping ratios:

$$\xi = \frac{b_w}{2.\sqrt{k_w.m_e}}$$

A simple ground foundation model was attached to the weighbridge mathematical representation so that all phenomena associated with vehicle passage were accounted for. The combination of a mass, spring and a viscous damper were found to be a a satisfactory approximation of the ground foundation. The values of the fictitious ground mass and the damping coefficient were taken from a vehicle/pavement bond graph simulation study conducted at Southampton University, [146]. The ground stiffness was calculated assuming a typical flexible road dynamic deflection of 0.5mm for a load of 5000kgf, (50kN).

The composite weighbridge-foundation model is shown in Fig. 2.12, and its parameter values are presented in Table 2.4.

The input to the model is the force F of the usual trapezoidal shape corresponding to the force applied by the two closely spaced moving tyres over the weighbridge module, (see the ideal area sensor signals in Fig. 2.7). The output of the weighbridge is obtained in terms of load-cell strain proportional to the displacement of the elastic element.

The modelling was carried out using the dynamic simulation package ***MEDIEM***, which is discussed in detail in Ch.4. The usefulness of the ground foundation model was evaluated by giving alternative values to the fictitious ground parameters and comparing the composite model outputs. The physical parameters of the weighbridge components were given two alternative sets of values such that to produce two distinctive types of systems in terms of their dynamic properties:

i) a system with light platform mass, $m_w = 30kgf$, high load-cell stiffness, (effective stiffness for all 4 load-cells $k_w = 3.0.10^9\ N/m$), and no damping added beyond that assumed inherent to the structure.

ii) a system with a heavy platform mass, $m_w = 160kgf$, low load-cell stiffness, (cumulative stiffness $k_w = 0.5.10^9\ N/m$), with no added damping, and with added damping.

The dynamic response of the TRRL weighscale platform was examined for two damping ratio values: $\xi = 0.1$ and $\xi = 0.6$. The dynamic errors, (dynamic to static readings ratio), can be computed as the amplitude ratio of a standard second order system:

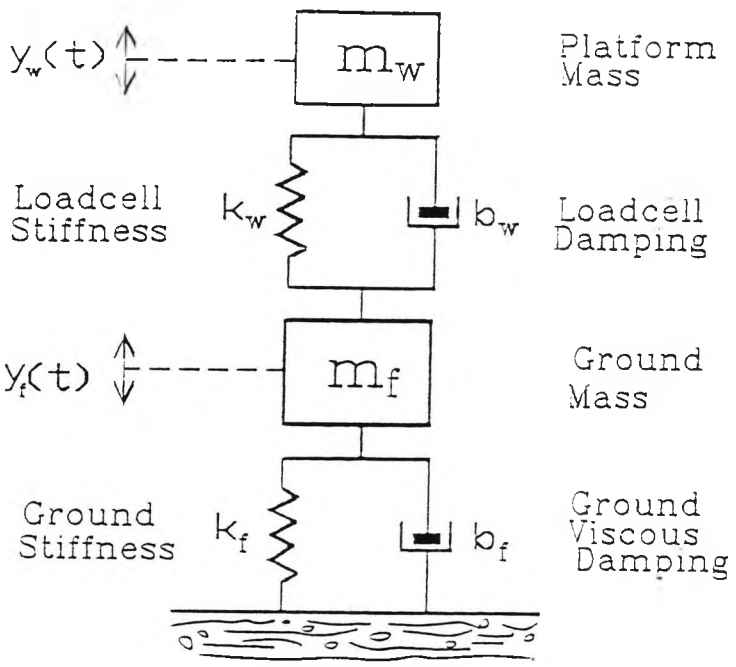

Fig.2.12 Weighbridge-ground foundation Model.

Parameter				Value
Platform Mass	=	m_w	=	*85.0 kgf*
Load-cell Stiffness	=	k_w	=	*2.35.10³ N/m*
Load-cell Damping	=	b_w	=	*24.0 kN/m/s*
Fictitious Ground Mass	=	m_f	=	*1000.0 kgf*
Fict. Ground Spring Stiffness	=	k_f	=	*1.0.10³ N/m*
Fict. Ground Viscous Damping	=	b_f	=	*500.0 kN/m/s*

Table 2.4: Weighbridge-Foundation Model parameters.

$$\left|\frac{x}{x_s}\right| = \frac{1}{\sqrt{[1 - (f/f_p)^2]^2 + 4\xi^2(f/f_p)^2}} \qquad (2.7)$$

where: $f = 1/T_r$ is the vehicle transit frequency,

f_p is the natural frequency of the platform, $(f_p = 317Hz)$,

ξ is the damping ratio.

The dynamic errors can be plotted as the difference between the static deflection of the plate, (0.5mm for the TRRL weighscale at 12tonnef load), and the dynamic signal - Figs. 2.15(a) and (b). The transit of a single axle over the weighbridge was simulated in that case.

The following observations were made:

– The foundation model has negligible effect on the compression of the weighbridge spring, which is proportional to load-cell output. The stiffness of the foundation, k_f was varied by a factor of 10 in both directions. Likewise ground foundation damping, b_f, and mass, m_f were varied substantially in both directions. All simulation results pointed to the relative insignificance of foundation properties to the dynamic response of the weighbridge to axle passages. This can be explained with the big differences in the adopted foundation fictitious mass and damping, and those of the weighbridge platform.

– The response of the light platform, (case i), appears to be adequate although it might be difficult to design a rigid module of such a light mass. The platform's resonance is well above the transit frequencies as well as the vehicle's natural frequencies of vibration - Fig. 2.13.

– The lower natural frequency of the heavier platform, (case ii), is apparently too close to the transit frequency, hence the pronounced ringing observed in the residency and latency signal plateaus - Fig. 2.14(a). In terms of accuracy, oscillations of that amplitude would not be acceptable. However, if additional damping is introduced in the system, ringing could be reduced to within

acceptable limits - Fig. 2.14(b).

– Considerable ringing was observed in the response of the TRRL weighscale module for the lower damping ratio $\xi = 0.1$ suggesting that the module should incorporate additional damping to minimise dynamic errors. Results for two damping ratios obtained through Eq.2.7 for two vehicle speeds are presented in Table 2.5, and simulation plots for axle passages are shown in Figs. 2.15(a) and (b), respectively for the two damping ratios.

Veh. Speed		*Damping ratio*	
[km/h]	*[mph]*	$\xi = 0.1$	$\xi = 0.6$
67.5	*42.5*	*1.004*	*1.001*
135	*85*	*1.017*	*1.005*

Table 2.5: Dynamic Error, (Dynamic to Static readings ratios), of TRRL weighscale module, $(f_p = 317Hz)$.

The results presented here should be confirmed with more detailed studies which may involve the study of rolling loads on the weighbridge module using FE methods.

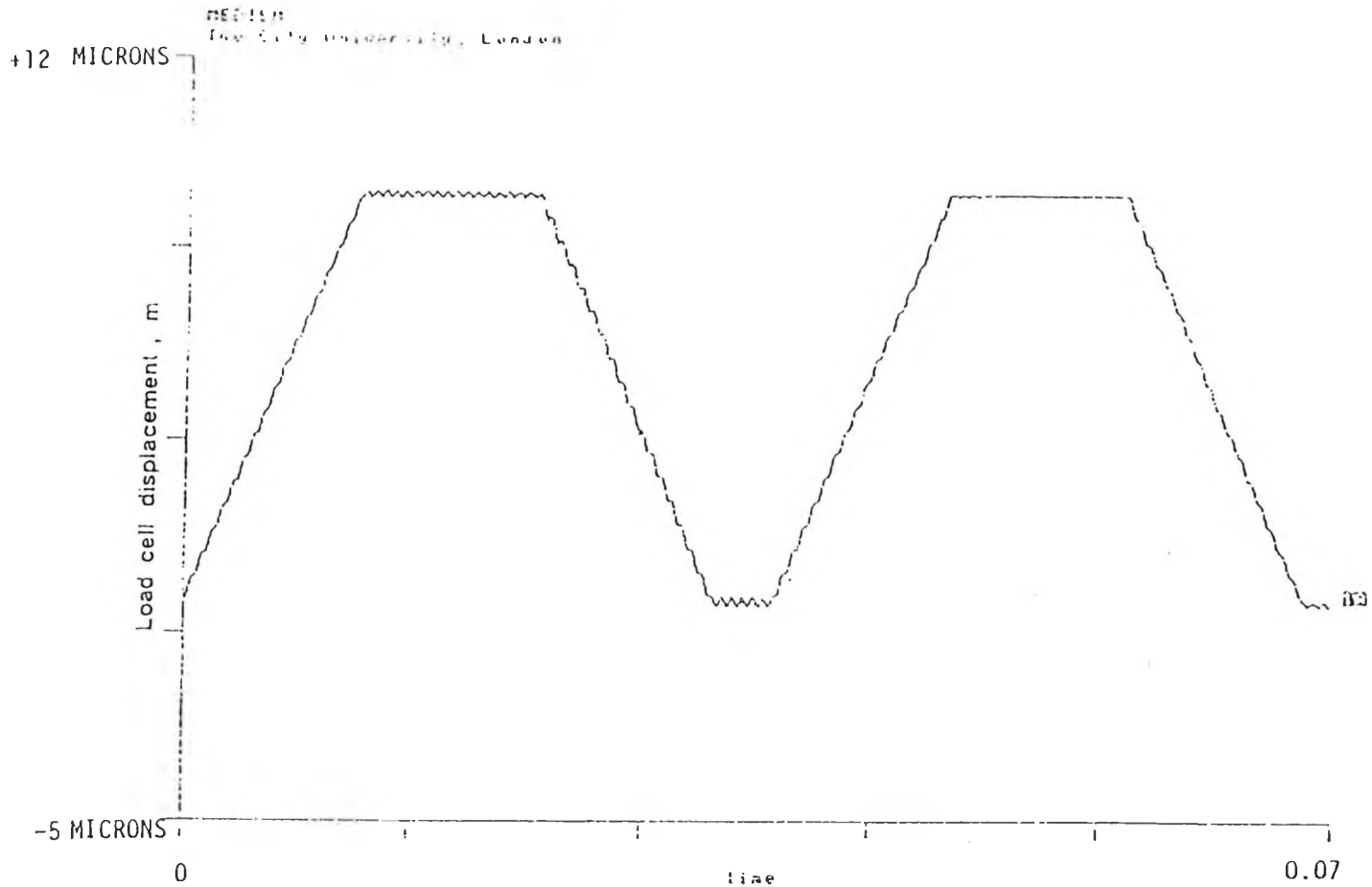

Fig.2.13 Dynamic response of a Load-cell Weighbridge
with a *High* natural frequency.

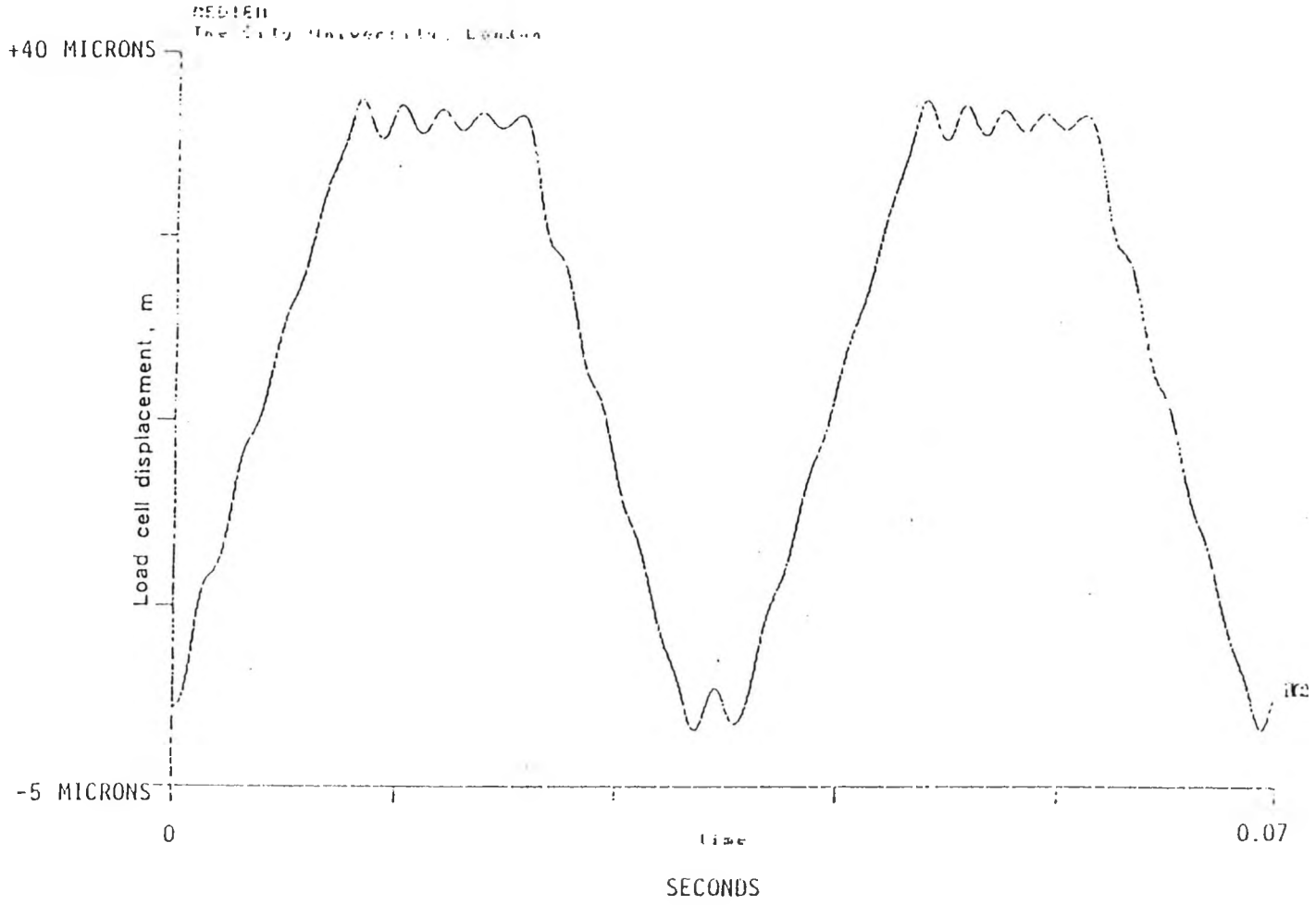

Fig.2.14 Dynamic response of a Load-cell Weighbridge with a *Low* natural frequency.
a) No added damping

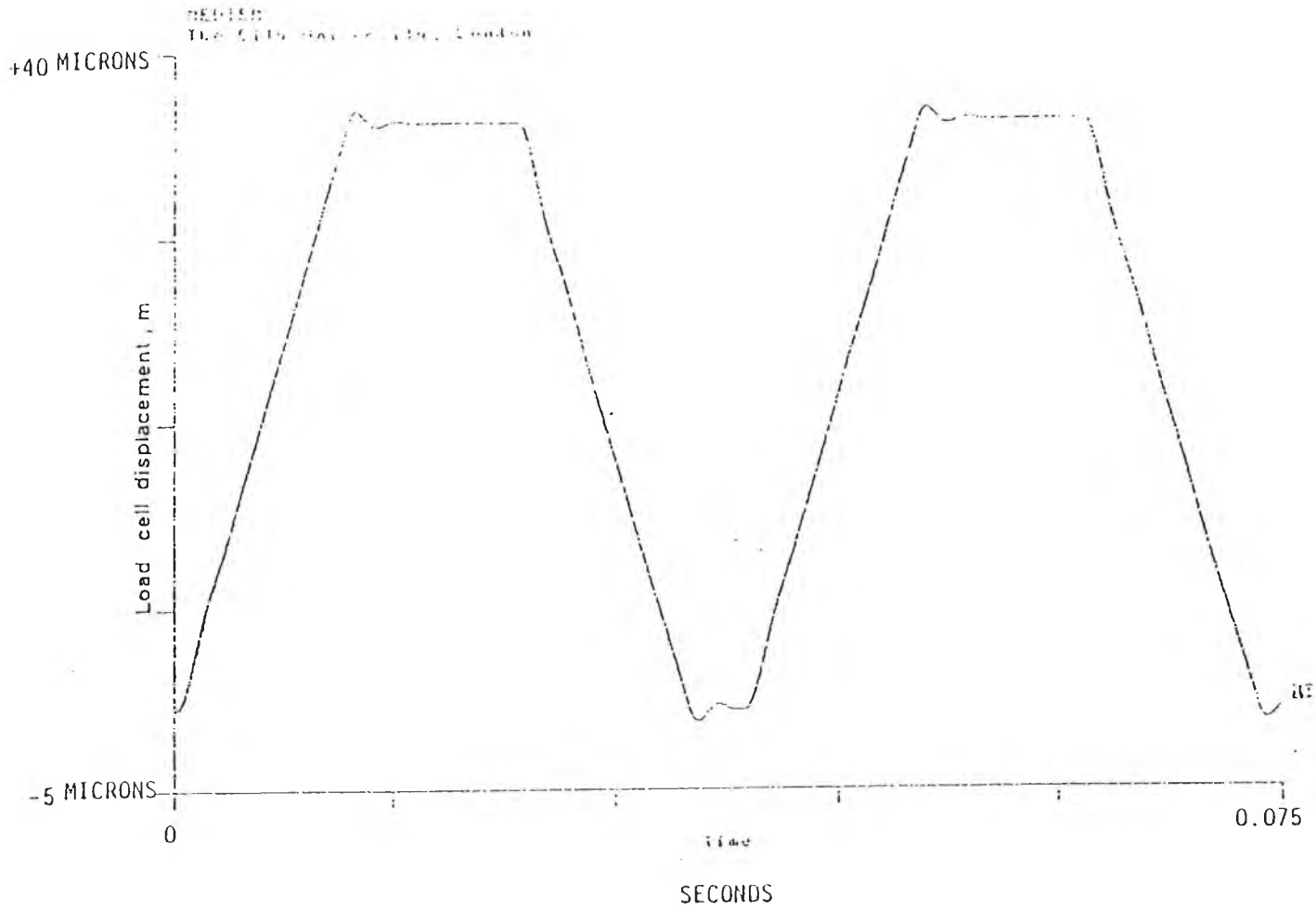

Fig.2.14 Dynamic response of a Load-cell Weighbridge with a *Low* natural frequency.
b) With added damping

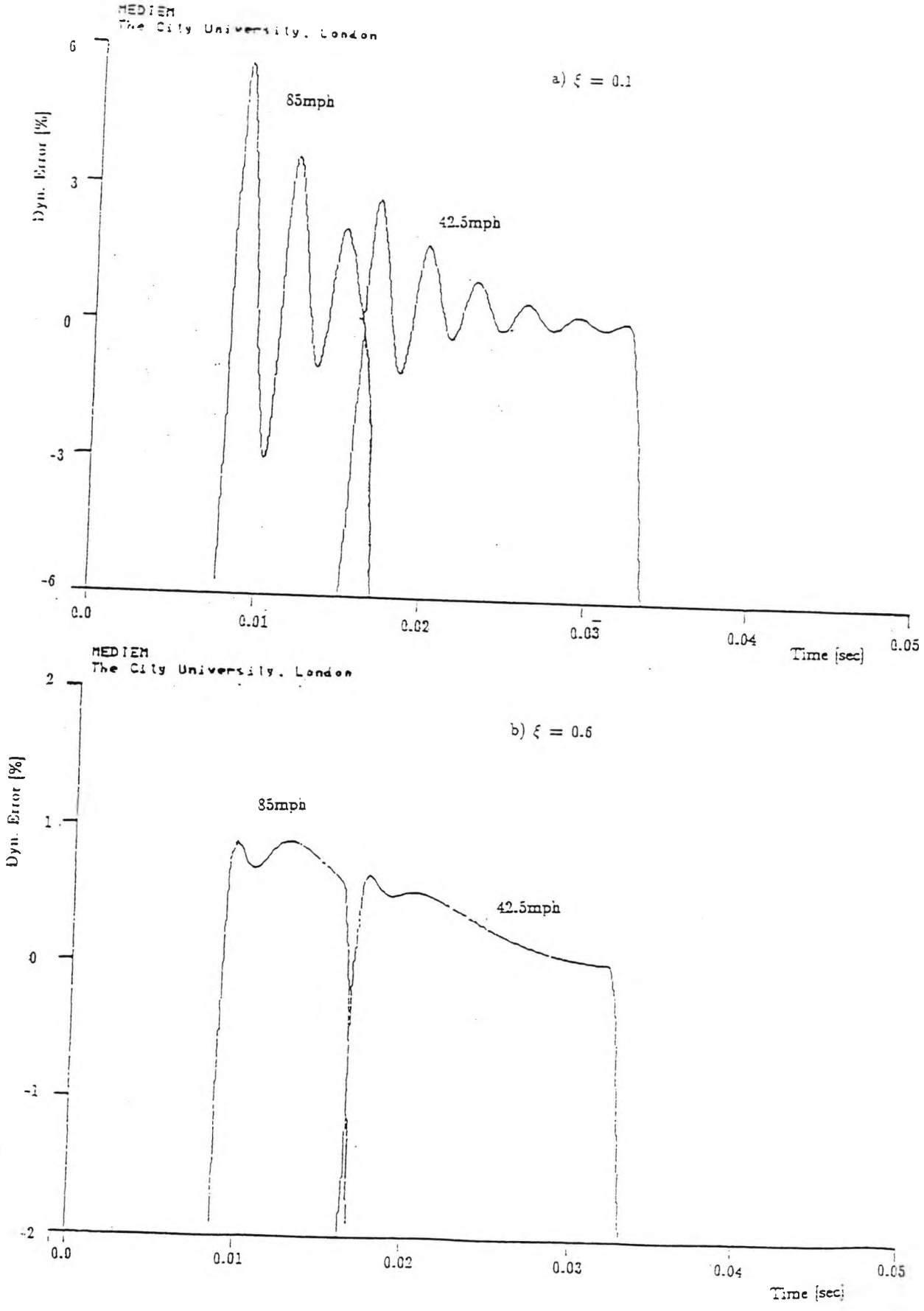

Fig.2.15 WIM Dynamic Errors for two Damping Ratios.

2. 5 SENSOR SIGNAL PROCESSING

In this section the key features of the electronic equipment used in modern WIM systems are discussed. A generalised electronic system configuration is presented applicable to the sensor systems described in the previous sections. Different signal detection and processing methods are reviewed and their features assessed in terms of complexity and measurement accuracy.

2. 5. 1 WIM System Electronics.

To process sensor signals and present the desired information WIM systems employ different measurement principles requiring different types of electronic circuitry. Most of the early WIM systems used resistive strain gages connected in bridge circuits the electrical outputs of which were photographed as oscilloscope traces or recorded on chart recorders, [38], [102]. Modern systems make extensive use of microprocessor based digital circuitry for real time signal processing, automated data classification, presentation and storage facilities. A typical WIM system electronic unit consists of two functional blocks: 1) Signal conditioner, and 2) Data management and control unit.

2. 5. 1. 1 Signal Conditioning Circuits. Normally sensor outputs are low energy analogue signals vulnerable to electrical interference and containing all the unwanted noise components due to vehicle vibration. An initial filtering and amplification electronic device is therefore necessary to make the signal safely transportable and suitable for further processing. For best results the circuit should be located as close as possible to the sensor itself. For analogue type outputs a local low noise preamplifier should be fitted to provide a low impedance drive to the cable link with the rest of the circuitry. Because of the large temperature variations on the road surface a temperature compensation circuit should also be provided in close proximity to the sensor. Immunity to electrical interference can be significantly improved by analogue to digital, (A/D) signal conversion prior to transmission.

Where sensors are the frequency varying elements in an oscillator circuit, the output can be directly transmitted as a frequency count. Electrical interference can be induced in sensors that exhibit high impedance, such as capacitive mats. The introduction of screening plates around such devices should be beneficial, but care must be taken not to swamp outputs with stray capacitance.

Some types of sensors exhibit nonlinear output relationships, (e.g. variable capacitance circuits operating on the principle of changing distance between capacitor's plates). Inherent sensor nonlinearities compensation is achieved by incorporating them into special operational circuits with inverse nonlinearity relationships. Linearisation algorithms or look-up table procedures are applied to digitised signals. Some other basic signal processing operations that can be undertaken in the signal conditioning block include: waveform sampling, initial filtering, integration, as well as some mathematical operations on the analogue or digital signal. In Fig. 2.16 where a schematic of a typical WIM system electronic unit is shown, this part of the signal conditioning block is denoted as the "*Preprocessor*".

The range of sensors used in current WIM systems provides a variety of system operating modes and signal processing requirements. These are summarised in Table 2.6:

Device	*Sensor Type*		
	Strain Gage Load-cell	*Variable Capacit./Induct.*	*Piezoelectric*
Output Type	*Analogue Pulse*	*AC Volt./Freq. Chnge*	*Analogue Pulse*
Preamplifier	*DC or AC*	*AC Brdg/Pulse Amp.*	*High Imp. Ch. Amp.*
Filters	*Low pass*	*Band pass*	*Low pass*
Spec. Converter	*A/D or V/f*	*Freq. counter or f/V*	*No*
Power Supply	*DC and AC*	*DC*	*DC*

Table 2.6 WIM Sensors signal conditioning circuits.

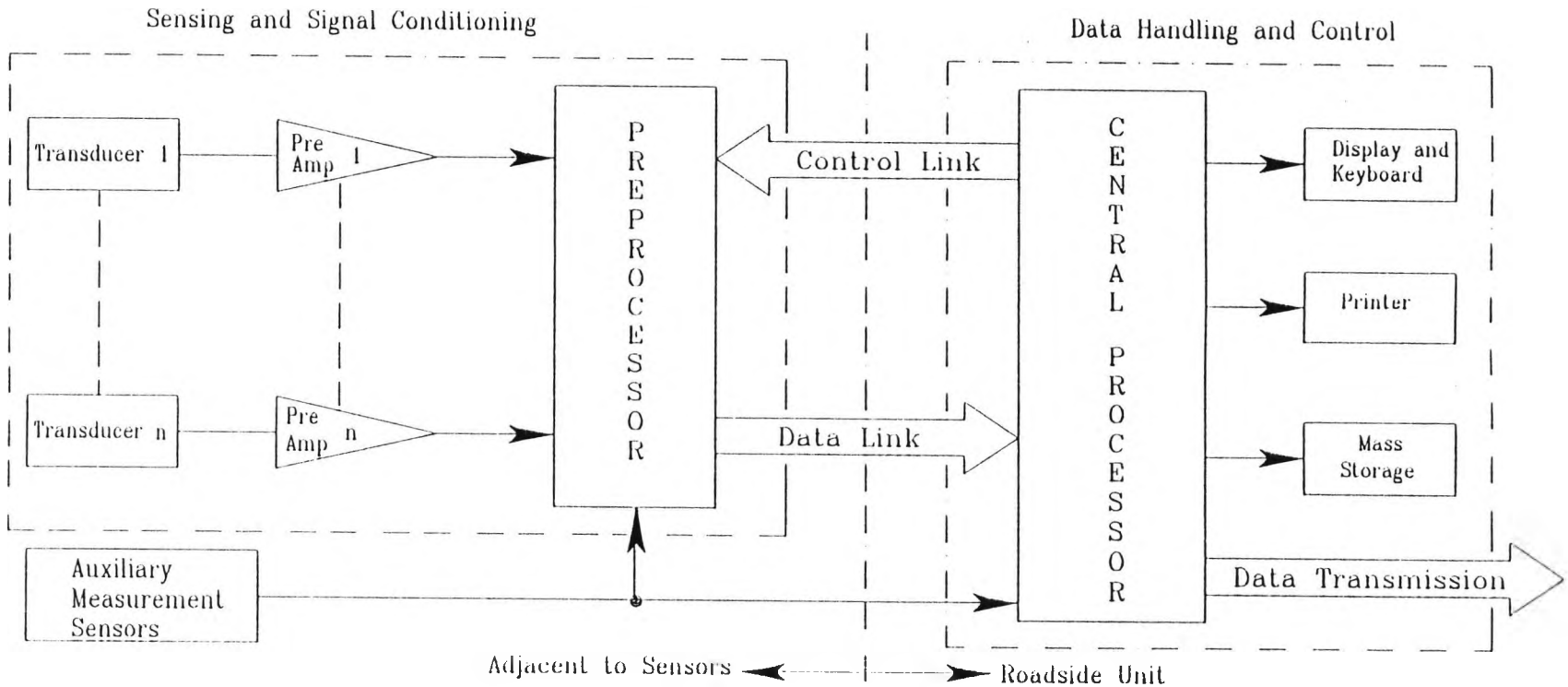

Fig.2.16 Block diagram of a typical WIM system electronics.

The frequency requirements for the signal conditioning circuits are determined by the maximum expected frequency of the sensor signal. Waveform sampling rates have to be set so that discretization errors do not occur. The integration constants and conversion times should not be larger than the minimum axle separation times, T_l. For AC excited bridges and variable frequency circuits the modulation carrier frequency should be at least 10 times higher than that of the sensor signal, so that demodulation circuits can respond to the highest expected signal frequencies.

2. 5. 1. 2 Data Management and Control Unit. This unit, which in most cases is located in a roadside cabinet, hut or a mobile van, interprets the preprocessed sensor signals to transform them into information as desired by the specific end user. In modern systems this is a microprocessor based device, *(central processor)*, programmed to scan the individual sensor channels and process the measurement signals to produce an indication or a record of the specific vehicle/axle passage. Different sensing system arrangements can be used to detect various aspects of vehicle traffic. For instance a line of sensing elements is capable of measuring half or full axle weight if it is stretched across a carriageway. In another arrangement of two rows of sensors separated by a known distance along the carriageway, it would be possible to obtain vehicle speed, axle separation, and possibly deduce vehicle class. Signals from inductive loops, piezocables, optical sensors, photocameras and other auxiliary sensors, can be included in the working algorithm to obtain the desired information. If the equipment is intended to work under operator's supervision, its hardware must include means of data input and indication: keyboard, switch panel, VDU, printer, etc. If unmanned operation is envisaged then mass storage devices are needed to keep the measurement records. Sometimes a data transmission link is provided to a remote central computer station.

Depending on the particular information tasks of the dynamic weighing system the Data management and control units present a great variety both in terms of hardware and software, [44], [49], [69], [150], [153]. A generalised structure of the unit is shown in Fig. 2.16 as part of WIM system electronics. A typical VDU screen display of a WIM monitoring station showing a readout of vehicle identification, speed, weights, dimensions, etc, is shown in Fig. 2.17.

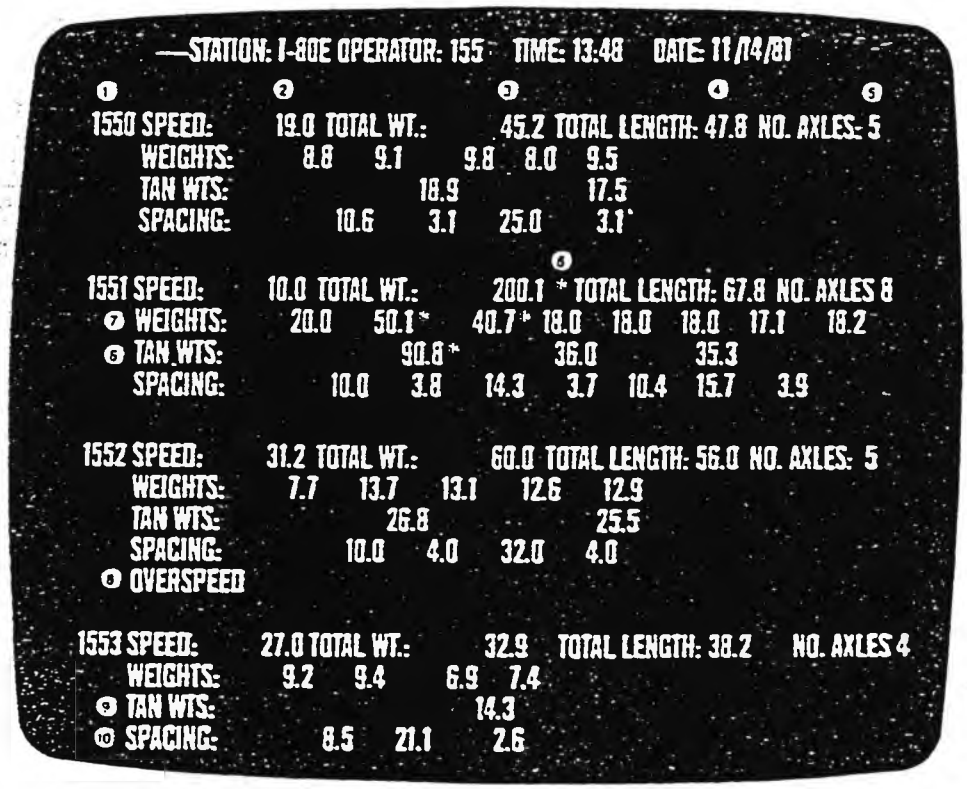

(1) vehicle identification
(2) speed across the WIM-scale
(3) total vehicle weight
(4) total vehicle length
(5) number of axles on vehicle
(6) * indicates overweight condition
(7) individual axle weights
(8) indicates overspeed
(9) tandem weights (accumulated weight of any 2 axles less than 1.5 m apart)
(10) spacing between axles

Fig.2.17 A typical WIM system VDU readout, (Streeter Amet).

2. 5. 2 Signal Detection Techniques.

The instantaneous pressure inputs experienced by WIM sensing systems represent samples of the dynamic loading applied by the vehicle to the road. The sensor output is a complex aperiodic signal which is a combination of the DC value of the static vehicle's weight superimposed with vehicle, and to a lesser extent, sensor vibrations. Which parts of the sensor signal are being sampled as well as the methods of extracting the useful information from the sampled signal are of primary importance to measurement accuracy and the nature of the measured quantity.

2. 5. 2. 1 Area Sensor Signal Detection. In area type sensors the trapezoidal shape of the signal generally allows for three methods of signal detection:

i) Peak detection. This is probably the simplest approach requiring least processing. The sensor output is fed into a peak detector circuit, (usually an analogue comparator and a "sample&hold" opamp). Through auxiliary position sensors the system registers when the tyre is about to step over the weight sensor and activates the peak detector. This information can be acquired by the weight sensor itself as the output begins to rise above the no-load output level. The detector then registers the peak signal value which is converted to its digital equivalent by the preprocessor and sent to the central processing unit. The peak signal value can also be selected after the A/D conversion through a short "maximum value" sort routine in the preprocessor. Finally the peak detector is reset by the signal falling below a preset minimum value. In both cases hardware is minimal in that only a peak detector and an A/D converter are necessary.

The major disadvantage of this technique is the considerable measurement error introduced by approximating the maximum measured peak of a dynamic signal to its static DC value. However in the cases when peak dynamic loads are the object of measurement, peak signal detection will obviously be the advantageous sampling method to use.

ii) Single sampling. If the WIM system is designed such that area sensor output is sampled once per axle passage somewhere during the flat part of the signal, Fig. 2.7, then the rise/fall parts of the signal will be eliminated. In terms of axle static weight, accuracy will then be limited to the signal oscillations

around the static DC value induced by vehicle and sensor dynamics. The problem arises however, of determining the moment when the tyre is positioned centrally over the sensor platform. When velocity or position auxiliary measurements are provided then the central processor should use these data to generate a "sample take" pulse at the correct moment of axle passage. If no speed or position information is available however, then this moment has to be determined in real time from the incoming sensor signal itself. A time delay of fixed or variable duration, (depending on vehicle speed) is usually introduced after the signal exceeds a predetermined value. This might pose some problems since real sensor signals are not as sharply defined as in the plot of Fig. 2.7.

iii) Multiple sampling. This is a technique similar to single sampling, but a number of samples is taken for processing along the waveform. Preferably again only the flat part of the signal is selected for sampling since only during T_r is the full weight of wheel supported by the sensor platform and transients are avoided.

2. 5. 2. 2 Line Sensor Signal Detection. In the case of line sensors the length of the sensor in the direction of travel is always smaller than a tyre contact length hence the sensor output at any moment in time represents only the load of a fraction of the tyre that sits on top of the sensor at that moment. To obtain the full tyre load the signal must be integrated over the complete tyre contact length, (see Sect.1.6.2). Either some method of analogue signal integration has to be applied over the signal area, or a number of samples have to be taken and numerically integrated over tyre residency time. Finally a single, (peak) sample might be taken and integrated over the residency time, however incurring the same errors characteristic of peak signal detection.

2. 5. 3 Signal Processing Methods.

Vehicle dynamic loads are composite oscillatory signals and if no filtering is applied, WIM systems errors might be as large as the peak vibration amplitudes. Elimination of vibratory components, therefore is of crucial importance for weighing accuracy when an estimate of the static weight has to be extracted.

The sensor output vibratory components can be divided into two categories: those originating in the weighing sensor, and those originating in the

moving vehicle. The former are caused by the impact of the tyres on the weighing sensor, and the vibration amplitudes and frequencies are a function of platform's physical parameters. By designing the sensor platform to have light mass, high stiffness, and therefore high natural frequency, the impact vibrations can be attenuated at source to an acceptable level. However, reducing vehicle associated oscillatory components may not be that easily accomplished. At high vibration frequencies conventional filtering techniques should prove effective, but where the vibration period is comparable with the weighing period, such techniques are inadequate. In general there are two basic approaches to vibration attenuation: ***Filtering*** and ***Integration***.

2. 5. 3. 1 Weighing signal Filtering. Vehicle suspension simulations and experimental studies have shown natural body frequencies as low as 1.5Hz and amplitudes approaching 30% of static vehicle weight.

Choosing filter parameters providing minimum response deviation from true static weight means finding the optimum compromise between rise time and ripple attenuation. Calculations for a simple **R-C** passive filter have shown maximum attenuation of 2.5 on a single sinusoid emulating ***body bounce*** vehicle vibration, [46]. A further disadvantage of conventional **R-C** filters when used at low frequencies is the large component values required to obtain the necessary time constants. This disadvantage can partly be overcome by using active filters. Increasing the order of the filter improves attenuation up to a point, but from then on performance will deteriorate as the order is increased.

The optimum design of a filter depends on the specific operating conditions such as vibration frequencies, ripple magnitudes and maximum acceptable time delay. A maximum flat 4-th order *Butterworth* filter seems to be well suited for the conditions specific of dynamic weighing. An attenuation of 7 is achievable with this filter in which the output does not exceed the input level. Higher attenuation can be obtained by allowing some overshoot in the response, but that in itself will introduce some error. A significant improvement in performance can be obtained by using customised filters with variable time constants. In the installation described in [46], the initial weight signal transient precharges in a short time the filter capacitor through a relatively low impedance, effectively setting the initial integration voltage to a value much closer to the true static weight. The filter is then switched back to a high time

constant best suited for attenuation. However, precise performance prediction of variable filters is extremely difficult and estimation by experimental methods is very time-consuming task. For filters performance comparison data see Table 2.7.

2. 5. 3. 2 Weighing signal Integration techniques. Integrating a sensor signal $W(t)$ over the weighing period is a common method to reduce vibration errors. It is realised either by analogue integration or by digital averaging. In principle the effect of both can be expressed mathematically by signal integration with respect to time over the weighing period T_r, and then dividing by time T_r:

$$\overline{W} = \frac{1}{T_r} \int_0^{T_r} W(t).\, dt$$

In practice the vibration superimposed on the static weight will contain several components of different frequencies, but to simplify the analysis vibration is represented by a single sinusoid of frequency f:

$$W(t) = W_m . (sin 2\pi ft + \theta) \qquad (2.8)$$

Assuming a weighing period $T_r = 1sec$, (i.e. accommodating one full vibration cycle), the vibration attenuation A at worst phase conditions will then be calculated as:

$$A = \pi . \frac{N}{sin \pi N} \qquad (2.9)$$

where N is the number of vibration cycles within the weighing period. The broken line plot in Fig. 2.18 shows the general increase in attenuation obtained with straight integration with increasing cycle number N. Infinite attenuation is obtained when whole numbers of cycles of the fundamental vibration are

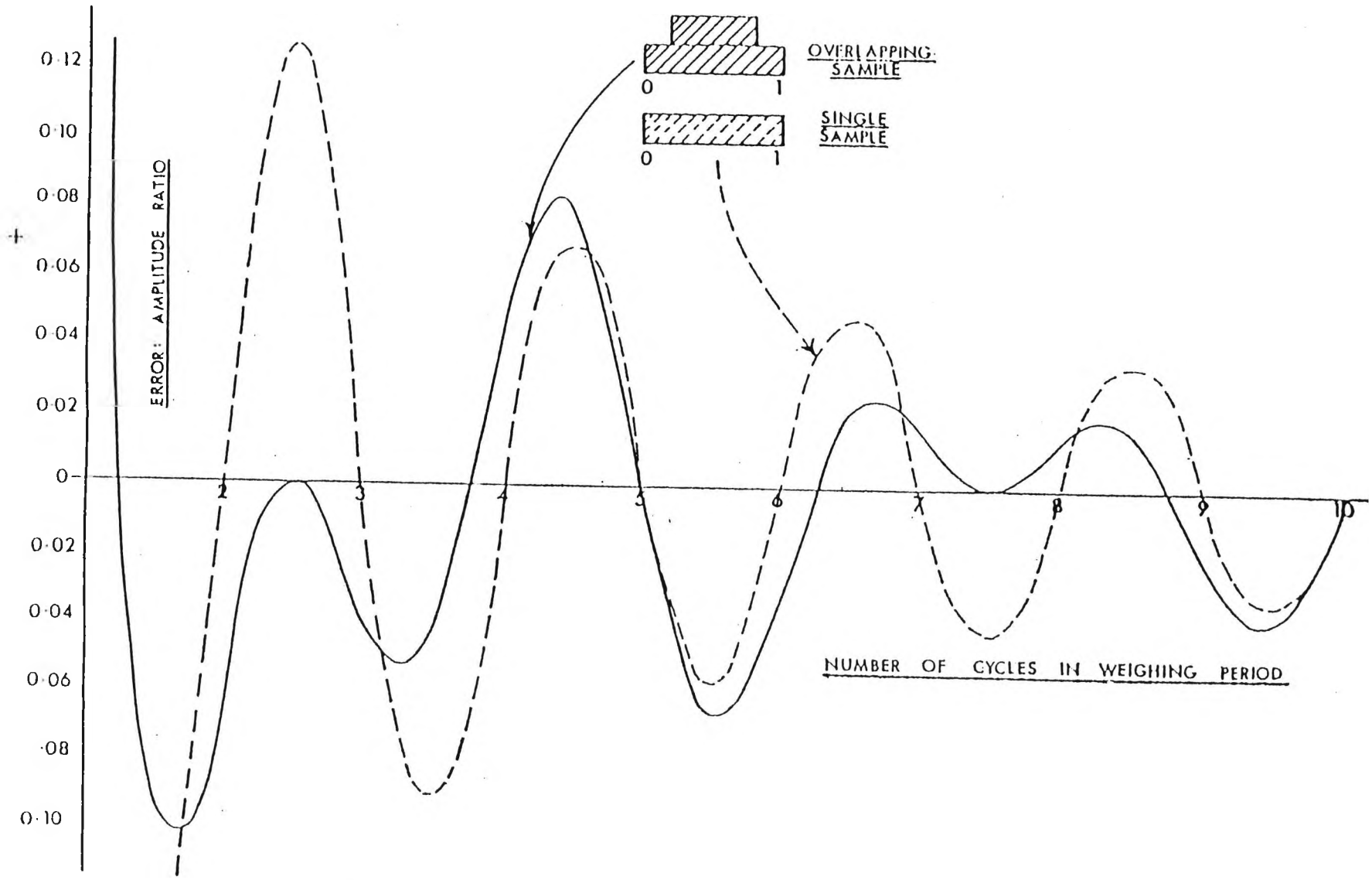

Fig.2.18 Vibration attenuation by straight integration and overlapping samples.

contained within the weighing period. In the practical case, however, the attenuation will be reduced by the presence of vibration frequencies other than the simple sinusoid whose effect has been plotted. It follows that for a given weighing period $T_r = \frac{l_s}{U}$, worst attenuation will result at low vibration frequencies, i.e. vehicle ***body bounce*** frequencies. For the TRRL standard vehicle used in this study body bounce natural frequency was found to be f_b=*1.62 Hz.* Assuming worst phase conditions and substituting in Eq.(2.9) for that frequency:

$$A = 1.62\pi = 5.1$$

If the vibration amplitudes were $\pm 10\%$ of DC static weight value, the resulting indication error would now be 1.96% of true static weight. It should be noted, however that to accommodate a full body bounce cycle on a TRRL type platform, $(l_s$=*0.6m)*, the vehicle horizontal velocity U has to be less than 3.5*km/h*, and for a wheel hop cycle, $(f_w$=*11. 7Hz)* - less than 25*km/h*. Therefore straight integration or averaging can be applied effectively only for low speed or quasi-static WIM systems.

2. 5. 3. 3. Combined signal processing techniques. A common solution for slow/midspeed operations is filtering out both high and low frequencies by combining low-pass filters and integrating circuits, [4], [86], [136], [154]. In one of the applications used in slow speed railway cars weighing, [154], attenuation of 130:1 is claimed with lowest vibration frequency of 3Hz. The signal is initially fed for a period of 2sec into a double pole low-pass filter having an AC response of at least 1/13 at 3Hz, and reducing the transient to within $1.7.10^{-4}$ of the static weight level. A subsequent 1sec long integration attenuates the vibrations by a further 1/20 giving the overall attenuation of 1/130 for the major vibration frequency. However, for a 3 second weighing period only very low passage speeds would be permissible, or in the case of uncoupled vehicles a very long platform would be required. The claimed accuracy of $\pm 0.15\%$ of true static weight refers to weighing railway cars at speeds up to 15mph only. If this technique were to be applied for motorway traffic conditions with existing installations, the overall attenuation will effectively be reduced to less than 1/10.

A method of improving attenuation without extending the weighing period has been achieved by integrating over a number of overlapping periods of diminishing duration, [46]. If digital processing is applied, the same effect is obtained by increasing/decreasing the sampling rate over the integration period. The greatest vibration errors occur where an odd number of half cycles is contained within the weighing period, as can be observed in the solid line plot of Fig 2.18. By "weighting" the peaks of vibration according to an appropriate set of binomial coefficients, alternate half-wave peaks are cancelled out. In principle the technique of "weighted averaging" involves multiplication of the weight signal by a "weighting function" $F(t)$, integration of the product over the weighing period, and finally division by the integral of $F(t)$ over the same period:

$$W(t) = \frac{\int_{-T_r/2}^{+T_r/2} [W_S + W_m . \sin(2\pi ft + \theta) . F(t) . dt}{\int_{-T_r/2}^{+T_r/2} F(t) . dt}$$

The vibration attenuation then will be:

$$A = \frac{\int_{-T_r/2}^{+T_r/2} F(t) . dt}{\int_{-T_r/2}^{+T_r/2} \sin(2\pi ft + \theta) . F(t) . dt}$$

The complexity and hence cost of the actual weighting function $F(t)$ derived for a particular application will depend on the accuracy requirements for the installation. Particularly good attenuation results have been achieved with a

"decay type" multicoefficient weighting functions. [46], [136]. Attenuations in excess of 600 are reported with correct coefficient selection for given frequencies down to 2.5Hz. However, as these weighting functions have to be tuned for a single set of frequencies, the described techniques are most suitable for installations measuring vehicles with very close natural frequencies, e.g. railway cars. A similar technique has been developed, [154], allowing for artificial signal values estimation when the weighing period is too short to ensure a sufficient number of samples to be taken. The reported accuracy is $\pm 0.5\%$ of static weight at speeds up to 6-8km/h, and $\pm 1.0\%$ at speeds 8-15km/h.

An original "integration-by-displacement" technique combines straight integration with a clever signal sampling method, [153]. The weighscale output is integrated over a short section of the plateau of the waveform, determined by comparing the outputs of the load-cells situated on the front side of the platform and those on the rear side. Compared to conventional ways of wheel position detection (pedal switches, light barriers etc.), this method has the advantage of eliminating errors caused by differences in wheel diameters and tyre contact lengths. The dual slope integration provides for inclusion of vehicle speed in the measurement thus allowing axle weight to be determined correctly regardless of integration time. Accuracy of 0.2% of rated weight has been achieved for speeds up to 20km/h, and 5% for speeds up to 70km/h, outperforming in this way conventional systems working on the principle of direct averaging.

Table 2.7 summarises the attenuation qualities of different filtering and integration techniques used in WIM systems:

Processing Technique	**Estimated Attenuation**
Simple R-C Filter	*2. 5*
Max. flat Butterworth Filter	*7. 0*
Simple Integrator	*8. 0*
Filter/Integrator combination	*10. 0*
Overlapping samples	*12. 0*
Second order Filter with overshoot	*25. 0*
Variable Filter	*50. 0*
Weighted averaging: COS function	*188. 0*
Weighted averaging: Function D(N, a, b)	*670. 0*

Table 2.7: Attenuation figures for Signal processing techniques in Weighing in Motion. Assumed weighing period: $T = 1.0s$; Minimum vibration frequency: $f_{min} = 2.5Hz$. *(From Ref. 46).*

In the case of line sensors some form of signal integration has to be provided over sensor signal duration, (residency time T_r). Vehicle horizontal velocity U has to be included in the algorithm, (See Eq.1.4), if a reasonable accuracy is required. A high speed A/D converter might be necessary capable of processing a sufficient number of tyre load samples so that representative integration results are obtained. The shortest tyre residency time for a vehicle with tyre print length $l_t = 0.25m$, and travelling at a maximum speed of 140km/h, will be $T_r = 6.4$ms. If 10 A/D conversions are required for the integration, then A/D conversion rates of better than 1.5kHz, (650μsec conversion time), will be necessary for the application.

Chapter III : Metrological Aspects.

INTRODUCTION

The survey of published literature revealed that no dedicated investigation into the problems of dynamic vehicle weighing as a measurement process has been undertaken by any of the authors. Nor is there an established consensus on a standard method of presenting the accuracy of the devices amongst equipment manufacturers and users.

Poor accuracy levels of dynamic weight measurements (rarely less than 10%), is one of the major disadvantages of the method compared to static weighing. Measurement data have a variety of applications requiring different interpretation of the input signals and sometimes different approaches to accuracy.

The purpose of this Chapter is to investigate the physical nature of dynamic weighing, provide definitions of its characteristics in metrological terms, and identify the main sources of measurement error.

Measurement qualifications such as accuracy, repeatability and reproducibility are applied to the specific conditions of in-motion weighing and the existing limitations are pointed out. Two types of weighing accuracy are defined and methods of their presentation are discussed. Special attention is paid to WIM systems calibration and the practicality of the present methods. The sources of weighing errors are outlined and classifications are provided on origin and error contribution basis. A section is dedicated on explaining the difference in the dynamic error interpretation depending on the purpose of measurement - true weight or dynamic wheel load. The sources of dynamic wheel force bias are treated in particular detail as they account to a great degree for the uncertainty of dynamic weighing results. Finally some methods for improving weighing accuracy in existing systems are presented and the conclusions on the metrological limitations of the technique are generalised.

3. 1 ACCURACY OF WIM SYSTEMS.

According to the adopted international vocabulary – [16], accuracy is *"the closeness of the agreement between the result of a measurement and the (conventional) true value of the measurand."*

Weighing in motion involves a considerable degree of uncertainty of the results due to the following factors:

- the output has to be extracted from a nonstationary in time and space signals;
- the system's input represents a random sample of the measured dynamic signal;
- the measurement period is too short compared to a complete signal cycle;
- the great number of vehicular, roadway and environmental factors (some of them of random nature), which influence the measurement.

The experimental axle load records taken by a series of weighbridges specially arranged along a track - Fig. 3.1, [74] represent typical patterns of the dynamic forces transmitted by vehicle tyres to roads. Along with the static weight value the signal contains a number of dynamic components appearing at different frequencies. A normal WIM sensor is usually much shorter and it "picks up" a randomly sampled portion of the dynamic force, thus introducing an element of uncertainty in each measurement. In practical terms for a population of measurements this would mean significantly reduced repeatability and increased standard deviation compared to similar population of static weighings. Consequently two types of measurement accuracy should be defined in dynamic vehicle weighing: ***Single sample accuracy,*** applied to individual measurements, and ***Statistical accuracy*** defined for multiple weighings, and requiring probabilistic approach.

3. 1. 1 Single Sample Accuracy.

It is determined for individual axle transits over a weighscale. In practice single sample accuracy should be established by direct comparison of the reading

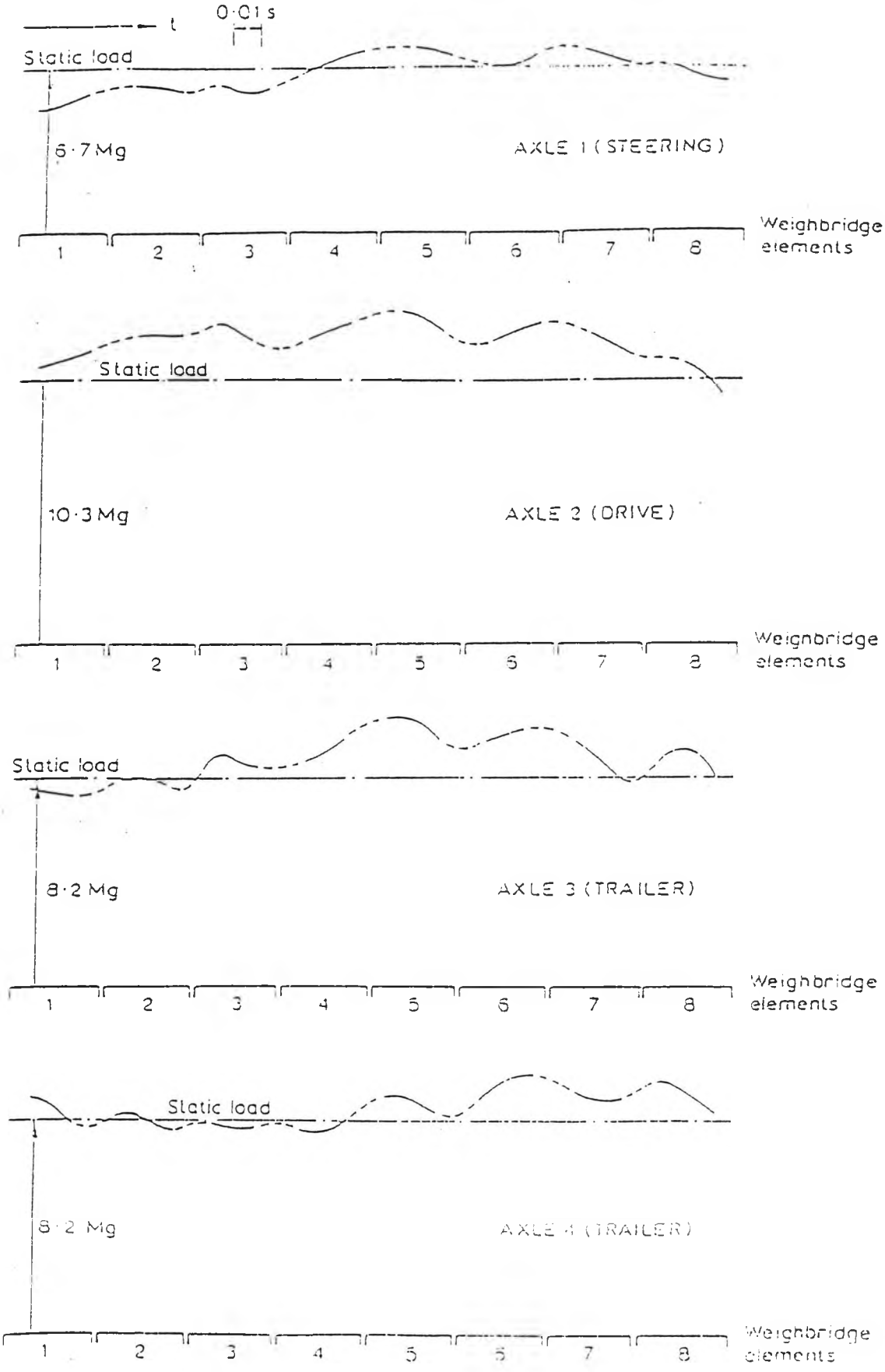

Fig.3.1 Variation of Dynamic axle Loads on a smooth Road profile.
(Vehicle at 66km/h)

with the true value of the measurand (if available). The single sample weighing error δ is given as:

$$\delta = \frac{w_i - W_s}{W_s} \cdot 100 \ , \ [\%]$$

where: w_i – the reading of the *i-th* measurement,
W_s – axle/vehicle static weight.

When the weighing is performed according to the requirements prescribed by the manufacturer, the accuracy of individual measurements should be within the limits given in the technical specifications of the equipment. However, the presence of some environmental or vehicular influencing factors may induce excessive systematic or random bias in the input and distort the measurement beyond the specified accuracy levels. Since the system input is a random sample of the dynamic wheel forces and hence a random function of the static weight, the individual sample accuracy will also acquire random character. Single sample accuracy, therefore is in close relationship with the ***repeatability*** of measurements. Multiple dynamic weighings of a single vehicle performed at virtually identical conditions have shown good repeatability, but this cannot be expected for different vehicles possessing different physical properties and thus having different dynamic behaviour even on identical tracks and at equal speeds.

3. 1. 2 Statistical Accuracy.

The statistical accuracy of a WIM system is defined on the basis of a large number of measurement results. The statistical model of a population of readings has to be built in the form of a ***Probability Density Function (PDF)***. The statistical accuracy is then established as the ***relative correlation*** "ϵ" of the results with the true value of the measurand, (in most cases the static weight). It is given as:

$$\epsilon = \frac{Population\ Mean - Static\ Weight}{Static\ Weight} \cdot 100, \ [\%]$$

Alongside with the ***population mean,*** other useful statistical parameters such as the standard deviations, ***(1σ, 2σ, 3σ*** levels), can also be obtained from the *PDF*. Thus the ratio between the standard deviation of the measured dynamic forces and the static weight, (or the population mean): σ_f/W_s, can be used as a measure of the aggressiveness of the traffic to the road structure and also of the quality of the road surface, [68].

In practice, if a WIM system can be designed to produce individual measurements with accuracies of around 10%, (single sample accuracy), then the correlation error, (statistical accuracy) will also be of the same order. Indeed, the correlation error will theoretically be zero if the errors for the individual measurements were random and Gaussian. This can be expected provided there is no input bias which would cause shift in the population mean from the true static weight thus introducing a systematic error. The problem of reducing the correlation error, therefore, involves the identification of sources of bias in the system input and finding ways to minimise their effect.

3. 1. 3 Weighing Accuracy Presentation.

Although WIM systems have been in use for more than three decades there seems to be no standard method of expressing the accuracy of the devices.

One of the most common measures is the mean error expressed as a percentage of individual weights, coupled with a confidence level. For example *"$\pm$ 10% at the 95 percent confidence level"* means that 95 out of 100 weight measurements taken fall within 10%, over or under, of the true static weights. However, if the accuracy levels are claimed with the indicated confidence, some instructions specifying the conditions at which the measurement should be taken have to be provided in the technical specifications of the equipment.

Another form of accuracy presentation that has been used by designers and manufacturers is the percent accuracy coupled with a standard deviation. This may be a better approach compared with the previous method, but it requires assumptions about the statistical distribution of the data. Statistical processing of weighing results – [135], has shown that normal distribution can be assumed applicable.

In any case there is a clear need to define a standard method of measuring and specifying accuracies so that users can easily compare products as well as the

experiences of other users.

3. 2 REPEATABILITY OF MEASUREMENTS.

Repeatability of the weighing results can be defined only for individual vehicles as obviously only then identical conditions can be insured for multiple measurements. Repeatability experiments have been carried out by various authors by repetitive wheel force measurements of a vehicle following the same track when approaching the scale and running at the same speed. During six runs of a test vehicle at 30mph, peak load variations within $\pm 3\%$ have been recorded by Whittemore et al – [150]. The experimental study of Leonard et al – [74], shows that the response of a TRRL type weighbridge is repeatable to within 2.5% provided the tracking and speed of the vehicle are consistent. Similar tests were conducted by Lee – [76], confirming the similarities in the pattern and magnitudes of wheel forces of individual vehicles recorded at similar conditions. However, repeatability cannot be expected to be within these limits when different vehicles are being weighed even if their static weights are identical. Their different physical parameters will lead to differences in their dynamic behaviour and hence the vertical forces applied to the sensor will also be different.

3. 3 REPRODUCIBILITY OF RESULTS.

Reproducibility is *"the closeness of agreement between the results of measurements of the same measurand. where the individual measurements are carried out at changing conditions"*– [16].

Reproducibility of dynamic weight measurements will be impaired mainly by the differences in the measurement conditions from site to site. Site-specific conditions such as road surface roughness, crossfall, sensor elevation, foundation, speeds of approach etc., will significantly affect the dynamic behaviour of the vehicle and hence the outcome of the measurement. Therefore, even though a

particular type of a WIM system can meet given tolerances at one site, this does not necessarily mean that it will perform within the same tolerances at another location. Any systematic bias in the results, however can be substantially reduced if the system is properly calibrated on site.

3. 4 CALIBRATION OF WIM SYSTEMS.

It was shown that perfect agreement between WIM weight estimates and static weight measurements cannot be expected due to the dynamic character of the measurand. The objective of calibration is to make the weights indicated by the WIM system for mixed traffic agree as closely as possible with the best estimates of the corresponding static weights that can be obtained feasibly in practice.

3. 4. 1 Factory Calibration.

The sensors that are used as the wheelforce transducers can be calibrated individually in the factory under static loads but the response of the roadway/vehicle/transducer system under dynamic loads cannot be easily evaluated in the laboratory. There is a complex interaction among the components of this physical system that is unique for every location and vehicle load that is applied to the transducer.

3. 4. 2 Site Calibration.

Two basic techniques can be used for on-site calibration of WIM systems:

- Static-weight loading;
- Dynamic loading.

3. 4. 2. 1 Static Loading. In this method, a known weight is applied to the transducer either by standard weight blocks or by the wheels of a standing test vehicle. This technique is more appropriate for low-speed WIM systems where the dynamic effects of the vehicle are relatively small.

3. 4. 2. 2 Dynamic Loading. The moving-vehicle calibration method is applicable for intermediate and high-speed systems when the dynamic interaction of the vehicle with the system is more pronounced. In this technique readings are taken from multiple runs over the transducer of a single test vehicle with known static axle weights at representative traffic speeds. The system is then adjusted so that best agreement is achieved between the mean values of the estimated from these runs axle weights and the corresponding static axle weights. More than one type of test vehicle, each making multiple runs, can also be used to obtain better representation of the various patterns of the roadway-vehicle-transducer interaction. In addition, laden weight on the vehicles can be varied to account for the differences in dynamic behaviour when changing the body mass of the vehicle.

The importance of on-site calibration and the relative effectiveness of the other calibration techniques is illustrated by experimental data in [84]. In the same paper, as well as in [104] correction expressions for the mathematical adjustment of the systems are also provided.

3. 5 SOURCES OF WEIGHING ERRORS.

The sources of inaccuracies of road vehicle WIM systems generally fall into two basic categories:

- Instrumentation errors,
- Dynamic effects errors.

3. 5. 1 Instrumentation Errors.

These are the errors of the equipment which determine its accuracy in measuring the applied dynamic forces. They can be traced down to the specific characteristics of the sensor system and the associated electronics. Some of them are: nonlinearity, frequency response, hysteresis effects, temperature dependence etc. The way to deal with them is quite straight forward and common to most instrumentation.

3. 5. 2 Dynamic effects errors.

These are inherent to the very concept of the in-motion method of weighing that vehicle weights can be estimated from instantaneous or discrete time measurements of the vertical component of the dynamic (continuously changing), load applied to the road by the tyres of a moving vehicle. Under some conditions that load may vary from twice the static weight to zero value when the wheels temporarily lose contact with the road.

Road surface profile prior to the weighscale and the speed of the vehicle are the most important factors determining the pattern and amplitudes of the dynamic forces. However, they are also affected by a number of other roadway, vehicular and environmental influences.

In Table 3.1 the most important factors influencing the weighing results and the accuracy of the measurement are classified in the two groups as outlined above with additional subclassification according to their origin:

Instrumentation Errors		*Dynamic Effects Errors*		
System	*Environment*	*Vehicular*	*Roadway*	*Environment*
Nonlinearity *Hysteresis* *Freq. Resp.*	*Temperature* *Moisture* *Dirt, Ice*	*Speed* *Acceleration* *Laden Weight* *Suspension* *Tyres* *Load distrib.* *Aerodynam.* *Wheel unbal.*	*Road profile* *Sensor level* *Crossfall* *Slope* *Curvature*	*Wind* *Temperature* *Ice*

Table 3.1 Factors influencing WIM system accuracy.

The practice has shown that the contribution of dynamic effects errors to the overall measurement error is significantly greater than that of the instrumentation. A series of tests with a capacitive mat system – [13], [14], have shown that only 10% of the overall error is due to instrumentation inaccuracy as opposed to more than 70% due to dynamic vehicle effects.

A clear distinction should be made, however, as to whether the measurement is aimed at obtaining the true static axle weights, or the dynamic loading of the pavement imposed by the wheels.

3. 6 PURPOSE OF MEASUREMENT CONSIDERATIONS .

As it was pointed out earlier in dynamic vehicle weighing measurands of interest can be either:

- Static (true) vehicle weight;
- Dynamic loads imposed on the pavement.

Both of them have to be derived from the same system input – the dynamic wheel forces transmitted to the sensor in the moment of contact. The different interpretation of the input signal dictates different approach to accuracy problems and the potential sources of measurement error.

3. 6. 1 True Vehicle Weight Measurement.

When the static weight is being measured the dynamic components of the input signal will appear as a noise and lead to errors. What is more, the dynamic effects normally comprise the largest share in the overall measurement error, to a large extent explaining the relatively poor accuracy of these systems compared with static scales. While weighing errors of 0.5% and less are standard requirements for static scales, accuracy of less than 5% is very difficult to achieve even for slow speed dynamic weighers.

To approximate static wheel loads it is necessary to minimise all effects except for gravity. The roadway factors can be controlled within a reasonable extent. Selection of sites with smooth surface, or adequate resurfacing prior to installation can help avoiding excessive vehicle vibrations on the scale. Careful installation and maintenance of the equipment and above all good scale levelling will eliminate sensor induced vibrations. Speed as well as braking/acceleration restrictions may be imposed to reduce oscillations and eliminate interference of spurious wheel forces. Weighing period is increased in this way too, allowing for a

sufficient portion of the signal to be sampled for processing.

However, some vehicular factors are not that easy to control. These include parameters such as tyre inflation pressure, laden weight, suspension nonlinearity, spring stiffness, damping, wheel unbalance etc. These parameters vary from one vehicle type to another and sometimes even between equivalent vehicles. This will introduce difference in the dynamic response of the various vehicles to equivalent measurement conditions and therefore produce weight estimations of variable accuracy and hence reduced measurement reliability.

Experiments and practice – [17], [84], [150] show that dynamic weighings are generally most accurate for gross vehicle weights and deteriorating for axle and single wheel weights respectively. This can be explained with the error compensating effect which summing or other mathematical operations have on the individual wheel/axle results. Operations combining the results of parallel measurements usually eliminate errors due to uneven load distribution, longitudinal or lateral vehicle body motions, aerodynamic effects etc. Examples of accuracies achieved with a typical "platform" type WIM system for gross, axle and wheel weight measurements, respectively are given in Table 3.2:

Measurement	*Expected Accuracy with respect to static weight – [%]*
Gross Vehicle Weight	*± 5. 8*
Axle Weight	*± 10. 8*
Wheel Weight	*± 13. 6*

Table 3.2 Results of Accuracy tests of a "platform" type WIM system. ***(From Ref. 91).***

3. 6. 2 Dynamic Load Measurement.

If the system, however, is to be used for estimation of the actual dynamic wheel loads *(static+dynamic)*, regardless of how they could vary from the static

weight, a different approach has to be applied towards dynamic vehicle effects. They are now part of the measurement and therefore should not be considered an error contributing factor. As the results are usually provided in statistical form, a measure of accuracy will be their representativeness, i.e. their closeness to the real pattern of pavement loading. This will depend on the one hand on the capability of the equipment to measure instantaneously applied vertical forces, i.e. on the instrumentation accuracy, and on the other – on the absence of any factors which could cause some systematic bias in the wheel forces of the vehicles.

3. 7 SOURCES OF DYNAMIC WHEEL FORCE BIAS.

Statistical processing of multiple dynamic weighings has shown that the results exhibit Gaussian distribution centred around the static weights of the measured vehicles, [74], [135], [150]. This allows a realistic estimate of dynamic road loading to be obtained from the PDF of a population of measurements on a given stretch of the road system, and also contributes to the reliability of individual weighings. Any source of bias in the dynamic vehicle forces therefore will cause a shift in the population mean and introduce systematic error in the estimates. The following factors have been identified as some of the potential sources of dynamic force input bias:

- **Roadway:** Typical examples are road crossfall, road curvature, slope, surface irregularities ahead of sensor, etc;
- **WIM equipment:** Typical examples of equipment induced bias factors are: protruding and/or unlevelled sensor, peak signal detection, road surface temperature, atmospheric pressure, moisture etc;
- **Vehicular:** Asymmetric dynamic wheel forces can be caused by suspension nonlinearities, wheel unbalances, crosswinds, etc.

3. 7. 1 Roadway Bias Factors.

These are usually due to unsuitable siting of the WIM installation, and/or poor preparation of the track preceding and immediately after the sensor. The

consequences are shift in the vehicle load distribution and asymmetric suspension excitation.

3. 7. 1. 1 Road Crossfall. The sensor configuration of some low-speed WIM systems provide for measuring only single wheel loads hence full axle weights have to be deduced by doubling the result. This technique assumes equal distribution of load between the two wheels and any lateral road slope, (crossfall), in the vicinity of the sensor will lead to systematic errors. Most such systems measure the nearside wheel loads which due to the natural road crossfall will tend to be overestimated as a result of vehicle tilt and corresponding shift in the centre of gravity of the vehicle. Crossfall measurements at 17 of the TRRL sites has produced a mean slope of 1 in 42, [91]. This has been calculated to give a weight transfer of approximately 5% on to the nearside wheels.

The effects on statically measured wheel loads of tilting vehicles or raising individual wheels and axles has been described in [112]. The results show that for rigid vehicles, side tilts of up to 160 mm cause less than 10% error in statically recorded weights. However, for articulated vehicles, errors in excess of 20% have been observed for the same tilt. In all cases there appears to be little dependence of the size of the error on the magnitude of the tilt.

The survey of existing WIM systems revealed that the majority installations measured the full axle weight. The few single wheel weighers mostly belonged to quazi-static, off-road systems specially prepared to ensure the horizontal positioning of the vehicle in all planes. It is therefore unnecessary to consider road camber/crossfall as a potential error factor in high speed vehicle weighing.

3. 7. 1. 2 Road surface quality. Road surface undulations in the area immediately adjacent to sensor will excite vehicle suspensions and bring about unwanted dynamic noise in the measured forces. Surface irregularities preceding sensor in the direction of travel will directly increase vehicle vibration amplitudes, whereas irregularities situated immediately after sensor platform will excite front wheel axles and vibrations will be transmitted through suspension and body to rear axles. A theoretical investigation into the magnitude of dynamic forces induced by road surface irregularities ahead of sensor is carried out in Ch.5.

3. 7. 2 WIM Equipment Bias Factors.

Poor sensor installation can induce considerable bias in suspension excitation and distort the measurements. A wrong signal detection or processing technique may cause readings bias either because of sampling the wrong part of the waveform, or using inadequate signal processing methods. Environmental factors such as temperature, pressure, moisture etc.. might affect the circuitry and introduce short term measurement bias.

3. 7. 2. 1 Sensor induced Impact Factor. Dynamic forces will arise when tyres hit the sensor when the sensor system, (e.g. loadcell supported platform, mat area sensor etc.), is not flush with road surface. These dynamic forces will be superimposed on the load signal, and will hence introduce weighing error. Raising the weighscale will lead to impact factors biased to >1, whereas "sunk" sensors will tend to underestimate the input. In each case the mean of a population of measurements will not be the static weight.

A computer simulation of an axle's passage over a step in the road (emulating the edge of a platform), was performed to evaluate the approximate magnitude of sensor impact factor errors. The impact factor generated by a sensing system of any step height h at moment of contact is:

$$IF_s = 1 + \frac{F_v}{W_s}$$

where F_v is the vertical force acting on the wheel and W_s is the static weight of the semiaxle. Expressions for the vertical velocity of the wheelcentre at the moment of impact were derived taking into consideration the enveloping properties of the tyre, (see Ch.3, Sect. 3. 4.). From there the equations for the vertical acceleration and force F_v were found and the following expression for the sensor induced Impact factor IF_s was arrived at:

$$IF_s = 1 + hd$$

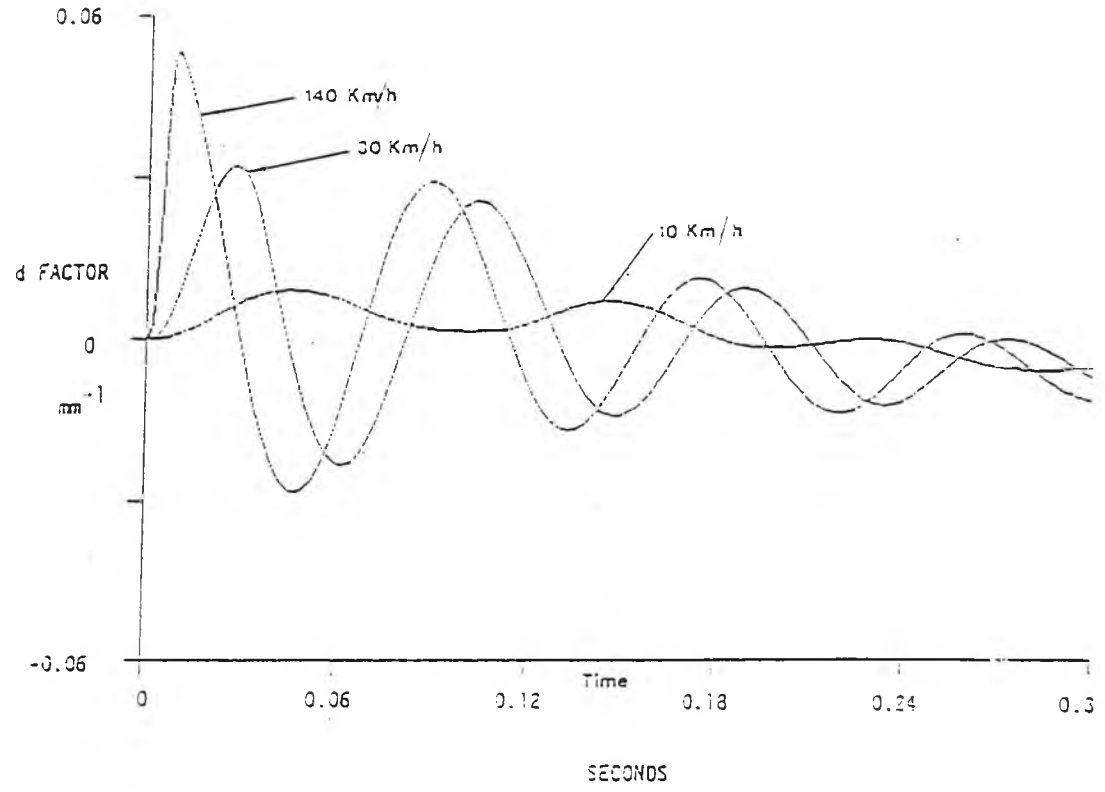

(a) Fully Laden Vehicle

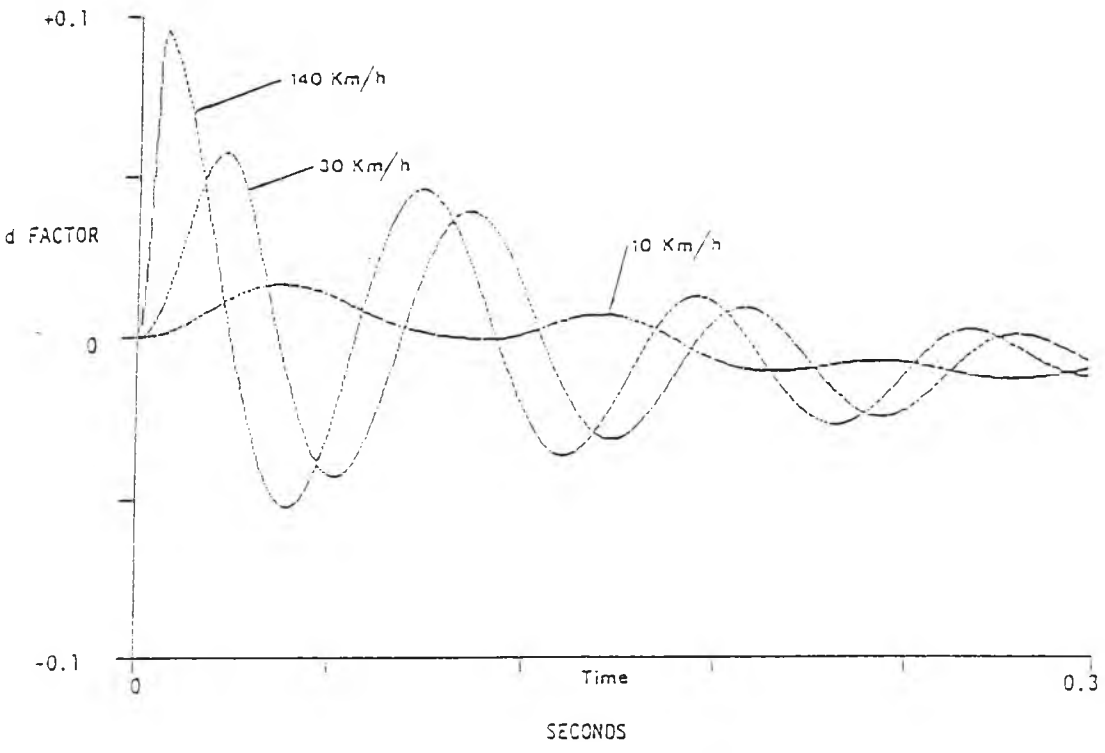

(b) Half Laden Vehicle

Fig.3.2 Dynamic Factor curves: $h = 10mm$.

where h is the step height in mm, and d is the following expression:

$$d = \frac{\pi^2}{2T^2} \cdot \sin\pi\left(\frac{t}{T} - \frac{1}{2}\right)$$

where $T = \frac{l_t}{U}$ is the time it takes the vehicle to travel its tyreprint length. Some computer generated plots of d for different vehicle speeds are shown in Fig. 3.2 (a), (b). For a step height of $h = 10$mm and fully laden vehicle - Fig. 3.2(a), the graphs indicate an impact factor IF ≈ 1.5 at 140km/h. Fig. 3.2(b) shows that the impact factor increases as laden weight is reduced. Impact factor values are significantly reduced at low speeds. In Figures 3.3(a),(b) the relative occurrence of the peak impact factor along sensor platform is shown. The heavy lines indicate the expected variation of the sensed signal during the residence time over a platform of length $l_s = 0.5$m. Fig. 3.3(a) applies to high speed signals (greater than 60 km/h) and Fig. 3.3(b) - to low speeds (less than 60 km/h). All the results are for an area type sensor which will always support a complete tyre print.

For a line type sensor (piezo cable, capacitive strip) the tyre will tend to envelop the sensor so impact factors will be reduced. When the sensor cable is buried into the pavement, (like some piezo cable installations) dynamic effects due to tyre-sensor interaction will virtually be absent.

Since the results are taken from a theoretical investigation they ought to be used only as an approximate guide. However, other theoretical [2], [30] and experimental studies [74], [116], [150] have reached similar conclusions. Some more detailed investigations into tyre enveloping effects as well as impact factors caused by road irregularities of common shapes were carried out in this study and are described later.

In general the results indicate that sensor induced impact factor is a major error contributing factor and that good sensor levelling is essential for a reliable measurement.

3. 7. 2. 2 Peak signal detection. Peak detection WIM systems incorporating line sensors, or the "broken bridge" area type sensor [128], can be used to measure instantaneously random values of the dynamic wheel forces. In

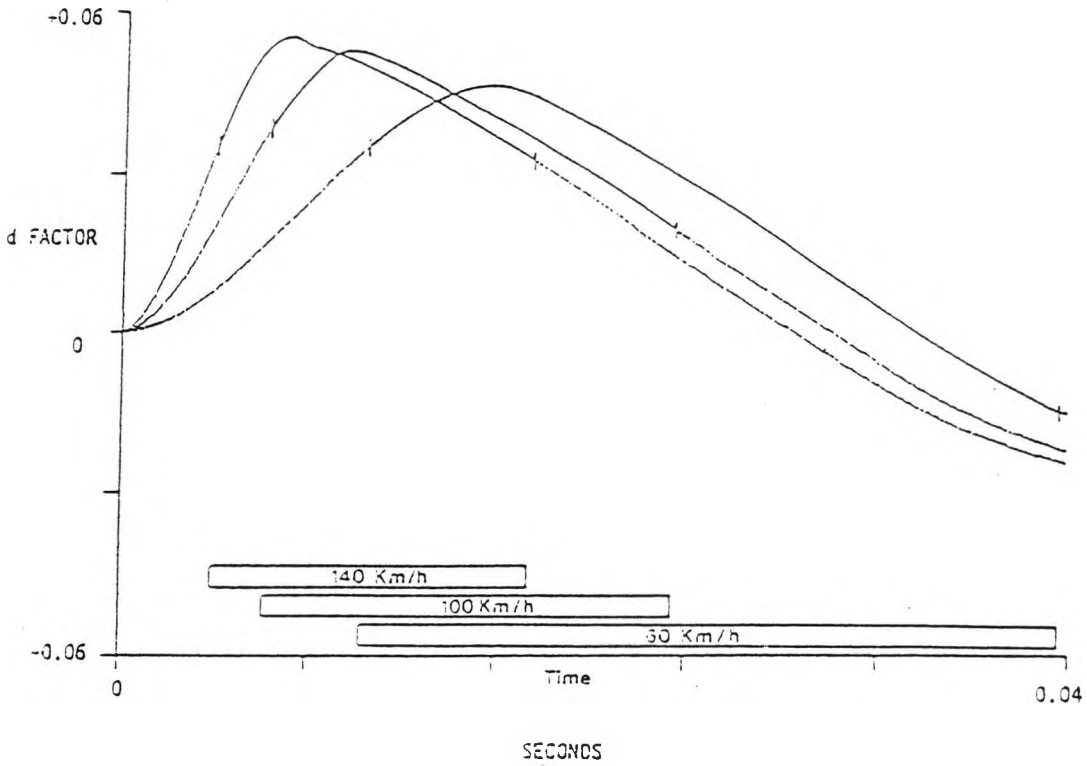

(a) High Speed transits

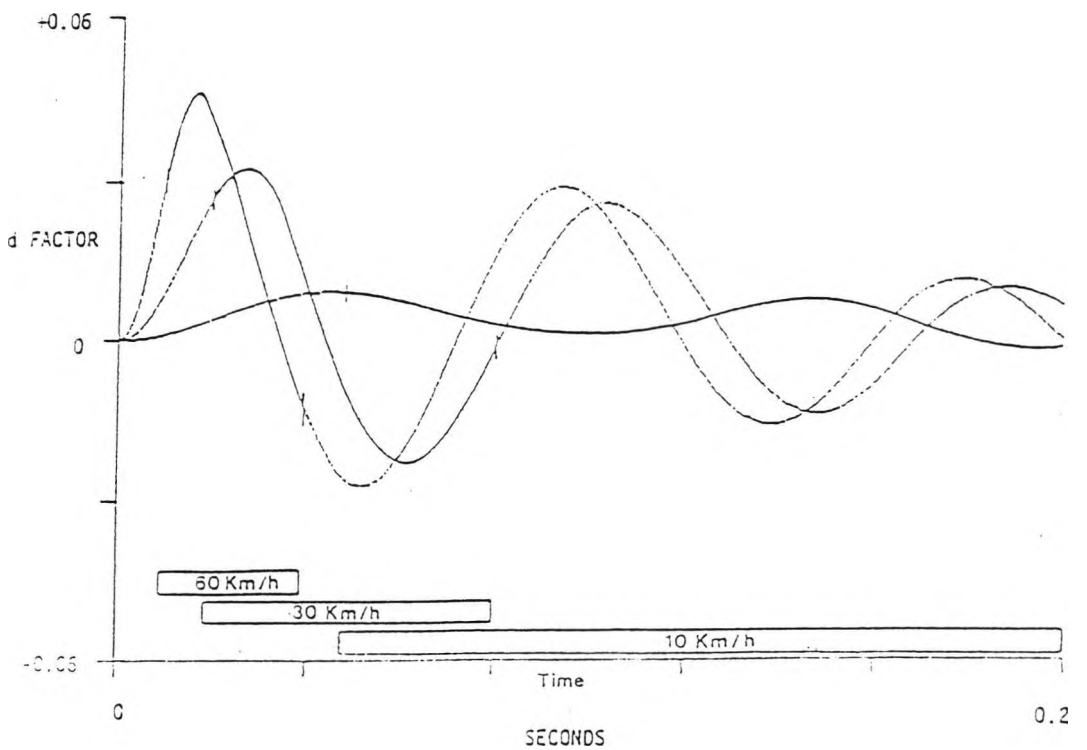

(b) Low Speed transits

Fig.3.3 Dynamic Factor curves and Area sensor positions: $l_s = 0.5m$

the absence of systematic bias and provided the distribution of the dynamic forces around the static weights is Gaussian, a representative estimate of the pavement loadings can be obtained in this way. However, peak signal detection can lead to considerable correlation errors, even if the population mean is not biased by any other factor.

a) Line sensors: For line sensors an error arises because tyre print area is dependent on laden weight, (see 1.6.2, Eq.1.4). Studies of tyre print areas [82], show that as laden weight increases, so does tyre print area with the width of the tyre b_t remaining almost constant, but the length l_t increasing. Since the ideal line sensor output, (Fig1.2) is proportional to the product $p_t x\, b_t$, and if we assume uniform pressure $p = W/l_t \; x \; b_t$ under tyre print then:

$$\textit{Peak sensor signal} \;\propto\; \frac{W}{l_t}$$

However, the proportionality will not hold when l_t does not stay constant with varying load. Depending on tyre inflation pressure l_t can change by as much as 50%, so the errors in assuming the peak signal as a measure of vehicle's weight can be quite large. As it was proved in Ch.1 this error will not arise if the sensor signal area rather than peak is used.

b) Area sensors: For area type sensor systems, (weighbridge platforms, pads etc.) the weighing period can cover from just a fraction of the signal's cycle to a number of cycles – Figs 2.9(a),(b), Figs. 3.3(a),(b). Peak signal detection could then lead to correlation errors as large as the peak amplitude of the vibrations.

To derive the statistical error due to peak signal detection ϵ_p we adopt a single frequency model for the dynamic wheel force transmitted to sensor platform:

$$W(t) = W_s + \; a.\sin(\omega t + \theta) \qquad (3.1)$$

where:

$\omega = 2\pi f$ and f is the wheel hop or body bounce frequency of the vehicle;

θ – phase angle, (angle of incidence);

W_s – vehicle static weight;

$1 \pm a/W_s$ – min/max peak impact factors.

As an axle passes over an area sensor a snapshot of the sinusoidal signal (Eq. 3.1) is taken during residency time T_r :

$$T_r = \frac{l_s - l_t}{U},$$

which is strongly dependent on the speed of the vehicle U, the characteristic vehicle vibration angular velocity ω, and the sensor and tyreprint lengths l_s, l_t respectively.

The vehicle dynamics period is $T_d = 2\pi/\omega$, so we can define a ratio of times:

$$\frac{T_r}{T_d} = \frac{1}{2\pi} \cdot \frac{(l_s - l_t).\omega}{U} = \frac{1}{2\pi} \cdot \bar{l},$$

where $\bar{l}$ is a dimensionless normalised length and:

$$\bar{l} = \frac{(l_s - l_t).\omega}{U}, \qquad (3.2)$$

or:

$$\bar{l} = 2\pi . \frac{T_r}{T_d}$$

It is assumed that each axle in a population encounters the sensor at a random phase angle θ, so that the sinusoid in Fig. 3.4(a) is effectively sampled randomly.

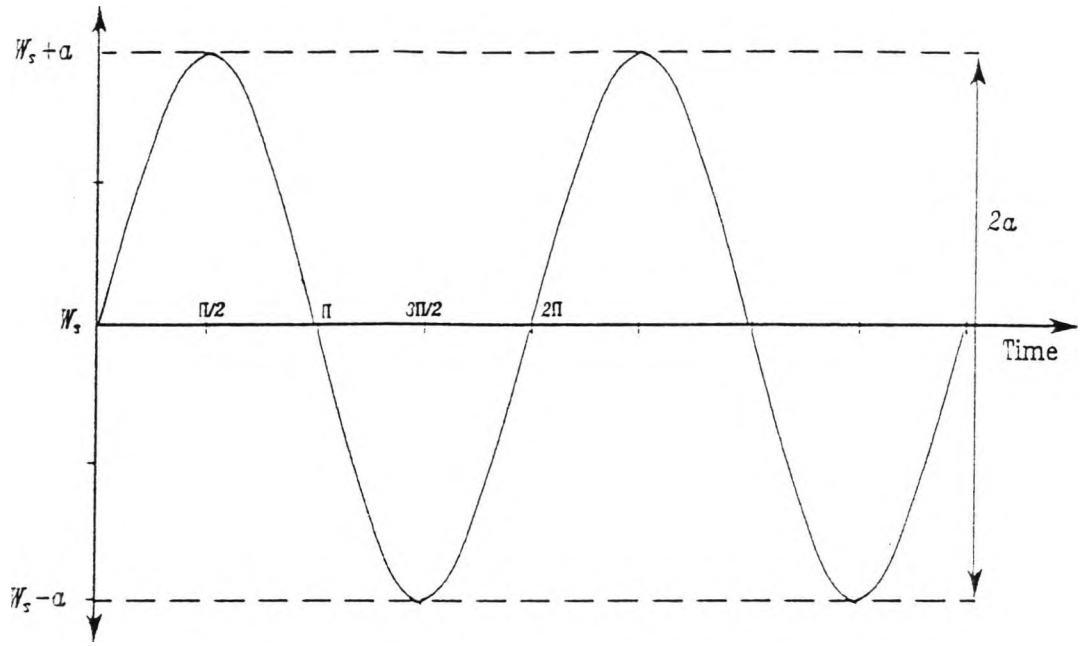

(a) Single Frequency Sinusoid signal

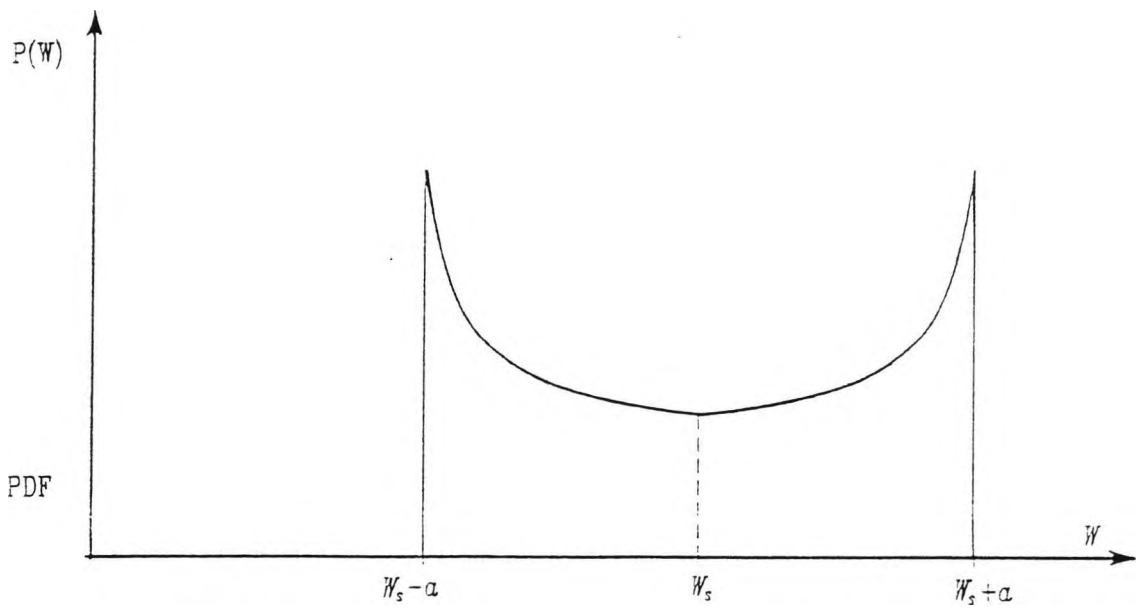

(b) Probability Density Function

Fig.3.4 Single frequency Dynamic Weight signal sampling.

Errors due to peak signal detection can be illustrated by two extreme cases:

(i) $\bar{l} \geq 2\pi$;
(ii) $\bar{l} \simeq 0$.

When $\bar{l} > 2\pi$ the vehicle axle will go through at least one complete cycle while the tyre is on the sensor platform. Peak detection will always pick up $(W_s + a)$, so the population correlation error will be:

$$\frac{\textit{Population Mean} - \textit{Static Weight}}{\textit{Static Weight}} = \frac{(W_s + a) - W_s}{W_s} = \frac{a}{W_s}$$

The PDF for this case would be a *Dirac* delta function located at $(W_s + a)$.

When $\bar{l} \ll 2\pi \simeq 0$ there will be no sampling bias and the PDF for a randomly sampled sinusoid will be produced - Fig. 3.4(b), with the mean $W_m = W_s$, so there will be no correlation error.

We now consider the intermediate case $0 < \bar{l} < 2\pi$. Fig. 3.5(a) shows the waveform of the peak detected signal as $\bar{l}$ is moved through the dynamic signal waveform. This will lead to the PDF shown in Fig. 3.5(b). To find the mean W_m for varying $\bar{l}$ the equation for the peak detected signal is required. In the range $\pi/2 < x < 3\pi/2$ it will be:

$$W_p = W_s + a \qquad \text{for} \qquad \pi/2 < x < \pi + \bar{l}/2$$

$$W_p = W_s + a.\sin(x - \bar{l}/2) \qquad \text{for} \qquad \pi + \bar{l}/2 < x < 3\pi/2$$

The probability that W_p lies between W_p and $W_p + dW_p$ is given by dx/π, where dx is the x intercept interval. The population mean W_m is therefore:

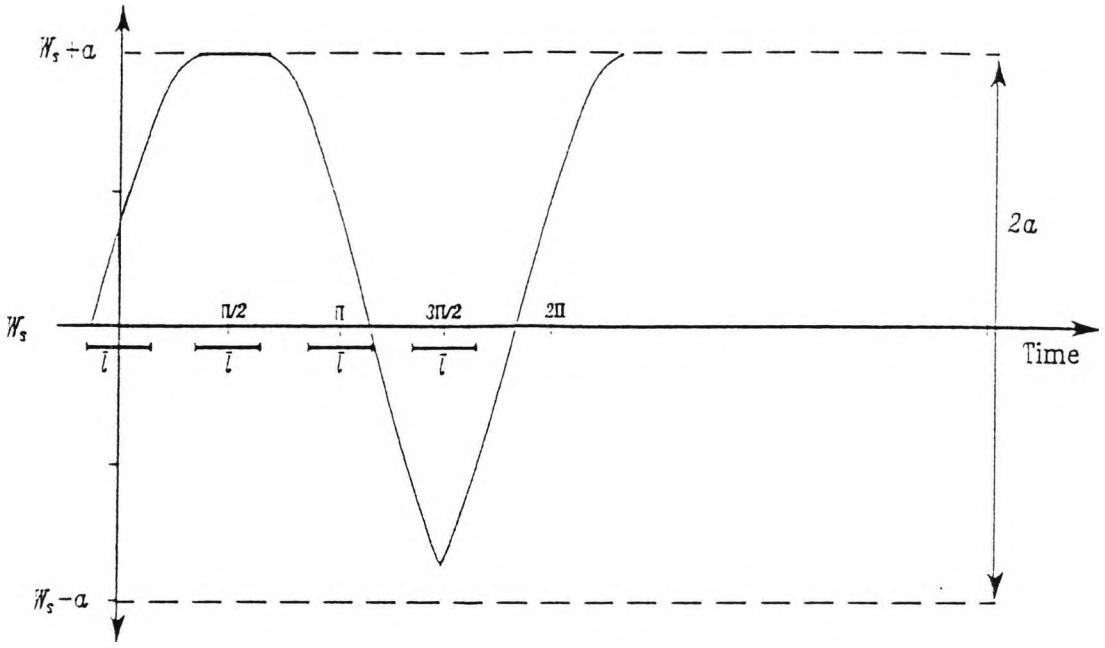

(a) Peak detected signal as a function of Sensor position

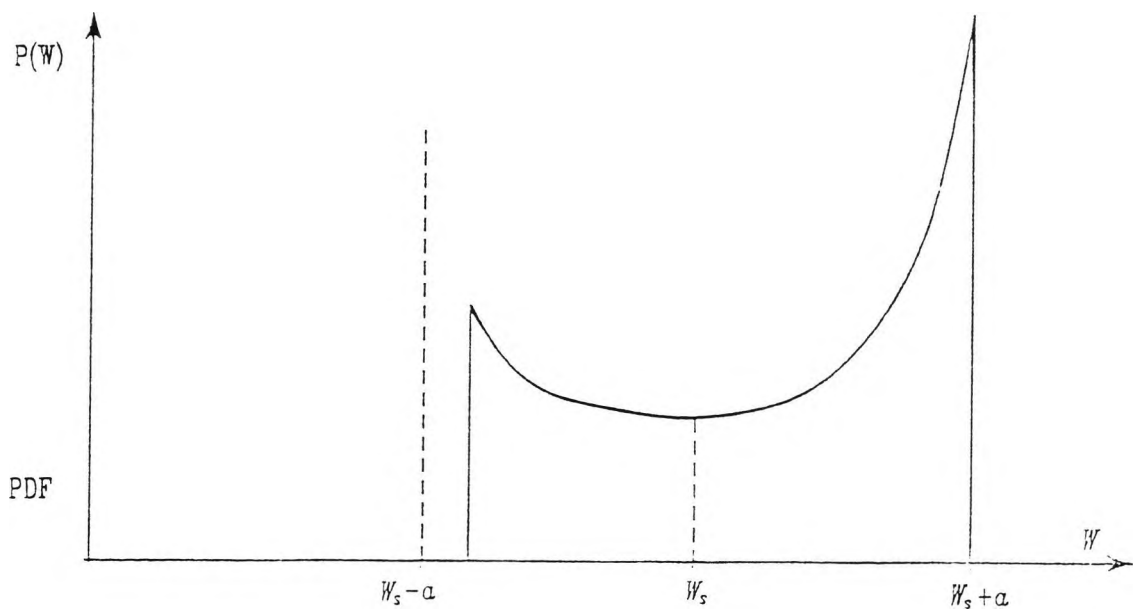

(b) PDF for a Peak detected signal

Fig.3.5 Correlation Error due to Peak Signal Detection.

$$W_m = \int_{\pi/2}^{3\pi/2} \frac{W_p}{\pi} . \, dx$$

$$= \int_{\pi/2}^{\bar{l}/2+\pi} \frac{(W_s + a)}{\pi} . \, dx + \int_{\bar{l}/2+\pi}^{3\pi/2} \frac{[W_s + a.sin(x - \bar{l}/2)]}{\pi} . \, dx$$

$$= W_s + \frac{a}{\pi} .[\bar{l}/2 + sin(\bar{l}/2)]$$

The population correlation error:

$$\epsilon_p = \frac{W_m - W_s}{W_s} ,$$

$$\epsilon_p = \begin{cases} \frac{a}{\pi . W_s} .[\bar{l}/2 + sin(\bar{l}/2)] & \text{for} \quad 0 < \bar{l} < 2\pi \\ \frac{a}{W_s} & \text{for} \quad \bar{l} \geq 2\pi \end{cases} \qquad (3.3)$$

It was shown earlier, (See Ch2., 2.4.2), that for most sensor platforms a complete vibration cycle can be accommodated only at vehicle speeds lower than 20km/h, and that is only for the wheel hop vibration, which has the shorter T_d. The case therefore, when $\bar{l} > 2\pi$, $(T_r > T_d)$ will only apply at very low measurement speeds, i.e. quasi-static WIM systems.

Assigning realistic values to the parameters and substituting in equations (3.2) and (3.3), the probable correlation errors arising from peak signal detection can be determined for typical WIM conditions. For the TRRL weighbridge $l_s = 0.6m$. A typical tyre print length value for an HGV is $l_t = 0.25m$. Then:

$$I = \frac{0.35.\omega}{U}$$

A vehicle speed of 80km/h = 22m/s was found to be representative for commercial vehicles traversing WIM sensors. The results of the experimental studies carried out by Leonard et al [74] show that for a number of HGVs travelling on a motorway class roads at different speeds (from 30 km/h to 80 km/h), Impact factors vary from 0.75 to 1.25. This corresponds to a value of 0.25 for the a/W_s ratio, which was used in the calculations.

The correlation error was then determined for the ***body bounce*** frequency of the standard TRRL vehicle $f_b = 1.67Hz$, which is representative of HGV body oscillation frequencies, and was shown to dominate the frequency spectrum of vehicle vibrations especially when fully laden. The value of $\epsilon_p = 0.0068 \simeq 0.7\%$ was obtained, showing that at such low frequencies when the waveform does not change substantially during the weighing period T_r, peak signal detection leads to relatively low population bias.

The same calculations were performed for the higher frequency of ***wheel hop*** oscillations $f_w = 11.7Hz$, and a value of $\epsilon_p = 0.0905 \simeq 9\%$ was obtained. The latter result shows that if peak signal sampling is applied to wheel hop vibrations a substantial bias will appear in a population of measurements due to the relatively large signal changes during the weighing period. Bias might increase at lower measurement speeds of travel and with unladen vehicles where the effect of wheel hop is more pronounced.

3. 7. 3 Vehicle dynamics Bias factors.

Asymmetric dynamic behaviour of the weighed vehicle will induce uncharacteristic wheel forces which will be transmitted to sensor and cause errors.

3. 7. 3. 1 Nonlinear vehicle suspensions. To illustrate this factor we consider the case of a linear suspension vehicle where no error would arise. The dynamic load $W(t)$ is again reduced to a single frequency oscillation about the static weight W_s, (Eq. 3. 1, Fig. 3.4(a)), and for the peak Impact factor we have:

$$IF = 1 \pm a/W_s$$

Assuming that each axle transit over the weighscale will have a different and random phase angle θ, then effectively the sinusoid will be sampled at random leading to the PDF plot shown in Fig. 3.4(b). When the PDF has no bias the population mean will equal the static weight, (correlation error = 0):

$$W_m = W_s$$

However, suppose the suspension is non-linear, or in some other way clipping occurs on the sinusoid - perhaps suspension "bottoms" - Fig. 3.6(a). This will lead to a shift of the mean from the static weight:

$$W_m \neq W_s ,$$

which can be seen from the resultant PDF graph in Fig. 3.6(b). That shift will introduce correlation error in the population of measurements.

These considerations are confirmed in a study of HGV suspension non-linearities effect on dynamic pavement loads [73], where experimental data from three typical HGV suspension systems are compared with one idealised linear model. The three suspension types have different degrees of divergence, (spring hardening rates) from the ideal linear spring load-deflection curve. Wheel load Power Spectral Density (PSD) curves showed that ***body bounce*** vibration of the vehicle is the predominant contributor to dynamic wheel loads, (see Fig. 2.5). The effects of suspension non-linearities are illustrated by comparison of the PSD curves of the wheel loads for the three suspension types. The maximum values of the PSDs are also plotted against vehicle speed. The results reveal the substantial variations in wheel load distributions with different degrees of

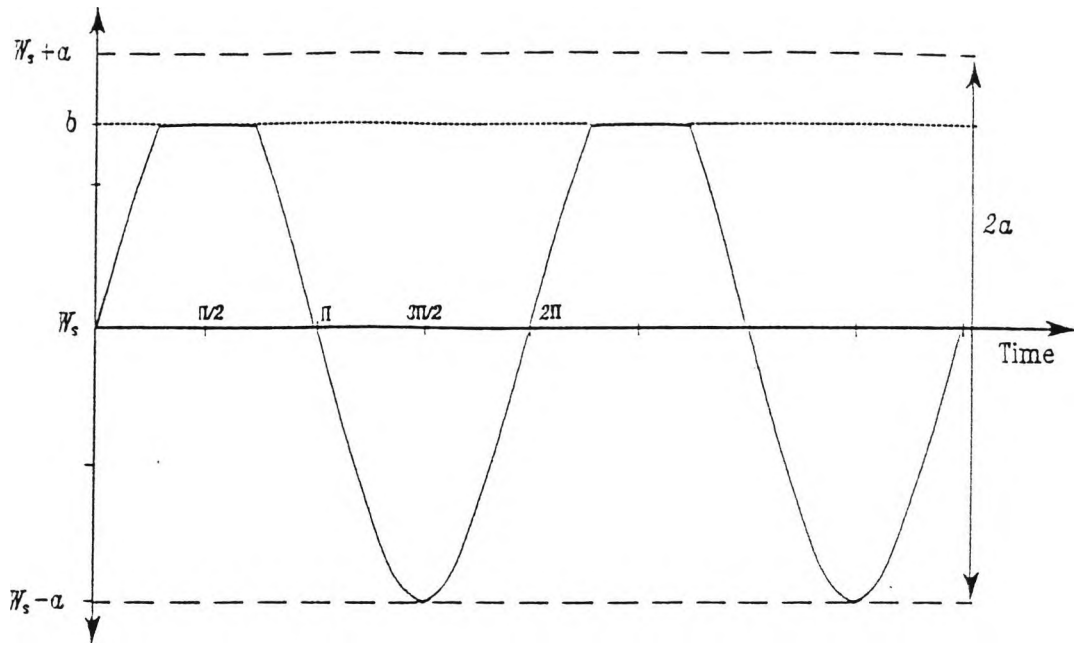

(a) Dynamic Weight variation

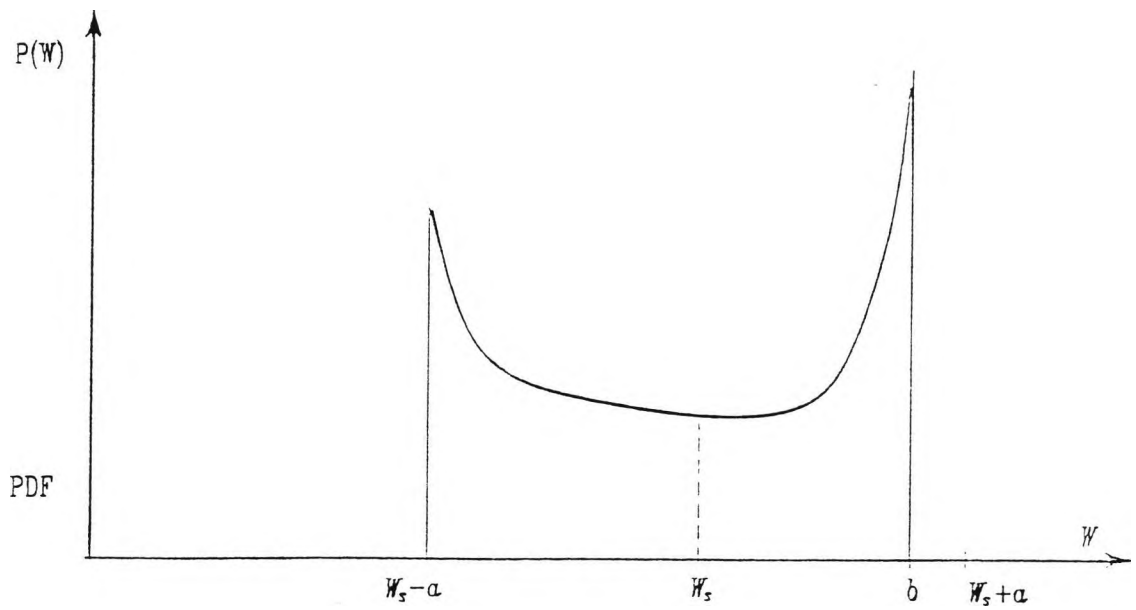

(b) PDF for a Non-linear suspension signal

Fig.3.6 Correlation Error due to Non-linear Vehicle Suspensions

suspension non-linearities, as well as the detrimental effect of progressive spring hardening on pavement loading.

3. 7. 3. 2. Wheel Eccentricity. Loads related to wheel rotation are another source of population bias. These vehicle generated forces are usually due to wheel imbalance associated with tyre deformity or rim assembly runout. Dynamic force records of unbalanced wheels show sinusoidal load variations with frequency corresponding to wheel angular velocity, [150]. Power Spectral Density analysis confirms the presence of several orders of wheel rotation frequency in the signal. Simple calculations for a HGV type tyre shows that the first order rotation frequency will coincide with body bounce frequencies for vehicle speeds in the range from 10km/jh to 35km/h. That is confirmed by experimental results presented in [150] showing excessive load variations for a speed of 32 km/h then gradually decreasing. The wheel hop resonance frequency remains out of the frequency range of wheel rotation and is approached at speeds higher than 140km/h.

3. 8 METHODS FOR IMPROVING WIM ACCURACY.

The main reasons for the limited accuracy levels which can be achieved when true static weights are sought, were found to be the dynamic character of the input signal and the short measurement period. These features are inherent to the method and they can only be overcome if some radically new approach is adopted for wheel force sensing and signal processing.

3. 8. 1. Multiple weighing sensors.

The use of long weighing platforms or multiple weigh transducers appears to be a possible solution, effectively extending the weighing period or increasing the number of gathered samples. The signal record obtained in this way will be of sufficient length to ensure that the filtered DC value should be much closer to the true static weight of the vehicle. An array of TRRL type platforms was used by Leonard et al [74] in their experiments to obtain continuous records of

dynamic wheel forces of commercial vehicles.

In another study, [44] the authors used 4 successive variably spaced dynamic scales to analyse the effect of multiple sensing on weighing accuracy. It was shown that accuracy gradually improved when considering the outputs of higher number of scales.

A multiple sensor installation used for high-speed weighing of railway cars is described in [66]. A comprehensive signal processing algorithm brings the mean error down to less than 1% and measurement variances to within 2%.

3. 8. 2. Output correction techniques.

The significance of applying an efficient signal processing method for dynamic errors attenuation was illustrated in Ch.2, (see Sect. 2. 5. 3, Table 2.7).

It has long been recognised in the field of measurement that accuracy and speed of measurement are contradicting requirements. It is a fact that high accuracy instruments have their own long response time, and those with good response characteristics lack measuring accuracy in general. Applying modern estimation theory Ono et al, [103] use the transient sensor output data to analyse the signal characteristics, thus reducing the measurement period length without sacrificing measurement accuracy.

Another method aimed at improving dynamic weighing accuracy takes account of the influence of vehicle speed on the weighing result. In most of the cases this would require the installation of a dedicated vehicle speed detector. Auxiliary speed measurements are taken at some WIM operations, and it was shown that vehicle speed information is essential if reliable line sensor measurements are sought.

Based on a series of preliminary tests the designers of the Saskatchewan scale, [53] have reached by regression the following a correction expression:

$$W_s = A + B \times \underline{Speed} + C \times \underline{Measured\ weight}$$

The obtained accuracy ranged between 12% and 2.5% respectively at the bottom

of the scale (tandem axles of 20 kN) and at the top of the scale (tandem axles of 80 kN).

A similar correction formula, though slightly more complex because it takes into consideration a number of influencing factors, was developed by the Danish Road Administration and used on their "Vibracoax" systems:

$$W_s = a + b.D + c.U + d(A) + e(V) + f(T) + g(L)$$

where: D - Measured dynamic load;
U - Vehicle Speed;
A - Number of axles, (1 to 3);
V - Vehicle types, (1 to 9);
T - Scale type, (1 or 2);
L - Traffic lane, (1 or 2).

Reported accuracy is ± 8kN in the 0 to 150kN range, i.e. $\pm 5\%$ of full scale.

3. 9 CONCLUSIONS.

The practice of true static weight measurement has shown that errors induced by dynamic vehicle effects constitute by far the greatest part of the overall measurement error. Road surface roughness, sensor levelling, vehicle speed and its physical parameters were identified as the main factors in the measurement environment that affect the dynamic behaviour of the vehicle and hence weighing accuracy.

When the true dynamic loads are the measurand of interest the results can be distorted by a number of roadway and vehicular factors which introduce systematic bias in the forces applied to the sensor.

It was concluded, therefore, that vehicle interaction with road surface and the sensor system in particular is of primary importance for the accuracy of the

obtained results in both types of measurement.

A detailed theoretical study into some aspects of the dynamic interaction between vehicle and road/sensor was undertaken by means of computer simulation. Mathematical models were created of vehicle tyre/suspension systems as well as of road profiles of deterministic nature. Vehicle runs were simulated for different conditions and quantitative data of expected dynamic errors were obtained. The influence of specific roadway and vehicular parameters was investigated and the corresponding conclusions were drawn which may be used by WIM system designers as well as in pavement loading studies.

Chapter IV: WIM System Mathematical Modelling.

INTRODUCTION.

The simulation of vehicle road interaction is normally preceded by the definition of the physical and mathematical models which behave analogous, (or at least similar) to the real system. Mathematical models are problem dependent, i.e only those motions of a vehicle have to be considered which are of importance for settling a specific design problem. The main advantage of the simulation software is its ability to generate, synthesise and finally solve the overall system equations from the model. Vehicle-road interaction modelling requires on the one hand a representative and validated vehicle model suitable for the intended simulations, and on the other – some mathematical representation of the road surface describing the irregularity with the desired shape and dimensions. The derivation of these models and the theory behind them is discussed in the following Chapter.

At first the theoretical background of physical system modelling is explained and the two main approaches in modelling are introduced. A detailed survey follows of existing mathematical vehicle models used by other authors in vehicle-road interaction studies. After a critical analysis of their qualities, a quarter-vehicle model is found to be adequate vehicle representation for the objectives of this study. The system equations are derived using the Bond graph methodology and model input formulation is defined for a common type of surface irregularity. Special attention is dedicated to pneumatic tyre modelling as it poses serious problems in finding the best compromise between realistic emulation of the tyre's elastic enveloping properties and the model's simplicity. Several types of existing tyre models are introduced and a new model is developed best suited for Bond graph modelling.

A computer modelling package is then introduced which has been used in some of the current dynamic vehicle modelling. The background of graphical simulation techniques is explained and some of the methods described. Finally the quarter-vehicle suspension model and its input/output representations are defined in the graphical environment as used in the subsequent simulations.

4. 1 MODELLING METHODOLOGIES.

Two approaches are presently being used to analyse and predict the response of vehicles traversing road surfaces of different profiles. Although inherently different in model representation, the nature of the computed results, computation times etc., each of them can provide valuable information on vehicles' behaviour.

4. 1. 1. Time Domain Modelling.

This technique simulates the dynamic response of the vehicle as a function of time. A set of differential equations is used to describe the vehicle system and the inputs are normally of deterministic character - i.e. step, pulse, ramp etc. The physical system parameters, i.e. spring rates, damping coefficients, sprung and unsprung masses etc., are represented as coefficients of the independent variables. Time domain analysis allows the use of nonlinear vehicle parameters and is well suited for simulating nonlinear effects owing to spring and damper nonlinearities, bump stops etc.

Alongside with the standard control inputs the forcing functions used in time domain vehicle simulations generally consist of elevation variations of the road profile. These variations are normally deterministic variables in the time domain. They might be generated by a set of measured elevations along a given path, or by properly filtered ***white noise*** signal. Since the function is a deterministic variable, it can vary in either statistically stationary or nonstationary manner without affecting the validity of the simulation. A generalised illustration of time domain modelling is shown in Fig. 4.1 (a).

The basic method of solving the set of differential equations is through a series of numeric integrations performed on a digital computer. The resulting information is usually presented as a list of dynamic response values as a function of time, or the corresponding plots. Time domain simulation produces informative and accurate results but a great deal of time is normally spend on

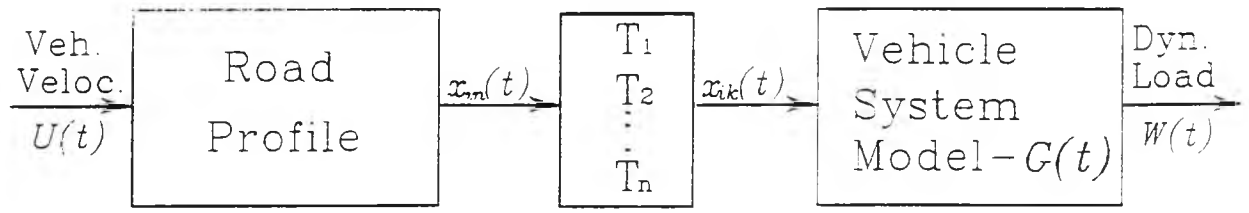

a) Time domain modelling

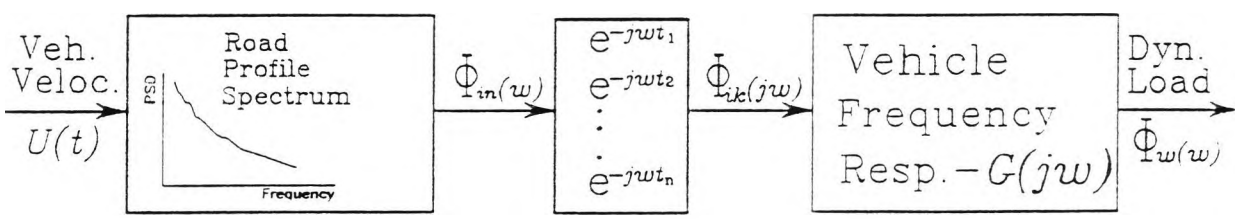

b) Frequency domain modelling

Fig.4.1 Mathematical modelling methods.

programming and running the simulation.

4. 1. 2. Frequency Domain Modelling.

Frequency domain model analysis represents the vehicle system with a frequency response function or an algebraic expression with the frequency as the independent variable. The vehicle system equations are transformed to their frequency response functions by the use of the Fourier transform. [80]. Time to frequency domain conversion requires linear coefficients in the differential equations representing the system. The forcing function is described statistically in the form of *Power Spectral Density, (PSD)* estimate. The stages in frequency domain modelling are depicted in Fig. 4.1 (b).

The method reduces simulation time and gives the analyst immediate feedback on any parameter changes made. The method however has its limitations. Certain assumptions have to be made in transforming the system differential equations to their frequency response functions and in transforming the deterministic representation of the terrain profile to its PSD estimate. The requirement for linear representation of system parameters limits the scope of simulation to linear systems. The computation of the PSD of a random variable requires that the variable be statistically stationary which restricts the simulation to steady state analysis.

4. 2 SURVEY OF VEHICLE MATHEMATICAL MODELS.

Creating a meaningful mathematical vehicle model remains a basic engineering art. The development of a suspension model is guided by the problems it is meant to handle, the configuration of the modelled vehicle, and the available mathematical tools. It is also important that the models are created with user-friendliness in mind, i.e. easy to understand and providing simple model input/output interface with the operator.

A satisfactory accurate prediction of dynamic loads of vehicles on roads in the time domain was achieved by Cox et al [30] using a simple model without

tyre damping and spring Coulomb friction elements. The simulation results were compared to experimental records gathered with an on-board system, and generally tended to overestimate wheel loads with 5 to 10%. However, that was one of the first attempts in dynamic vehicle modelling, (reported 1941) and was done without using computers.

A more elaborate model was developed by Whittemore et al for the computation of the dynamic behaviour of a truck suspension system, [150]. The modelling technique was confined to computing pavement loads for the right rear wheel set only – a version of the commonly known quarter-vehicle model. The physical parameters of the vehicle were established from static laboratory measurements and dynamic testing of a standard goods vehicle. The ability of the tyre to envelop small irregularities and the complex non-linear stiffness and friction characteristics of a 3-leaf spring were simulated, but the model did not include tyre damping. Analogue computer techniques were used for two reasons:

(i) they allow convenient programming of non-linearities and time lags,

(ii) model parameter values can be varied easily to study the effect of each of them on the dynamic loads.

Through that model the effect of parameter variation was examined by simulating passage over 12.7mm high step on an otherwise smooth profile at a constant speed. Each parameter was varied in turn keeping the other parameters constant. The accuracy of the prediction technique was evaluated against measured pavement loads. A more detailed tyre description, and building a half-vehicle model, including wheel hop and axle correlation effects were pointed out as potential refinements of the model.

Page used a similar quarter-vehicle model to simulate the dynamic behaviour of a single axle vehicle suspension system, [106]. Unlike the previous author however, the inherent friction suspension damping was represented by a single term and the effect of the tyre enveloping was taken into account by modifying the profile of the step-shaped surface irregularity. The effect of that smoothing process is showed to disappear at high speeds suggesting that the height of the obstacle and not its shape is of importance at those speeds.

The same model was later used by Laker, [71], [72] in his study of dynamic loads applied by vehicle suspensions over computer generated road

profiles of different roughness. A non-linearity was introduced in the otherwise linear model allowing the wheel to leave the surface when the displacement difference of the road profile exceeded the tyre deflection.

Using a more sophisticated twin-axle model Page, [107], theoretically investigated the behaviour of two types of linked-axle tandem suspension commonly fitted to heavy vehicles. He proved that within a known range of speeds the models applied considerably greater loads than did the unlinked suspensions. It was also shown that such suspensions tended to be underdamped because of the absence of shock absorbers. Those conclusions were later confirmed by experiments with eight heavy vehicles performed at the Transport and Road Research Laboratory, [74].

In their survey of analytical tyre models, Captain et al [21] used a two dimensional six degrees of freedom model (DOF), of a 3-axle cargo truck. The model incorporated a variety of non-linearities: dry friction, bump stops and wheel-lift-off. Agreement between computed and measured spectral densities of axle accelerations was very good for the most sophisticated tyre model used.

In his theses Cebon, [23] investigated the dynamic interactions between wheeled vehicles and the road surfaces relating them to road damage mechanisms. A thorough experimental examination of heavy vehicle leaf-springs is carried out and it is proved that empirical equations can be used to describe adequately their behaviour throughout the frequency range of importance to dynamic wheel forces. A tyre model realistically emulating short wavelength irregularities envelopment was developed and compared to other existing tyre models. The conventional methods for deriving and solving the equations of motion of non-linear multiple degree of freedom systems were simplified and made more compatible with digital computation. As a result three models of increasing complexity were created of a rigid 23 ton fuel tanker. The simplest was a two dimensional $4-\mathrm{DOF}$ representation of a single point tandem bogie suspension. The second one was also two-dimensional, "pitch-bounce" half-vehicle model, but with 7 degrees of freedom. The most complex model was a three-dimensional, $14-\mathrm{DOF}$ representation of the whole vehicle. The simple two-dimensional models were found to be sufficiently accurate for the simulation of dynamic forces generated by particular wheels of the vehicle at frequencies above the sprung mass resonances. At lower frequencies however, only the complex

three-dimensional model provided adequate accuracy. Tyre filtering was recommended if slow vehicle speed dynamic simulations are to be carried out.

Newland, [98], Robson [122], Czerny et al [33], Kozin et al [65], investigated vehicle's response to random surface profiles by means of multi-input 2 and 3 – DOF vehicle models. The models used are normally linear as most of the simulations are carried out in the frequency domain. Kallenbach, [59] used multi-body formalisms to develop a 9 – DOF linear model of a passenger car for the purpose of identification of vehicle parameters.

Other authors [55], [64], [120], [127], have created even more sophisticated theoretical models of vehicles, taking into account the multitude of phenomena affecting their motion. However, simplified models solving only one or two aspects of the problem have been used widely by researchers and have proved their sufficiency in most of the practical cases.

4. 3 VEHICLE – ROAD INTERACTION MODELLING.

4. 3. 1 Suspension Model Selection.

The simple quarter-vehicle suspension model was used in this study to simulate suspension responses to different types of road irregularities. The derivation of the model and its parameters were described earlier in Ch.2, Section 2.3.3.

The choice of the model was motivated by the following reasons:

i) The half-axle model is the simplest vehicle representation still capable of producing good simulation results. The fact that it is a single dimension model makes its analytical description easier and suitable for the computer aided modelling formalisms used.

ii) Other authors have used variations of the model for wheel-load prediction with good results – [30], [72], [106], [150].

iii) Road tests, [150] have shown that:

• Vehicle longitudinal pitch motions do not contribute significantly to front or rear axle loads. Therefore front axle loads can be studied without considering rear axle effects and vice versa. Fig 4.2 shows the degree of typical front to rear axle interaction. The trials have shown that when abrupt obstructions are encountered at the front axle, simultaneous rear axle loads never exceed 2% of front axle loads. Moreover front axle loads occurring simultaneously with abrupt obstruction at the rear axle are never more than 5% of maximum front loads.

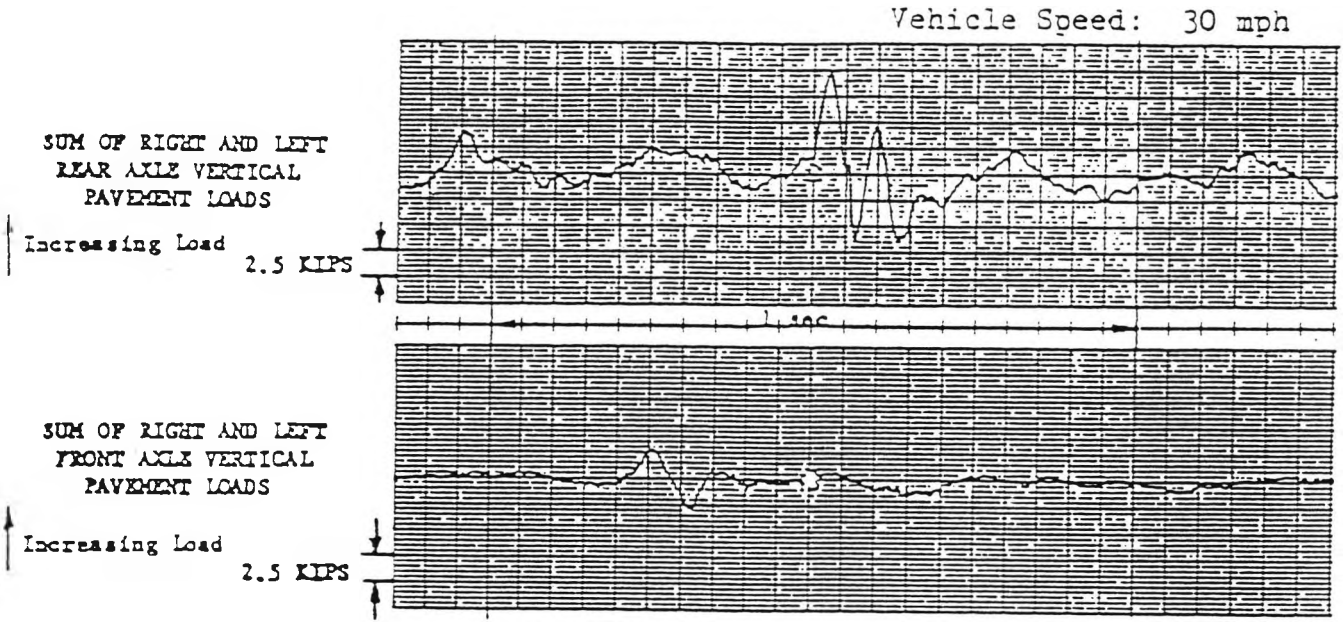

Fig.4.2 Simultaneous Front and Rear axle loads.
Vehicle Speed 30mph, [Ref. 133].

• Considerable degree of interference between different wheels of a single axle, (axle tramp coupling), has been observed suggesting that one side wheel loads are not always equal to half of the total axle loads. Left wheel dynamic forces measured when only the right wheels traversed an obstacle were typically 30% of the ones developed by the right wheel. Right wheel dynamic

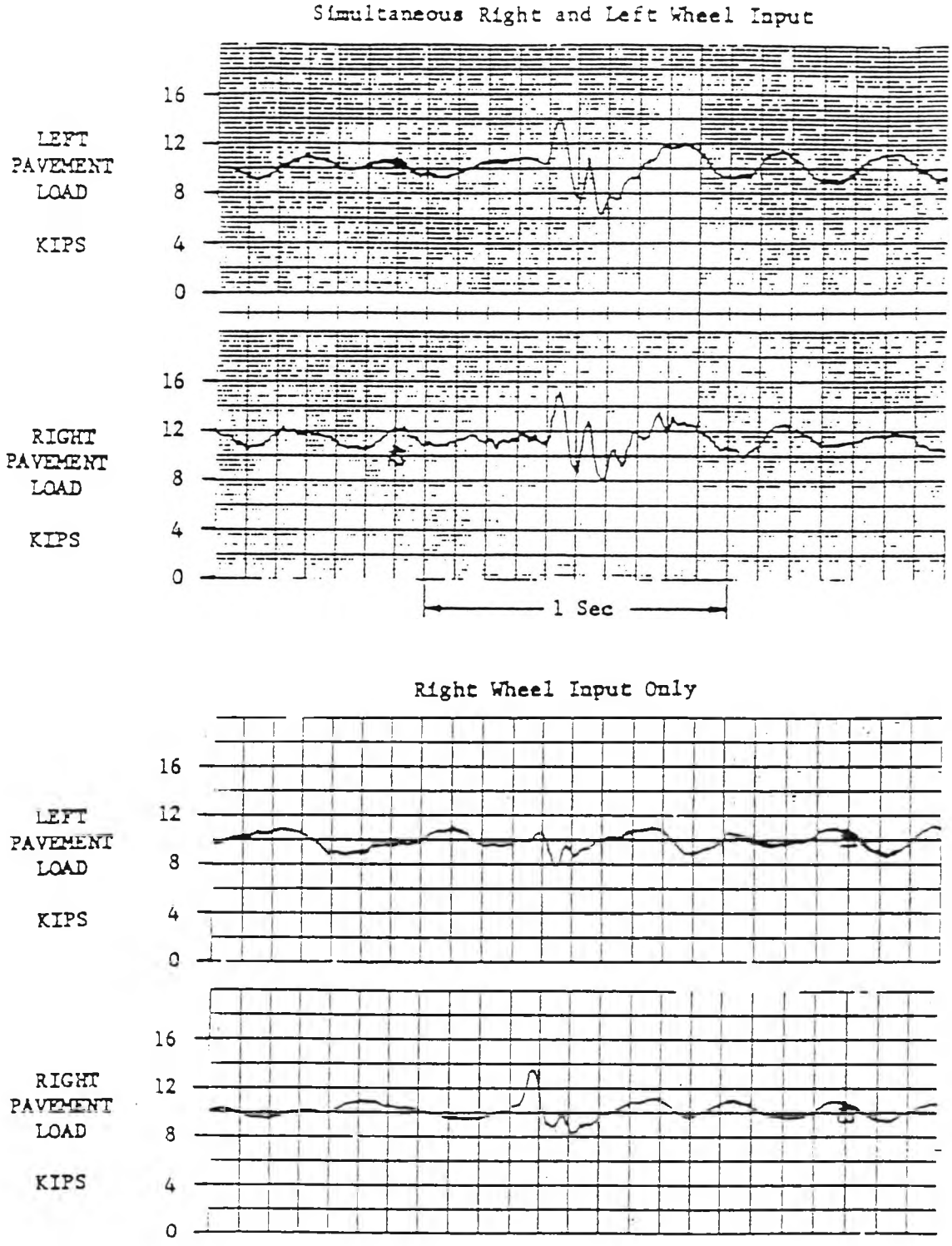

Fig.4.3 Inter-wheel load effects, (Tramp coupling).
Obstacle = 0.025m x 0.9m haversine bump, Vehicle Speed = 17mph, [Ref 133].

loads developed when only the right wheel traversed the bumps were 70% to 85% of the same wheel's loads in the case when both left and right wheels traversed the obstacle - Fig. 4.3. This seems to suggest that the negative errors of up to 30% have to be expected if wheel lateral interaction is not accounted for. However, if peak pavement loads are to be considered the difference becomes less than 12%. Moreover, road profile records show that many large motorway bumps occur simultaneously at the right and left wheels, especially if the surface prior to the weighscale is additionally prepared.

Some of the well established physical system modelling and graphical model representation methods were applied to the quarter-vehicle model to derive the system equations and achieve efficient and user friendly model interface and results representation.

4. 3. 2 Model Validation.

The purely theoretical character of the vehicle-road interaction study and the lack of corresponding experimental data to verify the results dictated that the validity of the selected model should be examined before proceeding with the simulation. Dynamic vehicle simulation is a complex process as the model has to reflect the complex non-rigid structure of vehicle body and incorporate the multitude of factors influencing its behaviour. However, depending on the aims of the simulation it is not always necessary for the model to cover all aspects of vehicle dynamic behaviour, and significant simplifications are therefore possible during model creation.

Before selecting the quarter-vehicle model for the current simulations previous work on vehicle/road interaction utilising similar modelling techniques was examined and it was found that in terms of dynamic forces transmitted to road modelling results are in good agreement with experimental data: [30], [72], [92], [106], [107], [150].

The earliest attempt at vehicle modelling performed by Cox et al, [30] made use of the quarter-vehicle model without tyre damping and leafspring friction. The simulation results were verified against experimental records gathered with an on-board system and generally tended to overestimate wheel loads with 5 to 10%. That was mainly due to the oversimplification of the model

and possible incorrect assumptions in the on-board measurement system.

The model developed by Whittemore for the computation of the dynamic behaviour of a truck suspension system, [150] was computing pavement loads for the right rear wheel set only. It was more complex in character incorporating non-linear stiffness and friction characteristics of a 3-leaf spring, as well as the ability of the tyre to envelop small road surface irregularities. However, no tyre/suspension damping was considered in the simulations. The accuracy of the technique was evaluated against measured wheel loads imposed by the moving vehicle on the pavement. Comparisons of computed signals with measured time records showed that peak loads were predicted with an average error of 2% (maximum error was 12%). Logarithms of computed and measured Power Spectral Density, *(PSD)* functions of the dynamic load showed an overall correlation of 7% with maximum error of 17%, but prediction accuracy deteriorated with frequencies higher than 7Hz.

The quarter-vehicle model was further refined by Page, [106] by adding a single term to reflect suspension friction damping, and representing the effect of tyre enveloping by modifying the profile of the step-shaped surface irregularity. The degree of agreement between computed data and experimental records is illustrated in Fig.4.8. The first peaks of computed and experimental tyre deflections correspond within 7%. At speeds below 20km/h there is substantial difference in the shape of the subsequent peaks, but above that speed agreement is satisfactory.

A variation of Page's model was therefore selected for the simulations in this study since vehicle behaviour at high speeds was of interest. The rigorous methodology of suspension parameter derivation as described in Ref. [106], also contributes to the close agreement between theoretical and experimental data. The model obviously cannot take into account the effects of longitudinal and lateral pitching motions of a real vehicle body, but those were considered to have minimal influence on motorway class roads, and especially in proximity to vehicle weighers.

4. 3. 3 The Vehicle Bond Graph Model.

Bond graphs are a graphical approach to physical systems analysis whose

relatively compact and orderly nature commends it as a basis for computer-aided modelling. This, coupled with the availability of low-cost, high speed interactive computer systems, distinguishes the approach as potentially the most useful of the systematic modelling methods.

Two modelling techniques based on the Bond graph methodology [60], [78], [146], [145], [149] were used to simulate the quarter–vehicle suspension model as described in Section 4.4.1.

Firstly the internal description equations of the system were derived and incorporated in a programme to calculate the dynamic wheel forces transmitted to the road. That programme was used for experimenting with a variety of pneumatic tyre models as discussed in Section 4.4 and also to investigate the mechanical resonances of the vehicle when passing over road bumps of different length – Ch.5. Then the dynamic simulation package **MEDIEM** (Section 4.5), based on the Structure graph technique was used for model creation and handling to perform most of the simulations subject of Section 3.4 and Ch.5.

The essential feature of Bond graph analysis is the representation of energy interactions between system components by a single line or ***energy bond.*** Pairs of variables called ***effort*** and ***flow*** are assigned to each bond. For mechanical systems the original Bond graph literature identifies Force/Torque as the *effort* variable and Velocity/Angular Velocity as the *flow* variable. Wellstead, (Ref.149) identifies effort and flow variables with the "across" and "through" type variables, effectively reversing the original assignment. This identification is also the one used in the Structure graph method and the **MEDIEM** package.

The quarter-vehicle suspension model is a two degree of freedom, translational motion mechanical system. It comprises ***Source, Storage*** and ***Dissipation*** elements and its dynamic behaviour is described by a set of vector velocities, displacements, forces and moments. The schematic representation of the quarter-vehicle suspension and the corresponding fully augmented Bond graph are shown in Fig 4.4(a) and (b), respectively.

The system is excited by an input received through the wheels in the form of vertical displacement corresponding to surface profile elevation ***y(t)***. The derivative ***y(t)*** – vertical velocity, is therefore selected as the model's *effort type* source element ***(SE).***

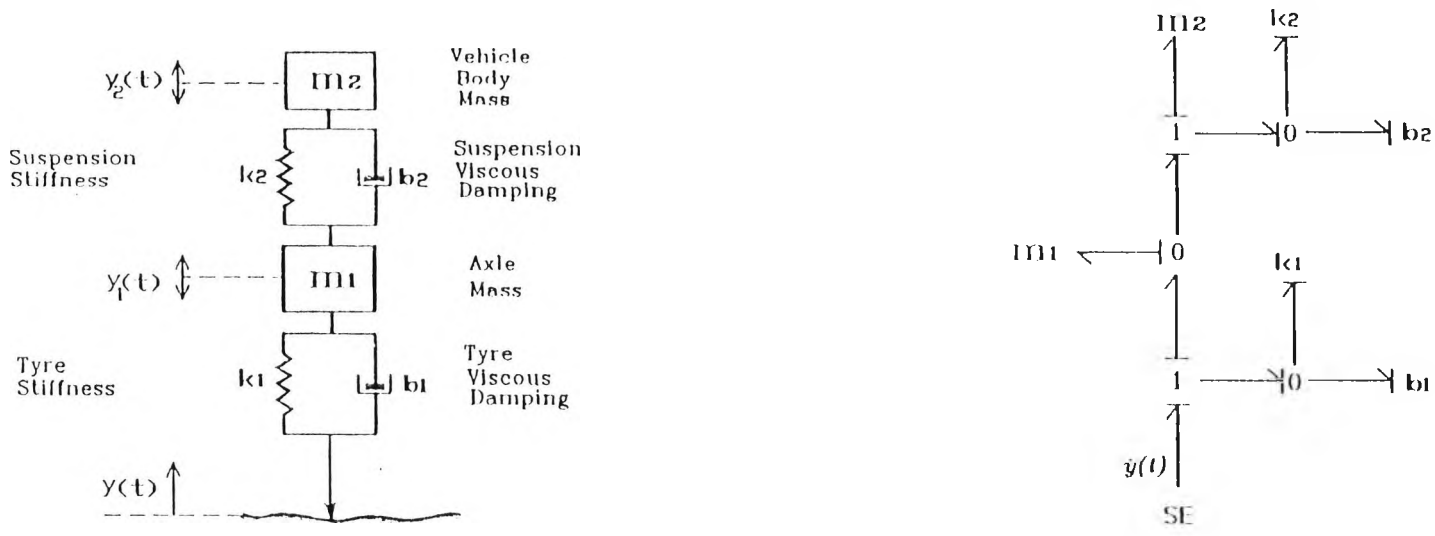

a) b)

Fig. 4.4 Bond Graph representation of the Quarter-vehicle model.

The viscous dampers b_1 and b_2 account for energy losses in the system. There are two modes of energy storage :

a) As the momenta p_1 and p_2 of the unsprung m_1 and sprung m_2 masses, respectively:

$$p_1 = \int_{t_0}^{t} F_1.dt + p_1(t_0) \quad ;$$

$$p_2 = \int_{t_0}^{t} F_2.dt + p_2(t_0) \quad ;$$

b) As deflections y_1 and y_2 of the tyre and suspension springs with spring stiffnesses k_1 and k_2, respectively:

$$y_1 = \int_{t_0}^{t} V_1.dt + y_1(t_0) \quad ;$$

$$y_2 = \int_{t_0}^{t} V_2.dt + y_2(t_0) \quad ;$$

The four storage elements provide the four states p_1, p_2, y_1, y_2 of the mechanical system. Assuming that at moment t_0 (reference position) the system is at rest i. e. $y_1(t_0) = y_2(t_0) = p_1(t_0) = p_2(t_0) = 0$, the state equations are readily obtained from the depicted bond graph structure as follows:

$$
\begin{aligned}
\dot{y}_1(t) &= \dot{y}(t) - \frac{p_1}{m_1} \;; \\
\dot{y}_2(t) &= \frac{p_1}{m_1} - \frac{p_2}{m_2} \;; \\
\dot{p}_1(t) &= k_1.y_1(t) - k_2.y_2(t) + b_1.\left[\dot{y}(t) - \frac{p_1(t)}{m_1}\right] - b_2.\left[\frac{p_1(t)}{m_1} - \frac{p_2(t)}{m_2}\right] \;; \\
\dot{p}_2(t) &= k_2.y_2(t) + b_2.\left[\frac{p_1(t)}{m_1} - \frac{p_2(t)}{m_2}\right] \;;
\end{aligned}
\qquad (4.1)
$$

When presented in a matrix form, equations (4.1) give the state space matrix of type:

$$
\dot{\underline{y}} = \underline{A} \,.\, \underline{y} + \underline{B} \,.\, \underline{u} \;; \qquad (4.2)
$$

where $\underline{y}$ is the states matrix and:

$$
\underline{y} = \begin{bmatrix} y_1(t) \\ y_2(t) \\ p_1(t) \\ p_2(t) \end{bmatrix} \;;
$$

$\underline{A}$ and $\underline{B}$ – parameter matrices :

$$\underline{A} = \begin{bmatrix} 0 & 0 & \frac{1}{m_1} & 0 \\ 0 & 0 & \frac{1}{m_1} & \frac{1}{m_1} \\ k_1 & -k_2 & -\frac{b_1+b_2}{m_1} & -\frac{b_2}{m_2} \\ 0 & k_2 & \frac{b_2}{m_1} & -\frac{b_2}{m_2} \end{bmatrix} \quad ; \qquad \underline{B} = \begin{bmatrix} 1 \\ 0 \\ b_1 \\ 0 \end{bmatrix} ,$$

and $\underline{u}$ is the input (control) vector: $\underline{u} = \mathring{y}(t)$. The state space description provided by Equations (4.1) and (4.2) form the ***internal*** model of the system entirely specifying its dynamic performance.

An alternative way of expressing the dynamic behaviour of the system is to reduce the full set of first-order state equations to a lower set of higher order differential equations in terms of the variables of interest. That expression is called the ***external*** model and it usually only partly describes the system. Examples of an *external* model description are Equations (2.2), (2.3) derived in Section 2.3.3.2 for the displacement variables y_1 and y_2.

The expression for the dynamic wheel force $F_w(t)$ imparted to the road was derived in general form earlier also in Section 2.3.3.2. Applying the bond graph technique we arrive at the following equation:

$$F_w(t) = k_1.y_1(t) + b_1\left[y(t) - \frac{p_1(t)}{m_1}\right] \quad ; \qquad (4.3)$$

which in matrix form can be written as:

$$\underline{f} = \underline{C} \cdot \underline{y} + \underline{D} \cdot \underline{u} \ ; \qquad (4.4)$$

where:

f – dynamic wheel force : $\underline{f} = F_w(t)$;
$\underline{C}$ and $\underline{D}$ – parameter matrices :

$$\underline{C} = \left[k_1, \ 0, \ -\frac{b_1}{m_1}, \ 0 \right] ; \qquad \underline{D} = b_1 ;$$

$\underline{u}$ is the input vector : $\underline{u} = y(t)$.

The matrix expressions (4.2) and (4.4) give the internal description of the model and the dynamic wheel force respectively. They can subsequently be used in the computer programmes for simulation of the suspension system.

4. 3. 4 Surface Irregularity Modelling .

Two types of deterministic road imperfections are considered in the simulations:

i) an abrupt step of variable height;

ii) a bump of rectangular cross section with variable height and length in the direction of travel.

In the model the tyre is represented by a spring and a damper having a point contact with the road surface. In practice the tyre has a finite length of contact with the surface and its carcass is flexible. These properties affect the way the tyre perceives an abrupt surface irregularity such as a step or bump. This is shown diagrammatically in Fig. 4.5.

In wheel position A the tyre is just touching the leading edge of a step, so beyond this position the wheel begins to rise and the tyre is indented by the sharp edge of the step as shown in position B. In position C the contact area of the tyre with the road surface is just completely on top of the step. Between

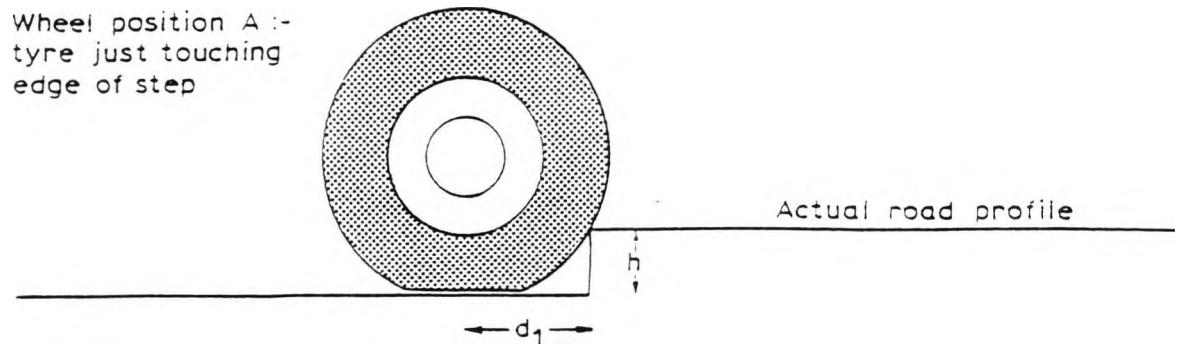

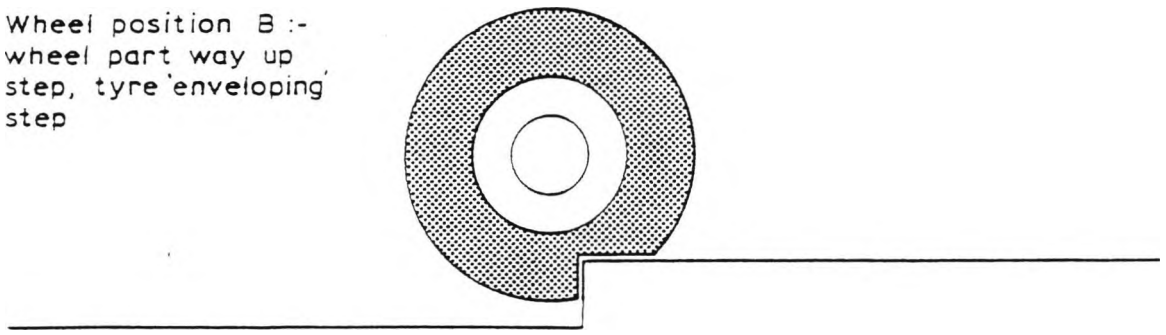

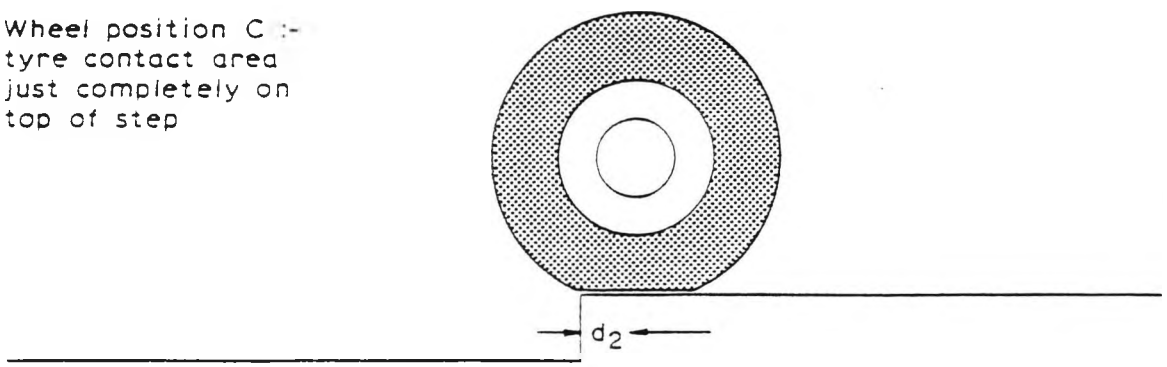

The step profile is smoothed as follows :-

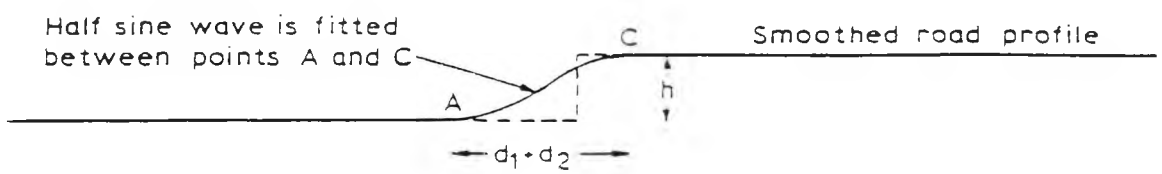

Fig. 4.5 Step shaped surface irregularity smoothing.

positions A and C – distance $(d_1 + d_2)$, the wheel rises smoothly through the height h of the step. As the point contact tyre model is incapable of accounting for this phenomenon it is therefore necessary for the profile of the irregularity to be modified to correspond to the smoothing effect of the real tyre.

For a step this has been done by fitting a half sine wave shape between points A and C to produce the smoothed profile in Fig. 4.6(a). Provided the step height h is relatively small compared to the tyreprint length l_t and the wheel radius r_w, the tyre will not hit the obstacle before the tyreprint reaches it. This will allow to substitute the distance $(d_1 + d_2)$ – Fig. 4.5, with the tyreprint length l_t:

$$l_t = d_1 + d_2 \ ;$$

For a typical goods vehicle $l_t = 0.25\ m$, [82]. With x and y the horizontal and vertical coordinates of the wheelcentre respectively, the equation for the latter's displacement by the smoothed profile is given by :

$$y = \frac{h}{2} . [1 + \sin \pi . (\frac{x}{l_t} - \frac{1}{2})] \ ; \qquad (4.5)$$

Differentiation by x gives :

$$dy = \frac{\pi . h}{2 l_t} . \cos \pi . (\frac{x}{l_t} - \frac{1}{2}) . dx \ ;$$

Time differentiation of the expression then provides :

$$\frac{dy}{dt} = \frac{\pi . h}{2 . l_t} . \cos \pi . (\frac{x}{l_t} - \frac{1}{2}) . \frac{dx}{dt} \ ;$$

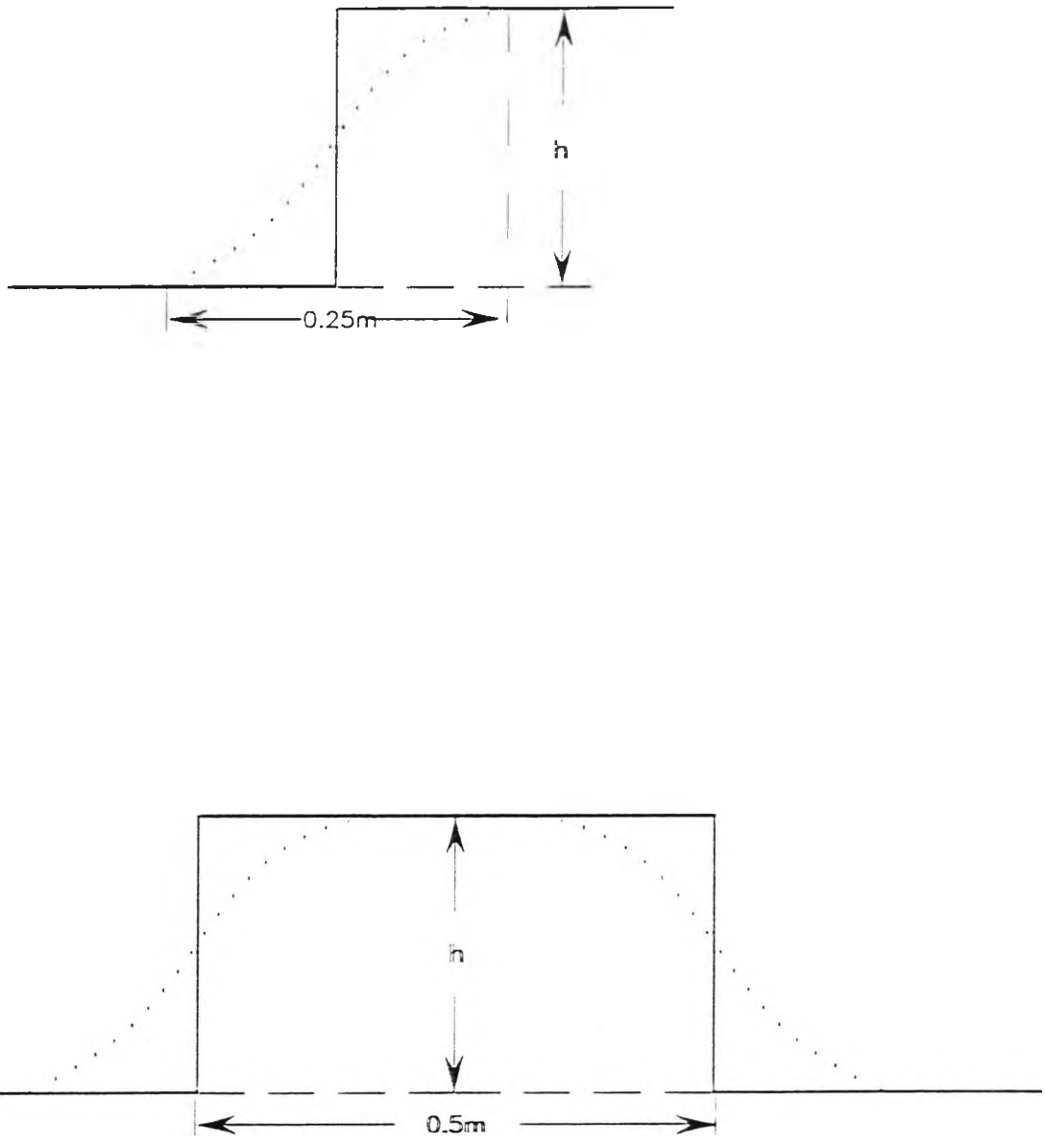

Fig. 4.6 Sine-wave smoothing of a step and a rectangular bump.
(Tyre print length $l_t = 0.25m$)

Now:

$$\frac{dy}{dt} = \dot{y}(t) \quad \text{-- vertical velocity ;}$$

$$\frac{dx}{dt} = U \quad \text{– horizontal velocity ;}$$

and $x = U \,.\, t$;

If T is the time to travel distance l_t (tyre transit time), then :

$$l_t = U \,.\, T ; \qquad U = \frac{l_t}{T} ;$$

resulting in the following expression for the vertical velocity of the wheel-centre :

$$\begin{aligned} \dot{y}(t) &= \frac{\pi.h}{2T} \,.\, \cos \pi.\left(\frac{t}{T} - \frac{1}{2}\right) \qquad \text{for} \quad 0 < t \leq T \\ \dot{y}(t) &= 0 \qquad\qquad\qquad\qquad\quad \text{for} \quad t > T \end{aligned} \tag{4. 6}$$

Likewise for a rectangular bump, sine wave smoothing occurs at both the leading and trailing edges of the bump. In Fig. 4.6(b) this is shown for a bump length of 0.25m and the vertical velocity of the wheelcentre is given by the Equations (4.7):

$$\begin{aligned} \dot{y}(t) &= \frac{\pi.h}{2T} \,.\, \cos \pi.\left(\frac{t}{T} - \frac{1}{2}\right) \quad ; \quad 0 < t \leq T \\ \dot{y}(t) &= 0 \quad ; \quad T < t < 2T \\ \dot{y}(t) &= -\frac{\pi.h}{2T} \,.\, \cos \pi.\left[\frac{(t-2T)}{T} - \frac{1}{2}\right] \quad ; \quad 2T \leq t \leq 3T \\ \dot{y}(t) &= 0 \quad ; \quad t > 3T \end{aligned} \tag{4. 7}$$

where the tyre transit time now comprises ascend/descend times plus flat part time, and for the chosen bump flat part length of 0.25m the transit time will be *3T*.

The effect of using the smoothing process is illustrated in Fig. 4.7 where passages of the *quarter-vehicle* suspension model over a $(40 \times 250)mm$ bump are simulated at speeds from 10 to 60km/h, [106]. At the two lower speeds the shape of the curves for smoothed and unsmoothed bumps is quite different, but at the higher speeds the curves following the initial peak are very similar except for a very small time difference. This suggests that at higher speeds it is likely to be the height of the obstacle and not its shape that is important. The validity of the technique was verified by Page through comparing theoretical and experimental values of tyre deflection against time for a range of speeds for the vehicle and its model – Fig 4.8. The shape and magnitude of the first peaks correspond well over the whole speed range. Agreement between theoretical and experimental results for subsequent peaks deteriorates, however it improves with speed. This may imply that the effective values of some of the vehicle parameters change with speed.

A similar smoothing technique has successfully been applied by Cox et al [30] to simulate the cushioning effect of a rolling tyre hitting a rectangularly shaped obstacle. The effective profile "seen" by the tyre has been approximated to an isosceles triangle of the same height, but almost three times as long.

The implementation of the technique using the computer simulation package **MEDIEM** is described in Section 4.5.3. A simulation run was performed with an unsmoothed impulse input having an amplitude corresponding to that of the smoothed half-sine wave for a given speed. The returned model output was profoundly unrealistic proving the necessity of the smoothing procedure.

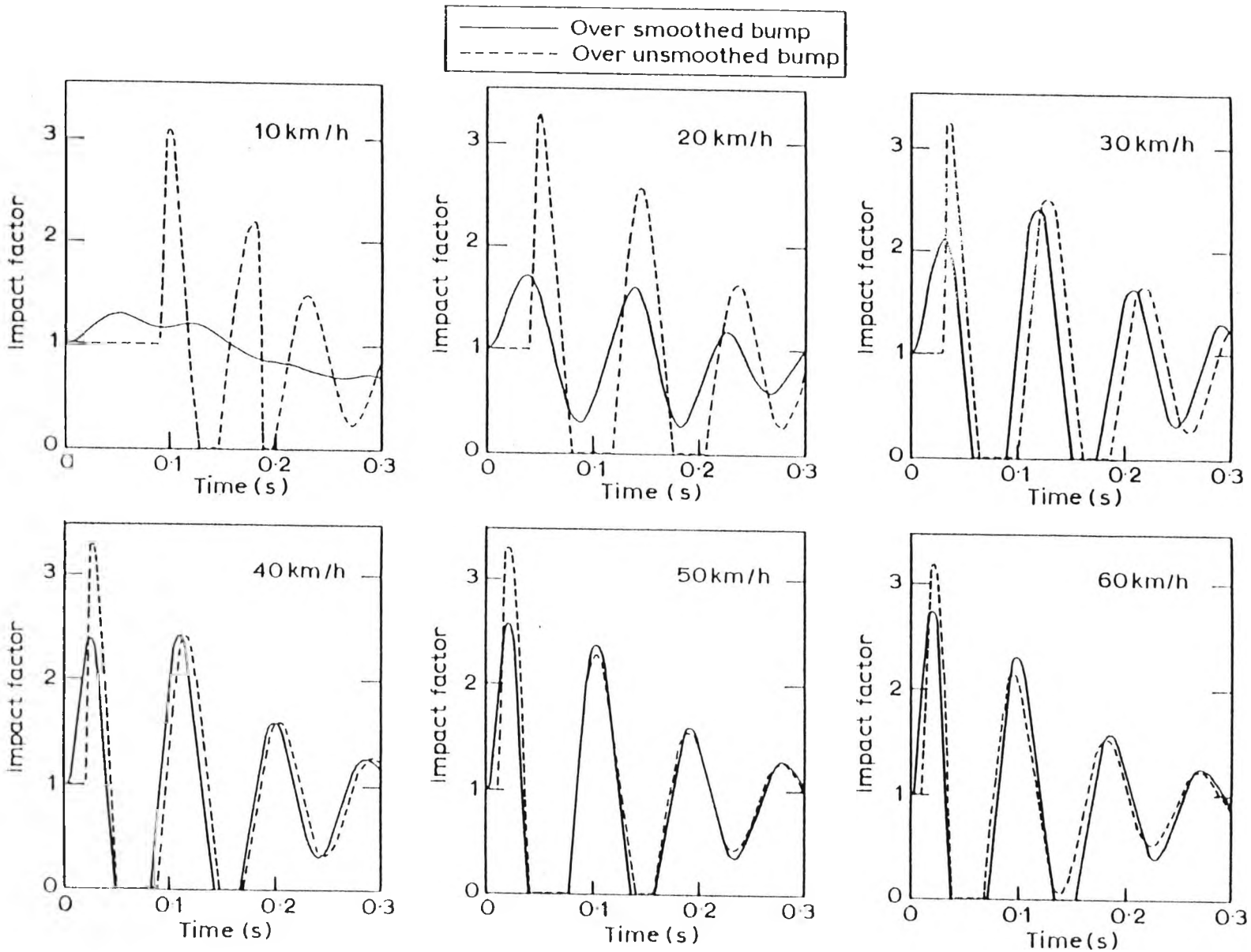

Fig. 4.7 Theoretical model of a test vehicle passing over *0 04m x 0.25m* smoothed and unsmoothed bump, [Ref. 89].

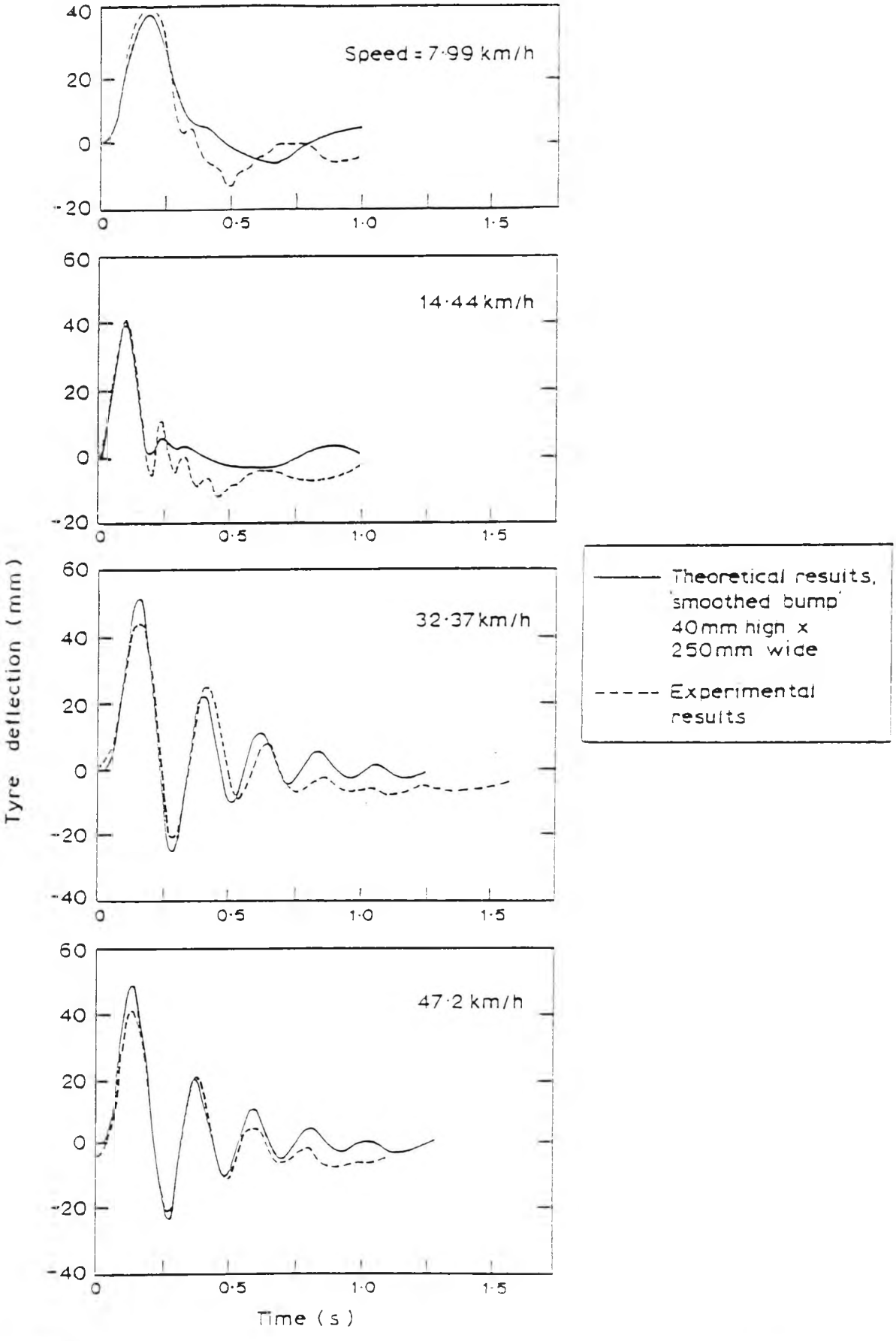

Fig. 4.8 Comparison of theoretical and experimental wheel – road surface irregularity interaction. [Ref. 89].

4.4 TYRE MODELLING.

Modelling tyre-terrain interactions is an important stage in developing the overall vehicle model, because most of the vehicle's external reactions occur at the interface between the tyres and the road surface.

The approach adopted in the models described so far has been to modify the shape of the obstacle into some mathematical curve to account for the smoothing effect of the tyre's elastic carcass. However, such approximations apply to a limited range of irregularity shapes and their validity is often difficult to verify. A better approach from a methodological point of view is to construct a tyre model capable of representing realistically the properties of the tyre and its interactions with the road surface.

4. 4. 1 Tyre Models Survey.

Many authors have dealt with the problem - [8], [9], [21], [34], [65], [81], [83], [99], [106], [127], [150], and a variety of pneumatic tyre mathematical models have been created. In terms of structure and complexity, tyre models may incorporate:

a) A single linear spring.

b) A linear spring and a damper.

c) A linear spring, a damper and an elastic stopper.

d) A linear spring, a damper, an elastic stopper and capability of leaving the ground.

A tyre model may consist of a single element comprising one of the above combinations or an assembly of such elements. Depending on the configuration of the model and its mode of operation three basic types can be outlined:

i) Point contact model. This is the simplest and most extensively used vehicle simulation tyre model. [21],[72],[99],[106],[107],[147],[150]. The tyre-terrain interaction is represented by a contact at a single point situated vertically beneath the tyre centre. The surface profile is followed by the contact point

acting as the model's input – usually after derivation in the form of vertical velocity. When traversing a small, sharp obstacle an actual tyre bridges and filters harsh contour changes whereas the point follower copies all edges and spikes – an unrealistic feature resulting in exaggerated system outputs. Therefore the use of this model is recommended for tyres operating on ground surfaces satisfying the following conditions:

- The surface in the path of the wheel has no step changes in its elevation or slope.
- The wavelength of surface variations is at least 1.5 times the length of the tyre print.
- A derivative can be defined for every point of the irregularity curve.

The limitations of the point contact model are demonstrated in the case of a step profile obstacle when the transmitted vertical velocity should have an instantaneous peak value of infinity resulting in an indefinite system response.

The dynamic force transmitted to the road is given by the sum of the spring and damper forces – Equation 2.4. Graphical representation of the model can be found in Fig. 2.3 and Fig. 4.4(a) as the tyre part of the quarter-vehicle models.

ii) Parallel spring model – [21], [65], [127]. This is a distributed contact model interfacing with the terrain through a tyreprint of finite length l_t, rather than a single point. Inflation pressure and carcass forces are simulated by a finite number of *parallel* spring and damper elements distributed uniformly over the contact length. Provided the elemental stiffness and damping are linear, this model is equivalent to a point contact model in which the local terrain elevation $y(x)$ is replaced with the average terrain elevation $\bar{y}(x)$, taken across the length, l_t. The whole wheel/half-axle mass m_1 is situated at the wheel-centre and the vertical wheel force, F_w at any moment of time is given by the sum total of the vertical forces of the distributed spring-damper elements along the tyreprint length, l_t:

$$F_w = k_{t'} \cdot \int_0^{l_t} y_1(x).dx + b_{t'} \cdot \int_0^{l_t} \dot{y}_1(x).dx \quad ; \qquad (4.8)$$

where $k_{t'}$, $b_{t'}$ are elemental stiffness and damping coefficients respectively, and $y_1(x)$ is the elemental vertical displacement.

In the tyre model surveys performed in [21] and [127] several parallel spring models are described and evaluated. A model of this type is described in [65] as a part of a linearised vehicle simulation to determine the effects of wheel base and other parameters on vehicle vibration levels.

iii) Radial spring model – [21], [34], [85], [127]. This is another type of distributed contact model bearing good physical resemblance to a real pneumatic tyre. Here the spring-damper elements are linked to the wheel-centre and angularly distributed over the footprint length. As the wheel passes over terrain surface, the thread in the tyreprint region envelops small irregularities through local deformations within the tyreprint. As in the previous model, the whole tyre mass is concentrated in the wheel-centre and the wheel force at any moment of time is given by the sum of all elemental spring and damping forces – Eq. (4.8).

A radial spring model which divides the tyre into independently deflecting segments was developed by Davis [34]. The tyre filtering effect for an arbitrary ground surface is simulated by redefining the terrain as an "equivalent ground plane" which reflects both the elevation and the slope characteristics of the original terrain. The individual deflecting forces in the radial springs reflecting the terrain irregularities are combined to produce the resultant force acting upon the tyre. The tyre area displaced by the terrain and the arc of the contact patch, together with the tyre force deformation curve determine the magnitude of the resultant tyre force.

The model developed by Albert [3], consists of a series of infinitely thin radial springs enveloping the surface profile by sensing the conditions existing over the whole contact patch. Here again the terrain is redefined into an "equivalent ground plane" contacting the tyre at only one point thus making it compatible with the point contact model, but for appropriately smoothed ground surface.

The *Adaptive footprint* model created by Captain et al [21] consists of a flexible thread band linked to the wheel-centre of angularly distributed stiffness and damping. In addition to the radial models described so far here the resultant tyre force is not vertical because of the existence of a non-planar tyreprint. Calculation of the appropriate components therefore allows determination of the vertical as well as fore-and-aft tyre forces. The model has been verified against field trial data and has shown good agreement both in terms of axle acceleration magnitude and frequency content. The model has then been used as a reference base for comparison of tyre models to develop guidelines for model selection.

The results of the simulations for three frequency bands are summarised in Table 4.1:

	RMS* – Tyre force ratio** ***(Normalised with respect to the Adaptive footprint model)		
Model Type	***0. 1 – 1 Hz***	***1 – 10 Hz***	***10 – 100 Hz***
1. Point Contact Model	*1. 32*	*2. 51*	*3. 54*
2. Fixed Footprint (Parallel spring)	*1. 0*	*1. 38*	*0. 46*
3. Adaptive Footprint (Radial spring)	*1. 0*	*1. 0*	*1. 0*

Table 4.1 Tyre models comparison, (Ref.21).

From the values in the table it can be concluded that substantial differences exist in the results for transmitted tyre forces of the three models. These differences tend to increase with frequency. While the adaptive footprint model performs well over a very wide frequency range, the parallel spring model can be a good alternative particularly where frequencies above the wheel hop are not of interest and the complexity of the radial spring model cannot be afforded.

As expected the response of the point contact model is significantly higher than that of the other models and has much greater high frequency content. These differences can be explained with the inability of the point contact model to filter out short wavelength irregularities. This model is therefore recommended only for basic simulations at low frequencies and where the road surface complies with the constraints outlined earlier.

4. 4. 2 The Parallel Element Model .

In this study the enveloping effect of the pneumatic tyre encountering a sharp obstacle was initially accounted for by modifying the step's profile into a half-sine wave. The simulation results were satisfactory – Fig. 4.7, Fig. 4.8, though the model still tended to overestimate the impact factor when compared with experimental data. The differences were expected to be even more pronounced when bumps relatively shorter than tyreprint length were simulated. A version of the parallel spring model was therefore developed to represent more realistically the tyre filtering effects – Fig. 4.9. For this purpose the tyreprint length l_t is divided into n elements each of length:

$$\Delta l = \frac{l_t}{n} ;$$

Corresponding stiffness and damping coefficients are assigned to the elements respectively:

Elemental tyre stiffness: $k_{t_i} = \frac{k_t}{n}$;

Elemental tyre damping: $b_{t_i} = \frac{b_t}{n}$;

Each element interacts with the obstacle's edge one at a time according to its horizontal position x_i, within the tyreprint. The inputs to the model are the elemental vertical velocities $\dot{y}_{1i}(t)$, calculated separately according to element's position x_i , with respect to obstacle. From the expression for the smoothed vertical displacement $y(t)$ – Eq. (4.5), we can write:

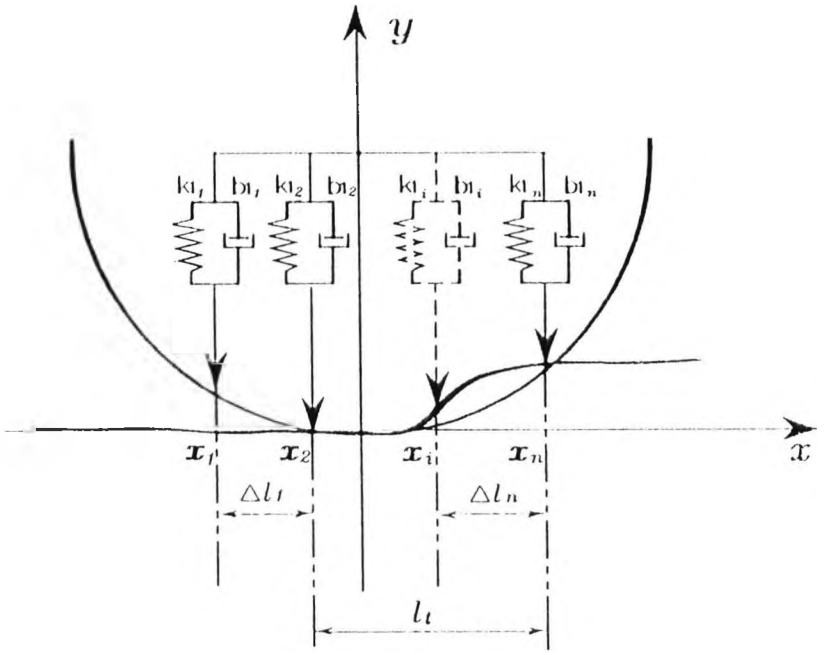

Fig. 4.9 Parallel element Tyre model.

$$y_i(t) = \frac{h}{2} \cdot \left[1 + \sin\pi \cdot \left(\frac{x_i}{\Delta l_t} - \frac{1}{2}\right)\right]; \qquad (4.9)$$

and the elemental vertical velocity $\dot{y}_i(t)$ is derived as:

$$\dot{y}_i(t) = \frac{n \cdot \pi \cdot h \cdot U}{2 l_t} \cos\pi \cdot \left(\frac{n x_i}{l_t} - \frac{1}{2}\right); \qquad (4.10)$$

where:

h – step height ;
l_t – tyreprint length ;
U – vehicle's horizontal speed ;
n – number of elements ;
x_i – element's horizontal position ;

The different tyre elements come into contact with the obstacle in succession after a time delay Δt_i depending on their horizontal position:

$$\Delta t_i = \frac{i}{n} \cdot \frac{l_t}{U};$$

The vertical velocity $\dot{y}_i(t) \neq 0$ only when the element is over the ascending/descending part of the bump. From Equation (4.10) it can be seen that increasing the number of elements n, will lead to greater amplitudes and higher frequencies for the elemental vertical velocities $\dot{y}_i(t)$.

In terms of Bond graph modelling the division of the tyre into independent elements will result in increasing the number of states of the system, from **4** in the case of the single spring-damper model, to **(n + 3)** when the latter is replaced by an array of **n** elements. The bond graph representation of the Parallel element model is shown in Fig. 4.10 where:

$$k_{t_1} = k_{t_2} = \ldots = k_{tn} = \frac{k_t}{n} \ ;$$

$$b_{t_1} = b_{t_2} = \ldots = b_{t_n} = \frac{b_t}{n} \ ;$$

The resulting **(n + 3)** state equations describing the system are:

$$\begin{aligned}
f(1) &= \dot{y}_{11}(t) = \dot{y}_1(t) - \frac{P_1}{m_1} \ ; \\
f(2) &= \dot{y}_{12}(t) = \dot{y}_2(t) - \frac{P_1}{m_1} \ ; \\
&\vdots \qquad\qquad\qquad\qquad \vdots \\
f(n) &= \dot{y}_{1n}(t) = \dot{y}_n(t) - \frac{P_1}{m_1} \ ; \\
f(n+1) &= \dot{y}_2(t) = \frac{P_1}{m_1} - \frac{P_2}{m_2} \ ; \\
f(n+2) &= \dot{p}_1 = \frac{k_t}{n} \cdot \sum_{i=1}^{n} y_{1i} + \frac{b_t}{n} \cdot \left[\sum_{i=1}^{n} \dot{y}_{1i} - n \cdot \frac{P_1}{m_1} \right] - k_2 \cdot y_2 - b_2 \cdot \left[\frac{P_1}{m_1} - \frac{P_2}{m_2} \right] \ ; \\
f(n+3) &= \dot{p}_2 = k_2 \cdot y_2 + b_2 \cdot \left[\frac{P_1}{m_1} - \frac{P_2}{m_2} \right] \ ;
\end{aligned} \qquad (4.11)$$

The first **n** equations of the set represent the vertical velocities of each of the **n** tyre elements, their sum at any instant acting as the system's input. Equation **f(n + 1)** describes vehicle body motion $y_2(t)$, while **f(n + 2)** and **f(n + 3)** are the expressions for the forces acting upon the unsprung – m_1, (axle) and sprung – m_2, (body) masses, respectively.

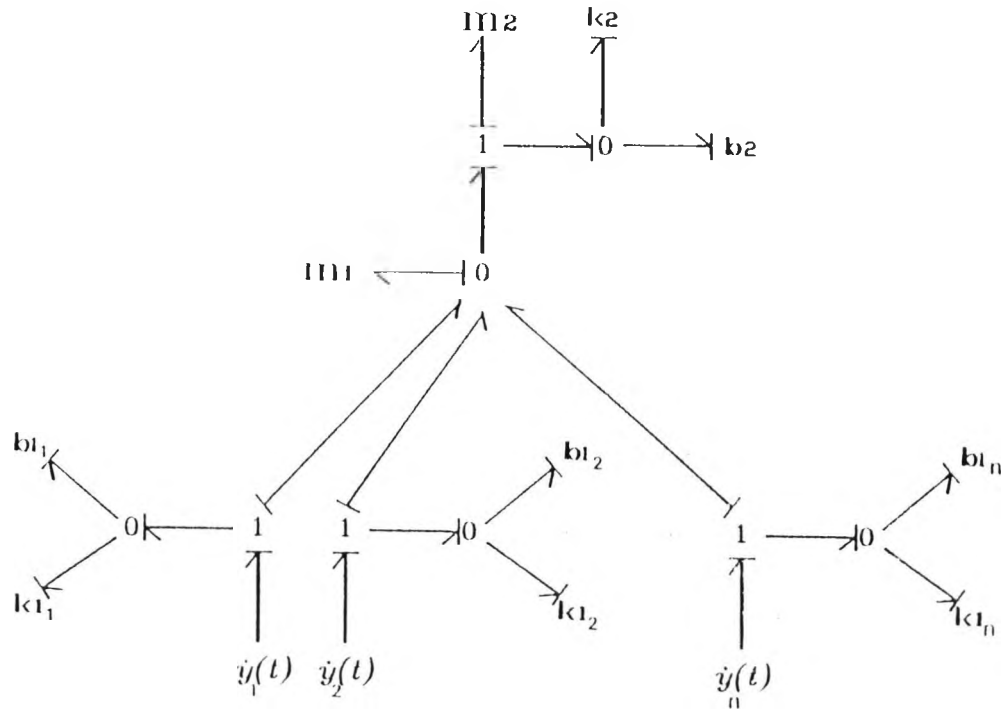

Fig. 4.10 Bond Graph representation of the Parallel element Tyre model.

The impact force exerted on the road at each moment will be the sum of all elemental tyre forces:

$$F_w = \sum_{i}^{n} F_{1i} = \frac{k_1}{n} \cdot \sum_{i}^{n} y_{1i} + \frac{b_1}{n} \cdot \left[\sum_{i=1}^{n} \dot{y}_{1i} - n \cdot \frac{P_1}{m_1} \right] \quad ; \qquad (4.12)$$

For the purposes of the study it is more appropriate to express the dynamic impact force in relation to the static semiaxle's weight. The resultant ratio is the familiar ***Impact Factor,*** which in most of the following simulations is used in percentage form as a measure of the extent to which the dynamic wheel forces exceed the corresponding static weights:

$$IF = \frac{F_w}{(m_1 + m_2) \cdot g} \quad ; \qquad (4.13)$$

Here the magnitude of ***IF*** was used to evaluate the validity of the Parallel elements tyre model. Three variations of the model were developed and tested, their tyre print length comprising $n = 2, 4$ and 10 elements, respectively. The Single point contact model as well as experimental data were used as a base for comparison.

Initially simulation runs of the models over a ***Step*** shaped obstacle were carried out at two different vehicle speeds. There were no significant differences in the shapes and timing of the different models' outputs apart from some higher frequency spikes on top of the first positive peak in the outputs of the multiple element tyre models – Fig. 4.11. These represent the higher characteristic frequencies of the separate tyre elements compared to the single spring–damper combination. The amplitude differences of the ***IF*** outputs of the four models were also small as can be seen in Table 4.2:

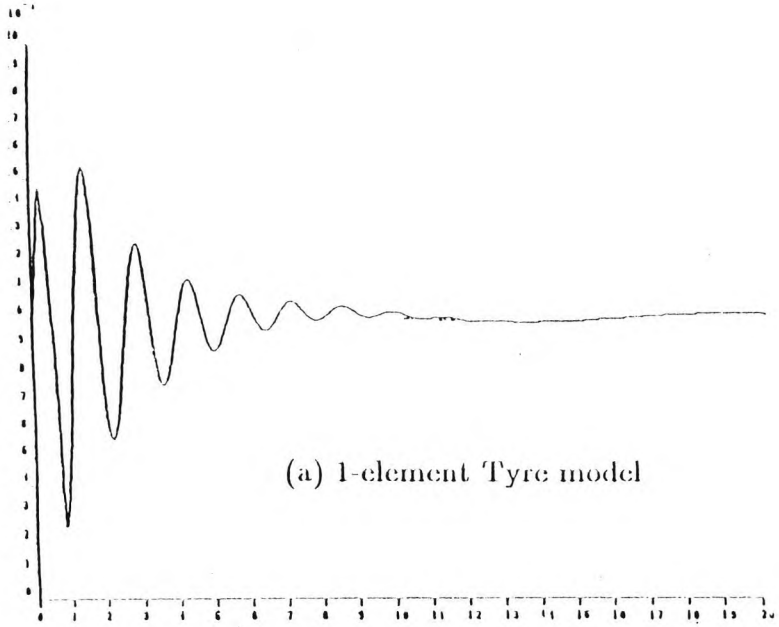

(a) 1-element Tyre model

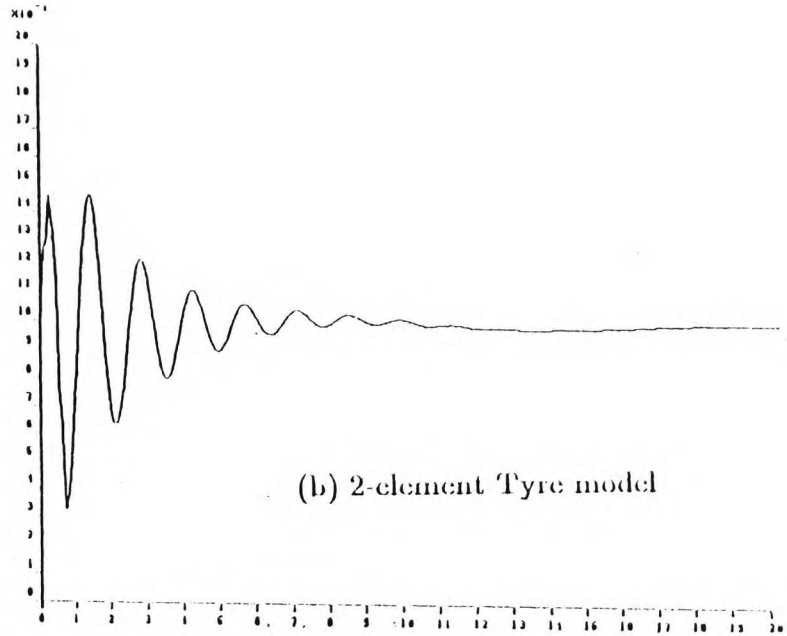

(b) 2-element Tyre model

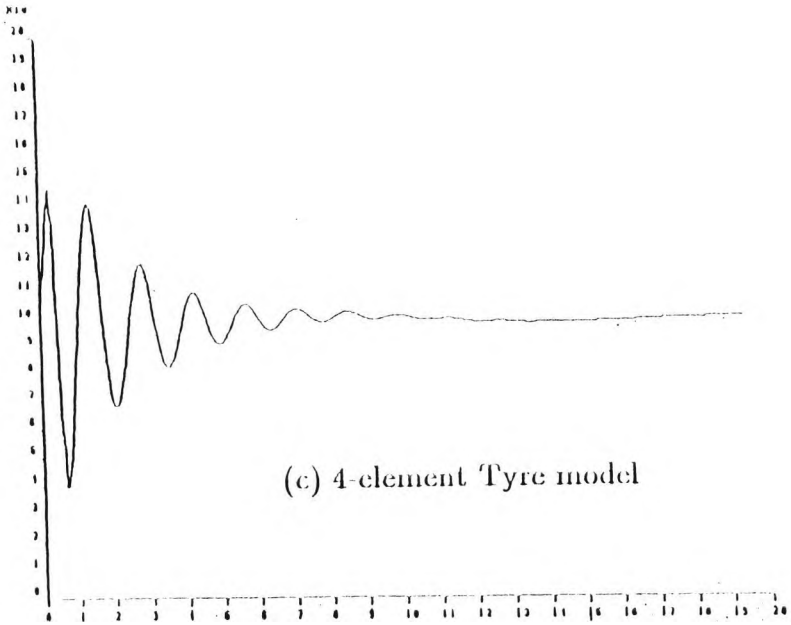

(c) 4-element Tyre model

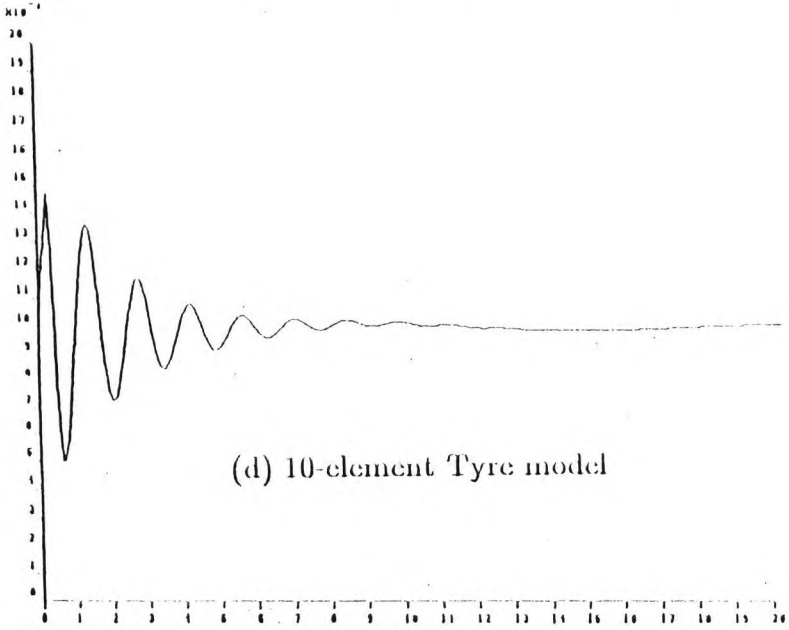

(d) 10-element Tyre model

Fig. 4.11 Comparison of different Parallel element tyre models - Step shape obstacle.

Tyre Model: (No of Elements) [n]	Peak No: (Amplitude normalised to Static weight)			
	First Positive	First Negative	Second Positive	First Body bounce
1	1. 33	0. 77	1. 27	1. 06
2	1. 32	0. 77	1. 26	1. 06
4	1. 3	0. 78	1. 25	1. 06
10	1. 26	0. 78	1. 25	1. 06

Table 4.2 Comparison of three *(2, 4, and 10 element)* Parallel element models with the Single point contact model: $U = 30$ km/h ; $h = 0.01$ m ;

Output amplitude differences of the same order were observed at the higher speed of 100 km/h showing that the different tyre models behave similarly over the whole speed range of the vehicle hitting a step type obstacle .

A further series of simulations were performed with the different tyre models this time with a ***bump*** shaped obstacle of the same height but different lengths in the direction of travel. A medium vehicle speed of 60km/h was chosen and three bump lengths l_b, (relative to tyre print length, l_t) were considered :

i) a relatively long bump : $l_b = 1.0 . l_t = 0.25$ m ;
ii) a medium length bump : $l_b = 0.5 . l_t = 0.125$ m ;
iii) a very short bump : $l_b = 0.1 . l_t = 0.025$ m ;

In terms of shape and timing the returned outputs of the different tyre models did not show considerable differences although for some combinations of l_b and the number of model elements n the amplitude of the second positive output peak exceeded the first.

Some of the important peak values of the dynamic wheel forces were extracted from the produced data for the long, medium and short bumps,

respectively. As anticipated the difference in the performance of the four tyre models depended considerably on the length of the obstacle. The tendency of the Single point contact model, ***(n = 1)*** to overestimate the wheelforces increased steadily with shortening the bump, thus highlighting the model's inability to account for the cushioning effect of the pneumatic tyre. The outputs of the Parallel element models ***(n = 2, 4, 10)***, showed progressively better agreement with experimental data of vehicle runs over road irregularities of similar dimensions and shape [21],[22].

The necessity of developing a multielement tyre model therefore becomes more obvious in the cases when the effect of road irregularities shorter than the tyreprint is being investigated, i. e. when the enveloping properties of the tyre can no longer be neglected. The choice of number of the spring-damper elements comprising the model depends chiefly on the shortest irregularity considered in the modelling and the required degree of accuracy of the results.

4.5 DYNAMIC MODELLING USING *MEDIEM*.

A major part of the computer simulations were performed using the ***Multi Energy Domain Interactive Element Modelling, (MEDIEM)*** programme package. The package was developed at the *Measurement and Instrumentation Centre* of *The City University* – London, for interactive mathematical modelling of lumped parameter physical systems in mixed energy domain environment, [1],[50],[51],[78],[79]. It has been extensively used mainly for dynamic simulation of different types of instrument transducers but the generalising character of the methodology makes it applicable to most physical systems operating in the allowed energy domains and provided they can be reduced to a finite number of lumped parameters.

The normal mathematical modelling procedures usually involve the "pencil and paper" approach for the formulation of the system's equations and limited use of computer power (usually in the final stage of the iterative solution routines). Compared to them ***MEDIEM*** both derives the system's state equations

and evaluates the time/frequency response after solving them. The package is based on a graphical language called ***Structure graphs***, allowing the user to describe the structures of lumped parameter systems in close correspondence with their engineering schematic.

4. 5. 1 Graphical Model Presentation Techniques.

When modelling real physical systems it is essential for the researcher to be able to proceed rapidly from an engineering schematic describing the elements of the system and their interconnections to a meaningful graphical representation. Three techniques have become firmly established in this area:

4. 5. 1. 1 Signal flow graphs. – Here the elements are represented by functional blocks exchanging signals in a specified way. System equations are therefore directly encoded into graphical form leaving only the calculation part to be carried out by the computer.

4. 5. 1. 2 Linear graphs. – Electric circuit analogies are used here in element's descriptions and their interconnections. Linear graphs offer sufficient capabilities when a single energy domain is being considered but fail for multifrequency systems when separate graph segments have to be used for the different energy domains.

4. 5. 1. 3 Bond graphs. – Among graphical techniques the bond graph method has the highest and most complete system information content. This is because of the rigorous rules of graph construction and equation formulation, the restricted set of permissible elements used and the capability to tackle multienergy systems by connected graphs. From a bond graph one can determine the state equations of a system in a straight forward manner by defined rules. This has led to the development of computer packages based on the bond graph methodology which both formulate and solve the differential equations from a suitably codified graph structure: *THTSIM* [145], *ENPORT* [124], etc.

However constructing a fully augmented bond graph of even a simple engineering system requires detailed knowledge of the methodology and some research experience. Moreover although the technique preserves the connectivity of the graph structure, the presentation loses its topological similarity with the real system.

4. 5. 2 Structure Graphs.

The structure graph technique was developed as a graphical simulation language from the Bond and Linear graph methods [51], [78], [79]. Its distinctive advantage is the high degree of topological resemblance of the engineering schematic of the system and its graphical representation. This makes the method more user-friendly and provides for a high degree of interaction in the course of modelling.

Fig. 4.12 is an illustration of the different graphical model presentation techniques and how they compare in terms of their similarity to the system's schematic. The Structure graph presentation – (d), bears by far the best resemblance to the schematic which would enable even an unexperienced user to build easily the structure. The Structure graph method uses a set of elements somewhat extended from those used in Bond graphs to include signal elements.

The set includes :

– L and C for energy storage .

– R for dissipative elements .

– ***TF*** *(transformer)*, and ***GY*** *(gyrator)* for energy transformation within or between energy domains.

– ***Source*** elements as inputs.

– ***Field*** elements to represent fields of type L, C or R .

– ***Signal*** elements to represent transfer of information without transfer of energy.

The other constituent parts of a structure graph are used to indicate element connectivity and information flow directions. These are :

– ***Nodes:*** these are reference markers on the graph and for the following system domains :

Electrical , ***Fluid*** , ***Thermal*** } *The node is a common positional point or across reference point. It is always static.*

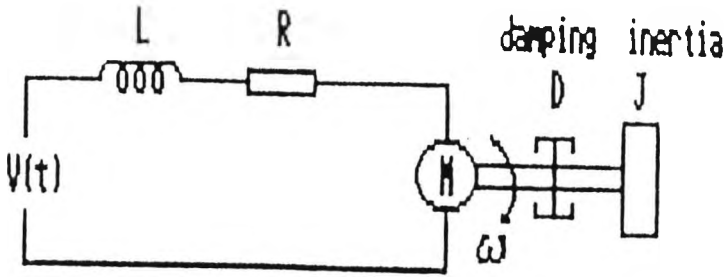

a) Schematic diagram

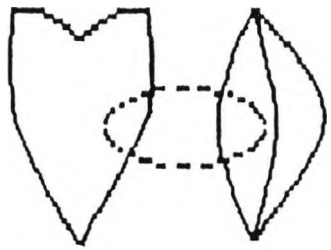

b) Linear graph

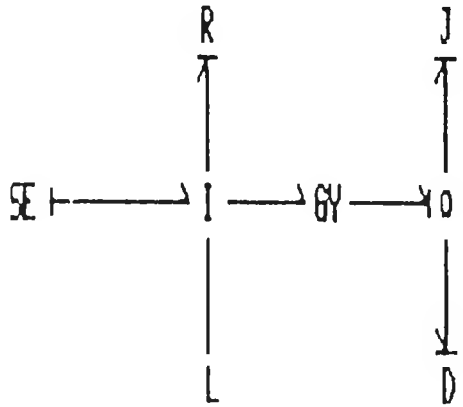

c) Bond graph

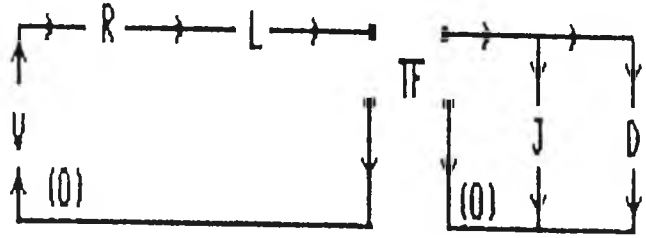

d) Structure graph.

Fig. 4.12 Electrical motor driving a frictional and inertial load.

Mechan. transl. } *The node represents a common*
Mechan. rotat. } *displacement point.*

One node, the zero, ***(0)*** node is used as a common reference point for all energy domains.

– Connecting lines or *edges:* They connect the elements to the nodes or other elements and are used for transmitting or receiving variable information.

– Joining lines: They join two identical nodes and serve only pictorial purposes.

– Arrows: They represent either:

- direction of a flow variable, or
- direction of signal transfer.

A more detailed presentation of Structure graphs elements is given in Appendix B. A structure graph is a collection of elements, nodes, connecting lines and arrows combined according to the following rules of construction:

1) There must be a node separator, (except for signal pickoffs), between any element topologically attached to another element.

2) Each edge must have an arrow even if this provides redundant information.

3) There must be an actual or implied common reference point, (the 0 node) for each separate graph segment.

With the earlier version of ***MEDIEM*** developed on a ***PDP–11*** minicomputer the user had to type in the structure graph as a series of alphanumeric input lines describing the interconnections of nodes and elements. A subsequent adaptation of the package for the ***ICL "PERQ"*** and the ***Whitechapel "MG –1"*** workstations made use of their better graphical capabilities to improve user interaction at the initial stage of graph formulation and facilitate better graphical output at the final stage of simulation.

4. 5. 3 The *MEDIEM* Quarter–vehicle Suspension Model.

The dynamic quarter–vehicle computer simulations in this study were performed on both the ***ICL "PERQ"*** and ***Whitechapel MG −1*** workstations and the model's structure graph as entered by the user is shown in Fig. 4.13. As can be seen the ***MEDIEM*** graphical representation corresponds closely to the schematic of the suspension system as shown in Fig. 2.9 and Fig. 3.1.

The two masses m_1 and m_2 are represented by the energy storage *Inductance* type elements ***L1*** and ***L2*** respectively.

The vehicle suspension and tyre springs are represented by the *Capacitance* type equivalent storage elements ***C1*** and ***C2*** with values:

$$C1 = \frac{1}{k_1} \quad \text{and} \quad C2 = \frac{1}{k_2}, \quad \text{respectively.}$$

The dampers are accounted for by equivalent energy dissipating, *(Resistance)* elements and:

$$R1 = \frac{1}{b_1} \quad \text{and} \quad R2 = \frac{1}{b_2}, \quad \text{respectively.}$$

The Single point contact tyre model was selected for the simulation because of ***MEDIEM 's*** inability to handle multiple system inputs separated by time delays. As a type of a translational mechanical system the vehicle suspension model will accept as an input either ***a mechanical force*** *(Through source)*, or ***a velocity*** *(Across source)*. The expressions for the vertical velocities corresponding to smoothed step/bump road profiles were developed earlier, (Equations 4.6, 4.7), and were used as the model's inputs. However, their implementation in ***MEDIEM 's*** environment would require the introduction of a combination of elements, (at least one of them nonlinear).

These elements are selected from the ***MEDIEM's*** standard set of elements

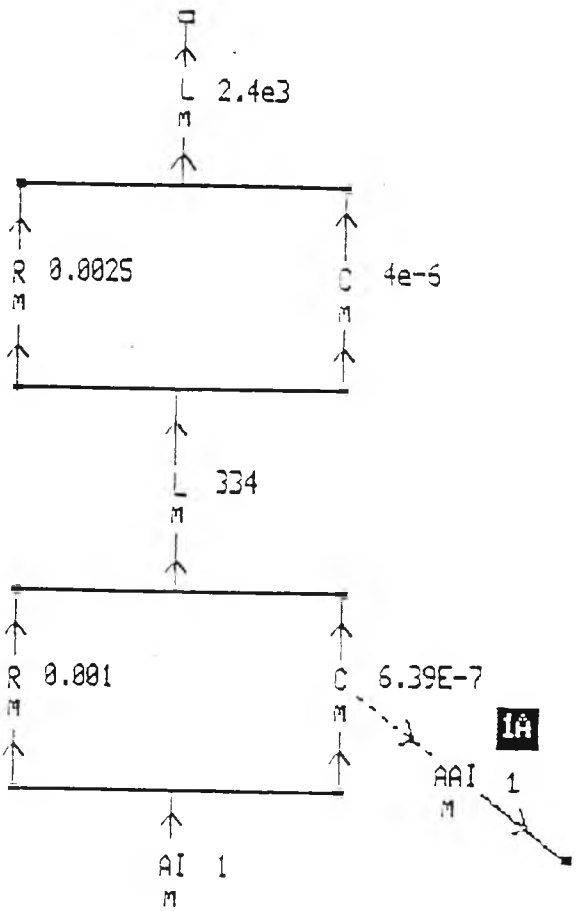

Fig. 4.13 MEDIEM graphical input of the Quarter-vehicle model.

to represent different parts of the input equations. An *Across Step* source element *(AS)* stands for the amplitude part of the vertical velocity expressions:

$$AS = \frac{\pi . h}{2T} \quad [m/s] \; ;$$

This arrangement makes the obstacle's height h indirectly accessible through the AS element thus allowing for easy step/bump height changes in the course of simulation.

A two-value *Across Ramp* element, *(AR)* specifies the rate of amplitude change *(ramp slope)*:

$$AR = \frac{1}{T} = \frac{U}{l_o} \quad [s^{-1}] \; ,$$

where: l_o – obstacle length in the direction of travel.

Vehicle speed can be indirectly controlled by accordingly changing the AR element values.

And finally a signal *Across-Across* transfer element, *(AA)* serves as the *non-linear* multiplying member:

$$AA = cos \; \pi . (\frac{t}{T} - \frac{1}{2}) \; ;$$

The element is entered in a table form for values of t relative to the residence time T during which the tyre is over the obstacle - see Table 4.3, element No 9.

A *Through* type output, (force) is selected over the model's input edge for the dynamic wheel force in the point of contact to be calculated and displayed. However, for the purpose of presenting the output in the form of the Impact Factor, *(IF)* , the value of AS has to be normalised to the static weight

```
fastep empty vehicle n=3mm,20mph,AR=1/T,T=0.02B,t=0.0,2.0,0.005,)
 Outputs are:
    th    9
 TIME: 0.000E+00   2.000E+00   5.000E-03  PLOTTING RATE IS :
 FREQ: 0.000E+00   0.000E+00   0.000E+00   LOG. IS -1.0
 PLOTTING IN TIME - RANGE IS : -5.000E+01   5.000E+01
 PLOTTING IN FREQUENCY - RANGE IS :  0.000E+00   0.000E+00
```

NO	ELEMENT	ARROW	NODE	CONNECT	DOM.	VALUE1	VALUE2
1	1	fr	4	0	m	2.000E+02	0.000E+00
1	1	to	0				
2	2	fr	5	0	m	2.500E-04	0.000E+00
2	2	to	4				
3	3	fr	5	0	m	4.000E-06	0.000E+00
3	3	to	4				
4	4	fr	12	0	m	1.000E-03	0.000E+00
4	4	to	9				
5	5	fr	12	0	m	6.390E-07	0.000E+00
5	5	to	9				
6	1	fr	9	0	m	5.000E+02	0.000E+00
6	1	to	5				
7	13	fr	0	0	m	1.630E-03	0.000E+00
7	13	to	14				
8	14	fr	0	0	m	0.000E+00	3.570E-01
8	14	to	16				
9	15	to	12	7	m	0.000E+00 0.000E+00 0.000E+00 0.000E+00 0.000E+00 0.000E+00 0.000E+00 0.000E+00 0.000E+00 0.000E+00 0.000E+00	0.000E+00 0.000E+00 0.000E+00 0.000E+00 0.000E+00 0.000E+00 0.000E+00 0.000E+00 0.000E+00 0.000E+00 0.000E+00

Table 4.3 MEDIEM model listing for a step profile.

of the semiaxle:

$$AS = \frac{\pi.h}{2.T.(m_1 + m_2).g} \quad ;$$

A list of the model parameter values as well as the conditions of simulation in the time domain is shown in Table 4.3. The list also illustrates the textual description of the model as it used to be entered with the older versions of ***MEDIEM***. In the current versions of the programme the parameter values are displayed in a condensed form on the graphical input screen. Nevertheless, the textual mode provides the user with the possibility for a quick look at their full values and also allows for convenient "on-line" parameter changes when model parameter variation effects are being investigated.

Chapter V: Dynamic Errors due to Road Surface Irregularities.

INTRODUCTION.

The nature and magnitude of dynamic wheel forces largely depends on the condition of the road surface. Even the best quality motorway class roads contain surface perturbations which may excite vehicle suspensions and cause considerable impact forces.

A study of the dynamic forces arising from the interaction of moving vehicles and road tracks of different description is undertaken in this Chapter to produce some quantitative data of the magnitude of those forces which could have crucial effect on the accuracy of WIM systems. The acquired data can also be used in pavement performance studies, vehicle modes of vibration, passenger comfort during travel, etc.

Two rounds of computer simulations were carried out accounting for vehicle interactions with road profiles of deterministic, and stochastic descriptions, respectively.

Time domain techniques were used to represent some common road surface perturbations of known shape. The ***MEDIEM*** package was applied to the quarter-vehicle suspension model and the tyre filtering effects were accounted for by suitably modifying model inputs. Road irregularity dimensions, as well as vehicle speed and physical parameters were varied within acceptable limits to investigate their influence on the dynamic wheel loads.

Vehicle behaviour on stochastic road surfaces was investigated in the frequency domain. A specific computer programme was developed to calculate and plot the Spectral densities of vehicle response to passages over road surfaces of relevant characteristics. The input description expression was chosen to represent motorway quality roads and the vehicle transfer function was derived from the quarter-vehicle system equations.

Most of the results are presented in both tabular and graphical form.

5. 1 DETERMINISTIC ROAD PROFILES.

Excessive suspension vibrations can be generated by the presence of abrupt surface irregularities such as the edges of weighing sensors, contraction joints of concrete carriageways, patches, potholes, bridge joints, etc. This will directly affect weighing accuracy when static vehicle weights are of measurement interest. When dynamic wheel loads are the object of measurement such irregularities will introduce high amplitude oscillations untypical of vehicle runs over normal road surface.

A study into the dynamic reaction of moving vehicles to such "isolated" track obstacles is therefore essential to obtain information about the nature of the impact forces and how they could influence the outcome of the measurement. Theoretical knowledge of the dynamic wheel forces could also be useful for the studies of pavement damage mechanisms and road structural design.

A theoretical investigation into the dynamic wheel forces generated by vehicles running over road irregularities of deterministic shape was carried out as part of this study and is described in this section.

Two sets of modelling experiments were carried out to investigate some common sources of dynamic measurement errors in WIM systems – unlevelled sensor platforms and road surface irregularities prior to weighscale. The computer simulations of vehicle-road interactions were oriented towards producing quantitative data for weighbridge designers and users in terms of WIM system construction and installation.

Simulating the dynamic response of vehicles traversing standard types of road profiles is necessary for a number of reasons:

- Most experimental studies – [114], [116], include vehicle runs over some sort of artificial road profiles – plank, ramp, bump etc., and therefore basis for comparison of experimental and theoretical results exists.

- Using profiles of standard shape and known dimensions makes it possible to obtain quantitative data about the dynamic behaviour of vehicles and

to assess the effect of different vehicle parameters and measurement conditions.

- Possibility to simulate and analyse the dynamic forces resulting from the tyres hitting an unlevelled sensor.

Two rounds of simulation trials were performed, the first dealing with the case of unlevelled sensor, and the second assessing the effect on the dynamic forces of road imperfections ahead of sensor.

5. 1. 1 Dynamic Errors due to Unlevelled Sensor.

With a very few exceptions WIM sensor platforms/cables always come into direct contact with the measured vehicle wheel or axle. Bad installation and maintenance may result in the platform not being flush with the road surface causing unwanted dynamic disturbances of the suspension. Unburied piezo or capacitive sensors standing proud of the road will have the same effect on the vehicle.

5. 1. 1. 1 Effect of Step Height. A series of simulations of wheel runs over steps of different heights were performed to emulate normal speed vehicle passages over WIM sensor platforms to various extent unflush with the road surface.

In Fig. 5.1 the *IF* outputs are plotted for two step heights showing that differences in output peaks of up to 50% have to be expected if the platform is lifted from 2mm to 5mm above the surface.

Data from these and other *IF* plots for different platform step heights are summarised in Table 5.1. Because of the linearity of the model the change in dynamic wheel forces is directly proportional to step height as can be seen in the plots:

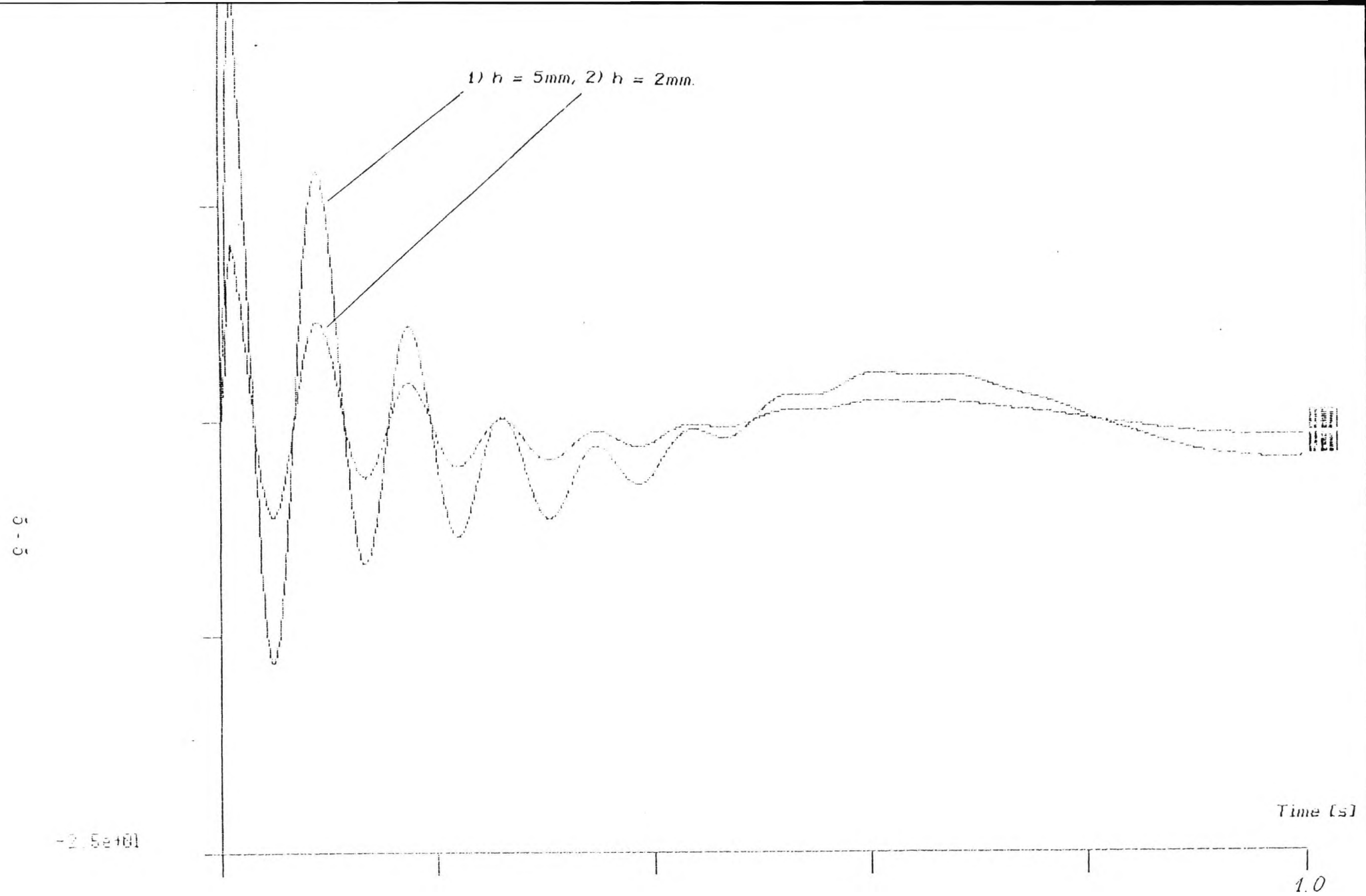

Fig. 5.1 Effect of Step height - *h, (Sensor unlevelling)* on *IF:*
U = 80km/h; 1) h = 5mm, 2) h = 2mm.

Platform Step Height - h [mm]	Peak No: (Amplitude normalised to Static Weight)			
	First Positive	First Negative	Second Positive	First Body Bounce
2	1. 12	0. 94	1. 06	1. 01
5	1. 26	0. 86	1. 14	1. 04
10	1. 51	0. 73	1. 28	1. 06
20	1. 86	0. 44	1. 57	1. 14

Table 5.1 *IF* peak values for vehicles running over platform steps of different height h ; $U = 80$ *km/h* .

On the other hand frequency content and timing of the signal are not affected by the step height. Additional simulations showed that the differences stay high even at low vehicle speeds. The analysis of simulation results proved that even small scale sensor unflushness with road surface could introduce significant dynamic weighing errors over the whole practical range of vehicle speeds.

5. 1. 1. 2 Effect of Vehicle Speed. The objective of this part of the simulations was to obtain information about the effect of speed on the results of axle weighings, when the tyres hit a step-shaped irregularity presumed to be the edge of the weighing platform.

Simulation runs were performed at five different vehicle speeds starting with *10km/h*, which is a normal operational speed for most of the present, (slow speed) WIM systems. The range of intermediate and high speed passages – *20km/h, 60km/h, 100km/h,* was covered more thoroughly. Finally a *140km/h* run was simulated mostly for theoretical purposes.

The important peak values information is shown in Table 5.2 and the *IF* output plots for the different speeds are displayed in Fig. 5.2. The graphs in Fig. 5.2 show that first positive peak amplitudes rise rapidly with speed to about

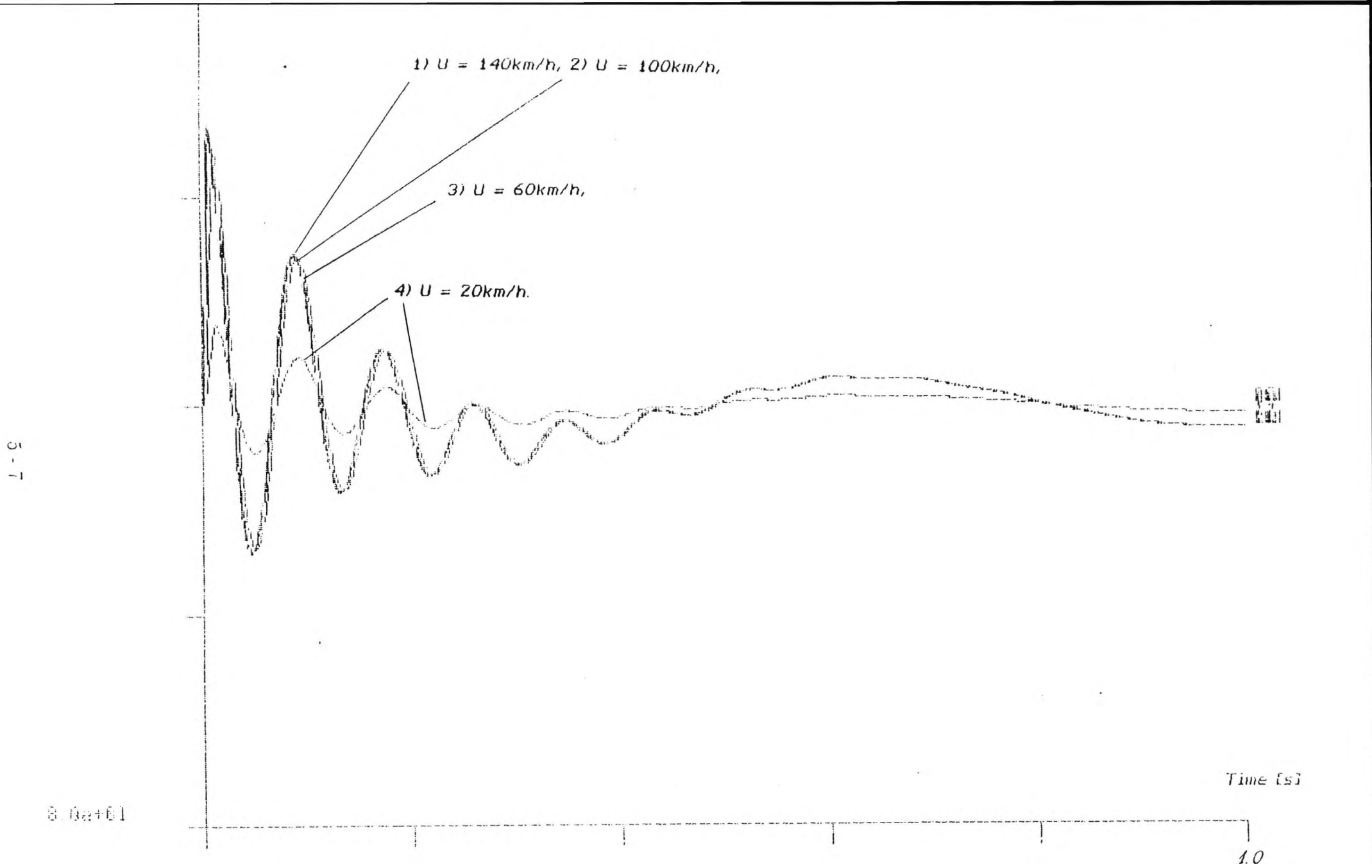

Fig. 5.2 Effect of Vehicle horizontal Speed - U on IF: $h = 0.01m$;
1) $U = 140km/h$, 2) $U = 100km/h$, 3) $U = 60km/h$, 4) $U = 20km/h$.

60km/h above which the effect gradually fades. This can be explained by the fact that at very high speeds the axle and the whole mass above the tyre will not have time to respond to surface irregularities, and the whole vehicle reaction will be provided solely by tyre deflection. Therefore with speed rising, the first positive peak amplitudes *(wheel hop)*, start to approach a maximum value approximately equal to the product of tyre stiffness and step height.

The same pattern of rapid amplitude increase with speed in the low speed range and almost none at higher speeds is observed with the other important *IF* peaks. This results in the characteristic "grouping" of the *IF* graphs for the speeds above *60km/h* – Fig. 5.2.

Vehicle Speed - U [km/h]	*Peak No: (Amplitude normalised to Static Weight)*			
	First Positive	*First Negative*	*Second Positive*	*First Body Bounce*
10	*1. 11*	*0. 93*	*1. 04*	*1. 01*
20	*1. 17*	*0. 84*	*1. 09*	*1. 02*
60	*1. 50*	*0. 74*	*1. 26*	*1. 05*
100	*1. 55*	*0. 70*	*1. 29*	*1. 07*
140	*1. 56*	*0. 69*	*1. 30*	*1. 07*

Table 5. 2. *IF* peak values for vehicles running over sensor platform at different speeds *U ; h = 0. 01 m ;*

In terms of WIM accuracy the vehicle speed effects may lead to extremely large measurement uncertainties in the range (10 – 60)km/h. Depending on the method of signal detection and processing, (peak detection being the worst case), repeatability errors as large as the differences in the *IF* peak values may occur.

Imposing speed limits in the region of the weighscale is a regular practice on present WIM sites though it may not be always applicable. For high speed WIM systems a speed correction factor may be introduced in the signal processing algorithm which would almost certainly require vehicle speed

measurement.

5. 1. 1. 3 Effect of Variation of Vehicle Parameter Values. In this part of the study the aim of the computer simulations is to investigate the contribution of each major vehicle component to the dynamic forces applied to the weighscale after hitting its edge. The investigation has to identify the technical parameters of the vehicle which are most crucial for its dynamic behaviour, but could also provide helpful information when vehicle suspensions and tyres are considered in view of minimal road damage caused by dynamic loading.

The parameters of primary importance for the dynamic behaviour of the vehicle and the corresponding model elements are expected to be:

- Tyre inflation pressure, (tyre spring stiffness – k_1) ;
- Vehicle laden weight, (sprung vehicle mass – m_2) ;
- Suspension stiffness, (suspension spring rate – k_2) ;
- Shock absorbers, (suspension damping – b_2) ;

During the simulation runs over a step of height $h = 0.01m$ and a constant speed of $U = 80km/h$, the value of each parameter was varied in turn within reasonable limits, keeping all the other parameter values constant.

The following observations were made for each of the variables:

i) Tyre inflation pressure: It has been shown – [119], that in the working range of car tyres the stiffness of the carcass increases linearly with inflation pressure. However, because of the many other factors influencing tyre stiffness, (tyre static load, differences in static and dynamic stiffnesses, roll frequency etc), no direct relationship between inflation pressure and tyre stiffness was used when the value of k_1 was varied. The simpler approach of assigning preset values smaller or greater than the reference value used so far in the model: $k_1 = 1564kN/m$, was applied instead.

The graphs of the IF for two different values of tyre stiffness k_1, are plotted in Fig. 5.3. Important peak values for two smaller, as well as two greater than the original k_1 values are displayed in Table 5.3. The graphs show considerable differences both in amplitudes and frequencies of the *wheel hop* oscillations while there is almost no change in the *body bounce* peaks.

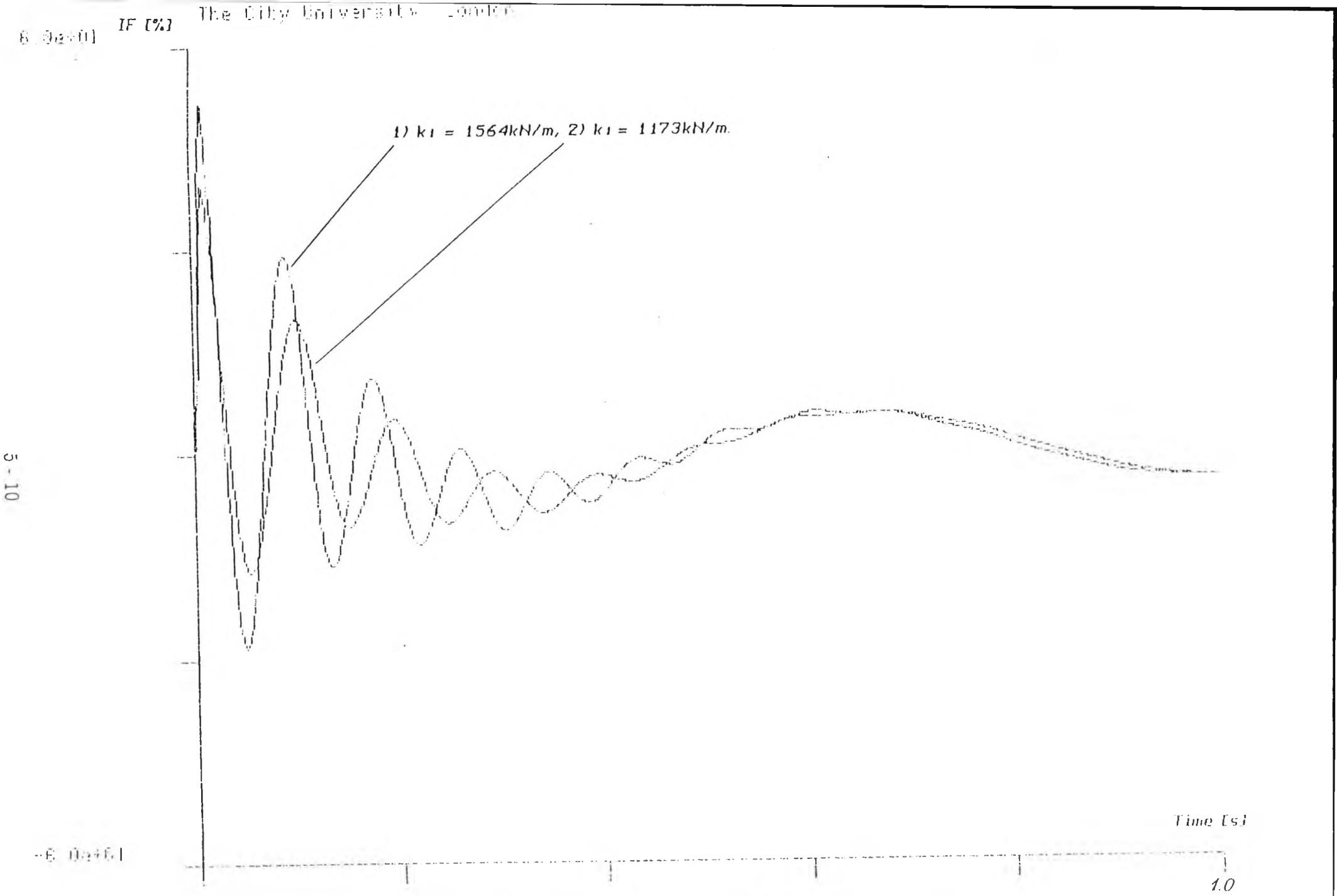

Fig. 5.3 Effect of Tyre Stiffness - k_1 on IF: $U = 80km/h$; $h = 0.01m$;
1) $k_1 = 1564kN/m$, *2)* $k_1 = 1173kN/m$.

Tyre Stiffness k_1 [kN/m]	Peak No: (Amplitude normalised to Static Weight)			
	First Positive	First Negative	Second Positive	First Body Bounce
$0.5.k_1 = 782$	1. 27	0. 92	1. 09	1. 06
$0.75.k_1 = 1173$	1. 41	0. 83	1. 20	1. 06
$1.0.k_1 = 1564$	1. 51	0. 73	1. 28	1. 06
$1.25.k_1 = 1955$	1. 61	0. 63	1. 39	1. 06
$1.5.k_1 = 2346$	1. 73	0. 52	1. 49	1. 06

Table 5.3 *IF* peak values for different Tyre stiffness values k_1 ; $U = 80\ km/h$; $h = 0.\ 01\ m$;

The steep rise in amplitudes with increase of tyre stiffness is due to the decreasing capability of the tyre to absorb the force of the impact and thus to "soften" the initial vehicle response. The frequency shift can be explained with the change in the *wheel hop* resonance, f_w (Eq. 2.5), when changing k_1.

ii) Vehicle Laden Weight: Unlike other model parameters the sprung vehicle mass, m_2, depends not only on the vehicle's design characteristics, but also on the carried load. In this respect it is the most changeable vehicle parameter of importance for its dynamic behaviour.

The results of previous theoretical and experimental studies – [74], [106], [107], generally prove that increasing the laden weight correspondingly increases the *total dynamic wheel load* while relatively reducing the *dynamic component* of this load.

The computer simulation runs of the model over a step of height $h = 0.01m$ for different values of the sprung mass m_2, lead to similar conclusions though in quantitative terms they reflect the parameter specifics of the test vehicle chosen for the model. Three values for m_2 were used apart from the reference value, to represent approximate estimates of empty, laden and fully laden quarter-vehicle weights.

The effect of varying laden vehicle weight on its dynamic behaviour is illustrated in Fig. 5.4 with the corresponding peak values are summarised in Table 5.4:

Sprung Mass Weight - m2 [kg]	*Peak No: (Amplitude normalised to Static Weight)*			
	First Positive	*First Negative*	*Second Positive*	*First Body Bounce*
Empty - 1800	*1. 64*	*0. 62*	*1. 36*	*1. 08*
Normal - 2400	*1. 51*	*0. 73*	*1. 28*	*1. 06*
Laden - 2800	*1. 45*	*0. 76*	*1. 25*	*1. 04*
Fully Lad. - 3200	*1. 37*	*0. 80*	*1. 22*	*1. 03*

Table 5.4 *IF* peak values for vehicles with different laden weights (sprung mass, m_2), running over platform step of height $h = 0.01m$ at speed $U = 80\ km/h$.

The results show greatest reduction in the amplitudes of the *first wheel hop,* and the *body bounce* peaks when increasing the laden weight of the vehicle. The frequency of the *body bounce* is affected too – increasing m_1 predictably increases the wavelength of the *body bounce* – Eq. 2.6.

From the point of view of weighing accuracy the changing dynamic behaviour of the vehicle with sprung mass variations would mean that different degree of dynamic effects interference will occur over the range of the loads carried by the vehicle. If adequate suppression of these effects is not provided in the measurement then the accuracy of weighing will depend on the widely ranging value of the sprung mass.

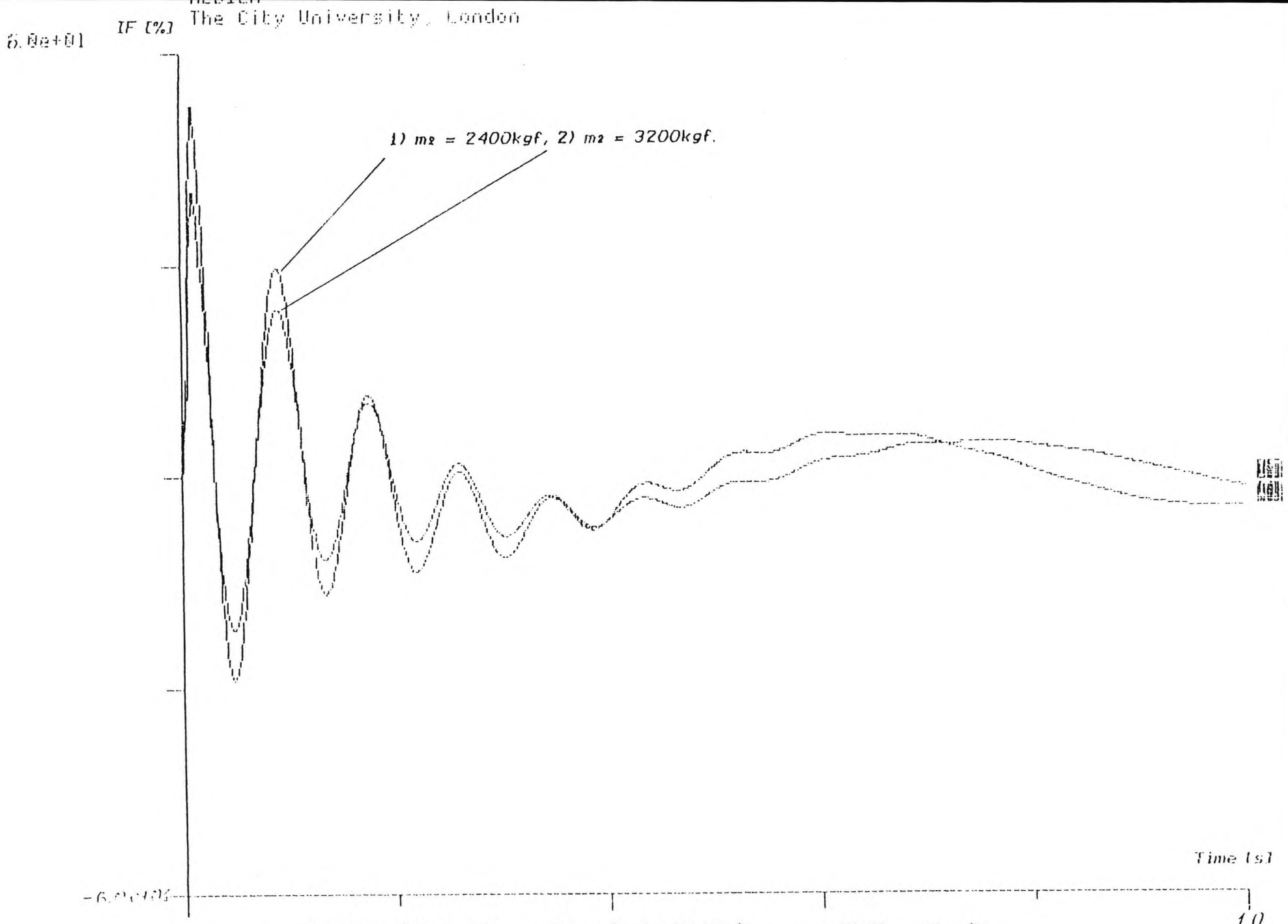

Fig. 5.4 Effect of Sprung Mass *(Laden Weight)* - m_s on *IF*: $U = 80km/h$; $h = 0.01m$; 1) $m_s = 2400kgf$, 2) $m_s = 3200kgf$.

iii) Suspension Stiffness: The major task of vehicle's suspension is to ensure safe and comfortable ride of passengers and cargo, i. e. to reduce the vertical accelerations on the vehicle's body. The properties of the suspension (stiffness and damping), however, may also have a considerable effect on the dynamic wheel forces applied to the road.

Suspension stiffness in our model is represented by the *suspension spring rate* – k_2. The reference value of $250kN/m$ was varied in steps of $\frac{k_2}{4}$, up and down, i. e. to simulate the effect of "stiffer" and "softer" suspensions, respectively. The resulting differences in the dynamic behaviour of the vehicle are illustrated in Fig. 5.5 and the major peak values of importance for the measurement are presented in Table 5.5:

Suspension Stiffness - k2 [kN/m]	*Peak No: (Amplitude normalised to Static Weight)*			
	First Positive	*First Negative*	*Second Positive*	*First Body Bounce*
0.5.k2 = 125.0	*1. 51*	*0. 66*	*1. 32*	*1. 03*
0.75.k2 = 187.5	*1. 51*	*0. 69*	*1. 30*	*1. 04*
1.0.k2 = 250.0	*1. 51*	*0. 73*	*1. 28*	*1. 06*
1.25.k2 = 312.5	*1. 51*	*0. 75*	*1. 28*	*1. 08*
1.5.k2 = 375.0	*1. 51*	*0. 77*	*1. 28*	*1. 11*

Table 5.5 *IF* peak values for different Suspension spring rates – k_2; $U = 80\ km/h$; $h = 0.01\ m$;

The simulation outputs confirm the prediction that suspension stiffness should mostly affect the oscillatory mode of the the sprung mass m_2. The amplitude differences of the first *wheel hop* peaks are negligible whereas the amplitudes of the second tend to fall slightly with increase of the suspension stiffness. However, the differences become obvious in the subsequent wheel hops and especially in the first *body bounce* peak. The latter's amplitude rises more

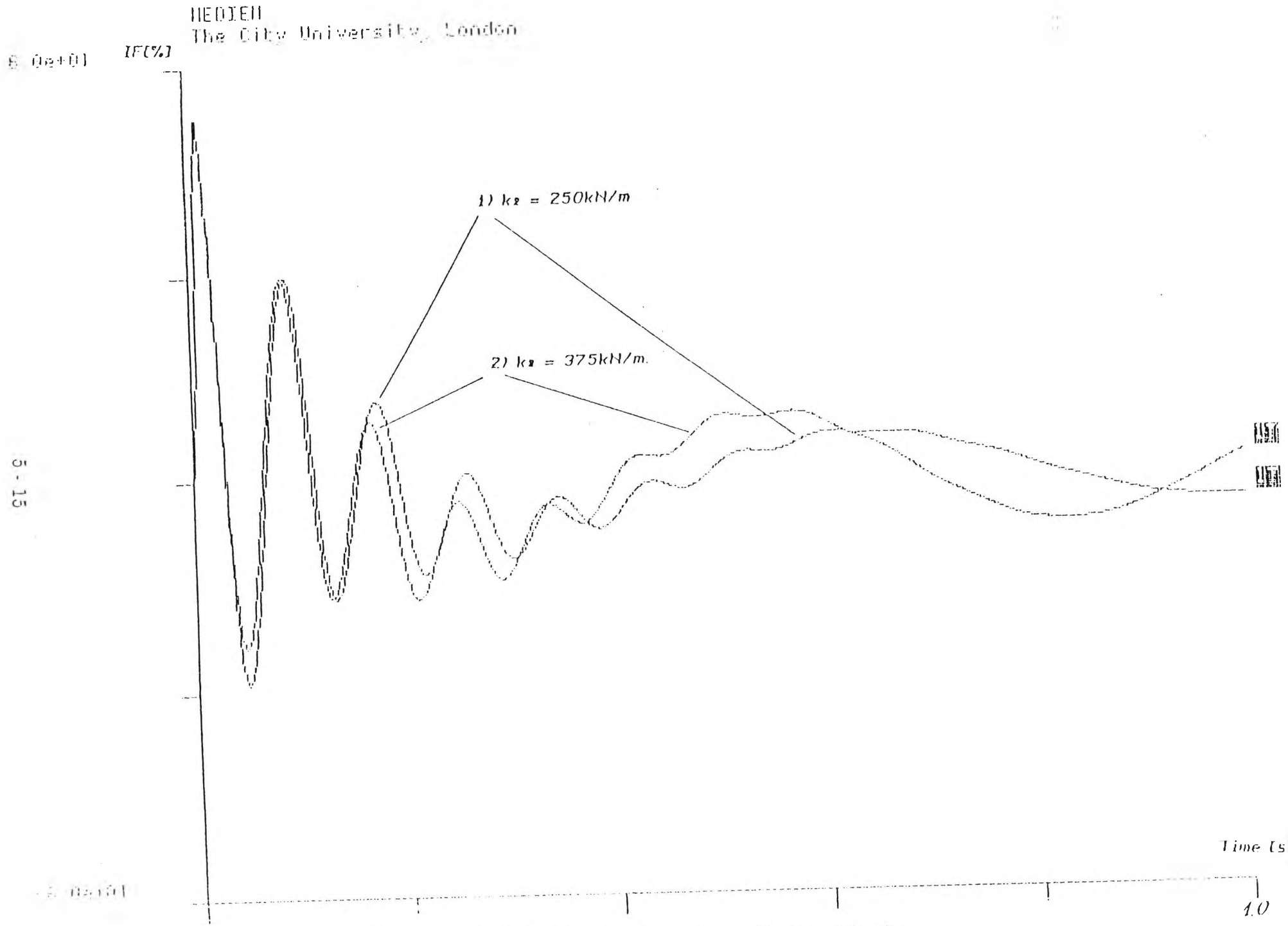

Fig. 5.5 Effect of Suspension Stiffness - k_2 on IF: $U = 80km/h$;

than three times when increasing the stiffness of the suspension from $0.5k_2$ to $1.5k_2$. A change in the wavelength is also observed which reflects the shift in the body bounce natural frequency of the vehicle f_b – Eq. 2.6.

A number of experimental studies have been also conducted to assess the dynamic performance of some existing types of HGV suspensions in terms of their pavement damaging potential – [74],[88],[135]. In this respect the air and hydraulically suspended vehicles have shown best results.

On the whole the simulation results did not indicate a particularly strong effect of suspension stiffness on the dynamic wheel forces. However, that effect was mainly displayed in the body bounce frequency region, which previously was shown to dominate the spectrum of the dynamic forces. On the other hand, except for very low speeds, body bounce will be out of reach for most WIM systems because of the time delay it takes the vehicle body to be excited after hitting the edge of the platform. Therefore the findings would apply chiefly to *slow-motion* and *quasi-static* axle weighers.

iv) Shock Absorbers: As it was pointed out earlier, these provide the major mode of energy dissipation in the system and therefore to a great extent determine the damping of the generated oscillations.

The same variation procedure as used with the other parameters was applied for b_2 (reference value: $b_2 = 4000\ N.s/m$) and the output graphs for the different values of b_2, as well as the important amplitude peaks are presented in Fig. 5.6 and Table 5.6, respectively.

The results show that increase of suspension viscous damping has little effect on the *first wheel hop* peak but provides a considerable reduction in the subsequent peaks and especially in the *body bounce* oscillations.

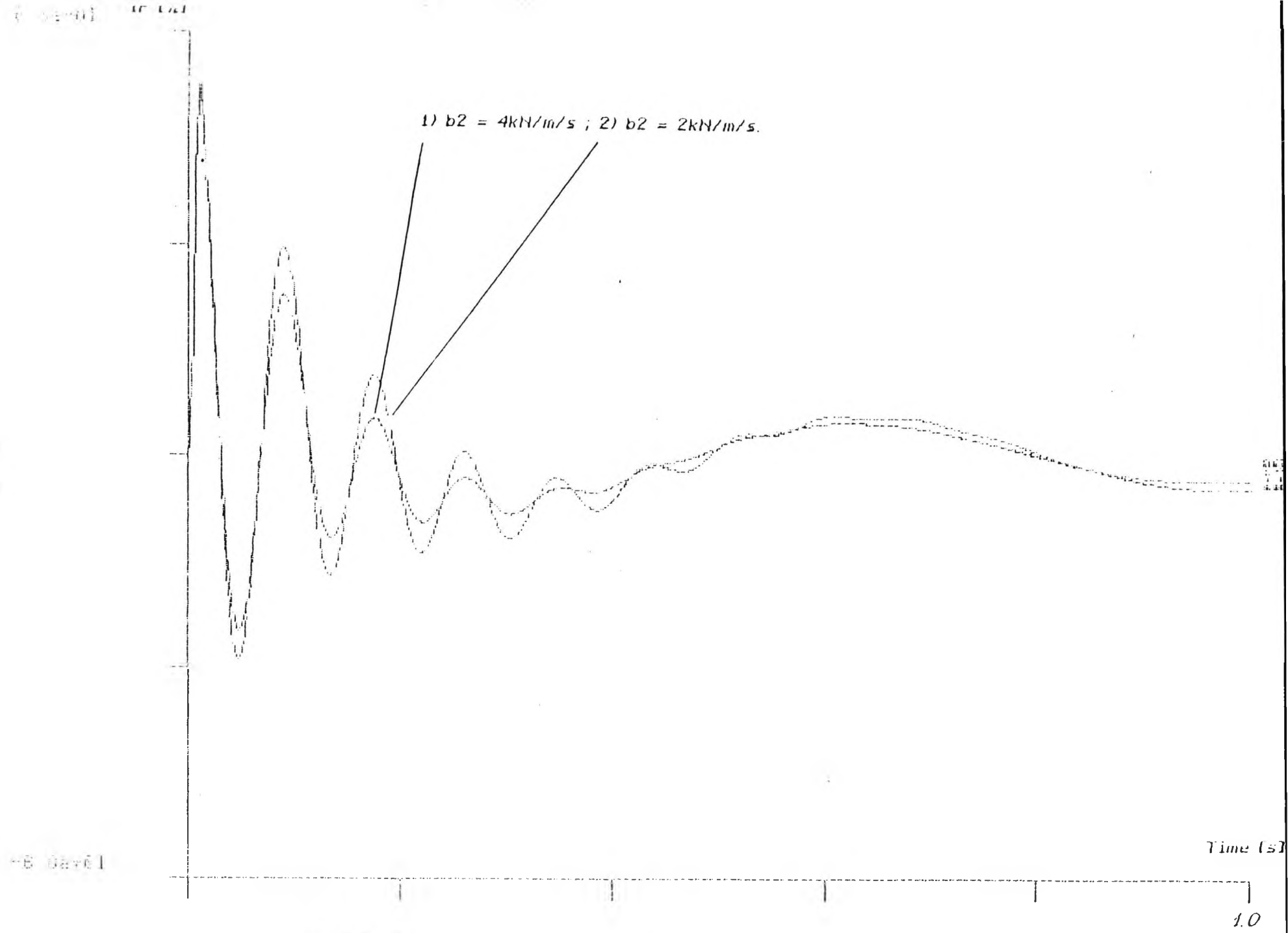

Fig. 5.6 Effect of Suspension Damping - b_2 on IE: U = 80km/h h = 0.01m

Suspension Damping — b_2 [kN.s/m]	Peak No: (Amplitude normalised to Static Weight)			
	First Positive	First Negative	Second Positive	First Body Bounce
$0.5.b_2 = 2.0$	1. 52	0. 65	1. 37	1. 09
$0.75.b_2 = 3.0$	1. 52	0. 67	1. 34	1. 07
$1.0.b_2 = 4.0$	1. 51	0. 73	1. 28	1. 06
$1.25.b_2 = 5.0$	1. 51	0. 75	1. 25	1. 04
$1.5.b_2 = 6.0$	1. 50	0. 8	1. 17	1. 02

Table 5.6 *IF* peak values for different Suspension damping coefficients – b_2; $U = 80$ km/h ; $h = 0.01$ m;

In terms of weighing accuracy the significance of suspension damping for dynamic effects induced errors will hardly be crucial, again because of the time delay necessary for the effect to take action and which will coincide with the weighing period.

v) **Other Parameters:** When within their operational ranges the remaining two system parameters – unsprung mass, m_1, and tyre damping, b_1. are relatively unimportant for the dynamic behaviour of the vehicle. However, amplitudes fall slightly with reduction of m_1, and some rise in *wheel hop* frequency, f_w, is also observed – Eq. 2.5.

Tyre damping, b_1, has even smaller effect – amplitudes fall slightly with increase of b_1. This may explain why in many tyre models the damping element is omitted.

5. 1. 2 Measurement Considerations.

The computer simulations described in this subsection give an insight into the process of the dynamic contact between the weighing sensor and the vehicle tyre passing over it. The dynamic errors are quantified for the specific model parameters and expressed as a fraction of the static vehicle weight.

The overall analysis of simulation results shows that a substantial dynamic component, *IF* is introduced in the signal, even by minor sensor unflushness with road. The magnitude of the dynamic component depends to a great extent on the height of the protruding sensor, but is also dependent on a number of additional factors associated with the vehicle's physical parameters, as well as the speed of passage. In Table 5.7 the ranges of change of the *IF* are shown when sensor step height ***h***, vehicle speed ***U***, and certain vehicle parameters are varied between their extreme practical values. Only the first positive *wheel hop* and *body bounce* peaks are featured as the *IF* is at its maximum there.

Parameter varied: (Range)		*h (2-20) mm*	*U (10-140) km/h*	*k1 (0.5-1.5) x k1*	*m2 (0.75-1.3) x m2*	*k2 (0.5-1.5) x k2*	*b2 (0.5-1.5) x b2*
Range of IF change: [%]	*Wheel Hop*	*74*	*45*	*46*	*27*	*0*	*2*
	B.Bounce	*13*	*6*	*0*	*5*	*8*	*5*

Table 5.7 *IF* span for full range parameters variation: $h = 0.01m$, $U = 80km/h$.

Although slightly exaggerated because of the use of the *Single point contact* tyre model, and by the fact that the results cover the whole *min−max* range of the parameters, the figures in the Table show the scale of the expected dynamic errors if the sensor is not level with ground. The measurement accuracy will be further deteriorated by the additional effects of vehicle parameter variations. These will cause differences in the dynamic response of the various vehicles or even same class vehicles but with one or more different parameters. Laden weight and tyre stiffness are the parameters most likely to fluctuate widely within their ranges even for same class vehicles.

The general conclusion can be made that considerable effort should be put in the installation and maintenance of weighing sensors so that minimal unflushness ($h \leq 2mm$) is ensured for reliable measurements.

5. 1. 3. Dynamic Errors due to Road Profile Irregularities ahead of a Sensor.

In the siting of permanent or temporary WIM systems it is also important to reduce dynamic errors from road imperfections ahead of the weighscale. The question is often asked as to how smooth the road surface should be on the approach of a weighscale installation.

A computer simulation study was undertaken at the request of the TRRL to provide some guidelines for WIM approach surface quality.

5. 1. 3. 1 Simulation Planning. Data was supplied from the TRRL about the vehicle weights when empty, half-laden and fully laden, and the corresponding half-axle values were calculated for m_2. The simulations consider two road profile imperfections ahead of the weighing sensor:

i) an abrupt step of variable height h;

ii) a bump of rectangular cross-section with variable length in the travel direction l_b, and variable height h.

At first an analysis was carried out to compare the dynamic response of the vehicle on encountering the two different types of obstacles. For each combination of road profile imperfection, vehicle weight and vehicle speed, the simulation allows a calculation of the dynamic error when the imperfection is a fixed distance ahead of the sensor. By varying the position and height of the bump (or step), and varying vehicle speed it is possible to build up a picture of the dynamic errors. These are presented both in tabular and graphical form in such a way that they may be used by an engineer in the siting of a weighbridge or in the assessment of errors in existing weighbridge installations.

Here again the dynamic error is expressed as a fraction of the vehicle static weight:

$$W_s = (m_1 + m_2).g \; ;$$

The element AS representing the amplitude of the input is given the value:

$$AS = \frac{\pi.h}{2.T.(m_1 + m_2).g} \cdot 100, \ [\%],$$

and the simulation results ***(Impact Factor)***, will then be percentage error of static weight.

For a fully laden vehicle moving at 60mph (96km/h), traversing a *step* of height $h = 10mm$, results are shown in Fig. 5.7. If these are compared with those for a *bump* of the same height and length $l_b = 0.5m$ – Fig. 5.8, it can be seen that setting time is considerably longer for the *step*. These results showed that it was necessary to consider both steps and bumps. It can also be seen from the graphs that the time taken for the error to be reduced below some specified value can be roughly discerned. For more accurate determination, the minimum and maximum values to be plotted can be selected within ***MEDIEM*** as can also the simulation time. For example in Fig. 5.9 the error has been set at $\pm 5\%$ and the time when it goes below that value can clearly be discerned. The time can be taken either as when the signal first comes within the specified error limits, or when the envelope of the peaks or troughs come within the error limits. Although a little more difficult to discern the latter was chosen. Fig. 5.10 shows how the $\pm 5\%$ error time would be discerned setting plotting limits within ***MEDIEM*** at $\pm 10\%$. With this error time and the vehicle speed U, the distance s can be determined.

Results for various step and bump heights, vehicle speeds and laden weights were obtained in this manner and are presented in the next subsection.

5. 1. 3. 2 Simulation Results. The three vehicle weights obtained from TRRL were:

a) Laden axle weight of 18000lbf = 4100kgf half axle weight comprising 3600kgf sprung weight and 500kgf unsprung weight.

b) Half laden: 9000lbf = 2050kgf half axle comprising 1550kgf sprung and 500kgf unsprung.

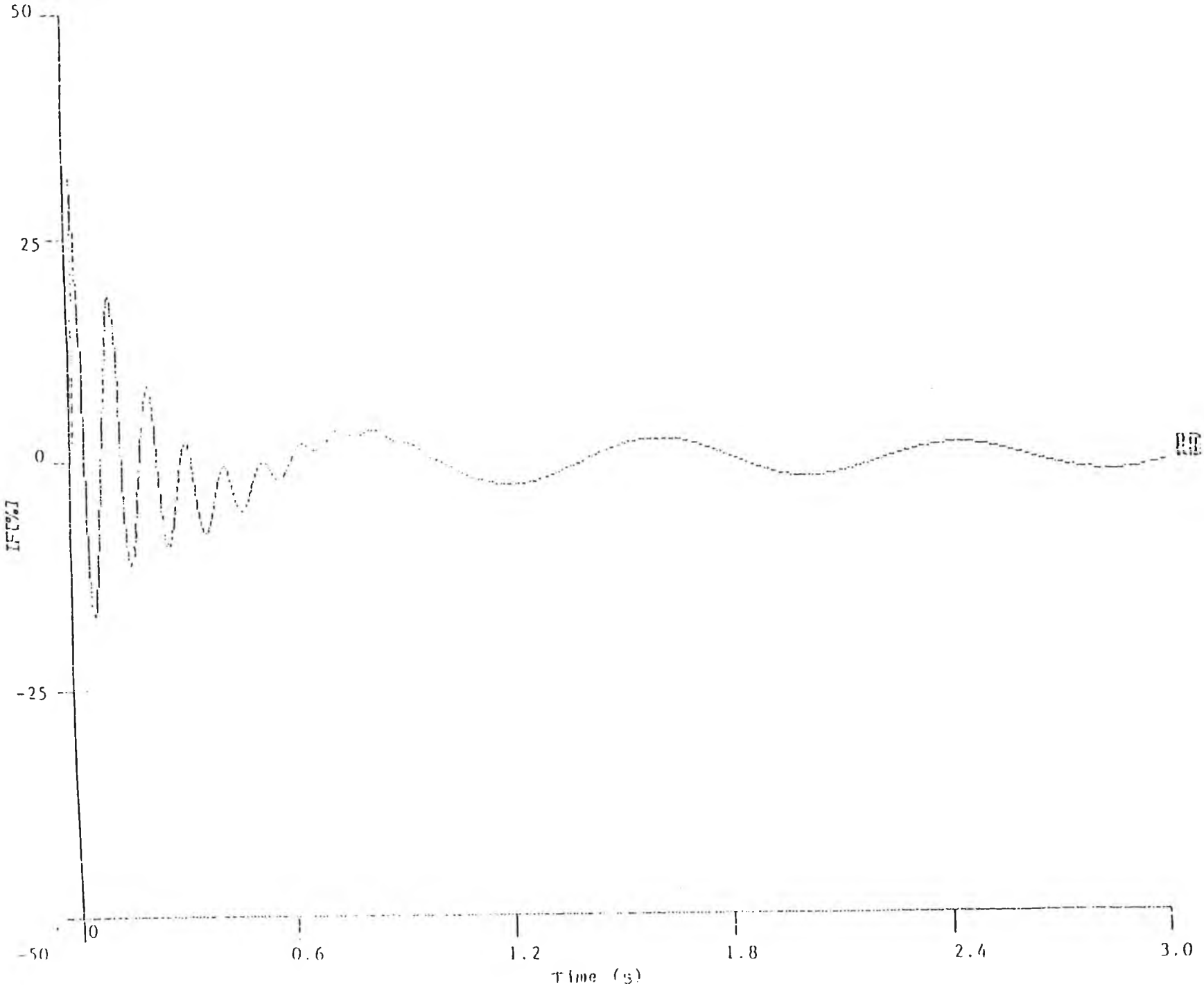

Fig. 5.7 Dynamic Error for a Step: $U = 96km/h, \quad h = 0.01m.$

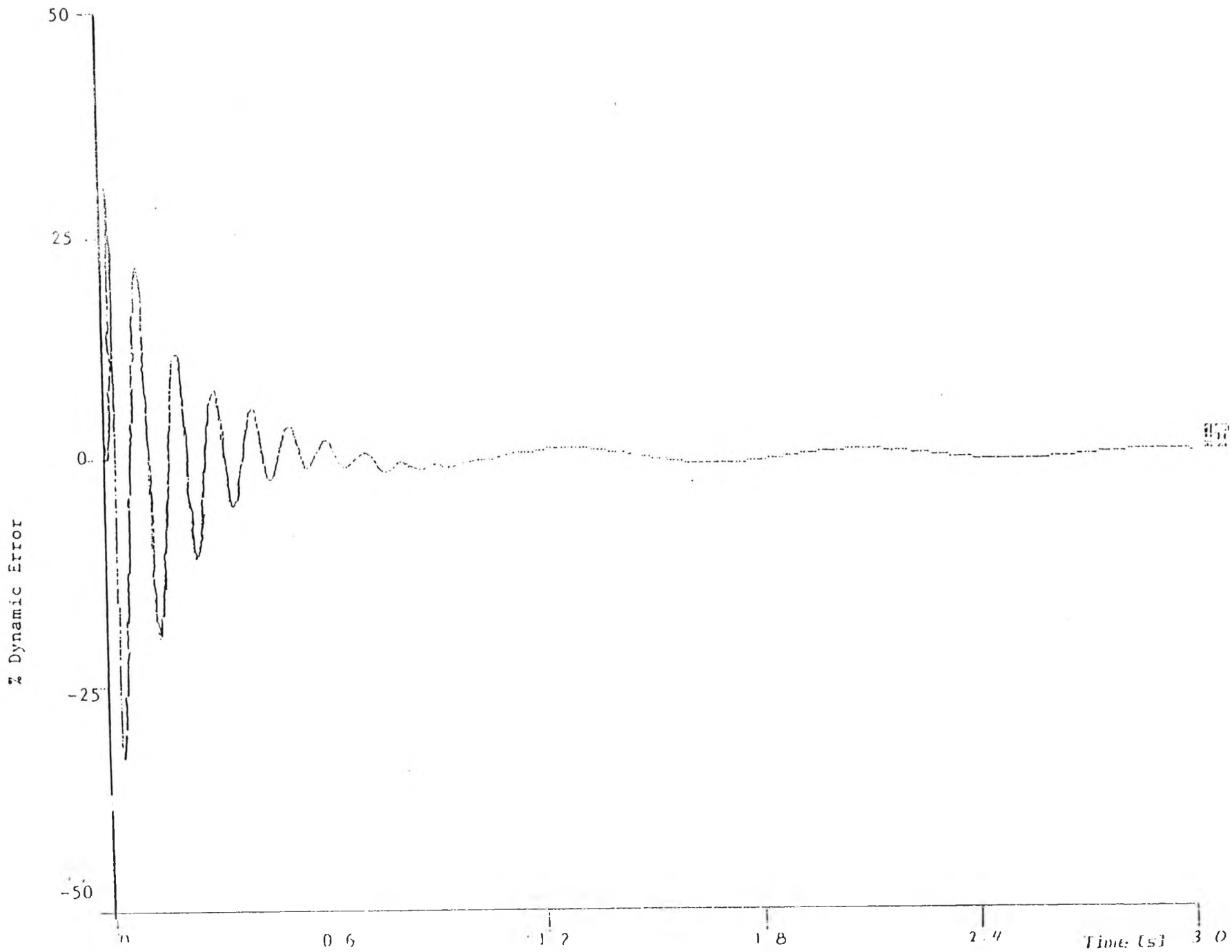

Fig 5.8 Dynamic Error for a Bump: $U = 96km/h, \quad h = 0.01m.$

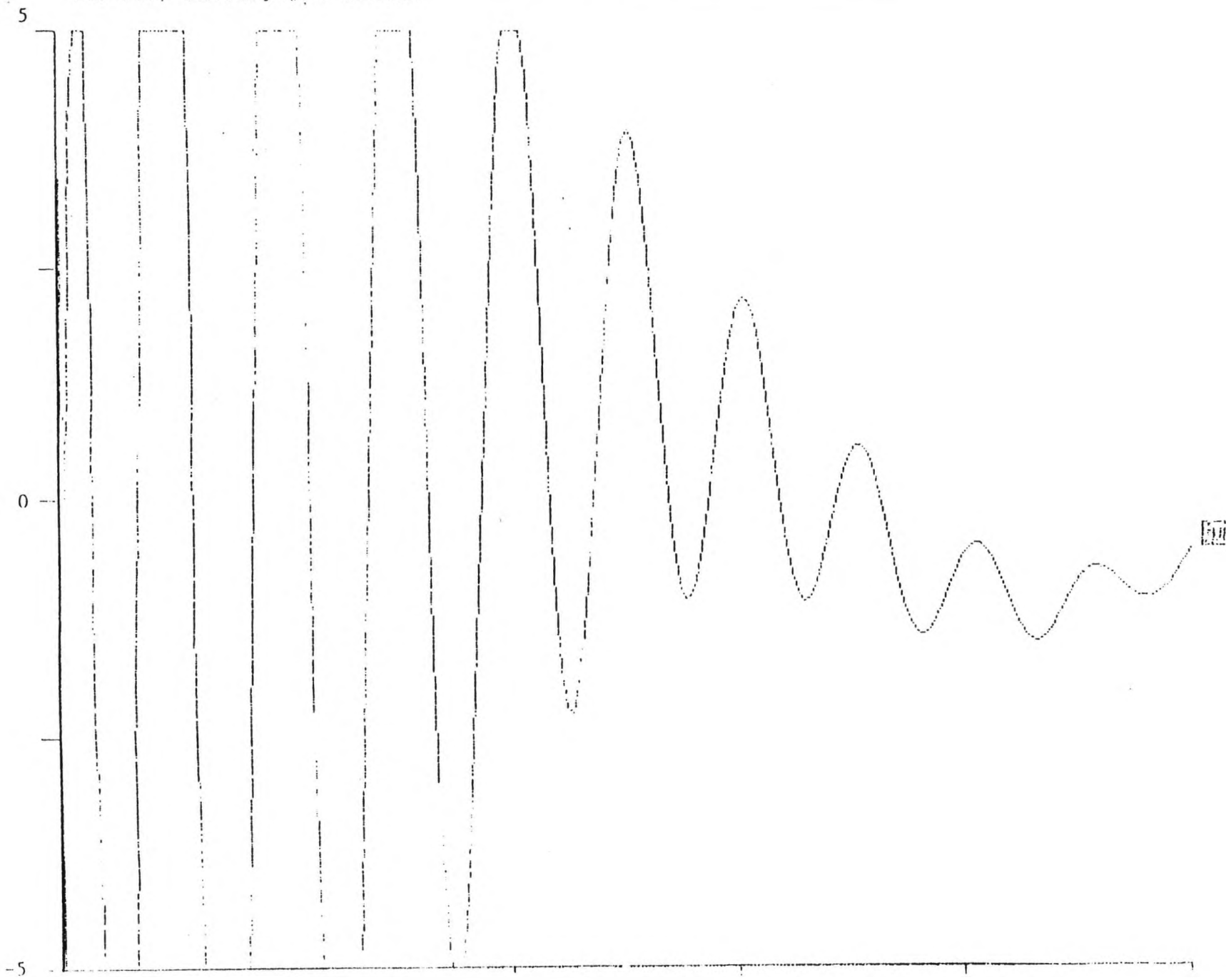

Fig. 5.9 Determination of time τ necessary for dynamic error ϵ to fall under a preset value, $(\epsilon = \pm 5\%)$.

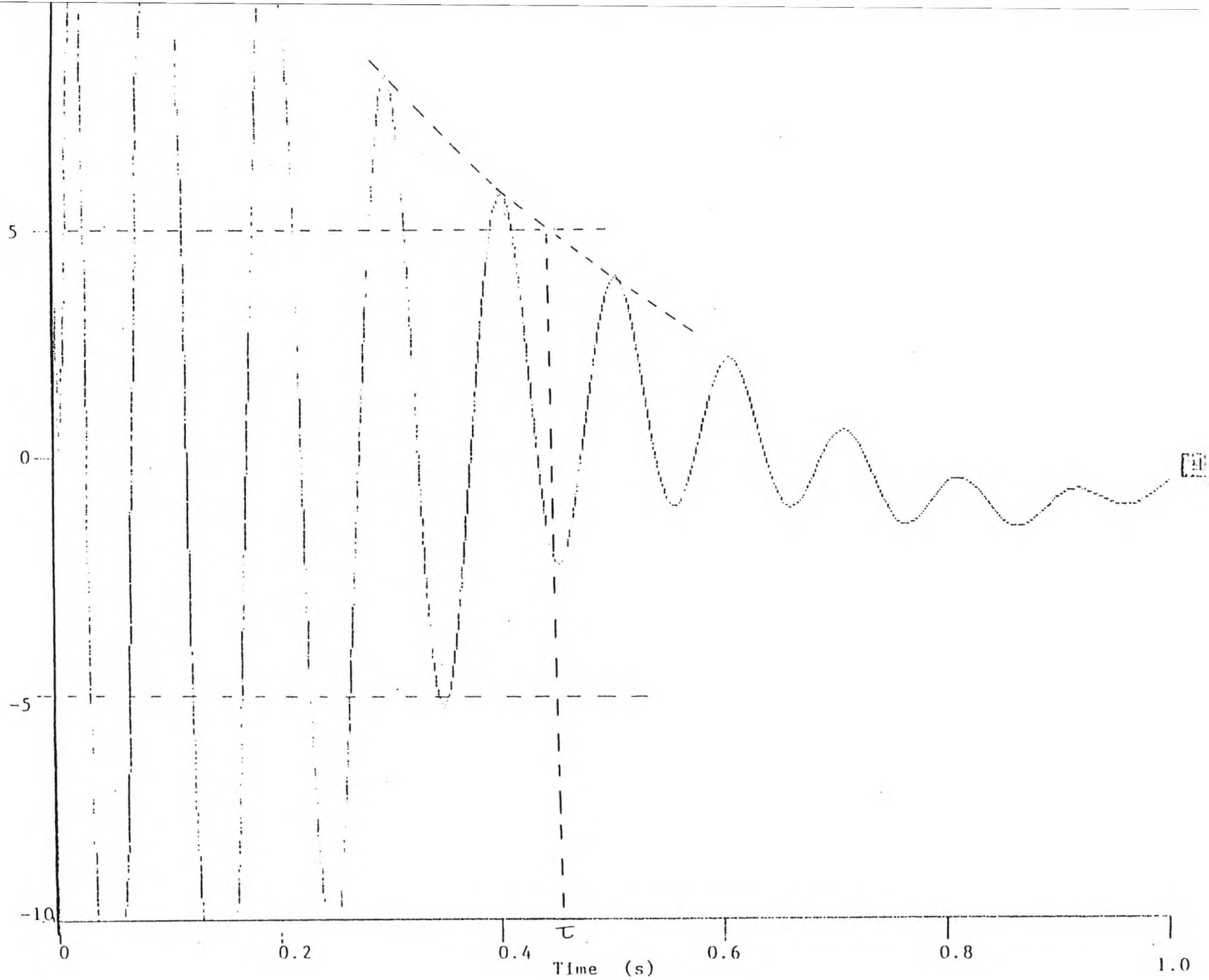

Fig 5.10 Methods for determination time τ for dynamic error ϵ to fall below $\pm$ 5%.

c) Unladen: 3000lbf = 700kgf half axle comprising 200kgf sprung and 500kgf unsprung.

Bump and step response simulations were required and errors up to $\pm 8\%$ were to be incorporated. Speeds up to 80mph (128km/h), had to be considered.

The basic model used in the simulations is a linear one. This means that the output (dynamic error), will be proportional to step, (or bump) height, h. For example, if the dynamic error falls below $\pm\epsilon$ after some time τ, then if the height is doubled to $2h$, the error will be less than $\pm 2\epsilon$ at precisely the same time τ. By choosing ϵ and h in a geometric series:

$$\epsilon = (1, 2, 4, 8)\% \quad \text{and} \quad h = (1, 2, 4, 8)mm,$$

we reduce the number of required simulations since there are only 7 independent ratios of $\epsilon/h = 1/8,\ 1/4,\ 1/2,\ 1,\ 2,\ 4,\ 8$ – Table 5.8:

Step (Bump) Weight - h [mm]	*Dynamic Error - ϵ [%]*			
	1	*2*	*4*	*8*
1	*1*	*2*	*4*	*8*
2	*1/2*	*1*	*2*	*4*
4	*1/4*	*1/2*	*1*	*2*
8	*1/8*	*1/4*	*1/2*	*1*

Table 5.8 Independent ϵ/h ratios used in the simulation, (underlined).

If linearity of the model was not used we would need to take all 16 combinations into account. Taking 4 speeds (20, 40, 60, 80mph), 3 laden weights and two road profiles (step and bump), this would entail $16x4x3x2 = 384$ separate simulations. With model linearity this was reduced to *168*.

Results are expressed in terms of distance ahead of WIM sensor which must be free of step or bump shaped irregularities of specified height. The results are presented in Tables 5.9 (a) and (b) respectively, only for *half-laden vehicle.* These were derived for different vehicle speeds and using the underlined ϵ/h combinations in Table 5.8. Plots of the results are shown in Figs. 5.11 (a) and (b), respectively, as families of curves labelled with ϵ/h values. The advantage of such a presentation is that the graphs can be used for ranges outside those specified, *(ϵ_{max}= 8%, h_{max}= 8mm)*. For example the $\epsilon/h = 1/8$ results correspond not only to *1%* error for 8mm step (or bump), but also to *2%* for a 16mm step (or bump).

Results are produced in the same way for fully laden as well as empty vehicles and can be found in Ref[2]. For the convenience of the user of these data, the results are also presented according to specified errors: ϵ = ***(1, 2, 4, 8)%***, with curves labelled according to height in *mm*.

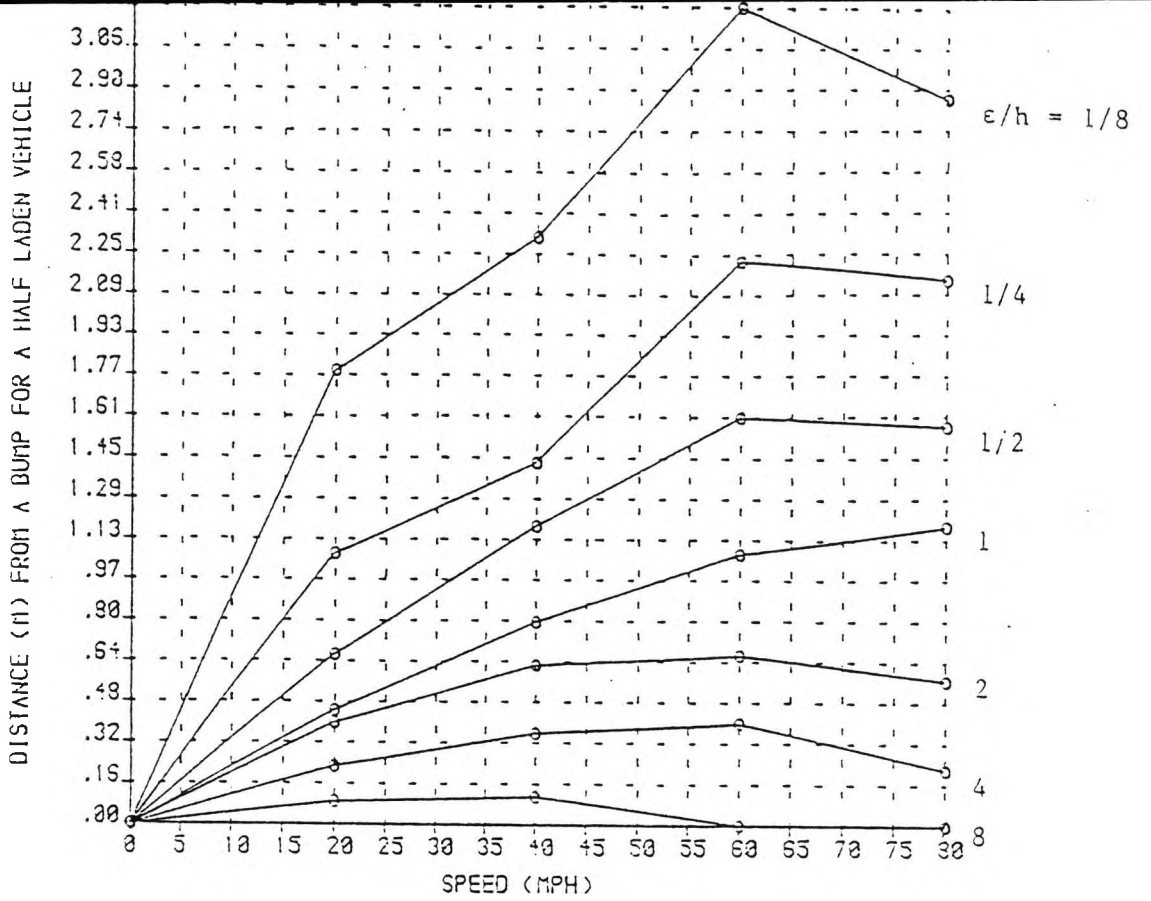

(a)

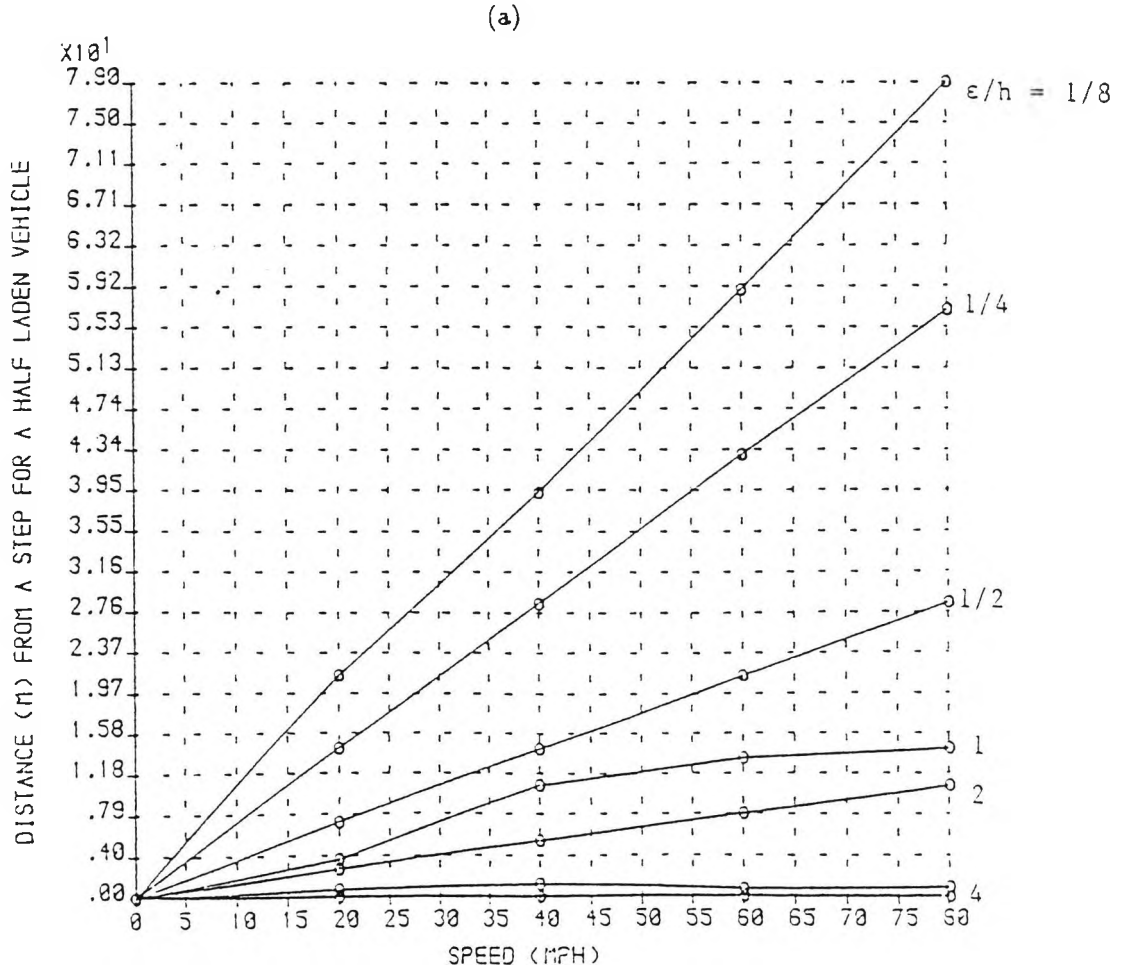

(b)

Fig. 5.11 Normalized Error Graphs. Half Laden Vehicle.

Speed [km/h]	ϵ/h ratio						
	1/8	1/4	1/2	1	2	4	0
0	0	0	0	0	0	0	0
20	17.9	10.7	6. 7	4. 5	4. 0	2. 3	0. 9
40	23.2	14.3	11.8	8. 0	6. 3	3. 6	1. 1
60	32.2	22.3	16.1	10.7	6. 7	4. 0	0
80	28.6	21.5	15.7	11.8	5. 7	2. 2	0

a) bump

Speed [km/h]	ϵ/h ratio						
	1/8	1/4	1/2	1	2	4	0
0	0	0	0	0	0	0	0
20	21.5	14.3	7. 2	3. 6	2. 7	0. 7	0
40	39.3	28.6	14.3	10.8	5. 4	1.25	0
60	59.0	43.0	21.5	13.4	8. 0	0. 7	0
80	79.0	57.0	28.6	14.3	10.7	0. 9	0

b) step

Table 5.9 Distances (m), for various speeds and normalised (ϵ/h) errors. Half laden axle: $m_2 = 1550kgf$; $m_1 = 500kgf$.

5. 1. 3. 3 Measurement Considerations. The aim of this part of the study was to show the trend on typical additional dynamic errors that occur when there is an abrupt road profile change ahead of an weighing sensor. It has been accepted that the road is perfectly smooth except for the addition of a step or a bump. Although the results presented in the figures and tables have been derived using a step and bump road profiles, they do apply to a negative step (step down), and a negative bump, (pot hole). The error, ϵ, is to be read $\pm\epsilon$.

Only a single vehicle suspension model has been used. Due to the simplified approach to tyre/road profile interaction, some over estimation of the wheel forces should be expected.

The obtained results show certain trends:

a) For the chosen bump length of 0.5m, steps produce greater errors than bumps. However, for certain combinations of bump lengths and vehicle speeds, the perceived input oscillation wavelength may coincide with some of the natural frequencies of the vehicle. This will cause resonant vibrations with amplitudes possibly greater than the ones obtained with step profile at the same speed. The peaks observed in the curves in Fig. 5.11(a) at 60m/h are an illustration of resonant vibrations caused by the combination of that speed and the bump length.

b) In terms of laden weights the largest errors, (or equivalently greatest distance ahead of a weighscale for fixed error), is that for a fully laden vehicle encountering large steps, $(\epsilon/h=1/8)$. For smaller steps the half-laden results are worse than the fully laden ones. The errors for the unladen case with steps are the least for all the laden cases except for small step heights. With bumps the half-laden results present the worst case for most bump heights. These are followed by those for the fully laden and then the unladen cases.

c) Looking at the magnitude of errors, the worst case corresponds to 114m for a step height of $\pm\, 8mm$ and an error of $\pm\, 1\%$. This occurs when the vehicle is travelling at 80mph. For bumps, (or potholes), the errors are significantly lower and the corresponding worst case distances, ($\pm\, 1\%$ error for $\pm\, 8mm$ bump height), fall to around 20 to 30m. It should be pointed out that all distances are with respect to the beginning of the step or bump.

5. 2 STOCHASTIC ROAD PROFILES.

The analyses of road profile records have shown that common road surfaces can be best represented as realisations of Gaussian and stationary random processes, provided that the effects of occasional large irregularities, (e.g. bumps and potholes) are removed from the considerations and treated separately. The probabilistic method of road roughness description enables the theory of random vibrations to be applied to the dynamic response analysis of vehicles traversing such tracks. A number of authors, [22], [24], [33], [40], [65], [67], [68], [71], [118], [122], [123], have used the methodology to derive useful information about dynamic wheel loads, vehicle vibrations, passenger comfort etc., resulting from vehicle interactions with road surface of stochastic description.

A frequency domain simulation was performed in this study to establish the relationship between road roughness, vehicle speed, and the magnitude of the dynamic wheel load exerted on the pavement - see Appendix C.

5. 2. 1 Road Surface Description.

In these simulations the road surface is represented as a single profile realisation of a stationary random function $Y(x)$, where x is the distance covered by the vehicle in forward direction. A simple expression was derived for the Power Spectral Density – S_y after an analysis of road spectra collected by MIRA, [70]:

$$S_y(N) = C.N^{-k}, \qquad (5.1)$$

where $'N'$ $[rad/m]$, is the wave number reciprocal to irregularity wavelength. $'C'$ and $'k'$ are parameters characterising the surface quality. Parameter $'k'$ lies within a relatively narrow interval: $k = 1.6$ to 2.8, and a value of $k = 2.5$ has been

adopted. The *'roughness'* coefficient C is selected from a table of values describing different qualities of road surface, [122]. The mean value of $C = 10.10^{-8}$ was chosen from the interval $C = 3.10^{-8}$ *to* 50.10^{-8}, corresponding to 'motorway' class quality surfaces.

The Power Spectral Density, (PSD) – $S_y(N)$ provides an invariant description of the road profile from which the excitation Spectral density $S_y(f)$ can be derived, where $f = N.U$, and U is the vehicle's forward velocity. Replacing in Eq. (5.1), we obtain:

$$S_y(f) = \frac{S_y(N)}{U} = C.\left(\frac{U^{k-1}}{f^k}\right) = C.\left(\frac{U^{1.5}}{f^{2.5}}\right), \ [m^2/Hz]$$

5. 2. 2 Vehicle model Transfer Function.

The quarter-vehicle model was used again to derive the system's equations of motion - Eq. 4.1. The corresponding harmonic transfer function $H(\omega)$, relating the system's excitation, (road profile displacement) to the system's response - the dynamic wheel forces F_w, (Eq. 4.3) imposed on the road, is as follows:

$$H(\omega) = -\frac{(k_1 + b_1.s).(m_1.m_2.s^2 + m_1.b_2.s + m_1.k_2 + m_2.k_2 + m_2.b_2).s^2}{(m_1.s^2 + b_1.s + k_1).(m_2.s^2 + b_2.s + k_2) + m_2.s^2.(k_2 + b_2.s)},$$

where m_1, m_2, b_1, b_2, k_1, k_2 are the systems parameters as per Table 2.1, and $s = j\omega$.

5. 2. 3 Dynamic load PSD and Dynamic Load Coefficient, (DLC).

From the theory of random vibration transmission through linear systems, [97], [98], for the dynamic response spectral density $S_f(f)$ we have:

$$S_f(f) = |H(f)|^2 . S_y(f),$$

where $f = \frac{\omega}{2.\pi}$, and for our model:

$$S_f(f) = [H(f)]^2 . C . \left(\frac{U^{1.5}}{f^{2.5}} \right);$$

Provided the process is Gaussian, all its essential characteristics can be determined from its PSD function. Assuming the mean square value of the response is zero, its variance, (dispersion) is readily obtained simply by integration over the frequency range:

$$\sigma_f^2 = \int_0^\infty S_f(f).df = C.U^{1.5}.\int_0^\infty \frac{[H(f)]^2}{f^{2.5}} . \, df,$$

The square root of the above expression is the standard deviation of the wheel load σ_f. For the relevant response prediction and to limit computational time, the profile spectrum frequencies are reduced to the 0 to 20 Hz band. In order to perform the calculations by a digital computer, the integration procedure is replaced by discrete summation:

$$\sigma_f^2 = C.U^{1.5}.\delta f.\sum_{i=1}^{n} \frac{[H(f)]^2}{f^{2.5}} \quad ,$$

and $n = \frac{20}{\delta f}$, $f = i.\delta f.$

The Dynamic Load Coefficient – *(DLC)*, is then estimated as the percentagewise ratio of the dynamic wheel force's standard deviation σ_f and the static half-axle weight W_s:

$$DLC = \frac{\sigma_f}{W_s} . 100, [\%] ;$$

The results for different vehicle speeds are presented in Table 5.10. These results are valid for a typical class of vehicle with fixed body load mass $M_b = 2400 kgf$.

U	km/h	20	40	60	80	100	120	140
DLC	%	3.13	5.28	7.15	8.87	10.49	12.03	13.5

Table 5.10 Dynamic Load Coefficient with fixed body mass $M_b = 2400 kgf$.

5. 2. 4 Load Weight Distribution Effect.

Usually in-motion weight measurements are performed on a multitude of vehicles of a given class, or in the more common case - on all vehicles passing through that stretch of the road. Statistical information is therefore available of axle load distributions of vehicles on selected stretches of the motorway network. When this information is presented as PSD of vehicle body masses, $P(m)$ it can be used to replace the fixed value of the body mass used in the previous subsection. The whole expected span of dynamic loads exerted on the road can then be obtained in this way.

The vehicle's dynamic response is thus weighted by the load PSD function against the whole body mass range:

$$S_f(f,m) = \int_{M_{b_{min}}}^{M_{b_{max}}} S_f(f) . P(m) . dm = \int_{M_{b_{min}}}^{M_{b_{max}}} [H(f,m)]^2 . S_y(f) . P(m) . dm ,$$

and for the variance:

$$\sigma_f^2 = C.U^{1.5}.\int_0^{f=20} \int_{M_{b_{min}}}^{M_{b_{max}}} \frac{[H(f,m)]^2}{f^{2.5}} \, . \, P(m) \, . \, dm \, . \, df \, ,$$

which in discrete form becomes:

$$\sigma_f^2 = C.U^{1.5}.\delta f.\sum_{i=1}^{n} \delta m \, . \, \sum_{j=1}^{r} \left\{ \frac{[H_{ij}(f_j, m_i)]^2}{f_j^{2.5}} \right\} . \, P(m_i) \, ,$$

where: $n = \frac{20}{\delta f}$, $r = \frac{M_{b_{max}} - M_{b_{min}}}{\delta m}$.

Sample results from HGV axle load measurements on a stretch of the M6 motorway were available from the TRRL in the form of histograms, and were used to construct the Probability Distribution function of body mass weights. Three body mass ranges were considered starting with the widest range of all measured HGV's, and subsequently narrowing the weight band leaving only the heavier vehicles with greatest contribution to road damage – Fig. 5.12. The *DLC* was now calculated as the ratio between the Dynamic load's Standard deviation and the mean value of the body mass $<M_b>$ in the respective range:

$$IF_d = \frac{\sigma_f}{<M_b>} \, . \, 100, \quad [\%].$$

The expected values are shown in Table 5.11:

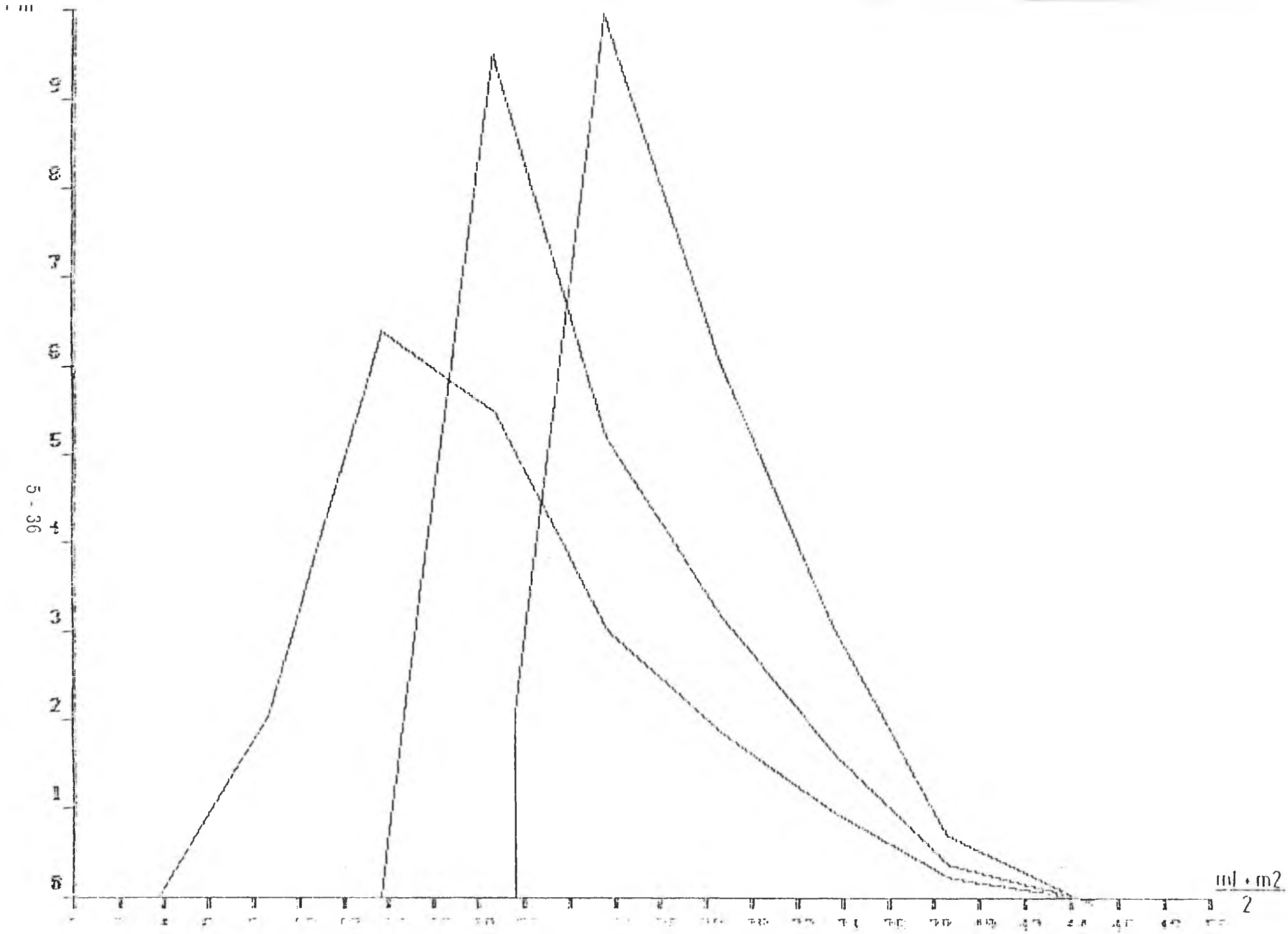

Fig. 5.12 DLC distributions for 3 vehicle body mass ranges.

U	km/h	20	40	60	80	100	120	140
DLC %	$<M_b>$ = 2705kgf	3.23	5.44	7.37	9.15	10.81	12.4	13.92
	$<M_b>$ = 2315kgf	3.43	5.77	7.82	9.7	11.47	13.15	14.75
	$<M_b>$ = 1866kgf	3.88	6.52	8.84	10.97	12.97	14.87	16.7

Table 5.11 DLC with Load weight distribution,
($<M_b>$ – *Statistical Mean of Half axle weight).*

The results from both this and the fixed body mass simulations exhibit a considerable increase of *DLC* with speed: more than *twice* between 40 and 120km/h, which is the range of speeds most likely for HGV's on motorways. Choosing 80km/h as the most representative, and comparing the results for all body masses (fixed and mean), one could conclude that the spread of pavements's dynamic loading around the static vehicle weight should not change much with the vehicle's load distribution.

However, the simulations showed the crucial effect of the road surface quality on the dynamic component of the wheel forces. To assess the relationship, the mean value of *'C'* used so far was replaced with its two extreme values corresponding to the best and worst quality motorways, respectively. The results in Table 5.12 indicate an expected increase of about *four* times in the value of the IF_d between the two extreme *'C'* values.

U	km/h	20	40	60	80	100	120	140
DLC %	$C = 3.10^{-8}$	1.72	2.89	3.92	4.86	5.75	6.59	7.4
	$C = 10.10^{-8}$	3.23	5.44	7.37	9.15	10.81	12.4	13.92
	$C = 50.10^{-8}$	7.02	11.8	15.99	19.84	23.46	26.9	30.19

Table 5.12 DLC on Road surfaces of different quality.

5 .2 .5 Tyre filtering Effects.

A further analysis was carried out on the filtering properties of tyres enveloping some of the short wavelength surface irregularities. We assumed that all vibrations generated by effective wavelengths twice the length of the tyreprint $l_t = 0.25m$, and shorter are being suppressed. For the highest induced vehicle vibration frequency of 20Hz the corresponding forward speed will be:

$$U = 2 \, . \, l_t \, . \, f_{max} = 2 \, . \, 0.3 \, . \, 20.0 = 43.2km/h.$$

In Fig. 5.13 the frequency response graph of the system shows the relative magnitudes and contribution to the Dynamic Load Coefficient of the body bounce and wheel hop frequency components respectively.

The calculations confirmed that DLC can be reduced by up to a *third* at low speeds, but above 40km/h tyre filtering becomes negligible. Assuming that a very small number of vehicles on motorways can be expected to travel at speeds lower than 40km/h, with the DLC values corresponding to those speeds being low anyway, the tyre filtering effect was not considered important for this study.

5. 2. 6 Simulation results Conclusions.

A basic vehicle suspension model describing just one vehicle was used throughout the whole last round of simulations. Nevertheless, some meaningful results were obtained leading to a better understanding of the dynamic interaction between real road surfaces and vehicles, and some useful conclusions were drawn:

i) The results are in qualitative agreement with experimental data gathered on typical road tracks with some common vehicle suspension systems, [74], [135].

ii) A considerable increase in the dynamic component of wheel forces on pavements has to be expected with rising vehicle forward speed and poorer road surface quality. On the contrary, the effect of changing the laden weight of the

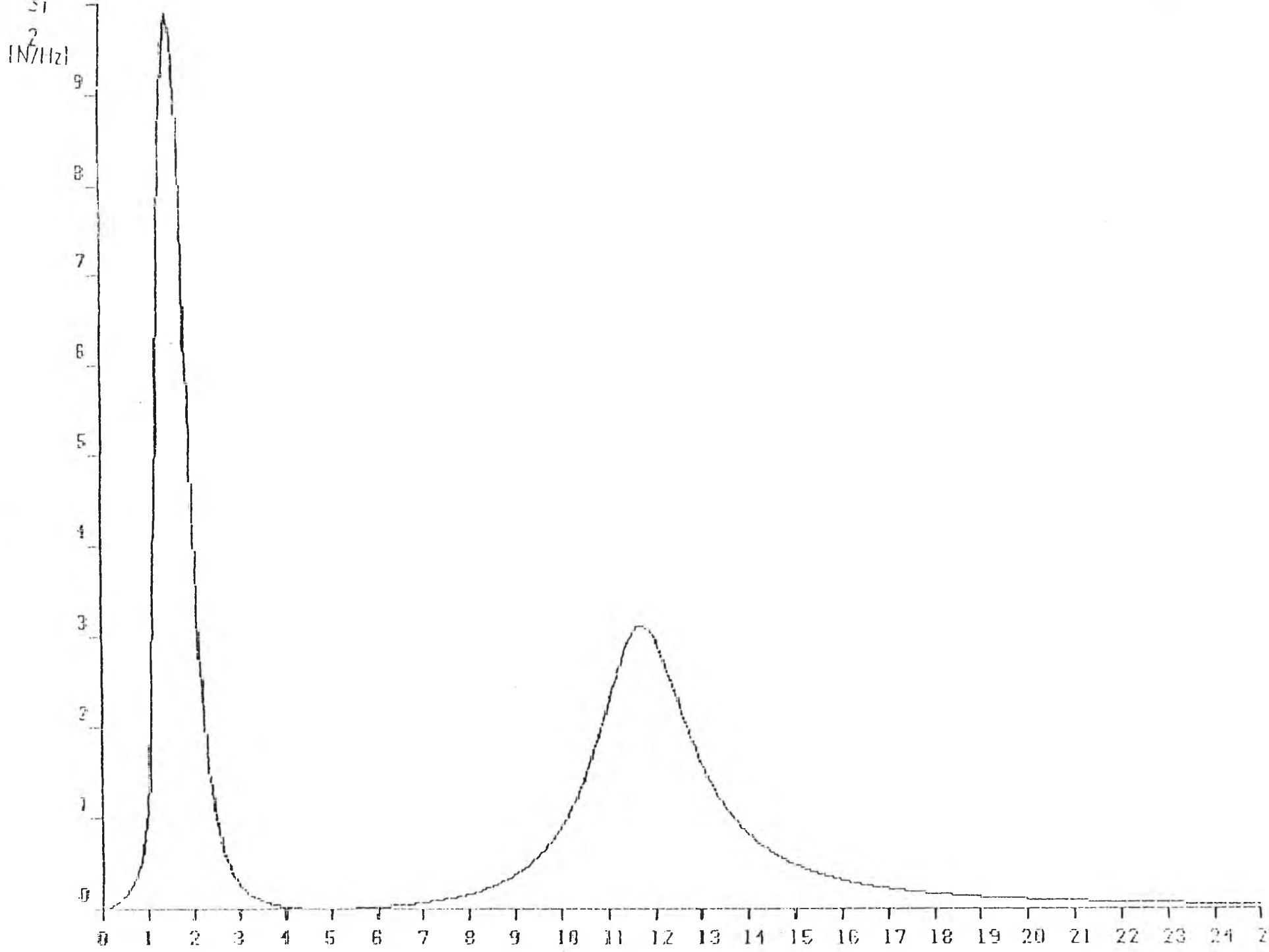

Fig. 5.13 Relative Frequency contributions of *Wheel hop* and *Body bounce*.

vehicle was proved to be insignificant in terms of change in the Dynamic Load Coefficient value.

iii) The tyre enveloping effects were found to be insignificant for the considered types of roads and probable vehicle speeds, and therefore ignored.

iv) Since the load distribution has a minor effect on the Dynamic Load Coefficient, a single vehicle could be used for routine measurements of road surface parameters.

A suitable "test" vehicle should be equipped with an on-board weighing system, [100] and run at constant speeds over some "standard" tracks with accurately established parameters C and k. The records of the dynamic wheel forces should be statistically processed to obtain the corresponding standard deviations. The "calibrated" vehicle could then perform constant speed rides over roads under study, with the collected date processed in a similar manner. Assuming a value of k equivalent to that of the "standard" track and using the previously developed relationships, the approximate values of the roughness coefficients C could be readily obtained.

Compared with the direct profile level measurement, [57], [70] this is a method of lower precision, but it could be more useful when overall mean road roughness characteristics of a certain motorway or a whole regional road system are required. A classification of roads and runways with respect to their surface quality was compiled in this way in Czechoslovakia, [68].

v) The predicted increase of the dynamic wheel force observed with rising values of C – Table 5.11, emphasises the detrimental effect of road surface quality deterioration. When expressed in terms of the *Fourth power law,* (Ch.1, Sect. 1.5.1) the fourfold increase in the dynamic wheel load with values of C ranging from poorest to best quality motorway surface translates into road damage increase from 1.21 to 2.06 respectively for the typical speed of 80km/h.

The magnitude of the measured dynamic load standard deviation could therefore be a valuable indicator of the extent of environmental damage on a particular stretch of the motorway system.

Chapter VI: Proposed Capacitive WIM Sensor and Measuring Circuit.

6. 1 CAPACITIVE WIM SYSTEMS.

The search for low cost easy to install WIM systems in the last decade has resulted in the gradual replacement of the traditional excavation type permanent load-cell platforms with light, surface mounted technologies employing new sensor principles. Most promising in that area have been the piezoelectric/resistive cables or films, as well as the capacitive mat/strip type sensors whose properties allow for very low profile, rugged and portable installations to be constructed at a relatively low cost.

A great deal of work has been carried out in the recent years to overcome some of the inherent deficiencies of the piezoelectric force transducer, [37], [52], [93], [132], [133]. Different methods of extrusion, pre-tensioning, polarisation, transportation and mounting of the sensors, have been tested with variable success. The pronounced sensitivity of the piezoelectric material to a number of factors such as bending, in-plane tensions, loading width/area, load location, temperature, electrical noise susceptibility, loading history etc., makes it difficult to achieve reliable measurements. The uses of the piezo-electric/resistive sensors therefore have been limited to cheap low accuracy weighing systems and simple axle detection installations.

On the other hand capacitive force/displacement transducers have made a steady progress in the recent years towards becoming the best candidate for low cost, portable high accuracy technique in dynamic vehicle weighing. Joint evaluation tests of different types piezo-electric and capacitive WIM sensors have proven the advantages of capacitive strip/mat sensors in terms of accuracy, reliability and immunity to measurement disturbances - Ref.[37]. A promising capacitive mat sensor design is also described in Ref.[29]. The low cost and easy installation of the sensor could allow sensor "tiling" of a relatively long stretch of road thus enabling taking uninterrupted wheelforce records to be taken. Multi-plate capacitive mat WIM sensors have been in use for a number of years, [12], [13], [86], [87], [141], [142], and have proved to be durable, reasonably accurate and resistant to error inflicting factors. However, their prohibitive price so far has prevented them from wider use especially where low cost automatic vehicle

classifying installations have been required. In recent years however, research and experimentation with simpler *strip* type capacitive transducers has shown good results, [29], [37], [126], which alongside with new techniques for signal conditioning and real time data processing make the sensor a viable and practical candidate option for WIM systems.

Following a study undertaken earlier at the Department on capacitive strip sensor profiles, it was decided to expand the research and develop a suitable electronic circuit interfacing to capacitive WIM sensors.

The development of a capacitive strip sensor and a compensating frequency modulating circuit for capacitance measurement is described in the following sections.

6. 2 PRINCIPLES OF OPERATION OF CAPACITIVE DISPLACEMENT TRANSDUCERS.

Capacitance, (C) is a measure of electrical impedance relating the charge on two conducting bodies to the potential difference between them:

$$C = \frac{Q}{V}, \ [F]$$

For an ideal capacitor consisting of two perfect conductors separated by a dielectric, the capacitance depends only on the surface geometry and the dielectric constant of the medium:

$$C = \frac{\varepsilon.\varepsilon_o A}{d}, \ [F] \qquad (6.1)$$

where: ε is the dielectric constant of the medium,
ε_o is the dielectric constant of the vacuum,
A is the area of the conductor plate,
d is the distance, (gap) between the conductor plates.

6. 2. 1 Capacitive Sensor Configurations.

Two configurations are used in capacitive sensor displacement measurements:

(i) Variable area: these transducers are inherently linear having simple mechanical design, (often "push-pull" couplings). They are normally used for large displacement ranges - up to 250mm, or angular - $0^{\circ} \pm 45^{\circ}$ range measurements. No variable area capacitive transducers have been reported yet in use for WIM purposes.

(ii) Variable gap: the capacitance/plate separation relationship is non-linear, (hyperbolic), therefore gap variation should be kept within relatively small limits if linearity is sought. Alternatively differential capacitor arrangements, compensating circuits, or digital signal processing might be used to offset nonlinearity. Small, (up to a few *mm*) displacement ranges are usually measured in this way, and a resolution of the order of 1 part per million can be obtained, i.e. ***1μm*** in ***1mm***. All present capacitive mat/strip WIM sensors employ variable gap type transducers.

6. 2. 2 Capacitance measuring circuits and Sensor performance.

In low capacitance transducers lead wire capacitance can be several orders greater than the working transducer capacitance. The effect is eliminated by careful design of the electronic interface circuits. Protection against external electrostatic fields is normally realised by shielding the sensor in a thin Faraday cage. Power is normally supplied from an AC source. Earlier measuring circuits invariably consisted of an AC bridge with the sensor capacitor forming one arm of the bridge and having AC voltage as output. In some recent developments, [41] the working capacitor is included in OpAmp circuits in which functions such as linearisation, rectification, pulse width modulation etc. can be performed. In this study and other developments, [90], the working capacitor is part of the resonance circuit of a sinusoidal generator. This allows the output to be provided directly in digital form which facilitates further signal processing and improves the overall measurement accuracy.

A typical capacitive mat sensor arrangement is shown in Fig. 6.1. The sensor is of differential construction and consists of a central electrode made of

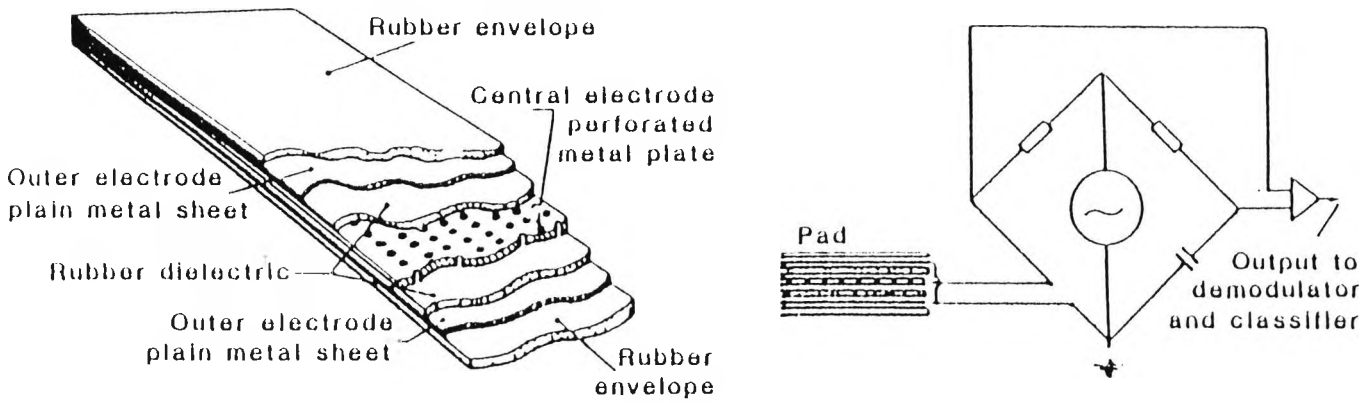

Fig. 6.1 Typical Capacitive weighmat sensor design.

perforated steel and two outer electrodes made of plain metal sheets. The plates are encapsulated in tough synthetic rubber compound. The sensor constitutes one of the arms of an AC bridge powered by an RF source. The amplitude modulated bridge output is passed to a the electronics block consisting of a preamplifier, demodulator, A to D converter and finally a data processing unit.

The performance of a capacitive weighpad was analysed by Basson, [14] by investigating the behaviour of a mechanical model of the weighpad under load. Empirical data on the deflection of the actual sensor was gathered from tests with wheel loads applied through different tyre contact areas, tyre inflation pressures etc. The results of the study indicated that the relationship between wheel load and the resulting weighpad capacitance change was linear and passed though the origin, [126]. There was also no apparent variation in the relationship for the range of wheel forces and inflation pressures found on a single or tandem axles.

6. 3 CAPACITIVE LINE SENSOR RELATIONSHIPS.

A capacitive line sensor is considered because of various advantages including the simplicity of construction, expected low sensitivity to bending, low temperature coefficient and the ability to test and calibrate with static loads.

A schematic of the concept from which a line sensor could be developed is shown in Fig. 6.2. The sensor body is a hollow extrusion of stainless steel, aluminium, or high strength plastic. Typical outer dimensions of the cross section of such a device would be 5mm thick and 12mm in the vehicle travel direction, (ie. $l_s = 12mm$). A typical strip length might be $1.0 - 1.5$m. The extrusion contains two copper electrodes bonded to the flat surfaces and separated by a gap d.

6. 3. 1 Sensor deflection sensitivity.

The concept is such that when a tyre print is over the line sensor the two electrode faces move together remaining parallel. The capacitance is then that of a parallel plate system as per Eq. (6.1). The sensitivity of the capacitor to plate

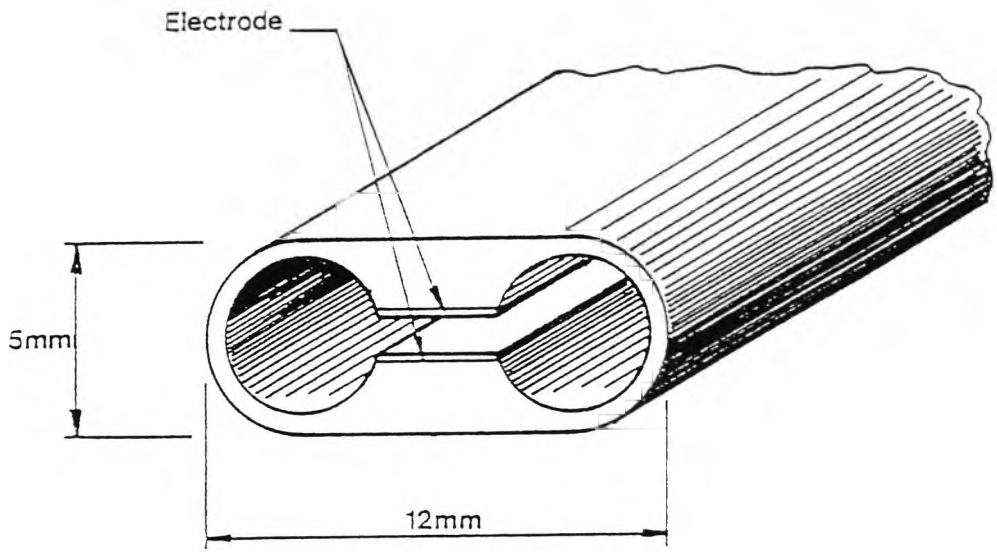

Fig. 6.2 Capacitive Line sensor concept.

separation d can be derived from the same equation:

$$\frac{\partial C}{\partial d} = -\frac{\varepsilon.\varepsilon_o A}{d^2} \qquad (6.2)$$

If we now denote the sensor capacitance when unloaded as C_o, and:

$$C_o = \frac{k_1.A}{d},$$

where: $k_1 = \varepsilon.\varepsilon_o$,

$A = l_e.\, b_e$, is the total electrode area.

Assuming that change in capacitance under load occurs only under the tyre print, i.e. only over strip length equal to tyre width b_t, then in loaded position the capacitance of the sensor will be C_w :

$$C_w = \frac{k_1.(A - A_w)}{d} + \frac{k_1.A_w}{d-x} = k_1.\left[\frac{A}{d} + \frac{A_w.x}{d(d-x)}\right] = C_o + \frac{k_1.A_w.x}{d(d-x)} \qquad (6.3)$$

where: $A_w = b_t.\, b_e$, is the electrode area under the tyre, (b_t: tyre print width),

x is electrode deflection.

The change in capacitance from unloaded to loaded mode is:

$$\partial C = C_w - C_o = \frac{k_1.A_w.x}{d(d-x)} \qquad (6.4)$$

hence the change in capacitance relative to the initial capacitance C_o is:

$$\frac{\partial C}{C_o} = \frac{A_w.x}{A.(d-x)} = \frac{A_w}{A}\cdot\frac{x}{(d-x)} = \frac{b_t}{l_s}\cdot\frac{x}{(d-x)} \qquad (6.5)$$

Judging from the last three expressions the capacitive strip sensor should exhibit sensitivity to tyreprint width. However, tests with experimental strip capacitors have confirmed that subject to sensor material and profile:

- the effect of tyre load on the sensor away from the contact area is minimal and can be ignored, hence sensitivity to tyre width should be low, [29].
- the relationship which is of primary importance for the measurement, i.e. between wheel load and sensor capacitance is linear and is not affected by tyre inflation pressures or wheel load range, [126].

The initial capacitances of practical capacitive strip sensors will be typically less than 100pF, therefore good sensitivity to plate separation is essential. From Equations (6.2, 6.4, 6.5) follows that sensitivity improves with reduced initial plate separation ***d***. It is desirable therefore that the electrode plates move parallel to each other under load and bending of the strip, in order to prevent contact, and also to keep the relationships valid.

6. 3. 2 Sensor Profile study.

A series of computer simulations have been carried out earlier at the Department on behalf of the TRRL to identify possible sensor profiles complying with the above condition. The concept was simulated using a finite element package on a highly interactive computer. Results are presented in Fig. 6.3, based on an elastic steel construction loaded with a typical HGV tyre print pressure, (only half of the profile is modelled because of inherent symmetry). Clearly the deflected shape (shown meshed with triangles), is such that the electrode surfaces move parallel to each other. The deflected shape is magnified by approximately 50 so the true change in electrode separation is 0.01mm for a 1mm nominal separation. In practice this change in separation will need to be larger, perhaps 10-20% of the nominal separation. Only then will there be reasonable changes in capacitance on loading. Some simulations with reduced wall thickness have shown that greater deflections are possible within the material's stress limits. Another possibility is to use materials with a lower Young's modulus such as hardened plastics or polymers. Such materials would lend themselves better to extrusion methods for production of the device. Production technology of such a design would involve making of two identical

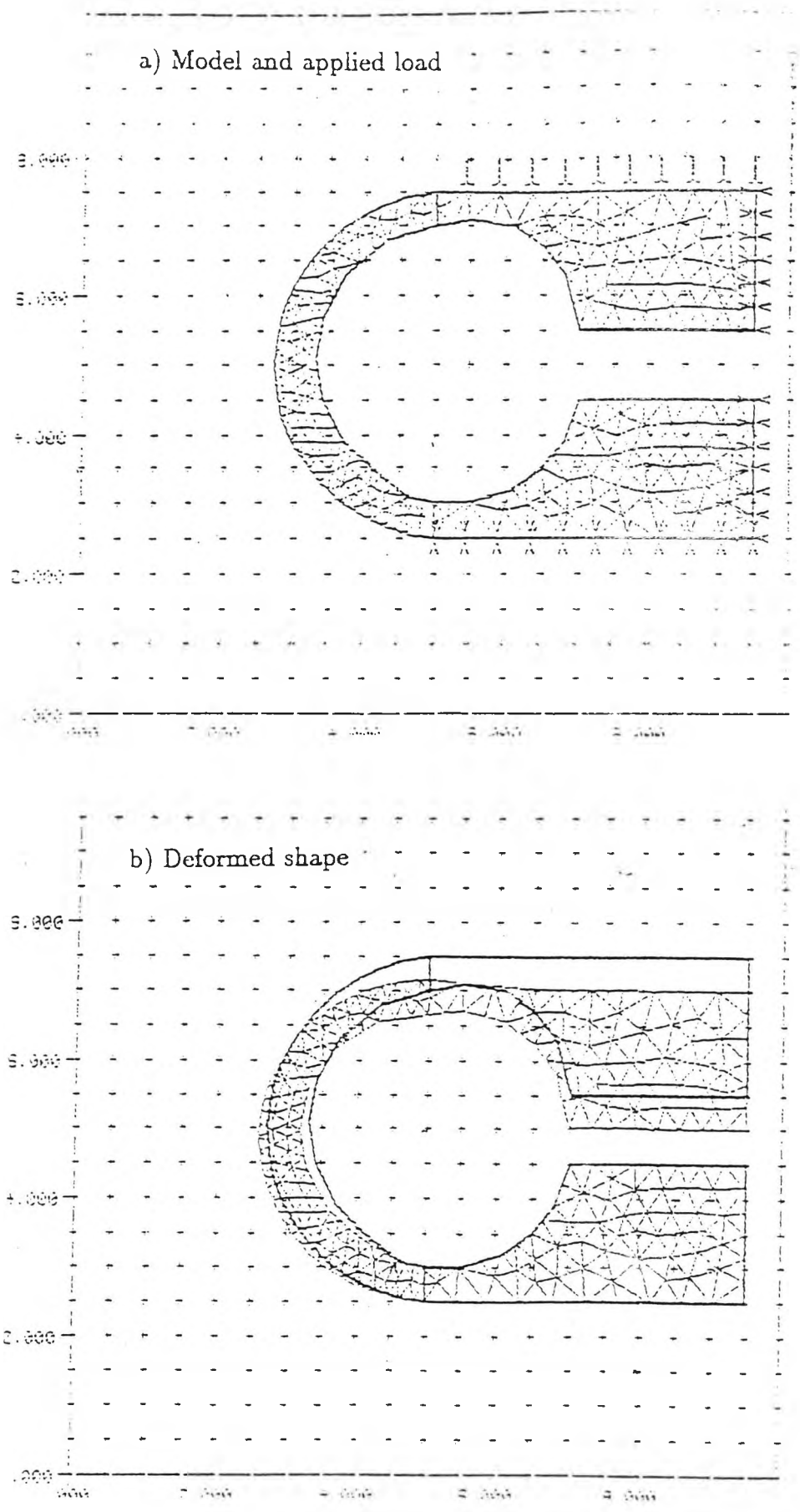

Fig. 6.3 Finite element modelling of the sensor profile.

parts - Fig. 6.3(a), and these would be spot welded or glued together after the electrodes have been installed on both sides. Both ends of the extrusion should then be sealed and the strip encapsulated in tough rubber compound shaped to form a gradual ramp up and down the sensor. The encapsulation might incorporate electrostatic screening mesh, and means of attachment to the road surface.

In case the response of the sensor to wheel load is nonlinear with large variations in gap ***d***, a three electrode system with two capacitances operating in push pull, (differential mode) can be used. When one capacitance increases the other decreases. Fig. 6.3(b) is a possible concept with one of the three electrodes being earthed. As can be seen when a load is applied, the top capacitor will decrease and the lower increase. Many differential bridge arrangements are available to measure the difference between the two capacitors which will be very nearly linear with applied load, [41].

Approximate calculations show that for a line sensor concept as shown, with electrode separation of 0.5mm, the nominal capacitance for a 1m sensor with air as dielectric will be:

$$C_o = 80pF$$

If a tyre print carrying the maximum load to be measured produced a 20% change in separation of 0.1mm (over the tyre print width of approximately 0.2m), then the change in capacitance is 4pF.

The range of loads to be measured in dynamic weighing is approximately 1 part in 400. This implies that it will be necessary to be able to measure 0.01pF. This should be possible with care taken to screen against stray capacitances, which will be much larger than this. To minimise stray capacitance problems in detection circuits the electronics will need to be placed as close to the sensor as possible. One option is to accommodate the preamplifier and signal conditioning circuitry in an integral box attached to the near end of the sensor.

The technological concept presented here has the advantage that a sensing strip to go within the space shown in Fig. 6.4(a) could be designed separately. This could be the differential electrode arrangement shown in Fig. 6.4(b). The rest of the structure when sealed together with the sensing strip inside would the also have the function of sealing and encapsulating the sensor. Also the sensor

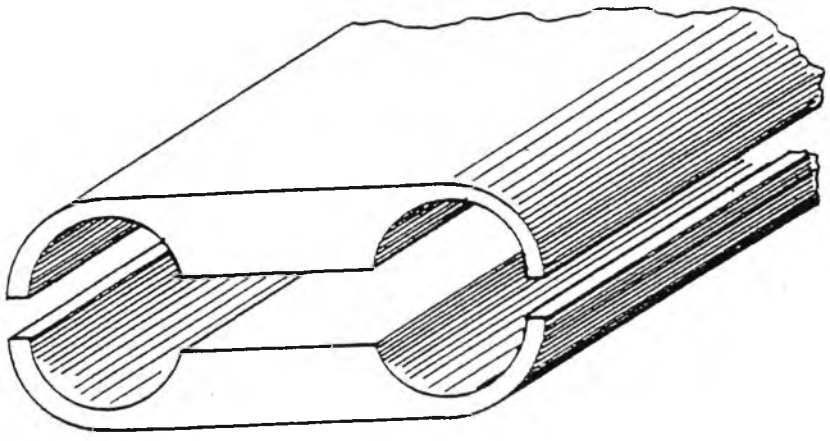

a) Extrusion halves

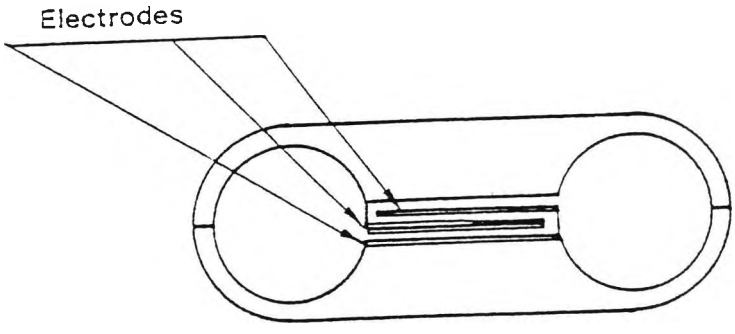

b) Electrode configuration for a differential capacitor

Fig. 6.4 Capacitive Line sensor construction details.

could be tested separately before assembly. The concept needs further exploration with regards to materials, measurement circuits and basic design using computer aided methods.

6. 4 CAPACITANCE MEASURING CIRCUIT WITH DRIFT CORRECTION.

After an extensive survey and evaluation of secondary signal converters for capacitive transducers, an oscillator circuit was selected as offering best performance and compatibility with the requirements of the project, as well as the modern data processing techniques. The bridge type circuits were found to be outdated, bulky and unstable. Other voltage output techniques, [41], [90] also lacked output stability, and the produced analogue signal was susceptible to RF and mains power interference.

Using the capacitive transducer as part of the tuning circuit of a sinusoidal generator ensured that the secondary signal was frequency, which can be measured with high accuracy. It is largely insensitive to electromagnetic noise, and converted to TTL/CMOS levels, is directly readable by digital logic devices. What is more, a digital frequency stabilisation technique was applied to compensate for the multiple error inflicting environmental factors causing slow frequency drift.

6. 4. 1 Principle of Circuit operation.

A block diagram of the device is shown in Fig. 6.5. Fast changes of sensor capacitance C_x under wheel load modulate the frequency of the free running Voltage controlled ***Oscillator***. The frequency is measured by a ***Counter*** and passed to a Data processing unit, ***(DPU)*** in which the raw frequency information undergoes further processing to produce a reading of axle load, or store the data in a desired form for classification. The frequency value measured by the ***Counter*** is also passed to a ***Storage*** device which retains the count for a certain period during which its output is smoothed by an ***Integrator***. The resulting voltage is used as the input to the Frequency control element, ***(FCE)*** which compensates

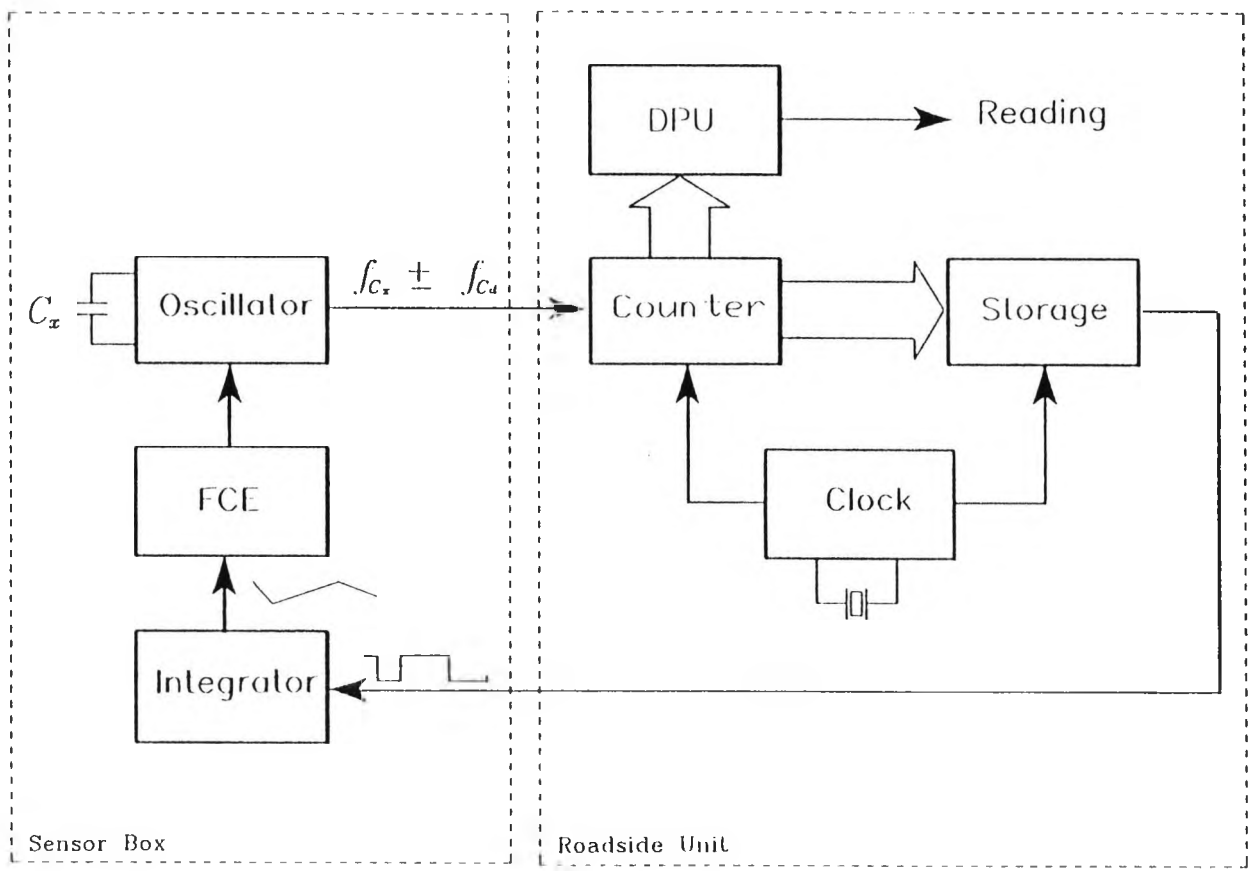

Fig. 6.5 Block diagram of the Frequency drift compensating circuit.

for frequency drift of the ***Oscillator***. Because of its large time constant the ***Integrator*** will not be able to follow the very short frequency peaks induced by wheel passages, and therefore will not distort wheel load measurements. It will however respond to slow frequency drift caused by changes in sensor/circuit temperature, atmospheric pressure, moisture etc.

6. 4. 2 Oscillator Circuit.

The sensor capacitor C_x forms part of the tuning circuit of the L-C type sinusoidal generator, T1 - Fig. 6.6. Half of the primary winding of inductance L closes the tuning circuit, and the oscillations are carried through the secondary to the emitter-follower, T2. The signal is then passed to the wide band amplifier IC1, - video OpAmp ***μA733*** with selectable gain, (pins 11 and 12), to attain the right amplitude levels for TTL/CMOS detection. Finally the high current matching stage T3, T4, gives the signal the correct output impedance and balancing before passing it to the counter and stabilisation circuits.

The Oscillator and Buffer Amplifier circuits assembly will normally be situated in close proximity to the sensor capacitor C_x for maximum noise immunity and the avoidance of stray capacitance along the lead wires. The expected frequency of the oscillator can then be derived using the expression:

$$f_x = \frac{1}{2\pi . \sqrt{L.C}} \qquad (6.6)$$

where: L is the inductance of the tuning circuit,

C is the combined capacitance of the sensor - C_x, the frequency control element - C_d, and the transfer capacitor - C_t.

6. 4. 3 Frequency Counter and Storage circuit.

This is the digital part of the device in which the sinusoidal signal arriving from the Oscillator is converted to CMOS levels, and counted with a very high accuracy using Quartz stabilised gate signal - Fig. 6.7. The coded output of the Counter is then passed to the Integrator for smoothing. The CMOS converted Oscillator output is also diverted to the Data processing unit for

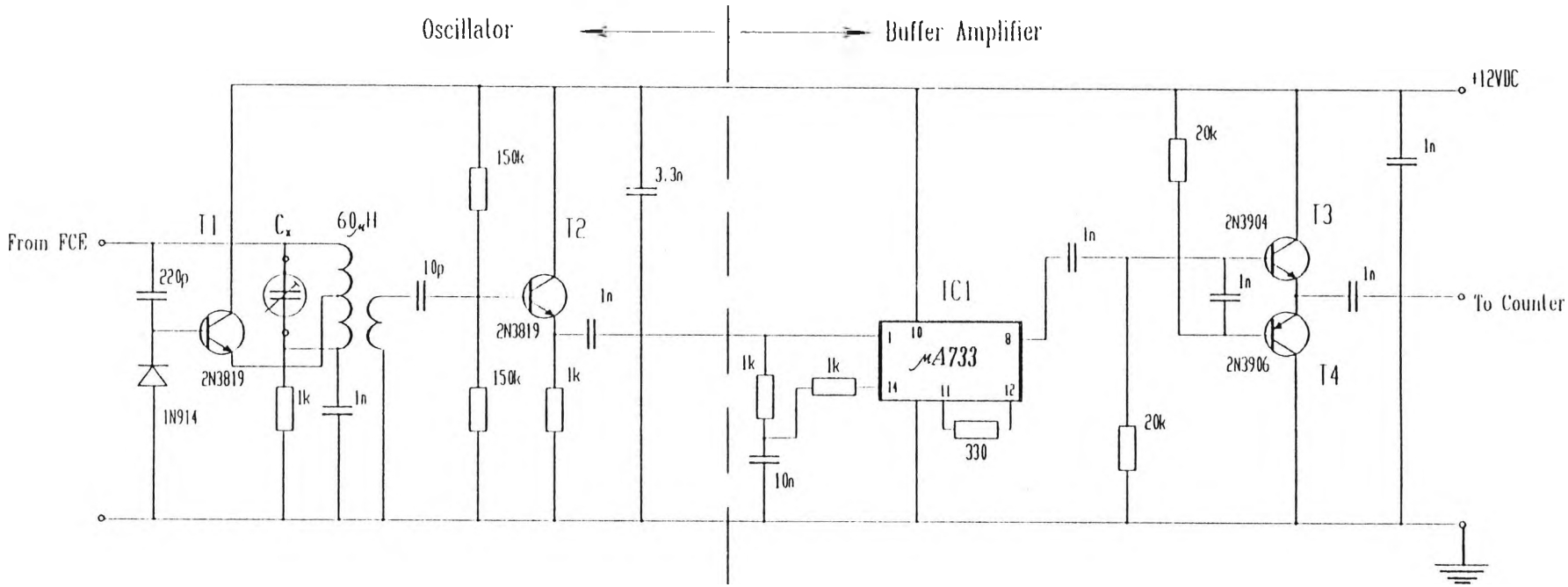

Fig. 6.6 Voltage Controlled Oscillator and output amplifier.

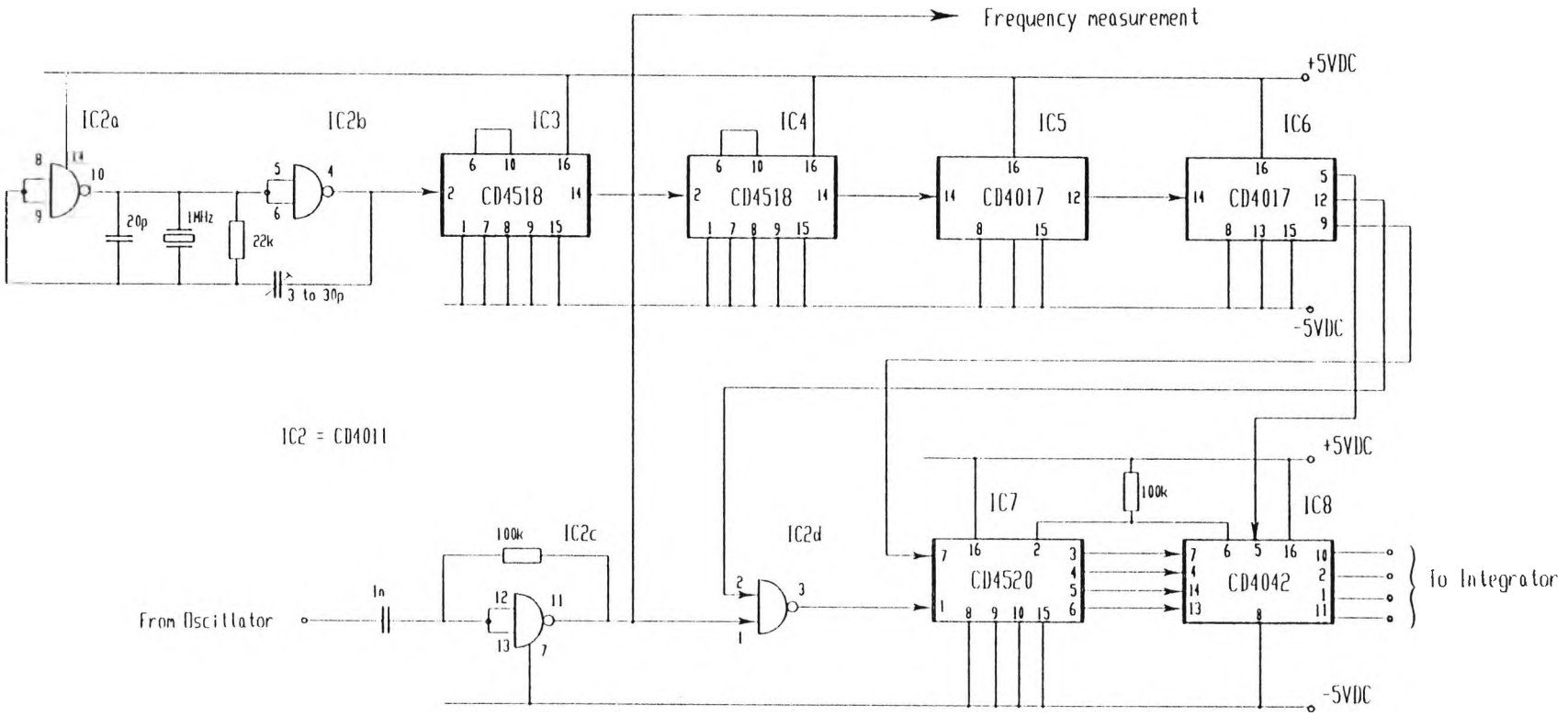

Fig. 6.7 Frequency counter and drift correction circuit.

further processing and extracting the wheel load information.

Integrated circuits IC2a and IC2b are connected to form a crystal oscillator generating a highly stable 1MHz reference frequency train. IC's 3, 4, and 5 are decade dividers reducing the 1MHz signal by 100, 100, and 10 respectively. Thus a square wave with a stable period of 0.1s is applied to the clock input of the decade counter IC6 which gives a decoded output in decade form, i.e. 0 to 9. The "carry" output - pin 12 of IC6, will be high for the first five counts and low for the higher five, which will give a square wave with half its period equal to 0.5s. The latter output is the counter's "gate" signal. Two other signals are required to operate the system - one to transfer the information from the input of the latch IC8 to its output, and one to reset the counter to zero prior to the start of the next counting period. From the timing diagram in Fig. 6.8 it can be seen that the outputs corresponding to counts of six and eight can be used to provide these functions.

IC2c is used in its linear mode to act as an input amplifier for the sinusoidal signal from the Oscillator and to convert this signal to CMOS logic levels. IC2d is the gate which allows the Oscillator signal to pass to the counter for a period of 0.5s. The signal is then counted in IC7. The output of the latch IC8 remains constant while Pin 5 is held at a low level. However, when Pin 5 is raised to high, the levels at the inputs (Pins 4, 7, 13, 14), are transferred to the outputs, (Pins 1, 2, 10, 11). As this transfer occurs after the counter has stopped counting, the transferred data will be stable. After Pin 5 returns to low level, a reset pulse is applied Pin 7 of IC7 returning the counter to zero in readiness for the next count. The whole system therefore cycles, and is updated with a period of 1s.

6. 4. 4 Integrator and Frequency Control.

It is now necessary to convert the coded digital output of the counter into an analogue correction signal. This is accomplished using the OpAmps IC9 and IC10 as a Digital-to-analogue Convertor, and Integrator respectively - Fig. 6.9.

Provided the OpAmp has very high input, and very low output impedance, for the gain of the amplifier IC9 we can write:

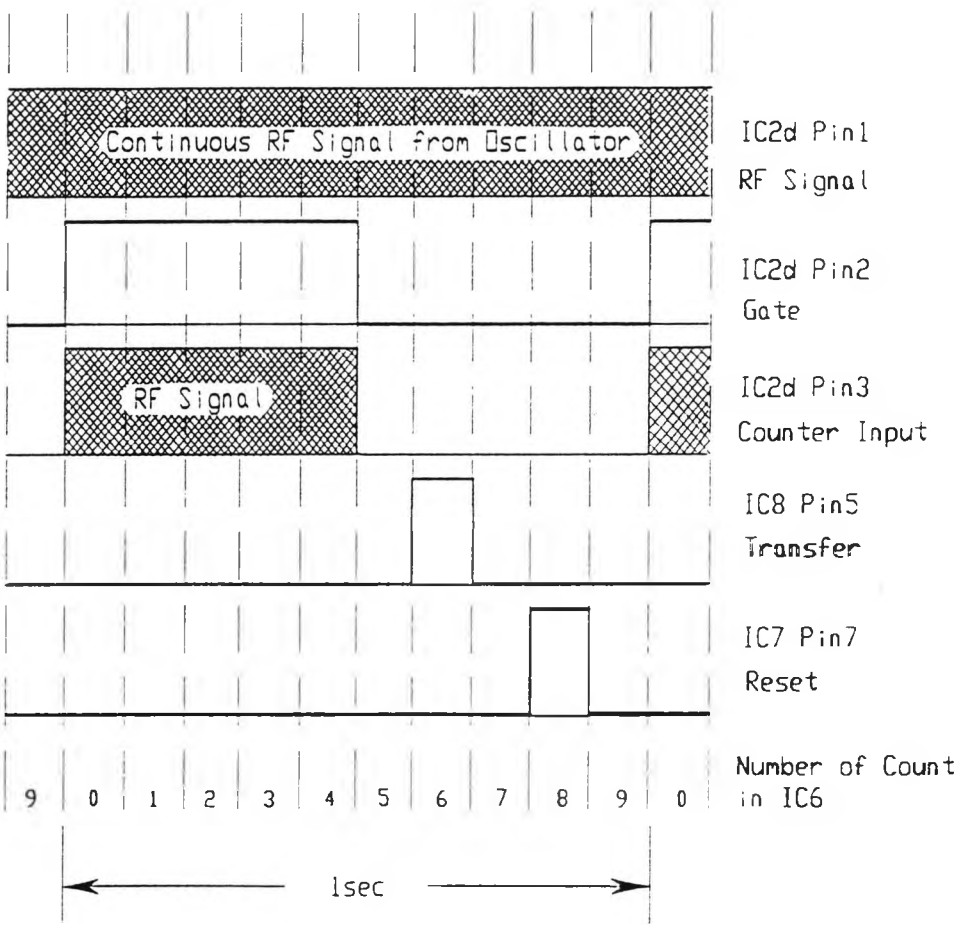

Fig. 6.8 Timing diagram of the frequency drift correction circuit.

$$K = -\frac{R_f}{R_{in}},$$

where: R_{in} is the series input resistor,
R_f is the feedback resistor.

With very high input impedance, practically no current will be flowing at the input pin 2 of IC9, therefore it can be assumed that this point is virtually at earth. As a result several inputs can be applied, and the gains of each of them can be varied by changing the value of R_{in} appropriately. The output will then be the sum of all the inputs multiplied by their respective gains set by their R_{in} resistors.

The counter used in the system is of the four-bit binary type, (divide by 16), and the truth table of the counter's four outputs for count from 0 to 15 is shown in Table 6.1. The CMOS logic of the system is run off ± 5Vdc, therefore a logic 0 is a level of -5Vdc, and a logic 1 is a level of $+5$Vdc.

	Output of IC7				
	1	2	4	8	
Count	Pin3	Pin4	Pin5	Pin6	Output of IC9
0	−	−	−	−	*+15*
1	+	−	−	−	*+13*
2	−	+	−	−	*+11*
3	+	+	−	−	*+9*
4	−	−	+	−	*+7*
5	+	−	+	−	*+5*
6	−	+	+	−	*+3*
7	+	+	+	−	*+1*
8	−	−	−	+	*−1*
9	+	−	−	+	*−3*
10	−	+	−	+	*−5*
11	+	+	−	+	*−7*
12	−	−	+	+	*−9*
13	+	−	+	+	*−11*
14	−	+	+	+	*−13*
15	+	+	+	+	*−15*

Table 6.1 Truth table of IC7, (4520 4-bit counter), and output of DAC, IC9. (" − " equals logic 0, " + " equals logic 1)

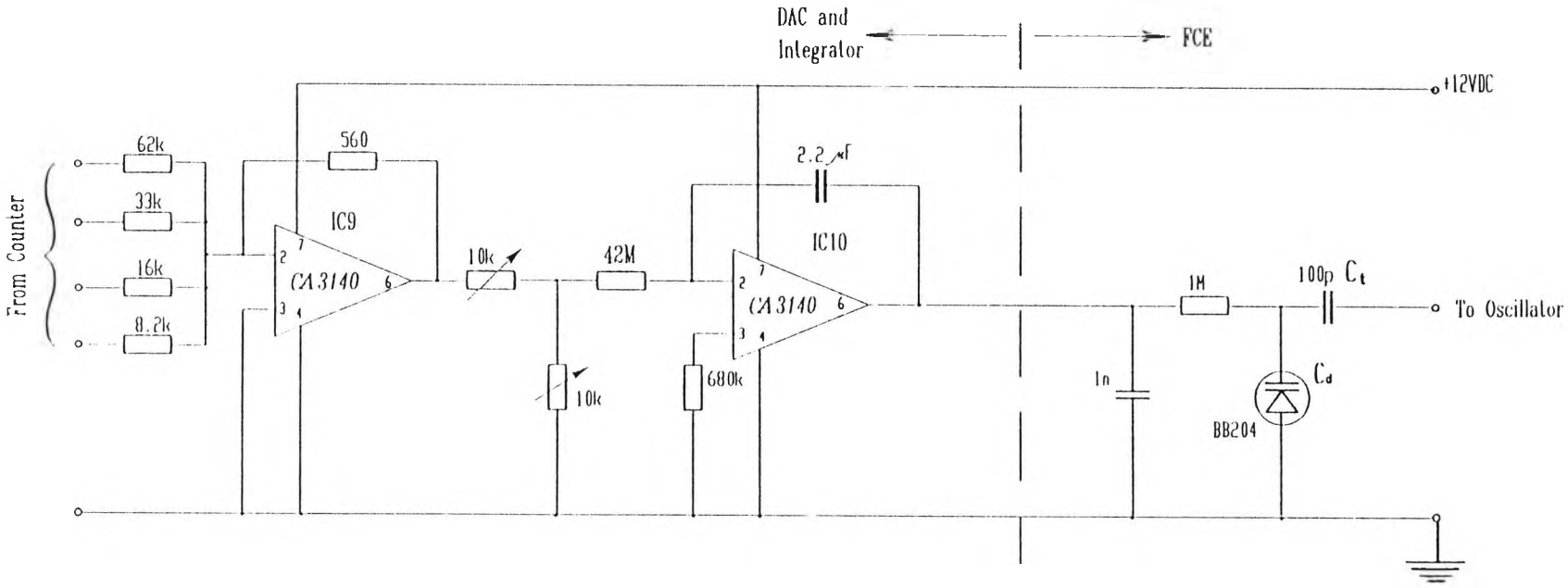

Fig. 6.9 Integrator and Frequency control element.

By examination of the truth table it can be seen that if the gain of IC9 is set at one for bit 1, two for bit 2, etc, then the output will be highest at both extremes of the count, i.e. 0 and 15, and lowest at the centre of the count i.e. 7 and 8. In this way the output of the OpAmp will be proportional to the detected error in frequency, i.e the size of the correction will increase with increasing frequency deviation from a stable point.

The second OpAmp, IC10 is connected as an integrator with a very large time constant, (90s). In this mode of operation if a positive DC level is applied to the input resistor, the output of the integrator will be a falling linear ramp until the low level of the OpAmp is reached. Likewise if a negative level is applied, output will ramp up until the upper limit is reached. In the present configuration the input voltage will be changing once every second as the latch is updated, hence the output of the integrator will be continuously rising and falling about a mean level. The rate of change of the ramp output will depend upon the output of the DAC, IC9, which itself is dependent on the value of the binary output of the latch IC8.

The Integrator's output is then applied as a correction voltage to the Frequency control element represented by the variable capacitance diode, *(Varicap)* - C_d, , connected across the Oscillator's tuning circuit. The Varicap is connected in parallel with the sensor capacitor C_x in the tuning circuit of the Oscillator thus influencing the generated frequency count. In this way the control loop will be closed and the stabiliser should correct for any slow frequency drift in the Oscillator.

6. 4. 5 Circuit performance and Experimental results.

Originally a simpler version of the stabilising circuit was developed using TTL logic and an R-C delay line to generate the "Counter Reset" signal. The Oscillator signal was passed through a decade counter and just the level of the least significant bit of the count was used to drive the Integrator. The circuit proved to be effective, but given the high current levels being switched which might upset the correction, as well as the high power consumption of TTL chips, a CMOS version of the device was developed. A more flexible frequency correction method was also implemented which is sensitive to the magnitude of frequency deviation thus eliminating the drawback of the original circuit of

"missing" some of the stable frequency points.

In the present circuit the oscillator is stabilised in a series of steps, each distanced 16 counts of the divider-counter away from the next. The resolution of the counter, i.e. the value of one count of the least significant bit in Hz, is equal to $1/T_g$, where T_g is the gate period in seconds. In this case $T_g = 0.5s$, hence each count has a value of 2Hz. It can be seen therefore that the oscillator will lock at $16x2Hz$ intervals, or every 32Hz, which is adequate for the generated frequency.

For a typical sensor capacitance value of $C_x = 80pF$ selected from a standard decade capacitor, an oscillator frequency of around 2Mhz was measured at Pin 11 of IC2, – Fig. 6.7, (see Eq. 6.6). For practical purposes though, a divider by 100 was connected between the output and the Frequency counter taking the frequency down to 20kHz.

The frequency drift of the Oscillator was monitored in the course of 4 hours after powering on the circuit, for two cases:

(i) Non-stabilised, stand-alone Oscillator – "open loop" case,
(ii) Stabilised Oscillator circuit as described above.

The results are illustrated in Fig. 6.10 showing that the greatest drift occurs in the initial half hour of the Oscillator's operation. The stabilising potential of the circuit is obvious as a drift reduction of more than 10 times was achieved. Experiments were also carried out with both configurations to test their sensitivity to known frequency destabilising factors. The ambient temperature was gradually increased by 100% through introducing a heat source in the vicinity of the device. Large frequency deviations, (up to 8%) were observed with the stand-alone oscillator, whereas no more than 0.45% drift was recorded with the stabilised circuit.

Using the stabilising device a long term stability of the Oscillator is achieved comparable with that of the reference crystal oscillator. Different versions of the circuit have been successfully applied to some FM transceiver devices, [6], [43], [134], [151], etc. and have shown very good results.

In the practical application of the device to a capacitive wheel load sensor only the analogue part of the circuit, i.e. the Oscillator, Buffer Amplifier, DAC,

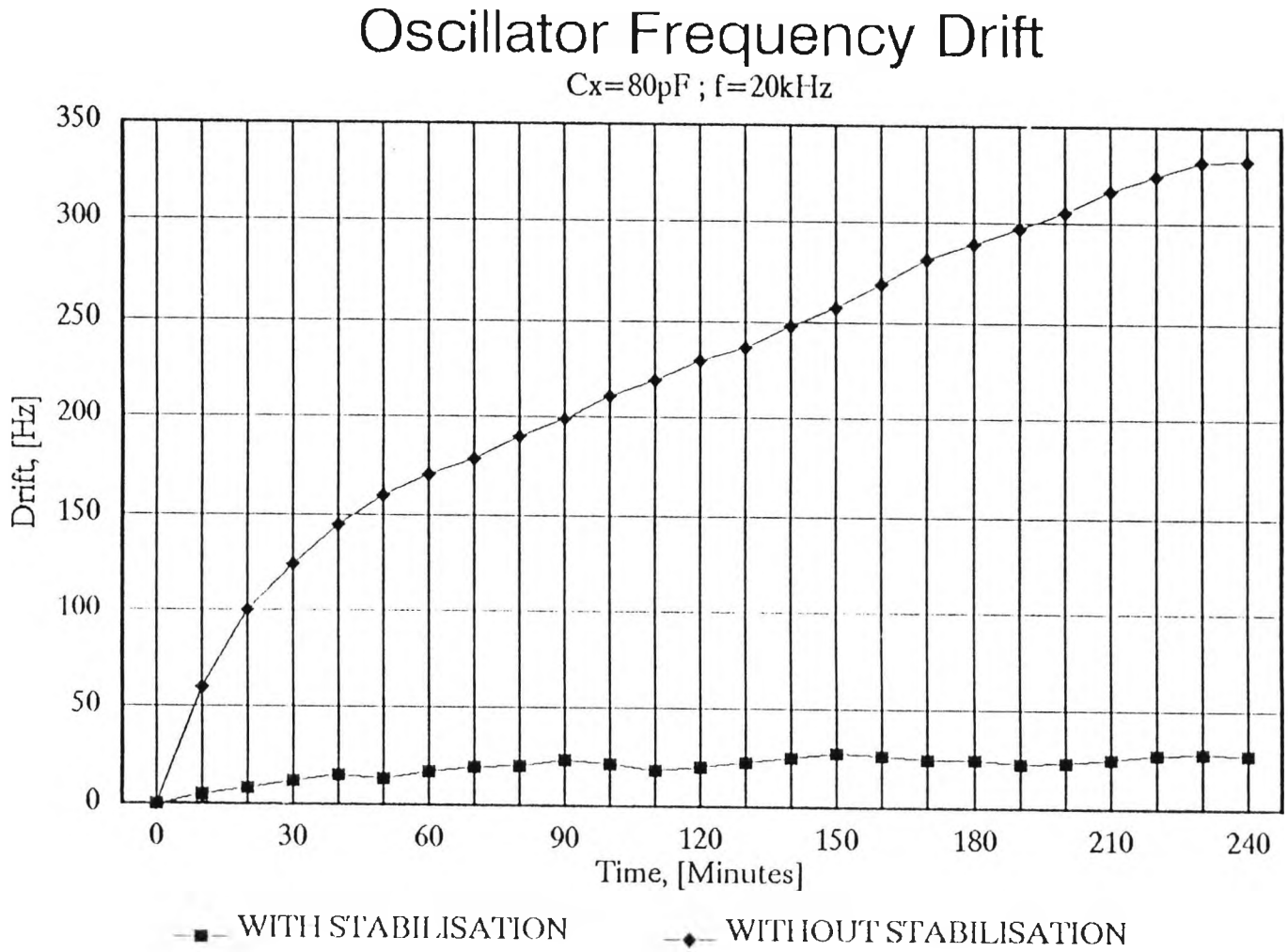

Fig. 6.10 Oscillator Frequency drift results.

Integrator, and the Frequency control element should be situated in close proximity to the sensor assembly. Using modern surface mounted devices and possibly hybrid IC's, those circuits can be accommodated on a surface no larger than 1-2in^2. Thus only digital signals and the power supplies are carried in the properly screened cable connection to the Roadside unit containing the digital circuitry, power supplies and data processing equipment. In the case when line type sensors are used the sensor signal should be combined with vehicle speed information to produce the required result - see Ch.1, Sect. 1.6.2.1.

Chapter VII: Study Conclusions.

7. 1 SUMMARY.

The objective of this study is to help solving some of the measurement accuracy and reliability problems of present WIM systems. The theoretical part of the study is focused on vehicle dynamic effects since they have long been identified as one of the major causes of error in high speed dynamic vehicle weighing. As part of the experimental work a concept for a capacitive strip sensor is suggested and a suitable measuring circuit is developed and tested.

Weigh-in-Motion technology is introduced by giving a brief description of the technique and its historical background, and outlining the major areas of application of the gathered data. A generalised functional model of the WIM process is presented, followed by a system classification based on various operational criteria. A detailed system analysis describes the functionality of the basic elements of the WIM process - vehicle suspension dynamics, sensor system, and signal processing. In the metrological analysis the standard measurement categories accuracy, repeatability, reproducibility etc., are defined for the technique, and the main sources of measurement errors are identified. The dynamic character of the measurement is found to be the single most important source of measurement errors resulting in the relatively poor accuracy of the method.

Mathematical models are presented of the vehicle suspension/tyres, and a rigid sensor platform with its ground foundation. A simple single wheel, (quarter-vehicle) suspension model is used and its major parameters and relationships are introduced. Methods of emulating the enveloping properties of the pneumatic tyre are also discussed. The models are later used in a series of vehicle - roadsurface dynamic interaction computer simulations. A locally developed interactive modelling package is used to run the simulations.

Two major sets of simulations are performed - 1) vehicle interaction with road profiles of deterministic shapes, accounting for dynamic vehicle effects induced by isolated surface irregularities and/or unlevelled sensor platforms, and 2) vehicle interaction with road surfaces of stochastic description, reflecting the

the interaction with natural type of road surface. The effects of different factors influencing the outcome of the measurement, e.g. vehicle speed, platform protrusion level, vehicle physical parameters etc., are investigated.

A concept for a capacitive line sensor is proposed in line with the trend of developing low-cost, easy to install WIM systems. The results of a finite element modelling undertaken in a previous study are presented to illustrate the derivation of a optimal sensor strip profile. Finally a frequency modulated capacitance measurement circuit incorporating frequency drift compensation is developed and tested with good results.

Most of the study results are presented in both tabular and graphical form. The corresponding conclusions are drawn on the basis of the obtained data, concerning the design, installation and usage of WIM equipment. However, the simulation results can also be used by pavement and road structure designers in relating pavement damage to the vertical dynamic wheel forces.

7. 2 STUDY FINDINGS.

Following the research described in this thesis the following conclusions can be drawn:

1) Compared to experimental data the simulation results slightly overestimate the dynamic wheel forces generated by wheel contact with an isolated obstacle of deterministic shape. This can be attributed mainly to the simple tyre model used, unable to account effectively for the tyre enveloping properties.

2) Incorrectly installed sensor, (unflush with road surface), induces considerable suspension excitations which may significantly distort the measurement. Furthermore, the magnitude of these excitations is strongly dependent on additional vehicular factors which will further increase the uncertainty of the measurement. Impact Factor values of up to 12% were obtained at vehicle speeds of 80km/h with only 2mm sensor unflushness.

3) The effect of vehicle speed variation is most strongly pronounced in the intermediate speed range: 10km/h – 60km/h, leading to simulated first IF peak

differences of 39% for the step of height h = 0.01m. Above that speed the IF peaks show a tendency of slowly approaching a maximum value determined by the tyre stiffness and the step height. The speed sensitivity of WIM equipment has to be compensated either by enforcing site speed restrictions, (slow speed systems), or introducing speed correction algorithms in the signal processing part.

4) From the vehicle's physical parameters, variations in tyre stiffness and laden weight will cause greatest differences in the dynamic behaviour of the vehicle. The fact that these are the most 'unstable' vehicle parameters will further reduce the reliability and accuracy of the measurement. It is therefore advisable that the calibration procedure should incorporate multiple passages of different types of vehicles, (and with different laden weights), to partly compensate for the effect of variation of these parameters. The effect on the IF magnitude of other vehicle parameters – suspension stiffness, suspension and tyre damping, unsprung mass etc., is not that strongly pronounced, though some differences in the frequency response of the vehicle suspension are observed.

5) The magnitudes of dynamic errors induced by road imperfections ahead of sensor do not necessarily follow the same relationships to vehicle parameters as the ones induced by unflush sensor edges. For example the dynamic errors of unladen vehicles are not always greater than those of laden or half-laden vehicles at similar conditions. For the bump length chosen for the simulations, step-shaped profiles generally produce greater errors. In terms of the distance ahead of sensor which has to be free of irregularities of specific shape and height, the worst case corresponds to a step-shaped irregularity of the maximum simulated height of h = 8mm and minimum allowed error of $\epsilon = 1\%$.

6) The simulation results of vehicle interaction with road surfaces of stochastic description are in qualitative agreement with experimental data gathered on typical road tracks with some common vehicle suspension systems.

7) A considerable increase in the dynamic component of wheelforces on pavements has to be expected with rising vehicle speed and deteriorating road surface quality.

8) Unlike the case with isolated surface irregularities, here the effect of changing vehicle laden weight was proved to be insignificant. Tyre filtering was also found to have little effect on reducing the dynamic wheelforces for the considered types of roads and vehicle speeds.

9) Since the load distribution has a minor effect on the generated dynamic

wheelforces, a single vehicle could be used for routine measurements of road surface parameters. Compared with the direct stylus, or laser assisted profile level measurement this is a method of lower precision, but it could be more useful when overall mean road roughness characteristics of a certain motorway or a whole regional road system are required.

10) The predicted increase of the dynamic wheel force observed with road surface deterioration emphasises the detrimental effect of low surface quality on pavement durability. The magnitude of the measured dynamic load standard deviation could therefore be a valuable indicator of the extent of environmental damage on a particular stretch of the motorway system.

11) The work done on the capacitive strip sensor indicated the viability of the concept as a promising candidate sensor assembly for a low-cost temporary system. Recent publications on the matter have confirmed the potential of capacitive sensors in WIM technology.

12) The frequency drift compensating circuit demonstrated excellent stability. A production version of the device should show good performance in the adverse road surface environment.

7. 3 RECOMMENDATIONS FOR FURTHER WORK.

Although the study gives a general insight if the WIM process and points out the major problems concerned with its accuracy, it analyses in detail only one aspect common to WIM systems – the errors due to dynamic vehicle effects resulting from the wheels interaction with road profiles of different descriptions. Research in the area can be expanded in the following directions:

1) Improvement of the vehicle model for the simulations to account for the distribution of forces and momenta over the whole vehicle structure, as well as to change parameter values so that to cover more vehicle types. Improvement of the tyre model is especially important in order to provide a realistic representation of tyre enveloping of short surface irregularities.

2) Investigate the nature of load distribution on weighscale platform and develop on this basis guidelines for platform design and loadcell specifications.

3) Study the possibilities of wider applications of new types of force transducers to replace the commonly used resistive loadcell weighscales. Expand the work on capacitive strip/mat sensors and perform "live" trials of the devices on laboratory test rigs or with vehicles on test tracks. Interface the frequency output of the capacitance measuring circuit to a microprocessor device and develop signal processing and data handling assembly language routines.

4) Evaluate the feasibility of a multisensor WIM system – an array of multiple sensors in the direction of travel to pick up a number of discrete samples of the applied wheel forces. Perform engineering calculations on the dimensions, sensor positioning and alignment, and the possible traffic restrictions which have to be imposed on the measured vehicles. Develop specifications for the dynamic response of the equipment and real-time software for the signal processing algorithms.

Appendix A

CLASSIFICATION OF WIM SYSTEMS CURRENTLY IN USE.

Identification	Weigh in Motion Scale	TRRL High Speed Weighbridge	Bascille De Pesage Dynamic	Bast Bending Plate Dynamic Weighbridge
Developer	University of Saskatchewan	Transport and Road Research Laboratory	Laboratoire Central Des Ponts et Chausees	Bundesanstalt Fuer Strassenwesen
Manufacturer/Distributor	International Road Dynamics CMI Dearbourne	Trevor Deakin	Angers C.E.C.P.	Messdata, Seimens-Allis Corp Process-Automatisierungstechnik
References	3, 10, 48, 49 *	3, 9, 14, 39 *	3, 6, 13	3, 14, 48
Deck Height Above Pavement (mm)	0	0	0	0
Sensor Base Depth Below Pavement (mm)	203	205	150	40
Deck Area (mm)	1420 x 760	600 x 600	1510 x 440	1250 x 500
Deck Surface Material	Steel	Hiduminium (Aluminium Alloy)	Bare Steel or Asphalt Coating	Steel Coated with Vulcanised Synthetic Rubber
Sensor Type	Hydraulic Pressure Chamber with Strain Gauges	Wire Strain Gauges on Steel Prisms	Piezoelectric Quartz Crystals	Strain Gauged Bending Plate
No of Sensors per Deck	1	4	3	1
Wheel/Axle Weigher	Wheel	Wheel	Wheel	Wheel
Max Vehicle Speed (mph/kph)	More than 62/100	>75/120		81/130
Rated Axle Load (Tonnes)	20	20	>23	>25
Max Overload (%)	10			
Axle Weight Accuracy	±5% at 90% Confidence	±10% Statistical	±5% up to 50mph/80kph	±5% up to 81mph/130kph
Gross Vehicle Weight Accuracy				
Output Resolution				
Microprocessor Based	Yes		Yes	Yes
Power Supply	110V AC 60Hz	Mains with 2 hour Failure Protection	220V AC	12V Battery
Temperature Range Sensor (°C)	-50 to +50			-60 to +80
Temperature Range Analyser/Display (°C)	+5 to +50			-60 to +80

Table A.1 High Speed Permanent Weighbridge Systems - Specifications.

Identification				
Developer	Otto Graf Intitute	Bureau of Public Roads		
Manufacturer/Distributor			Streeter-Amet	Radian Corporation
References	3	3	48	48
Deck Height Above Pavement (mm)		0	0	0
Sensor Base Depth Below Pavement (mm)	1200	1600	203	90
Deck Area (mm)	3700 x 1400	3050 x 900	1473 x 686	1372 x 457
Deck Surface Material				
Sensor Type		Strain Gauge Load Cells		Strain Gauge Load Cells
No of Sensors per Deck	2	4	4	8 Active 8 Dummy
Wheel/Axle Weigher	Axle		Wheel	Wheel
Max Vehicle Speed (mph/kph)		40/64	55/88	
Rated Axle Load (Tonnes)				
Max Overload (%)				
Axle Weight Accuracy	± 5% Statistical	±5%	Statistical ± 5% at 90% Confidence	±10% at 90% Confidence
Gross Vehicle Weight Accuracy				±5% at 90% Confidence
Output Resolution				
Microprocessor Based	NO	NO	YES	IBM XT Microcomputer
Power Supply				
Temperature Range Sensor (°C)	Thermostatically Controlled			
Temperature Range Analyser/Display (°C)				

Table A.1 High Speed Permanent Weighbridge Systems - Specifications.

Identification			Fast Weigh	Lee Portable Electronic Scale	Vibra-Koaxialkabel Vibracoax
Developer		National Institute for Road Research	Case Western Reserve University	Highway Research Board	
Manufacturer/Distributor	Streeter-Amet	Plessey South Africa Golden River Vaxjo (Sweden)	Bridge Weighing Systems Inc.		Messdata Philips
References	48	48, 3, 9, 46 *	48, *	9	3, 11, 14, 17, 47
Deck Height Above Pavement (mm)		9.5		0	0
Sensor Base Depth Below Pavement (mm)		0		30	
Deck Area (mm)		1830 x 508		1270 x 500	3mm wide
Deck Surface Material		Rubber	Bridge Pavement	Metal	Pavement
Sensor Type	Capacitive	Capacitive	Re-Useable Strain Transducers	Load Cells	Piezoelectric Cable
No of Sensors per Deck		1		8	1
Wheel/Axle Weigher		Axle	Axle	Wheel	Axle
Max Vehicle Speed (mph/kph)		No Restriction			
Rated Axle Load (Tonnes)		29			
Max Overload (%)					
Axle Weight Accuracy		±10% at 95% Confidence	15%	15%	
Gross Vehicle Weight Accuracy		±0.25 tonnes	4%		
Output Resolution					
Microprocessor Based	YES	YES	YES		
Power Supply	110V AC (Petrol Generator)	Sealed Lead-Acid Batteries 6V 10 A	Mobile Supply		
Temperature Range Sensor (°C)		0 to 80			
Temperature Range Analyser/Display (°C)		-40 to 80			

Table A.2 High Speed Temporary Weighbridge Systems - Specifications

Identification	ADS Weighbridge	Logaload	Eaziwey	Dynamic Axle Weigher	DAW 310
Developer			Hull University		
Manufacturer/Distributor	Weighwrite	Trevor Deakin		Talent	Prozess-Auto-matisierungstechnik
References	3, 14 *	*	2	*	*
Deck Height Above Pavement (mm)	0	0	0	0	0
Sensor Base Depth Below Pavement (mm)	241	147		270	23
Deck Area (mm)	3040 x 760	1200 x 750	3090 x 750	3000 x 750	1250 x 508
Deck Surface Material		Zinc Spayed Steel			Steel covered with Vul-canised Neoprene rubber
Sensor Type	Hydraulic Cells with Strain Gauge Pressure Transducers		Strain Gauge Load Cells	Electronic Load Cell Cells	Bending plate with 10 strain gauges
No of Sensors per Deck	4		4		1
Wheel/Axle Weigher	Axle	Wheel	Axle	Axle	Axle
Max Vehicle Speed (mph/kph)	2.2/3.5	3.75/6	5/8	10/16	16 (25)
Rated Axle Load (Tonnes)	15	20	20	15	20
Max Overload (%)	33				50
Axle Weight Accuracy	±0.33% of full scale	±0.2%	0.1% in Static Mode		
Gross Vehicle Weight Accuracy					±1 to ±3% up to 5 Kph ±3 to ±5% from 5-10 Kph
Output Resolution	10kg	10kg	10kg		10 Kg
Microprocessor Based		YES	Rockwell AIM 65		YES
Power Supply		Battery 12V DC			220V at 50-60 Hz or Battery
Temperature Range Sensor (°C)	-5 to + 70 or -42 to +50	-15 to +55			-40 to +80
Temperature Range Analyser/Display (°C)	0 to 50	-5 to +50			-10 to +50

Table A.3 Static and Low Speed Permanent Weighbridge Systems - Specifications.

Identification	Lynx Weighbridge	Moduline Weighbridge	5155 Weighbridge	5152 Weighbridge
Developer				
Manufacturer/Distributor	Solidate Ltd	Solidate Ltd	Avery	Avery
References	*	*	*	*
Deck Height Above Pavement (mm)	0 or 275	0	340 or 0	0
Sensor Base Depth Below Pavement (mm)	390 or 0		0 or 370	1080
Deck Area (mm)	3000 x 5000 to 24000	3000 x 15000 or 18000 or 24000	3000 x 5000 to 24000	3000 x 12000 to 18000
Deck Surface Material	Concrete or Steel	Concrete		Concrete
Sensor Type	Shear Beam Load Cell	Load Cell	Load Cells	Load Cells
No of Sensors per Deck			4/6/8/10	4
Wheel/Axle Weigher	Vehicle	Vehicle	Vehicle	Vehicle
Max Vehicle Speed (mph/kph)	0	0	0	0
Rated Vehicle Load (Tonnes)	Up to 80	40/50/60/75	20/40/60/80	40/50/60
Max Overload %	50			
Axle Weight Accuracy				
Gross Vehicle Weight Accuracy				
Output Resolution		10 or 20 kg		
Microprocessor Based				
Power Supply	Mains	mains		
Temperature Range Sensor (°C)				
Temperature Range Analyser/Display (°C)				

Table A.3 Static and Low Speed Permanent Weighbridge Systems - Specifications.

Identification	Hydraulische Wiegeschwelle			Rigidec Static
Developer	Bundesanstalt Fuer Strassenwesen	University of California	Institut Fuer Material-prufung (Hanover)	
Manufacturer/Distributor				Mangood Ltd
References	9, 3	3	3	*
Deck Height Above Pavement (mm)	0		0	0
Sensor Base Depth Below Pavement (mm)	850		160	
Deck Area (mm)	3750 x 600		8000 x 500	3000 x 7500/9000/15000/18000
Deck Surface Material			Asphaltic Fine Concrete	Concrete
Sensor Type	Hydraulically Driven Inductive Transducer	Strain Gauged Bending Girder	Strain Gauged Bending Load Cells	Load Cells
No of Sensors per Deck	1	2	16	4 or 6
Wheel/Axle Weigher	Axle		Wheel	Vehicle
Max Vehicle Speed (mph/kph)	>3/5	?	?	0
Rated Vehicle Load (Tonnes)				30/40//50/60/80
Max Overload (%)				
Axle Weight Accuracy	6.4% Statistical			
Gross Vehicle Weight Accuracy				
Output Resolution				10 or 20kg
Microprocessor Based				
Power Supply				Mains
Temperature Range Sensor (°C)	-5 to +30			
Temperature Range Analyser/Display (°C)				-10 to +50

Table A.3 Static and Low Speed Permanent Weighbridge Systems - Specifications.

Identification	Weigh-In	DIY Weighbridge	British Aerospace Weigher	Hawkley S.A.
Developer				
Manufacturer/Distributor	Weighwrite	Weighwrite	Talent Weighing Ltd	Hawkley
References	*	*	*	*
Deck Height Above Pavement (mm)	0		0	0
Sensor Base Depth Below Pavement (mm)			121	
Deck Area (mm)	2600 x 760	3040 x 5500	2591 x 432 or 3050 x 762	2600 x 600
Deck Surface Material	Concrete	Steel or Concrete		Steel
Sensor Type			BAe Hydrostatic Load Cell	Hydraulic Cell and Gauge
No of Sensors per Deck				
Wheel/Axle Weigher	Axle	Vehicle	Axle	Axle
Max Vehicle Speed (mph/kph)	0	0	0	0
Rated Axle Load (Tonnes)	12	26 (whole vehicle)	15 or 20	16
Max Overload (%)				63
Axle Weight Accuracy	±0.25% of Full Scale	±0.12% of Full Scale		±15% of Full Scale
Output Resolution				50kg
Microprocessor Based			NO	NO
Power Supply	240V or 110V	240V or 110V Protection	None Required	None Required
Temperature Range Sensor (°C)				-20 to +40
Temperature Range Analyser/Display (°C)				

Table A.3 Static and Low Speed Permanent Weighbridge Systems - Specifications.

Identification			Dynamic Weighing Plate	Statical Wheel Load Scale	Saw 10C
Developer	Statens Vaginstut (Sweden)	University of Texas		Heini	
Manufacturer/Distributor			Prozess-Automatisierungstechnik	Prozess - Automatisierungstechnik	Prozess - Automatisierungstechnik
References	3	3	50, "	"	"
Deck Height Above Pavement (mm)	0	0			29
Sensor Base Depth Below Pavement (mm)	110	50	0		0
Deck Area (mm)	1400 x 300	1370 x 510			560 x 382
Deck Surface Material			Steel Coated with Polydirectional Rubber	Aluminium	Aluminium Alloy
Sensor Type	Strain Gauge Load Cell	Pressure Pickups with Coil Springs	Wire Strain Gauges on Bending Plate	Hydraulic (Liquid Sandwich)	Strain Gauged Bending Plate
No of Sensors per Deck	3	8	1	1	1
Wheel/Axle Weigher	Wheel	Wheel	Wheel	Wheel	Wheel
Max Vehicle Speed (mph/kph)	12/20	7	6/10	0	0
Rated Axle Load (Tonnes)					10
Axle Weight Accuracy		±10%		±2%	±25kg up to 2.5T ±50 kg up to 10T
Gross Vehicle Weight Accuracy			±3%		
Output Resolution			10kg	50kg	50kg
Platform Weight (Kg)			75	19.8	22.5
Power Supply			12V Auto Battery		6 x 1.5V rechargeable or disposable batteries
Temperature Range Sensor (°C)	Thermostatically Controlled				-10 to +50
Temperature Range Analyser/Display (°C)			-10 to 50	-10 to +50	-10 to +50

Table A.4 Static and Low Speed Temporary Weighbridge Systems - Specifications.

Identification	Checkweight MK 4	TRRL Portable Wheel Weigher	MIN.10.T	Highwayman	Telub 1203
Developer		Transport & Road Research Laboratory			
Manufacturer/Distributor	Talent Weighing Ltd		Trevor Deakin	Hawkley	Vaxjo
References	*	14, *	*	*	*
Deck Height Above Pavement (mm)		90	53	70	85
Sensor Base Depth Below Pavement (mm)	0	0	0	0	0
Deck Area (mm)	430 x 280	500 x 700	480 x 500	520 x 250	400 x 500
Deck Surface Material		Aluminium	Aluminium Alloy	Metallic	Magnesium Alloy
Sensor Type	Hydrostatic Load Cell	Load Cells		Hydraulic	Strain Gauges
No of Sensors per Deck	1	6		1	4
Wheel/Axle Weigher	Wheel	Wheel	Wheel	Wheel	Wheel
Max Vehicle Speed (mph/kph)	0	0	0	0	0
Rated Axle Load (Tonnes)	9	10	20	6.5	10
Max Overload (%)					50
Axle Weight Accuracy	0.5% of full scale	±2%	±2% of full scale	±2% of full scale	±1% of full scale
Output Resolution	100Kg	10kg	10kg		10kg
Platform Weight (Kg)	28	47	29	26	30
Power Supply	None Required	12V Battery	12V Battery/Mains	None Required	10 x 1.2V NiCd Batteries
Temperature Range Sensor (°C)	-30 to +70		-10 to +50		-40 to +60
Temperature Range Analyser/Display (°C)	-30 to +70				-40 to +60

Table A.4 Static and Low Speed Temporary Weighbridge Systems - Specifications.

Appendix B

USING *MEDIEM* WITH GRAPHICAL MODE OF MODEL ENTRY

The representation of a system within *MEDIEM* is invoked graphically. This is referred to as Graphical Model Input, (GMI). The GMI screen consists of a fixed horizontal menu line followed by a submenu of elements, used in *MEDIEM,* as shown in Fig. B.1. The menu and the set of elements are selected by a mouse-driven cursor. A brief description of the menu commands is given below:

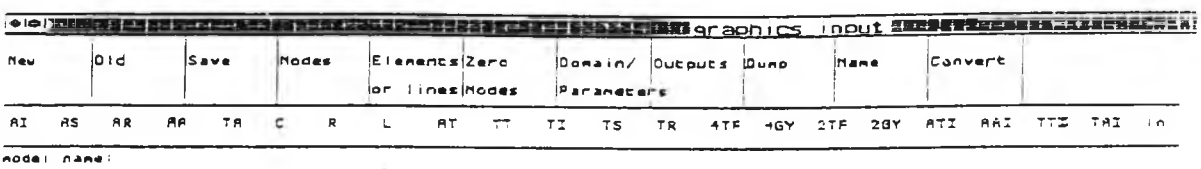

Fig. B.1 *MEDIEM* Menu structure for Graphical model input.

Menu commands:

- *NEW* clears the screen of any existing structure graphs.
- *OLD* enables the user to retrieve a structure graph stored on disk.
- *SAVE* enables a structure graph to be stored on disk.
- *NODE* allows the user to place the position of the nodes which separate the elements on the screen.
- *ELEMENTS or LINES* allows the user to select and place any of the elements in the submenu, between two nodes.
- *ZERO NODES* allows the user to change a solid node to a hollow node which represents "ground".
- *DOMAIN/PARAMETERS* allows the user to specify which domain an element is in, e.g. electrical, mechanical etc., and to enter its corresponding value.
- *OUTPUTS* enables the user to specify which of the elements will have their associated variables displayed. The user may choose the output to be an

ACROSS or *THROUGH* variable, (see Table B.1).

- *DUMP* sends the screen image to a printer.
- *NAME* allows the structure graph to be named. The name is then displayed at the top of the graph.
- *CONVERT* converts the structure graph image into a state-space matrix from which the user can display the outputs in either the frequency or time domain.

The outputs may be either tabular or graphical.The menu layout is such that in constructing a structure graph, the user would effectively work the menu from left to right. For all energy domains Structure graphs use *Through, (TH),* and *Across, (AC)* variables. These are described in Table B.1:

Domain Variable	Electrical	Mechanical Translational	Mechanical Rotational	Fluid	Thermal
AC	*Voltage*	*Velocity*	*Angular Velocity*	*Pressure*	*Temper.*
TH	*Current*	*Force*	*Torque*	*Mass* Flowrate*	*Heat Flowrate*

Table B.1 Variables used in Structure graphs.
(If incompressible Volume Flowrate can be used)*

Table B.2 gives the element list implemented within *MEDIEM*.

Name	Expression	Structure graph symbol
Across Source	AC	A – Where A – can be: AI Across Impulse AS Across Step AR Across Ramp
Through Source	TH	T – Where T – can be TI Through Impulse TS Through Step TR Through Ramp
Resistance	AC = R.TH	R
Capacitance	TH = C.AC (Electrical, Fluid, Thermal)	C If Linear initial value is AC(ϕ)[a] If Non-linear initial value is AC(ϕ).C(ϕ)
	AC = C.TH (Mechanical Translation, Mechanical Rotation)	C If Linear initial value is TH(ϕ) If Non-linear initial value is TH(ϕ).C(ϕ)
Inductance	AC = L.TH (Electrical, Fluid, Thermal)	L If Linear initial value is TH(ϕ) If Non-linear initial value is TH(ϕ).L(ϕ)
	TH = L.AC (Mechanical Translation, Mechanical Rotation)	L If Linear initial value is AC(ϕ) If Non-linear initial value is AC(ϕ).L(ϕ)
Transformer	AC1 = TF1.AC2 TH2 = TF2.TH1	TF
Gyrator	AC1 = GY1.TH2 AC2 = GY2.TH1	

[a] (ϕ) is the value at the start of simulation.

Signal Elements

Name	Expression	Structure Graph Symbol
Across to Across	AC2 = K.AC1	AA
Across to Across and Integrate	AC2 = $\int$K.AC1 + AC2(ϕ)	AAI
Across to Through	TH2 = K.AC1	AT
Across to Through and Integrate	TH2 = $\int$K.AC1 + TH2(ϕ)	ATI
Through to Across	AC2 = K.TH1	TA
Through to Across and Integrate	AC2 = $\int$K.TH1 + AC2(ϕ)	TAI
Through to Through	TH2 = K.TH1	TT
Through to Through and Integrate	TH2 = $\int$K.TH1 + TH2(ϕ)	TTI

Multiport Elements

Name	Expression	Structure Graph Symbol
Resistance Field	$AC_i = \sum_{j=1}^{N} R_{ij} TH_j$	RF (Linear only)
Conductance Field	$TH_i = \sum_{j=1}^{N} G_{ij} AC_j$	GF (Linear only)
Capacitive Field	$AC_i = \sum_{j=1}^{N} \frac{1}{C_{ij}} \int TH_j + AC_i(\phi)$	CF (Linear only)
Inductive Field	$TH_i = \sum_{j=1}^{N} \frac{1}{L_{ij}} \int TH_j + TH_i(\phi)$	LF (Linear only)

Table B.2 The *MEDIEM* Basic Set of Elements.

Appendix C

FORTRAN-77 LISTING OF PROGRAM *DLCSYM* FOR CALCULATION OF VEHICLE RESPONSE TO STOCHASTIC ROAD PROFILES

```
C*************************************************************************
C****Dynamic Load Evaluation of Vehicle Response to Stochastic Road Profiles.**
C*************************************************************************

C       ********************Local Scalars:*****************************
C       m1 -Axle mass-[kg]                  !
C       m2 -Body mass-[kg]                  !
C       k1 -Tyre Stiffness-[N/m]            ! System Physical Parameters
C       k2 -Suspension Stiffness-[N/m]      !
C       b1 -Tyre Damping-[N.s/m]            !
C       b2 -Suspension Damping-[N.s/m]      !
C       u  -Vehicle Horizontal Velocity [km/h]
C       w  -Angular velocity [rad/s]
C       f  -Road profile equvalent frequencies [Hz]
C       SR -Road profile Spectral density function [m2/Hz]
C       SW -Dynamic Load Spectral density function [N2/Hz]
C       SS -Dynamic Load variance [N2]
C       SD -Standard deviation [%]
C       H  -Complex System transfer  function [N/m]
C*************************************************************************
        real m1,m2,k1,k2,b1,b2,f,w,PI,SR,SW,SS,ABSH,u,step,SD
        complex i,H
        m1=334.0
        m2=2400.0
        k1=1564000.0
        k2=250000.0
        b1=1000.0
        b2=4000.0
        i=(0,1)
        PI=3.14159265
        step=.05
C*************************************************************************
        print*,'SRESP2'
        print*,''
C******************** Forward Speed Setting: ********************************
        do 5, u=20.0,140,20.0
          SW=.0
          SS=.0
*     *************** Frequency Integration Loop: ******************
        do 10, f=step,30.0,step
            w=2.0*PI*f
*     ******** Calculation of Rd Profile values for current frequency:********
            SR=(10.0e-8*((u/3.6)**1.5))/(f**2.5)
*     ******** Calculation of Transfer function values for current freq:******
            H=-((k1-b1*w*i)*(m2*w*w*i*i*(m1*w*w*i*i-k2-b2)-m1*w*w*i*i*(k2+b2-w
))/((m1*w*w*i*i+b1*w*i+k1)*(m2*w*w*i*i-b2*w*i+k2)+m
            ABSH=ABS(H)
*     ****** Calculation of Dyn.load Spectral Density Function:*************
            SW=ABSH*ABSH*SR
*     ****** Frequency Integration to calculate Variance:****************
            SS=SS+(SW*step)
  10    continue
C*************************************************************************
*     ****** Calculation of Standard Deviation:**********************
        SD=(SQRT(SS/(((m1+m2)*9.8)**2.0)))*100.0
*       *********Print Results:**********************************
        print*,''
        print*,u,SD
        print*,''
   5    continue
        stop
        end
C*************************************************************************
```

```
c*** Dynamic Load Evaluation of Vehicle Response to Stochastic Road Profiles +
c***       considering Vehicle Body Mass Statistical Distribution:          ****
c*************************************************************************

c*** mresc3.f - Half Axle Weights above 1700.0 kg considered only(Heavy veh.)**
c*************************************************************************

              ********** Local Scalars:***********
        m1 -Axle mass [kg]              :
        m2 -Body mass [kg]              :
        k1 -Tyre Stiffness [N/m]        : System Physical Parameters
        k2 -Suspension Stiffness [N/m]  :
        b1 -Tyre damping [N.s/m]        :
        b2 -Suspension damping [N.s/m]  :

        u  -Vehicle Horizontal Velocity [km/h]
        f  -Road profile equvalent frequencies [Hz]
        w  -Angular velocity [rad/s]
        SR -Road profile Spectral density function [m2/Hz]
        SW -Current Dynamic Load Spectral density function [N2/Hz]
        SM -Dynamic Load Spectral density function [N2/Hz]
        SS -Freq. integrated SM (Variance) [N2]
        SD -Standard deviation [%]
        H  -Harmonic System tranfer function
        bnd-Body mass P.D.F band width
        M  -Current body mass value [kg]
        MM -Body mass mean value [kg]
        PD -Band P.D.F. value
        PT -Previous band P.D.F. value
        PM -Current Body mass P.D.F. value
*************************************************************************
        real m1,m2,M,MM,k1,k2,b1,b2,f,w,PI,PD,PM,PT,SR,SW,SM,SS,SD,ABSH,u,step
d,mstep
        complex i,H
        m1=324.0
        k1=1564000.0
        k2=250000.0
        b1=1000.0
        b2=4000.0
        i=(0,1)
        PI=3.14159265
        step=.05
        mstep=10.0
        bnd=500.0
*************************************************************************
        print*,'MRESPC-Heavy Vehicles only:'
        print*,''
              ********** Vehicle Speed setting:**********
        do 5, u=20.0,140.0,20.0
        SW=.0
        SS=.0
              ********** Freq. Integration Loop:**********
           do 10, f=step,30.0,step
            w=2.0*PI*f
        ******* Calculation of Rd. prof. values for current freq:*******
            SR=(10.0e-8*((u/3.6)**1.5))/(f**2.5)
            PT=0.0
            SM=0.0
            MM=.0
               **********Body mass integration Loop:*********
            do 20 m2=1350.0,4550.0,mstep
               if(m2.LE.1366.0)then
               PD=.0
                 else:if((m1+m2).LE.2200.0) then
                  PD=.473
                  MM=MM+M2-2.5*bnd-0.5
                  else:if((m1+m2).LE.2750.0) then
                   PD=.
```

```
                    PT=.476
                    PD=.261-PT
                    M=m1+m2-3.0*bnd-699.0
                    elseif((m1+m2).LE.3200.0) then
                     PT=.261
                     PD=.181-PT
                     M=m1+m2-4.0*bnd-699.0
                     elseif((m1+m2).LE.3700.0) then
                      PT=.151
                      PD=.081-PT
                      M=m1+m2-5.0*bnd-699.0
                      elseif((m1+m2).LE.4200.0) then
                       PT=.081
                       PD=.0184-PT
                       M=m1+m2-6.0*bnd-699.0
                         elseif((m1+m2).LE.4834.0)then
                           PT=.0184
                           PD=.0024-PT
                           M=m1+m2-7.0*bnd-699.0
                           else
                             PD=.0
                             PT=.0
               endif
*       *******Calculation of Current Body mass P.D.F.:****************
          PM=(PT+(PD/bnd)*M)*mstep/bnd
*       ***Calculation of Transf.Funct.values for current Body mass & frec.*-
            H=-((k1+b1*w*i)*(m2*w*w*i*i*(m1*w*w*i*i+k2+b2)-m1*w*w*i*i*(k2-b2
))))/((m1*w*w*i*i+b1*w*i+k1)*(m2*w*w*i*i+b2*w*i+k2)+m
            ABSH=ABS(H)
*       ******** Current value of Dyn. load Sp.Density func.**********
            SW=ABSH*ABSH*SR
*       ******** Calculation of Dyn. load Sp.Density func.**********
            SM=SM+SW*PM
            MM=MM+(PM*m2)
  20      continue
*       *******Frequency Integration to obtain variance:***********
            SS=SS+(SM*step)
  10    continue
*****************************************************************************
*       ********Calculation of Standard Deviation:***************
        SD=(SQRT(SS/(((m1+MM)*9.8)**2.0)))*100.0
*       ************** Print Results:**********************
        print*,''
        print*,'SD
        print*,''
  7     continue
        print*,'MM=',MM
        print*,''
        stop
        end
```

REFERENCES AND BIBLIOGRAPHY

[1] ABDULLAH F., FINKELSTEIN L., 1982.
"A Review of Mathematical Modelling of Instrument Transducers."
Acta IMEKO Separatum, Budapest, 1982.

[2] ABDULLAH F., POPOV P.A., 1987.
"Dynamic Errors due to Abrupt Road Profile Changes ahead of a Weighscale."
Confidential Report for TRRL, The City University, London, Dec., 1987.

[3] ALBERT C.J., 1961.
"A method for simulating Tyre enveloping power in calculations of Vehicle ride performance."
Rep. No YM-1424-V-300, Cornell Aeronautical Lab., Buffalo, N.Y.,Nov. 17 1961.

[4] "Arrangement for Weighing Oscillatory Load."
U.S. Patent No 3.173.503, March 1965.

[5] BALAZ V. KUDJAK V., 1985.
"Controlled Oscillators and their active nad passive Frequency stabilization."
Katedra radioelektroniky, EF SVST, Bratislava, Czechoslovakia., March, 1985.

[6] BAILEY A.L., 1981.
"The Rx 80, Mk 2.", (part 3).
Radio Communications, U.K., March, 1981.

[7] BAILEY W.N., ABDULLAH F., 1989.
"Interactive Graphics-based Computer-aided System dynamic Modelling."
Trans. Inst. of Measurement and Control., Vol.11, No 3. July-Sept., 1989.

[8] BAKKER E., NYBORG L., PACEJKA H.D., 1987.
"Tyre Modelling for use in Vehicle Dynamic Studies."
SAE Paper 870421., 1987.

[9] BAKKER E., PACEJKA H.D., LIBNER L., 1989.
"A new Tyre Model with application in Vehicle Dynamic Studies."
4th Autotechnologies Conference - Monte Carlo, SAE Paper 890087, 1989.

[10] BANKE J., 1980
"Automatic recording of axle-load in Denmark 1967-1980."
Report for the Org. for Economic Co-operation and Development Seminar on Road Traffic Information, 1980.

[11] BARNETTI & WEST, 1983:
"New Load Sensor for truck self weighing systems"
SAE Technical Paper No 830108, 1983.

[12] BASSON J. E. B., 1971;
"Measuring Transient Loads"
U.S. Patent No 3782486, May 12, 1971.

[13] BASSON J. E. B., 1975.
"Dynamic Weighing of Motorvehicle Axles."
NIRR Rep. No RP3/75, 1975, Pretoria, South Africa.

[14] BASSON J. E. B., 1977.
"The development and evaluation of a Capacitive sensor for the Axle Weight Analyser"
NIRR Rep. No RP14/77, 1977, Pretoria, South Africa.

[15] BELLINI W.R., THROWER E.N., 1968.
"A Digital Computer program to Simulate the Passage of a Vehicle over a road surface."
RRL Rep. LR181/1968.

[16] BIPM, IEC, ISO, OIML Standards - 1989.
"International Vocabulary of Basic and General terms in Metrology."
The Int. Bureau of Weights and Measurements - BIPM.
The Int. Electrotechnical Comission - IEC.
The Int. Organization for Standardization - ISO.

The Int. Org. of Legal Metrology - OIML.

[17] BODE O. et all.
"Comparison of different methods of determining the Dynamic Wheel load." - From Ref. 22.

[18] BOSCH H.R. 1985;
"Federal Highway Admin. WIM research Program Past-Present-Future"
Proc. of the 2-nd Nat. Conf. on WIM Technology and Applications, Atlanta, GA, May,1985.

[19] BOSWIJK R.H., GLASBERGER R.M.. 1977;
"Voorontwerp vegbelastings classificatie systeem"
Interner Bericht CL 77/4, Rijkswegenbouwlaboratorium, Delft, Jan. 1977.

[20] BREYER G., 1979.
"The Selection of suitable Weighing equipment for wheel loads in Austria."
Res. project of Bundesministerium fur Bahnen und Technik, 1979.

[21] CAPTAIN K.M., BOGHANI A.B., WARMLEY D.N., 1979.
"Analytical Tyre Models for Vehicle Dynamic Simulation."
Vehicle Sys. Dynamics - Aug./1979, p. 1-32.

[22] CEBON D., 1985.
"An Investigation of the Dynamic Interaction between wheeled vehicles and road surfaces."
PhD Dissertation, University of Cambridge, 1985.

[23] CEBON D., 1985.
"Road damaging effects of Dynamic axle loads."
Proc. of the 9th IAVSD Symp. on the Dynam of Veh. on Roads and Tracks. Linkoping, 1985.

[24] CEBON D., 1989.
"Vehicle-Generated Road Damage: a Review"
Vehicle System Dynamics, No 18, 1989, p. 107-150.

[25] CHADICK J.F., 1985;
"Weight Enforcement, State of Delaware"
Proc. of the 2-nd Nat. Conf. on WIM Technology and Applications, Atlanta, GA, May,1985.

[26] CHATIGNY J.V., 1984.
"Piezofilm yields Novel Transducers."
Electronics Week, U.K., Aug.6, 1984.

[27] CLAUWERT C., 1987;
"Traffic Analysis and measurement of Axle loads by using an Instrumented Bridge Joint - Principles and first results."
Belgian Road Research Centre Report, 1987.

[28] COLE D.J., CEBON D., 1988.
"Simulation and Measurement of Vehicle response to
Road roughness"
Proc. Inst Acoustics, Vol.10, Part 2, 1988.

[29] COLE D. J., CEBON D., 1989;
"A Capacitive Strip Sensor for measuring Dynamic Tyre forces"
Proc. 2nd Int Conf. on Road Traffic Monitoring, IEEE, London, Feb. 1989.

[30] COX H.L., AUGHTIE F., BROWN A.F.C., 1941.
"The Computation of Wheel Impact Forces."
Journ. of the Inst. of Automotive Eng., Vol. 10(3), 1941, p. 45-74.

[31] CUNNAGIN W.D., 1986.
"Use of WIM systems for Data collection and enforcement."
Rep. TRB/NCHRP/SYN124 - Transp. Res. Board, Washington DC, Sept. 1986.

[32] CUNAGIN W.D., KENT P.M., SUMMERVILLE F.K., 1982.
"Truck Weighing in the U.S.A: Past trends and Future Prospects"
Federal Highway Administration, (Dep. of Transportation) Rep. 1982.

[33] CZERNY L., POPP K., ,1984
"Nonstationary Random Vibration of Vehicles on Irregular guideways."
Rep. Institute of Mechanics, University of Hannover, FRG.

[34] DAVIS D.C., 1975.
"A Radial Spring Terrain-enveloping Tyre Model."
Veh. System Dynamics, Apr,1975, p.55-69.

[35] DAVIS P., AYLAND N., 1985.
"New Developments in WIM".
SAE - Paper No 851454/1985.

[36] DAVIS P., BETTISON M., SALTER D.R., 1982;
"Fundamental properties of Piezo-electric Axle Load Sensors"
Project Report to TRRL - Ph. 1., Nov. 1982.

[37] DAVIES P., SOMMERVILLE F.K., 1986;
"Low cost Axle load determination"
Australian Road Research Board. pp. 29-29, Aug., 1986, ARRB, Victoria.

[38] DEARINGER J.A., 1961.
"Dynamic Weighing of Vehicles."
Public roads, Oct. 1961, p. 200.

[39] DICKERSON R.S., MACE D.G.W., 1981.
"Dynamic Pavement Force Measurements with a Two-axle Heavy goods Vehicle."
TRRL Rep. SR688/1981.

[40] DODDS C.J., ROBSON J.D., 1973.
"The description of Road surface roughness."
Journal of Sound and Vibration. - Vol. 31(2), 1973, p. 175-183.

[41] DOEBELIN E.O., 1984.
"Measurement Systems - Application and Design." - 3rd Edition,
Mcgraw Hill 1984.

[42] "Dynamic Axle Load Measurements Trial."
OECD/TRRL Seminar, June 1986, LF1040,1041.

[43] EASTON R.C., 1979.
"AFC Cirquit for VFO's."
Ham Radio. - June, 1979.

[44] ERICKSON E., 1974.
"Automatic Weighing of Vehicles in Motion and Collection of Traffic data by Electronic Methods."
Michigan Dept. of State Highways and Transportation, 1974.

[45] "Electronic Weighing in Industrial Processes."
Ch. 6: "In Motion Weighing" - p. 162-186.
McGraw Hill, 1982

[46] FERGUSON A.C., 1969.
"Weighing Vehicles in Motion."
Measurement and Control. - Vol.2 Dec. 1969.

[47] FISHER J.W., HUCKINS H.C., 1962.
"Measuring Dynamic wheel Loads."
Highway Res. Board - Spec. Rep. 73/1962.

[48] FRYBA L., 1987.
"Dynamic Interaction of Vehicles with tracks and Roads."
Veh. System Dynamics, 16/1987, p. 129-138.

[49] FUJII M., KAMATSU Y., 1984.
"Compact and Light Weight Vehicle Weighing System."
Proc. of the 10th Conf. of IMEKO - TC-3- Kobe, Japan 9/84.

[50] GARDNER P., 1985.
"The Use of Microcomputers for the Mathematical Modelling of Instruments."
PhD Thesis, The City University, London, 1985.

[51] GARDNER P., ABDULLAH F.,
"MEDIEM: A Microcomputer Package for Modelling Mixed Energy Engineering Systems."
Conference on Engineering Software for Microcomputers,
The City University, 1984.

[52] GLOAGAN M., HERBEUVAL M. - 1982.
"Detection of road traffic by Piezo-electric transducer"
Res. Report - LEAA, Nancy, France, 1982.

[53] GOLDEN J.M., 1982.
"A Note on the University of Saskatchewan WIM Scale."
An Foras Forbatha Teoranta. - Rep. No RC256, Dublin, Dec. 1982.

[54] HANSSEN S.C., ;
"New Transducer, a unique concept for weighing."
(From Ref. 147)

[55] HUNT H.E.M., 1989.
"Stochastic Modelling of Vehicles for calculation of Ground vibration."
Proc. of the 11th IAVSD Symposium: Dynamics of Vehicles on roads and tracks - Kingston , Ontario, Aug., 1989.

[56] JACKS M. J. ;
"The need for WIM in a comprehensive Size and Weight Enforcement Program"- Proc. of the 2-nd Nat. Conf. on WIM Technology and Applications, Atlanta, GA, May,1985.

[57] JORDAN P.G., 1984.
"Measurement and Assessment of Unevenness on Major roads."
TRRL Rep. 1125, 1984.

[58] ISHKHANOV I.A., 1985.
"Some Dynamic errors in Weighing during motion."
Izmeritel'naya Tekhnika, No 1, Jan. 1985, USSR, p.24-26.

[59] KALLENBACH R., 1987;
"Identification methods for Vehicle System Dynamics."
Vehicle Sys. Dynamics, No16/1987, p. 107-127.

[60] KARNOPP D., 1976;
"Bond Graphs for Vehicle Dynamics."
Vehicle System Dynamics, 5/1976, p. 171-184.

[61] KARRER H.E., VIRGIN G.L.,1964.
"Dynamic Force Measurement."
Instr. Soc. of America - 19 Annual ISA Conference & Exhibit -
Oct. 12-15, 1964 - New York).

[62] KELLER H., 1970;
"Achswagung von Kraftfahrzeugen mit verschiedenen Weigeverfahren"
Strasse und Autobahn, Vol.21, No5, 1970, pp.183-194.

[63] KENNEDY C.K., LISTER N.W., 1978.
"Prediction of Pavement performance and the Design of Overlays."
TRRL Rep. LR833/1978.

[64] KORTUM W., SCHIEHLEN W., 1985.
"General purpose Vehicle System Dynamics Software based on
Multibody formalisms."
Veh. System Dynamics, 14/1985, p. 229-263.

[65] KOZIN F., BOGDANOFF J.L., 1960.
"On the Statistical Analysis of the Motion of simple two-dimensional
Linear Vehicles moving on a Random track."
Int. Journ. of Mechan. Science., Vol. 2, 1960, p. 168.

[66] KRONMULLER H., 1983.
"Fast Measuring with Microcomputer for On-Line Weighing."
Measurement, vol.1, No.3, July-Sept 1983.

[67] KROPAC O., SPRINC J., 1982.
"Identificatioon of the System Vehicle-Road Parameters."
Vehicle System Dynamics. Nov., 1982, p. 241.

[68] KROPAC O., SPINC J., PROCHAZKA M., 1987.
"Classification of Roads and Runways with respect to unevenness of their pavement."
Acta Technica - CSAV. Feb. 1987, p.202.

[69] KRUKAR M., HENION L., 1980
"The Use of Automatic Vehicle Identification Devices with WIM Systems - The Oregon Experiment."
Res. Report, Oregon Department of Transport, Highway Division, U.S.A., 1980.

[70] LaBARRE R.P., FORBES R.T., 1970.
"The Measurement and Analysis of Road surface roughness."
MIRA Report No 5 1970.

[71] LAKER I.B., 1976.
"The Use of Random Sequences in the Identification of Vehicle Dynamics."
TRRL Rep. 216 UC/1976.

[72] LAKER I.B., 1978.
"The Dynamic response of a Single Wheel suspension to Computer generated road profiles."
TRRL Rep. SR 360/1978.

[73] LeBLANC P.A., WOODROOFE J.H.F., YUAN B., PLOEG H.L., 1987.
"Effect of Heavy Vehicle Suspension Nonlinearities on Pavement Loading."
Vehicle Sys. Dynamics, 1987.

[74] LEONARD D.R., GRAINGER J.W., 1974.
"Loads and Vibrations caused by 8 commercial vehicles with grossweights exceeding 32 tons."
TRRL Rep. LR 582/1974.

[75] LEE C.E., IZADMEHR B., MACHEMEHL R.B., 1985.
"Demonstration of WIM systems for Data Collection and Enforcement."
Res. Rep. 557-1F. Dec. 1985, CTR-The Univ. of Texas at Austin.

[76] LEE C.E., 1974 ;
"The History and Development of Weigh-in-motion systems."
Proc. of 1st Nat. Conference-workshop on Automating data collection
for Transportation planning, Orlando, Florida, 1974.

[77] LEE C.E., 1966;
"A Portable Electronic Scale for Weighing Vehicles in Motion",
Highway Research Record 127 - Highway reseach Board, Washington D.C.
1966, pp22-23.

[78] LIEBNER R., 1981.
"Interactive Functional Modelling of Instruments."
PhD Thesis, The City University, London, 1981.

[79] LIEBNER R.D., ABDULLAH F., FINKELSTEIN L., 1982.
"Structure Graphs: a new approach to Interactive Computer Modelling of
Multienergy domain systems."
Journ. of Dyn. Sys., Meas. and Control., Vol.104, 1982, p. 143-150.

[80] LINS W.F., HOOGTERP F.B., PRADKO F.,1969.
"Comparison of Time domain and Frequency domain Analysis of Off-road Vehicles."
SAE Earthmoving Industry Conference - Central Illinois Section, Apr., 15-16,
1969.

[81] LIPPMANN, PICCIN W.A., BAKER T.P., 1966.
"Enveloping Characteristics of Truck Tyres."
Transactions SAE Vol.74 (1966).

[82] LISTER N.W., NUNN D.E., 1968.
"Contact Areas of Commercial Vehicle Tyres."
TRRL Rep. LR 172/1968.

[83] LOZIA Z., 1987.
"A Two-dimensional Model of the Interaction between a Pneumatic Tyre and an even and uneven road surface."
Inst. of Transport, Warsaw University of Technology., 1987.

[84] MACHEMEHL R.B., LEE C.E., WALTON C.M., 1975.
"Acquiring Traffic Data by In-motion Weighing."
Transportation Engineering Journal, TE4, Nov., 1975.

[85] MARGOLIS D.L., 1981
"Bond Graphs as a Simulation Modelling Formalism."
Paper, Dept. of Mech. Eng., U-ty of California, Davis, CA., 1981

[86] "Method and Aparatus for Dynamically Weighing Objects in Motion."
British Patent No 1,077,508, Oct. 1964.

[87] MILLER R.P., 1969;
"Electrical Weighing Apparatus using a Capacitive Flexible Mat"
U.S. Patent No 3565195, Apr. 16, 1969.

[88] MITCHELL C.G.B., 1987.
"The effect of the Design of Goods Vehicle Suspensions on Loads on Roads and Bridges." - TRRL Report 1987.

[89] MITSCHKE M., 1961.
"Influence of Road and Vehicle Dimensions on the Amplitude of Body motions and Dynamic wheel loads."
SAE preprint 310C, Jan. 1961.

[90] MIAZAKI S., ISHIDA A., 1984.
"Capacitive Transducer for measurement of Vertical foot force."
Journal of Medical and Biological Eng. and Computing. - July, 1984.

[91] MOORE R.C., HODGE A.R., SPINDLOW J.R., 1982
Paper to "OECD Seminar of Freight Vehicle Measurements in the U.K".–TRRL, 1982.

[92] MOORE R.C., 1985
"High Speed Axle Load measurements – A European Perspective."
Paper to II National WIM Conference, Georgia.
Dept. of Transportation, Atlanta, GA., May 1985.

[93] MOORE R. C., BETTISON M., DAVIES P., STEVENSON J., FISHER J. ; "Piezoelectric axle load sensors" - Proc. of IEE Int Conf. on Traffic Data Collection, Publ. No 242, London, 1984.

[94] MOSES F.,GHOSN M., 1981;
"Weighing Trucks in motion using instrumented highway bridges"
FHWA Rep. OH-81/008, 1981.

[95] MOSES F. GHOSN M., 1983;
"Instrumentation for Weighing Trucks in motion for Highway Bridge Loads" Rep. No FHWA/OH-83/001, Case West Res. U-ty, Dept of Civil Eng., Cleveland, OH, Aug, 1983.

[96] NAPIER C., THOMMAS R., 1985;
"Impact of Truck size and weights on Highway Pavements and Bridges"
Proc. of the 2-nd Nat. Conf. on WIM Technology and Applications, Atlanta, GA, May,1985.

[97] NEWLAND D.E., 1984;
"An Introduction to Random Vibrations and Spectral Analysis"
Second edition, Longman, London.

[98] NEWLAND D.E., 1987;
"General Linear theory of Vehicle Response to Random Road Roughness."
Acta Technica - CSAV, Feb. 1987, p.202.

[99] NEWLAND D.E., 1986.
"The effect of a Footprint on perceived Surface roughness."
Proc. of Royal Soc. London, A405/1986, p.303-327.

[100] NEWTON W.H., 1987;
"Trials of three On-board Axle weighing Sytems for HGV's"
TRRL Rep. No 103, 1987.

[101] NORDVALL J.O.,
"New Magnetoelastic Load Cells for high precision Force measurement and Weighing." - From Ref. 147.

[102] NORMAN O. K., HOPKINS R. C., 1952;
"Weighing Vehicles in Motion"
Bull. No 50, HRB, National Research Concil, Washington D.C., 1952.

[103] ONO T., KAMEOKA K., NAKAJIMA K., 1979.
"Studies on Dynamic Measurement Methods of Mass and Weight."
Bulletin of the ISME, vol.22, No.166, April 1979.

[104] Organization for Economic Co-operation and development. 1986.
"Freight Vehicle overloading and Load Measurements."
Road Transport Research programme – Report by Working Group,
Seminar on Freight Vehicle Overloading and Load Measurement,
TRRL - June 1986.

[105] PACEJKA H. B., 1985.
"Modelling Complex Vehicle Systems using Bond Graphs."
Journ. of the Franklin Institute, vol.319, 1985, p. 67-81.

[106] PAGE. J., 1973.
"Dynamic Behaviour of a Single Axle Vehicle Suspension System –
a theoretical study."
TRRL Rep. LR 580/1973.

[107] PAGE J., 1973.
"Dynamic behaviour of two linked twin-axle Lorry Suspension
Systems: a theoretical study."
TRRL Rep. LR 581/1973.

[108] PAGE J., 1976.
"Dynamic Wheel load Measurements on Motorway bridges."
TRRL Rep. LR722/1976.

[109] PAGE J., 1974.
"Dynamic behaviour of Two-axle suspension system: a theoretical and experimental study."
TRRL Rep. SR119/1974

[110] PAGE J., 1974.
"A Review of Dynamic Loading caused by Vehicle Suspensions."
TRRL Supl. Rep. 82UC/1974.

[111] PELTIER B., 1982
"Application of Piezo-electric Axle Load Sensors in France."
Rep. - Setra, DTSC, France, 1982.

[112] POTOCKI F.P.,1981.
"The Effect of Vehicle Tilt on Measured Wheel Loads."
TRRL report SR708/1981.

[113] POTTER J.F., 1982
"Dynamic behaviour of pavements loaded by Vehicles with Tandem and Tri-axle arrangements."
TRRL Working Paper PD8 - 1982.

[114] POTTER J.R, 1968.
" Dynamic Impact Pressures generated on the Road by Sprung and Unsprung Vehicles."
TRRL Rep. LR137/1968.

[115] PRIEST R.A.F., MOORE R.C., 1985.
"The Estimation of Traffic for Road pavement Design".
TRRL Rep. SR 720/1981.

[116] PRUDHOE J., 1988.
"Slow Speed 'Dynamic' Axle Weighers: Effect of Surface Irregularities."
TRRL Res. Rep. 134/1988.

[117] PUCKET R.E., 1964.
"Selecting the Best scale for In-Motion Weighing."
Public Roads, Vol.33, No3, Aug. 1964, p. 45-47.

[118] RAO B.K.N., JONES B., 1975.
"Laboratory simulation of Vibratory Road surface."
Journal of Sound and Vibration. - Vol. 41(1), 1975, p. 73-84.

[119] RASMUSSEN R.E., CORTESE A.D., 1968.
"Dynamic Spring Rate Performance of rolling tyres."
SAE Paper 680408, 1968.

[120] RILL G., 1989.
"Demands on Vehicle Modelling"
Proc. of the 11th IAVSD Symposium: Dynamics of Vehicles on roads and tracks - Kingston , Ontario, Aug., 1989.

[121] ROBERTSON N.I.D., 1986.
"Dynamic Force Measurement."
Transducer Technology 9/1986.

[122] ROBSON J.D., 1979.
"Road surface description and Vehicle response."
Int. Journal of Vehicle design. - Vol. 1(1), 1979.

[123] ROBSON J.D., DODDS C.J., 1975.
"Stochastic Road Inputs and Vehicle Response."
Vehicle System Dynamics. - May 1975, p. 1-13.

[124] ROSENBERG R.C., 1974.
"A User's Guide to ENPORT-4."

Wiley, New York, 1974.

[125] SALTER D.R., DAVIES P., BETTISON B., 1981;
"The development of detectors for the measurement of moving wheel loads"
14 Ann. UTSTG Conference, U-ty of Leeds, U.K., 1981.

[126] SALTER D.R., DAVIES P. 1987;
"Development and Testing of a Portable Microprocessor-based Capacitive WIM System"
TRRL. Transportation Research Record 997.

[127] SCHURING D., BELSDORF M. R., 1969.
"Analysis and Simulation of Dynamical Vehicle-Terain Interaction."
Rep. of Cornell Aeronautical Lab., Inc., Buffalo, N.Y. - May, 1969.

[128] SCHWADERER W., REIMUND W., 1959.
"The Automatic Axle-load Scale at Grunbach."
Strasse und Autobahn, No2, 1959.

[129] SHARP R.S., HASSAN S.A., 1984.
"Performance of Passive, Active and Semi-active Car-Suspension Systems."
Proc. Inst. of Mech. Engineers. - Vol. 200(D3).

[130] SHARP R.S., CROLLA D.A., 1987.
"Road Vehicle Suspension System Design – a Review"
Vehicle System Dynamics, No 16, 1987, p. 167-192.

[131] SIFFERT M., 1974;
"L'Exploitation des Bascules Dynamiques" , (Dynamic Weighing by Piezo-electric Cables).
Bulletin de Liason des Laboratoires des Ponts et Chausees, No 70, III-IV 1974, pp25-44.

[132] SOMMERVILLE F.K., 1986;
"Low cost Dynamic Axle load Measurement"
Ph.D. Thesis, University of Nottingham, 1986.

[133] STEWART P.M., 1989;
"New Sensors for Axle detection and Weigh-in Motion"
Proc. 2nd Int Conf. on Road Traffic Monitoring, IEEE, London, Feb. 1989.

[134] SPAARGAREN K., 1977;
"Drift Correction Cirquit for free running Oscillators"
Ham Radio, Dec., 1977.

[135] SWEATMAN P.F., 1980.
"Effect of Heavy Vehicle Suspensions on Dynamic Road Loading."
Res. Rep. ARRB No 116, 1980.

[136] "System for Measuring the weight of Dynamic Loads."
US Patent No 3.063.635, Nov.1962.

[137] "The AASHO Road Test", 1962.
Rep. 5 - Pavement Research. - Highway Res. Board, Spec. Rep. 61E, 1962.

[138] TRRL, 1982.
"Fundamental properties of Piezo-electric Axle load Sensors."
Project Rep. - Ph. 1, TRRL, Nov. 1982.

[139] TRRL, 1983.
"An automatic method to count and classify Road Vehicles."
TRRL Rep. SR757/1983.

[140] TRRL, 1982.
"A Note on the University of Saskatchewan Weigh-in-Motion Scale."
TRRL Rep. RC256/1982.

[141] TROTT J.J., GRAINGER J.W., 1968.
"Improvements in Capacitors."
UK Patent No 1234083, April 2, 1968.

[142] TROTT J.J., GRAINGER J.W., 1968.
"Design of a Dynamic Weighbridge for recording Vehicle wheel loads."
TRRL Rep. LR219/1968.

[143] TROTT J.J., WILLIAMSON P.J., 1959
"Measuring, classifying and counting wheel loads of moving vehicles."
The Engineer, Dec. 1959, pp. 859-862.

[144] URQUHART F.A., RHODES A.H., 1987
"The Relationship between payload distribution and observed axle loading"-
Rep. of the Transport Operations Res. Group, U-ty of Newcastle upon
Tyne, 1987.

[145] VanDIXHOORN J.J., 1977.
"Simulation of Bond Graphs on Minicomputers."
Journ. of Dyn. Sys., Meas. and Control., March 1977, p. 9-14.

[146] VIRCHIS V.J., HAMMOND J.K., 1986.
"Dynamic Simulation with Independent variable transformation using
Bond Graphs."
Proc. of the Dynam. of Vehicles on Roads and Tracks Conference -
Linkoping, 1986.

[147] WEBBER J. M. et al (SIRA Ltd), and ABDULLAH F., RAHMAN M.M.
(CityUniversity), 1985.
"Feasibility Study of Dynamic Weighbridge Systems"
SIRA Ltd. Project Report A/7189 for TRRL, 1985.

[148] "*WEIGHMAN* and accessories User's Manual."
Golden River Ltd., 1979.

[149] WELLSTEAD P.E., 1979.
"Introduction to Physical System Modelling."
Academy Press, 1979.

[150] WHITTEMORE A.P., WILEY J.R., SCHULTZ P.C., POLLOCK D.E., 1970.
"Dynamic pavement loads of Heavy highway vehicles."
NCHRP Rep. 105, HRB Washington DC., 1970.

[151] WINTER T., 1978.
"A Digital Oscillator Stabilizer."
Radio Communications, Aug., 1979.

[152] W & T Avery Ltd, 1989.
"CTH Mk II Digital Indicator System."
Specifications leaflet, GEC Avery, Smethwick, Warley, W.Midlands, 1989.

[153] YOSHIKAWA H., 1984.
"In-motion Axle weigher."
'Recent Advances in Weighing Technology' Conf., Sept. 1984.

[154] ЛИПМАН А.Е., ШАПИРО А.И.;
"Автоматизированная Система Взвешивания в Движении"
УДК 681. 269.7.